ADVANCED RAMAN AMPLIFICATION TECHNIQUES FOR HIGH CAPACITY AND BROADBAND COHERENT OPTICAL TRANSMISSION SYSTEMS

MD ASIF IQBAL

Doctor of Philosophy

ASTON UNIVERSITY

January 2018

Aston University

Advanced Raman Amplification Techniques for High Capacity and Broadband Coherent Optical Transmission Systems

Md Asif Iqbal

Doctor of Philosophy

January 2018

SUMMARY

This thesis presents a detailed study of different advanced Raman fibre laser (RFL) based amplification schemes and the development of novel broadband distributed and discrete Raman amplifiers in order to improve the transmission performance of modern high capacity, long-haul coherent optical systems. The numerical modelling of different Raman amplifier techniques including power distribution of signal, pump and noise components, RIN transfer from pump to signal, broadband gain optimization and so on have been described in details.

The RIN and noise performances of RFL based distributed Raman amplifiers (DRAs) with different span lengths, forward pump powers and input reflection levels have been characterized experimentally. It has been shown through coherent transmission experiment that, in order to improve pump power efficiency, a low level of input reflection up to ~10% can be allowed without increasing the Q factor penalty > 1dB due to additional signal RIN penalty.

A novel broadband (>10nm) first order Raman pump is developed for use as a forward pump in long-haul transmission experiment. Significant signal RIN mitigation up to 10dB compared with conventional low RIN, narrowband sources was obtained for bidirectional DRA schemes. Long-haul coherent transmission experiments with 10×120Gb/s DP-QPSK system were carried out in a recirculating loop setup using the proposed broadband pump in bidirectional and backward only pumping configurations. The maximum transmission reach up to ~8330km was reported with first order broadband pumped bidirectional DRA, with transmission reach extensions of 1250km and 1667km compared with conventional backward only and first order semiconductor pumped bidirectional pumping scheme respectively.

Finally, a novel design of bidirectional broadband distributed DRA is proposed to reduce the noise figure tilt and improve the WDM transmission performances. Furthermore, broadband discrete Raman amplifier schemes in dual stage configuration are also shown for high gain, high output power, low noise and low nonlinear performances.

Keywords: Raman amplification, fibre amplifiers, fibre lasers, coherent communications, nonlinear amplifiers.

2

ACKNOWLEDGEMENTS

First of all, I am grateful to the almighty for giving me the knowledge and strength to carry out the research works in this thesis. I would like to take the opportunity to acknowledge and thank several people who have helped me in many different ways during the work for this thesis. Firstly, my supervisor Dr Paul Harper who has guided me throughout the whole project and has always been there with useful advices. I am also thankful to my associate supervisor Dr Wladek Forysiak for his utmost interest and inspiration during the project. I express my gratitude to the EU Marie Skłodowska Curie early stage researcher fellowship that I enjoyed during the last 3 years in ICONE project. I am grateful to all my placement supervisors, Dr Seb Savory, Dr Juan Diego Ania-Castañón, Dr Andre Richter and Dr Steve Desbrulais for their continuous support and help during my time in their respective institution. I would like to especially thank Dr Mingming Tan for his continuous support in different experimental works and useful discussion on numerous research ideas. I am also grateful to Dr Lukasz Krzczanowicz, Dr Ian Philips and Dr Atalla El-Taher for helping me in the experimental setup of broadband distributed and discrete Raman amplified transmission system as shown in chapter 7. I am also thankful to AIPT Lab technician Mrs Swaroopa for helping me in the lab with many technical issues. I also appreciate the comments and suggestions of Dr Ian Mcclean from II-IV, on many different technical results over numerous conference calls.

I must thank Dr Juan Diego Ania-Castañón, Giuseppe, and Francesca from IO-CSIC, Madrid and Auro from AIPT to help me in the numerical modelling of Raman amplifiers and with many useful discussion over different research works. The part of the experimental works on Raman fibre laser based distributed amplification as described in chapter 5 was obtained in collaboration with Giuseppe during his secondment at AIPT in 2015.

I would like to thank my AIPT colleagues Mohammed, Abdallah, Morteza, Pavel, Sam, Tingting, Vladimir, Dr Filipe Ferreira and Dr Marc Stephens for their day-to-day support during my PhD. My special thanks go to all of the AIPT members for the great working environment and constant support. I am also grateful to all my ICONE friends, Auro, Giuseppe, Francesca, Simone, Tu, Marti, Ksenia, Aditya, Jaime, Faruk, Oskars, Hou-man, Hugo and Noreen for their great company during the journey in ICONE project.

Most importantly I would like to thank my parents and my wife Onia for their constant inspiration, support and patience. I am really fortunate to have such a strong support from them in difficult times.

TABLE OF CONTENTS

ABBREVIATIONS

ADC	Analog-to-Digital Converter
AGC	Automatic Gain Control
AOM	Acousto-Optic Modulator
AWG	Arrayed Waveguide Grating
CUT	Channel Under Test
CW	Continuous Wavelength
DBP	Digital Back Propagation
DCF	Dispersion Compensating Fibre
DCM	Dispersion Compensating Module
DCRA	Dispersion Compensating Raman Amplifier
DDG	Digital Delay Generator
DFB	Distributed Feedback
DGD	Differential Group Delay
DP	Dual Polarised
DRA	Distributed Raman Amplifier
DRS	Double Rayleigh Scattering
DSP	Digital Signal Processing
DWDM	Dense Wavelength Division Multiplexing
ECL	External Cavity Laser
ENF	Equivalent Noise Figure
ESA	Electrical Spectrum Analyser
FBG	Fibre Bragg Grating
F-P	Fabry-Perot
FOPA	Fibre Optic Parametric Amplifier
FSR	Full Scale voltage-Range
FWHM	Full Width at Half-Maximum

FWM	Four Wave Mixing
GFF	Gain Flattening Filter
GVD	Group Velocity Dispersion
HD-FEC	Hard Decision – Forward Error Correction
HNLF	Highly Nonlinear Fibre
ISI	Inter Symbol Interference
LO	Local Oscillator
LW	Linewidth
MIMO	Multi-Input Multi-Output
MPI	Multi-Path Interference
MZM	Mach-Zehnder Modulator
NF	Noise Figure
NFT	Nonlinear Fourier Transform
NLSE	Nonlinear Schrödinger Equation
NPS	Nonlinear Phase Shift
OADM	Optical Add Drop Multiplexer
ODE	Ordinary Differential Equation
OPC	Optical Phase Conjugation
OSA	Optical Spectrum Analyser
OSNR	Optical Signal to Noise Ratio
OTDR	Optical Time Domain Reflectometer
PBC	Polarisation Beam Combiner
PBS	Polarisation Beam Splitter
PC	Polarisation Controller
PDG	Polarisation Dependent Gain
PDM	Polarisation Division Multiplexing
PMD	Polarisation Mode Dispersion
POLMUX	Polarisation Multiplexer

PPG	Pulse Pattern Generator
rDFB	Random Distributed Feedback
RFL	Raman Fibre Laser
RIN	Relative Intensity Noise
SBS	Stimulated Brillouin Scattering
SE	Spectral Efficiency
SSMF	Standard Single Mode Fibre
SOA	Semiconductor Optical Amplifier
SPM	Self-Phase Modulation
SPV	Signal Power Variation
SRS	Stimulated Raman Scattering
SYNTH	Synthesizer
TE	Transverse Electric
TIA	Trans-Impedance Amplifier
TM	Transverse Magnetic
TW	Travelling Wave
URFL	Ultra-long Raman Fibre Laser
WSS	Wavelength Selective Switch
XPM	Cross Phase Modulation

LIST OF FIGURES

16

LIST OF TABLES

CHAPTER 1

INTRODUCTION

The breakthrough of modern fibre optic communication system happened at the advent of low loss optical fibres (below 20dB/km) [1] and simultaneous introduction of optical sources (GaAs semiconductor laser) [2] near 1µm during 1970s. The first generation of optical fibre communication operated near 0.8µm with GaAs semiconductor laser and the system bit rate was limited up to 45Mb/s with maximum repeater spacing of 10km. But at the early 1980s the second generation of optical fibre communication became popular near 1.3µm because of lower fibre loss below 1dB/km and minimum dispersion. Optical sources and detectors using InGaAs technology were used for the operation near 1.3µm. At the end of 1980s, commercial system operating at a bit rates up to 1.7Gb/s with a repeater spacing about 50km also became available [3]. Later minimum loss of single mode silica fibre of 0.2dB/km was achieved around 1.55µm which led to the introduction of third generation of fibre optic communication in 1990s with bit rates up to 10Gb/s. One of the problems of third generation systems was high dispersion near 1.55µm, which was then solved with the introduction of dispersion shifted fibre. Electrical regeneration was used with repeater spacing of about 60-70km. In 1990s, the implementation of efficient amplification using erbium doped fibre amplifier (EDFA) and the use of wavelength division multiplexed (WDM) signals introduced fourth generation, where repeater spacing was also increased further (60-80km) with overall improved transmission reach.

The introduction of EDFAs which amplify signals in the lowest loss third window of silica based single mode fibre brought out revolutionary breakthrough in the modern fibre optical transmission systems increasing the system capacity in the order of 10s of Tb/s by early 2000. The current fifth generation transmission systems focuses on increasing the system bandwidth beyond conventional C band combining S, C and L band using advanced amplification techniques and new generation of low loss fibres from 1300 to 1650nm.

However, due to the exponential growth of current internet traffic, a "capacity crunch" of the installed transmission system based on single mode fibre has been predicted at the end of this decade [4, 5]. The growth rate of current network traffic is more than 20% per year and CISCO VNI has predicted the public network demand as 130 exabytes (1018 bytes) per month in 2018 [6].

The capacity of a single additive white Gaussian noise (AWGN) channel can be expressed using Shannon's theory as [7]:

$$C = B \log_2 \left(1 + SNR\right) \tag{1.1}$$

$$\text{with, } SNR \equiv \frac{P_S}{N} = \frac{P_S}{N_0 R_S} = \frac{E_S}{N_0} \tag{1.2}$$

where, SNR represent the signal-to-noise ratio, P_S and N are the average signal and noise power in a limited bandwidth B respectively. The symbol rate of signal, energy per symbol and noise power density are given by R_S, E_S and N_0 respectively. Current telecommunication systems is based on coherent technologies and many advanced techniques are being exploited in order to combat the exponential increase in bandwidth demand [6]. The capacity of a single mode fibre is limited, however maximum information capacity can be achieved by:

(i)   Improved spectral efficiency

(ii)   Improved SNR

(iii)   Extended transmission bandwidth

Spectral efficiency is defined by the ratio of total capacity to the system bandwidth (measured in bits^{-1}s^{-1}Hz^{-1}). Higher spectral efficiency can be achieved by using higher order modulation formats, encoding more number of bits per symbol. But the system reach of WDM systems with higher order modulation formats are highly dominated by the channel filtering, intrachannel and interchannel crosstalk due to nonlinearities [8]. The highest spectral efficiency reported so far is 15.3 bits^{-1}s^{-1}Hz^{-1} using DP-2048QAM but with a maximum distance up to only 150km [9]. Higher order modulation formats require higher SNR performance, which could be met by simply increasing the signal launch power into the fibre, but unfortunately the Kerr nonlinear penalties limit the performance when input power is increased beyond certain limit. So the use of improved spectrally efficient modulation formats beyond the most popular dual-polarised QPSK (DP-QPSK) is still challenging in trans-oceanic submarine systems.

The SNR can be improved by either increasing the launch signal power into the optical fibre or by reducing the noise generated in the system. Using fibre with large effective core area allows more signal power into the fibre and increases the SNR without increasing the fibre nonlinearity [10]. Reducing the fibre loss can also improve the fibre nonlinearity tolerance [11, 12], however scaling of signal power is bit worse than that of increased effective area because of longer interaction

22

length for fibre nonlinearity. Thus 1dB improvement in span loss provides less than 1dB improvement in optical signal to noise ratio (OSNR) [10].

The noise in long-haul coherent transmission systems mainly comes from the amplified spontaneous emission (ASE) noise generated from the amplifiers. Better design of optical amplifier with low noise figure (NF) can improve the SNR performance and increase system capacity. Distributed Raman amplification has much better noise performance than most popular EDFAs which has a quantum limited noise figure of minimum 3dB. Advanced design techniques of distributed Raman amplifiers (DRAs) using higher order pumping [13, 14] and ultra-long Raman fibre laser based bidirectional pumping scheme [15] can be used to improve the noise performance.

All the above techniques can improve SNR allowing increase in system capacity, however capacity increases logarithmically with SNR as shown in Eq. (1.1). A significant increase in capacity is possible by increasing the system bandwidth (*B*) which is outside the *log* in Eq. (1.1). The WDM system bandwidth mainly depends on the amplification bandwidth. In currently deployed system with EDFAs, the system bandwidth is limited within ~35nm in C band (1530-1565nm), however record transmission capacity (70.4Tb/s) in a wideband coherent transmission experiment have been demonstrated recently over >7500km using combined C+L band EDFAs with about 10THz usable optical bandwidth, coded modulation with advanced constellation shaping, digital nonlinearity compensation techniques and advanced filtering techniques [16]. Broadband Raman amplification has the benefits of continuous wideband transmission capability and better noise performance compared with EDFAs. Coherent WDM transmission over continuous 73nm bandwidth covering C+L band in all-Raman transmission experiment has also been demonstrated to allow transmission capacity >9Tb/s over 6000km using standard DP-QPSK modulation format [17]. Recently a revival of semiconductor optical amplifier (SOA) for broadband application has been demonstrated in a breakthrough experiment with ultra-wideband SOA based coherent WDM transmission >100nm continuous optical amplification with up to 100km distance [18].

The capacity demand can also be solved by using the spatial dimensions: *N* number of spatial modes in multi-/few-mode fibres or *N* number of parallel single mode cores in multi-core fibre or even combining both in a multi-mode, multi-core fibre in spatial division multiplexing (SDM) configuration. Recently the record capacity of 10.16 petabits/s in a dense SDM/WDM transmission over 6-mode 10-core fibre across C+L has been demonstrated up to maximum distance of 11.3km [19]. But due to the fundamental issues related to cost and power consumption required for

amplification and digital signal processing, the future of SDM technologies in real system is still not promising.

In this thesis, we focus on advanced design of distributed Raman amplification technique based on stimulated Raman scattering (SRS) to improve the SNR by improving the noise performance and mitigating the fundamental issue of relative intensity noise (RIN) transfer from pump to signal. Novel Raman fibre laser based bidirectional DRAs have been proposed in order to order to simultaneously improve the noise performance and mitigate intensity noise transfer from pump to signal. The resultant improvement in SNR will allow performance improvement of long-haul coherent WDM systems such as increase of the maximum reach. The improvement of SNR inside the *log* term of Shannon's capacity theorem as shown in Eq. (1.1) will allow the use of higher order modulation formats and increase the system capacity.

Moreover, we also demonstrate experimentally and numerically the improved design of broadband distributed and discrete Raman amplifiers over continuous C and L bands. The overall amplification bandwidth extension with reasonable gain flatness is achieved by combining multiple pumps at suitable wavelengths. Overall the noise figure performance is also improved by applying novel bidirectional pumping schemes. The improved noise performance with extended bandwidth allows system designer to work outside the *log* of Eq. (1.1) in order to increase system capacity linearly with the amplifier's bandwidth. The techniques used can also be used in multi-core fibre in SDM systems with multiple parallel single mode fibre cores in order to further increase the system capacity.

1.1   Thesis Organisation

This thesis consists of eight chapters. In chapter one, the historical overview of fibre optic transmission system so far and the scope of this thesis have been given very briefly.

The introduction of coherent optical transmission systems including the basic design of transmitter, coherent receiver and fibre optic transmission line setup in a recirculating loop is covered in chapter 2. This chapter also discusses the basic transmission impairments including both linear and nonlinear impairments that limit the signal performance in fibre optic transmission systems.

The theoretical backgrounds of different optical amplification techniques are explained in third chapter. The principles of operation, characteristics, advantages and challenges of Raman amplifiers are discussed in details. The basic principle, design, advantages and disadvantages of

other popular amplification techniques: EDFA, SOA, fibre optic parametric amplifier (FOPA) and rare-earth doped fibre amplifiers are also explained briefly.

A detail description on the numerical modelling of Raman amplifiers is given in chapter 4. All relevant equations of average power model and references to numerical simulation of basic design and different advanced distributed Raman amplification techniques: higher order bidirectional pumping, ultra-long Raman fibre laser based amplification are provided. Examples of signal power variation (SPV) along the amplifier span for different pumping schemes, contour plot of different amplifier characteristics such as: OSNR, SPV along the amplifier span are provided. Modelling of RIN is also presented with brief discussion.

In chapter 5, we show different pumping schemes with Raman fibre laser (RFL) based DRAs. Ultra-long RFL (URFL) based bidirectional DRA scheme has already been demonstrated as the best choice for quasi-lossless signal transmission with a cost effective higher order pumping scheme using a pair of passive fibre Bragg gratings (FBGs) at 1st order pump wavelengths [15]. However the high RIN transfer counter-balances the improved OSNR benefits and degrades the transmission performances as shown in [14, 20]. RIN mitigation in RFL based DRA removing input reflection has been proposed recently in a random fibre laser configuration [21], however the requirement of very high forward pump power compromises the pump power efficiency. In order to improve the pump efficiency and improve the design without compromising the signal RIN penalty, here we investigate different RFL based DRA schemes mainly their signal RIN, power distribution properties with respect to different forward pump powers and input reflection levels. Intra-cavity lasing mode structures at different span lengths and input reflectivity levels are also investigated in order to determine the type of lasing created inside the cavity and related 1st order lasing RIN performances are also presented in details. Moreover, SPVs corresponding to different pumping schemes are shown to determine the OSNR improvement. Finally, the simultaneous impact of RIN and OSNR improvements due to reduced SPVs using bidirectional pumping are characterized through long-haul coherent transmission experiments and results are given to compare the performance of different pumping schemes.

The most critical performance limiting factor in bidirectional Raman amplifiers is RIN transfer from forward propagating pumps to signal [22]. The RIN induced penalty outperforms the advantages of improved noise performance of DRAs. High forward pumping is essential to get quasi-lossless transmission along the span but that comes with a penalty of RIN transfer mainly

from forward pump(s) to signal. So RIN mitigation techniques are required in order to use forward pumping scheme in DRA.

In chapter 6, a novel RIN mitigation technique in 2nd order-, 1st order- bidirectional and backward only pumped distributed Raman amplifiers has been demonstrated using a broadband (>10nm of 3dB bandwidth) and incoherent 1st order pump source. The experimental design of the broadband pump generation technique, measured signal RIN and power profiles are compared with conventional Raman pumping schemes. The optimum level of forward pump power for minimum signal RIN penalty are also determined for respective pumping configurations. Performance benefits from simultaneous RIN mitigation and OSNR improvements are demonstrated using long-haul coherent transmission experiments with 10×120Gb/s DP-QPSK WDM system in a recirculating loop setup and are also compared with conventional Raman pumping schemes.

Chapter 7 focuses on the design of wideband distributed and discrete Raman amplifiers providing continuous bandwidth over C and L bands. As mentioned in Eq. (1.1) that system capacity can be increased linearly by extending the amplification bandwidth. The bandwidth extension capability by combining multiple pumps and the low noise figure properties of broadband distributed Raman amplification can be very attractive for long-haul, high capacity transmission system [17]. On the other hand, discrete Raman amplification has its own benefits and challenges. Discrete Raman amplifiers use short length of gain fibres with high nonlinear coefficient and thus require less pump powers, which makes the power handling issues much easier [23]. However performances are limited by increased nonlinear penalties [24] and higher noise penalty mainly from double Rayleigh scattering (DRS) [25]. In chapter 7, the numerical and experimental design methods of broadband Raman amplifiers with flat gain profiles are described both for distributed and discrete configurations. A detail design of broadband Raman amplifier with different number of pumps are presented. We also show briefly the optimization of pump powers in a multi-pump Raman amplifier using genetic algorithm method, in order to obtain minimum gain variation across the bandwidth. Moreover, for distributed Raman amplifiers, different bidirectional pumping schemes are proposed and compared to improve the noise figure tilt across wide bandwidth. A novel forward pumping scheme combining a 2nd and 1st order Raman pumps is reported to improve the noise performance in the low wavelength signals which are affected by more thermally generated noise due to being closer to the longer wavelength pumps and limits the transmission performance. Finally, the performance benefits of the proposed bidirectional pumping schemes are compared with other conventional pumping schemes, in a 70nm bandwidth distributed Raman amplifier using a long-haul coherent WDM transmission experiment.

Chapter 7 also describes the design of a dual stage broadband discrete Raman amplifier for high gain, high output power, low noise and low nonlinearity operations. Characterisation of discrete amplifiers in terms of net gain, noise figure and nonlinear phase shifts are described for different gain fibres i.e. highly nonlinear fibre (HNLF), dispersion compensating fibre (DCF), inverse dispersion fibre (IDF). Design criteria of multi-stage discrete Raman amplifiers with low noise and nonlinear penalty, which can be used in high capacity transmission systems are reported. Transmission experiment results are also shown for both single and dual stage configurations.

Finally, chapter 8 is the conclusion of the thesis providing overview of main contributions and potential future works.

1.2 Publication List

1.2.1 Publications included in this thesis

1. **M. A. Iqbal**, M. Tan, L. Krzczanowicz, A. El-Taher, W. Forysiak, P. Harper and J. D. Ania-Castañón, "Noise and transmission performance improvement of broadband distributed Raman amplifier using bidirectional Raman pumping with dual order co-pumps," Opt. Express 25(22), 27543-27550 (2017).

2. **M. A. Iqbal**, M. Tan and P. Harper, "On the mitigation of RIN transfer and transmission performance improvement in bidirectional distributed Raman amplifiers," J. Lightwave Technol. 36(13), 2611-2618 (2018).

3. **M. A. Iqbal**, M. Tan and P. Harper, "Enhanced transmission performance using backward-propagated broadband ASE pump," IEEE Photonics Technology Letters, 30(9), 865-868 (2018).

4. G. Rizzelli, **M. A. Iqbal**, F. Gallazzi, P. Rosa, M. Tan, J. D. Ania-Castañón, L. Krzczanowicz, P. Corredera, I. D. Phillips, W. Forysiak, and P. Harper, "Impact of input FBG reflectivity and forward pump power on RIN transfer in ultralong Raman laser amplifiers," Opt. Express 24(25), 29170-29175 (2016).

5. L. Krzczanowicz, **M. A. Iqbal**, I. D. Philips, M. Tan, P. Skvortcov, P. Harper, and W. Forysiak, "Low transmission penalty dual-stage broadband discrete Raman amplifier," Opt. Express 26(5), 7091-7097 (2018).

6. M. Tan, P. Rosa, S. T. Le, **Md. A. Iqbal**, I. D. Phillips, and P. Harper, "Transmission performance improvement using random DFB laser based Raman amplification and bidirectional second-order pumping," Opt. Express 24(3), 2215-2221 (2016).

7. **M. A. Iqbal**, M. Tan, and P. Harper, "Transmission performance improvement using broadband incoherent counter-pumped distributed Raman amplification," in Proc. OFC 2018, paper Th1C.2.

8. **M. A. Iqbal**, M. Tan, and P. Harper, "Evaluation of RIN mitigated dual order bidirectional distributed Raman amplification using a broadband first order forward pump," in Proc. ECOC 2017, paper P1.SC1.13.

9. **M. A. Iqbal**, M. Tan, and P. Harper, "Enhanced long-haul transmission using forward propagated broadband first order Raman pump," in Proc. ECOC 2017, paper P2.SC6.25.

10. **M. A. Iqbal**, M. Tan and P. Harper, "RIN reduction technique for dual order forward pumped distributed Raman amplification," in Proc. CLEO/Europe-EQEC 2017, paper CI-2.2.

11. **M. A. Iqbal**, M. Tan, L. Krzczanowicz, P. Skvortcov, A. El-Taher, I. D. Philips, W. Forysiak, J. D. Ania-Castañón, and P. Harper, "Performance characterisation of high gain, high output power and low noise cascaded broadband discrete Raman amplifiers", in Proc. ICTON 2017, paper We.D5.4. (**Best student paper award**).

12. **M. A. Iqbal**, M. Tan, A. El-Taher and P. Harper, "RIN and transmission performance improvement using second order and broadband first order forward Raman pumping," in Proc. OECC and PGC 2017, paper. P2-050.

13. **M. A. Iqbal**, G. R. Martella, F. Gallazzi, Mingming Tan, P. Harper and J. D. Ania-Castañón, "Performance improvement of broadband distributed Raman amplifier using bidirectional pumping with first and dual order forward pumps," in Proc. ICTON 2016, paper Tu.P.30.

14. **M. A. Iqbal**, M. Tan, L. Krzczanowicz, G. Rizzelli Martella, F. Gallazzi, A. El-Taher, W. Forysiak, P. Harper, and J. D. Ania-Castanon, "Noise performance improvement of broadband distributed Raman amplifier using dual order bidirectional pumping," in Proc. ACP 2016, OSA Technical Digest (online), paper AF4G.2.

15. L. Krzczanowicz, **M. A. Iqbal**, I. Phillips, M. Tan, P. Skvortcov, P. Harper, and W. Forysiak, "Low penalty, dual stage, broadband discrete Raman amplifier for high capacity WDM/metro networks," in Proc. OFC 2018, paper W3D.3.

16. M. Tan, **M. A. Iqbal**, S. K. Turitsyn and P. Harper, "Mitigating RIN-penalty to enhance the transmission performance in distributed Raman amplification system," in Proc. OECC and PGC, Jul. 2017, paper oral 3-2T-3 (invited).

17. M. Tan, P. Rosa, **M. A. Iqbal**, S. T. Le, I. D. Philips, S. K. Turitsyn and P. Harper., "Raman fibre laser based amplification in long-haul/unrepeatered coherent transmission systems," in 19th International Conference on Transparent Optical Networks (ICTON), Jul. 2017, paper We.C5.5 (invited).

18. G. Rizzelli, **M. A. Iqbal**, P. Rosa, M. Tan, L. Krzczanowicz, I. Phillips, W. Forysiak, J. D. Ania-Castañón, and P. Harper, "Impact of front-FBG reflectivity in Raman fiber laser based amplification," in Proc. CLEO 2016, paper SF1F.6.

19. G. Rizzellli, **M. A. Iqbal**, F. Gallazzi, P. Rosa, M. Tan, P. Corredera, J. D. Ania-Castañón and P. Harper, "FBG reflectivity impact on RIN in ultralong laser amplifiers," in Proc. ECOC 2016, paper CLEO 5.3.

20. M. Tan, V. Dvoyrin, **M. A. Iqbal**, S. K. Turitsyn, and P. Harper, "Evaluation of long-haul coherent transmission performance using low RIN forward Raman pump," in Proc. ACP 2016, OSA Technical Digest (online), paper AF3D.2.

1.2.2 Publications not included in this thesis

1. M. A. Z. Al-Khateeb, **M. A. Iqbal**, M. Tan, A. A. I. Ali, M. McCarthy, P. Harper, and A. D. Ellis, "Analysis of the nonlinear Kerr effects in optical transmission systems that deploy optical phase conjugation", Opt. Express 26(3), 3145-3160 (2018).

2. A. D. Ellis, M. Tan, **M. A. Iqbal**, M. A. Z. Al-Khateeb, V. Gordienko, G. S. Mondaca, S. Fabbri, M. F. C. Stephens, M. E. McCarthy, A. Perentos, I. D. Phillips, D. Lavery, G. Liga, R. Maher, P. Harper, N. Doran, S. K. Turitsyn, S. Sygletos, and P. Bayvel, "4 Tb/s Transmission reach enhancement using 10×400 Gb/s super-channels and polarisation insensitive dual band optical phase conjugation," J. Lightwave Technol. 34, 1717-1723 (2016).

3. F. Gallazzi, G. Rizzelli, **M. A. Iqbal**, M. Tan, P. Harper and J. D. Ania-Castanon, "Performance optimization in Ultra-long Raman laser amplified 10x30 GBaud DP-QPSK transmission: balancing RIN and ASE noise," Opt. M. Tan, P. Rosa, S. T. Le, V. Dvoyrin, **M. A. Iqbal**, S. Srikanth, S. K. Turitsyn and P. Harper, "RIN mitigation and transmission performance enhancement with forward broadband pump," IEEE Photonic Technology Letters 30(3), 254-257 (2018).

4. M. Tan, P. Rosa, S. T. Le, V. Dvoyrin, **M. A. Iqbal**, S. Srikanth, S. K. Turitsyn and P. Harper, "RIN mitigation and transmission performance enhancement with forward broadband pump," IEEE Photonic Technology Letters 30(3), 254-257 (2018).

5. G. Saavedra, M. Tan, D. J. Elson, L. Galdino, D. Semrau, **M. A Iqbal**, I. D. Phillips, P. Harper, A. D. Ellis, B. C. Thomsen, D. Lavery, R. I. Killey, and P. Bayvel, "Experimental Analysis of nonlinear impairments in fibre optic transmission systems up to 7.3 THz," J. Lightwave Technol. 35(21), 4809 - 4816 (2017). Express 25(18), 21454-21459 (2017).

6. A. El-Taher, M. Tan, **M. A. Iqbal**. L. Krzczanowicz, I. D. Philips, W. Forysiak and P. Harper, "High gain, flattened, discrete Raman fiber amplifier and its transmission performance," in Proc. CLEO/Europe-EQEC 2017, paper CJ-P.15.

7. L. Krzczanowicz, I. D. Philips, **M. A. Iqbal**, M. Tan, P. Harper and W. Forysiak, "Hybrid discrete Raman/EDFA design for broadband optical amplification in metro WDM systems," in Proc. ICTON 2017, paper We.D5.5.

8. F. Gallazzi, G. Rizzelli, **M. A. Iqbal**, M. Tan, P. Harper and J. D. Ania- Castañón, "Optimal balance of RIN and ASE impairments in ultra-long Raman laser amplified 10x30 GBaud DP-QPSK transmission", in Proc. CLEO/Europe-EQEC 2017, paper CI-2.1.

9. F. Gallazzi, G. Rizzelli, **M. A. Iqbal**, M. Tan, P. Harper and J. D. Ania- Castañón., "Balancing RIN and ASE noise in ultra-long Raman laser amplified 10x30 GBaud DP-QPSK transmission," in Proc. OPOTEL 2017.

10. M. A. Z. Al-Khateeb, M. Tan, **M. A. Iqbal**, M. McCarthy, P. Harper and A. D. Ellis, "Four wave mixing in distributed Raman amplified optical transmission systems," in Proc. IEEE Photonics Conference (IPC) 2016, pp. 795-796.

11. M. Tan, P. Rosa, **M. A. Iqbal**, I. Phillips, J. Nuño, J. D. Ania-Castanon, and P. harper, "RIN Mitigation in second-order pumped Raman fibre laser based amplification," in Proc. ACP 2015, OSA Technical Digest (online), paper AM2E.6.

12. G. Saavedra, D. Semrau, M. Tan, **M. A. Iqbal**, D. J. Elson, L. Galdino, P. Harper, R. I. Killey, and P. Bayvel, "Inter-channel stimulated Raman scattering and its impact in wideband transmission systems," in Proc. OFC 2018, paper Th1C.3.

13. G. Saavedra, M. Tan, D. J. Elson, L. Galdino, D. Semrau, **Md. A. Iqbal**, I.D. Phillips, P. Harper, N. Mac Suibhne, A. D. Ellis, D. Lavery, B. C. Thomsen, R. I. Killey, and P. Bayvel "Experimental investigation of nonlinear signal distortions in ultra-wideband transmission systems" in Proc. OFC 2017, pp. 1-3.

14. L. Galdino, G. Saavedra, D. Semrau, D. J. Elson, D. Lavery, M. Tan, **M. A. Iqbal**, P. Harper, R. Killey and P. Bayvel, "Digital Back-Propagation Performance in Wideband Optical Fibre Transmission Systems" in Proc. ECOC 2017, pp. 1-3.

15. A. D. Ellis, I. D. Philips, M. Tan, M. F. C. Stephens, M. E. McCarthy, M. A. Z. Al-Kahteeb, **M. A. Iqbal**, A. Perentos, S. Fabbri, V. Gordienko, D. Lavery, G. Liga, M. G. Saavedra, R. Maher, S. Sygletos, P. Harper, N. J. Doran, P. Bayvel and S. K. Turitsyn, "Enhanced superchannel transmission using phase conjugation," in Proc. ECOC 2015, pp. 1-3.

CHAPTER 2

COHERENT FIBRE OPTIC COMMUNICATION SYSTEMS

A coherent fibre optic communication system is typically consisted of a transmitter with higher order amplitude/phase modulation, an information carrying channel based on optical fibre and a coherent receiver, which recovers the amplitude and phase information of the received optical carrier by demodulating it using a local oscillator (LO). Coherent detection receiver is expected to consist of high-speed analog-to digital converters (ADCs) and advanced digital signal processing (DSP).

In this chapter, we briefly discuss the main optical subsystems of a long-haul coherent WDM transmission systems.

2.1 Transmitter

In the transmitter, incoming information bit stream can be encoded both on the amplitude and phase of each polarisation state of the optical carrier wave according to a given modulation format. If we consider the electric filed of a laser signal with amplitude A_S, phase φ_S and angular frequency ω is expressed as:

$$E_S(t) = A_S \sin(\omega t + \varphi_S)$$

(2.1)

The information is modulated in the amplitude and phase in case of amplitude modulation (AM) or amplitude shift keying (ASK) for digital modulation and phase modulation (PM) or phase shift keying (PSK) respectively. Both amplitude and phase are encoded in order to increase the transmitted information rate and also known as quadrature amplitude modulation (QAM). Eq. (2.1) can be further expressed as:

$$E_S(t) = A_S \sin(\omega t)\cos(\varphi_S) + A_S \cos(\omega t)\sin(\varphi_S) = a_S \sin(\omega t) + b_S \cos(\omega t)$$

(2.2)

where, $a_S = A_S \cos(\varphi_S)$ and $b_S = A_S \sin(\varphi_S)$. Eq. (2.2) is a sum of two AM signals modulated on a carrier with same frequency but in quadrature phase. The modulated signal is represented in a constellation, which is the representation of amplitude and phase encoded information bits, known as *symbol* in a complex plane.

2.1.1 Mach-Zehnder modulator (MZM)

Mach-Zehnder modulator (MZM) is usually used to modulate the information data stream onto the optical carrier. MZMs are based on interference principle of light and usually realized in LiNbO$_3$ by exploiting the electro-optic effect.
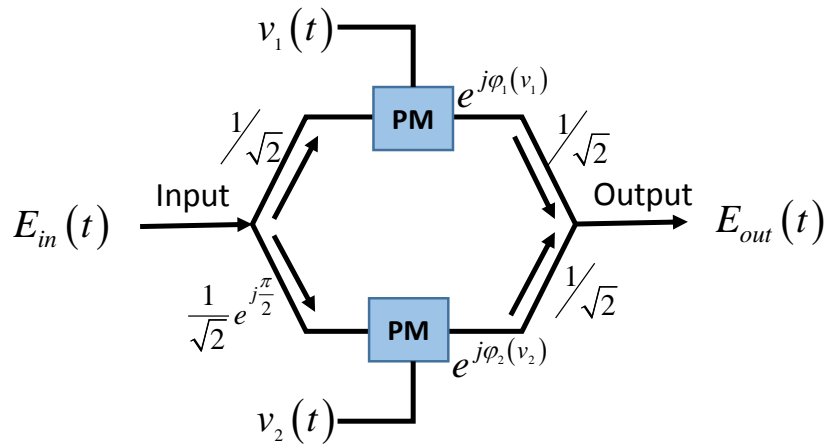
Figure 2. 1. A simple operational diagram of a MZM (PM = phase modulator)

Figure 2. 1 shows a simple diagram of MZM, in which the input optical field is divided into two separate paths using an input 3dB coupler, before going through a phase modulator placed in both or one of the paths. A $\dfrac{\pi}{2}$ phase shift is applied by the 3dB coupler between the two fields. $v_1(t)$ and $v_2(t)$ are the voltages applied in the phase modulator of upper and lower path respectively to change the phase in each path [3]. In dual drive MZMs, the phase modulators in both arms are usually operated independently compared with the single-drive MZMs. Then at the output of MZM, the two fields interfere with each other constructively or destructively depending on the modulated phases. So the output power depends on the relative phases between the fields which determines the maximum and minimum transmission when the phase difference is 0 and π respectively. The output optical field can be defined as:

$$E_{out}(t) = H(v_1, v_2) E_{in}(t) \tag{2.3}$$

$$H\left(v_1, v_2\right) = \frac{1}{2}\left\{e^{j\varphi_1(v_1)} + e^{j\varphi_2(v_2)}\right\} = e^{j[\varphi_1(v_1)+\varphi_2(v_2)]/2}\cos\left\{\frac{\varphi_1(v_1)-\varphi_2(v_2)}{2}\right\} \tag{2.4}$$

$H\left(v_1, v_2\right)$ represents the ideal transfer function which is essentially determined by the phase difference of the optical fields of two respective paths. The voltage-modulated optical phases of the upper and lower arms of the MZM are given by φ_1 and φ_2, which are linear functions of the drive voltages in the phase modulators. The voltages required to have π phase shift in the upper and lower arms are specified as V_{π_1} and V_{π_2} respectively. The phase of the respective optical field with applied drive voltage can be defined as:

$$\varphi_1\left(v_1\right) = \frac{\pi}{V_{\pi_1}}v_1, \qquad \varphi_2\left(v_2\right) = \frac{\pi}{V_{\pi_2}}v_2 \tag{2.5}$$

The linear change in phase with respect to applied voltage is shown in Eq. (2.5). Now the transfer function can be simplified as following considering, $V_{\pi_1} = V_{\pi_2} = V_\pi$:

$$H\left(v_1, v_2\right) = \exp\left(j\frac{\pi(v_1+v_2)}{2V_\pi}\right)\cos\left[\frac{\pi\left(v_1-v_2\right)}{2V_\pi}\right] \tag{2.6}$$

At identical phase shift condition, a pure phase modulation is achieved with the consideration that:

$$\varphi(t) = \varphi_1(t) = \varphi_2(t) \qquad \text{and} \qquad v(t) = v_1(t) = v_2(t) \tag{2.7}$$

$$H\left(v_1, v_2\right) = \exp\left(j\frac{v\pi}{V_\pi}\right) \tag{2.8}$$

The transfer function now represents a simple phase modulator operating in a push-push mode [26]. If the voltage applied in each arm is such that $v_1 = -v_2 = v/2$, the phase term of the optical field transfer function in Eqn. (2.6) vanishes and a chirp-free condition with pure amplitude modulation is achieved and the transfer function can be expressed as:

$$H\left(v_1, v_2\right) = \cos\left(\frac{v\pi}{2V_\pi}\right) \tag{2.9}$$

The phase term omission allows for the chirp free condition in a push-pull operation when equal but opposite voltages are applied in the arms with alternative phase shifts. The power transfer

function can be obtained by squaring the optical field transfer function and Eq. (2.9) can be written as:

$$H_P\left(v_1, v_2\right) = \frac{1}{2} + \frac{1}{2}\cos\left(\frac{v\pi}{V_\pi}\right) \tag{2.10}$$

H_P represents the power transfer function in push-pull operation. The modulation in intensity can be achieved by operating the MZM at the quadrature point, with a DC bias voltage of $-\dfrac{V_\pi}{2}$ and modulation with an input voltage swing of V_π peak to peak as shown in Figure 2. 2(a). Moreover, when the MZM is operated at the minimum transmission point with DC bias point at $-V_\pi$ and a peak to peak input voltage swing of $2V_\pi$, a phase shift of π is occurred at the crossing point of minimum transmission as shown in Figure 2. 2(b) [26].
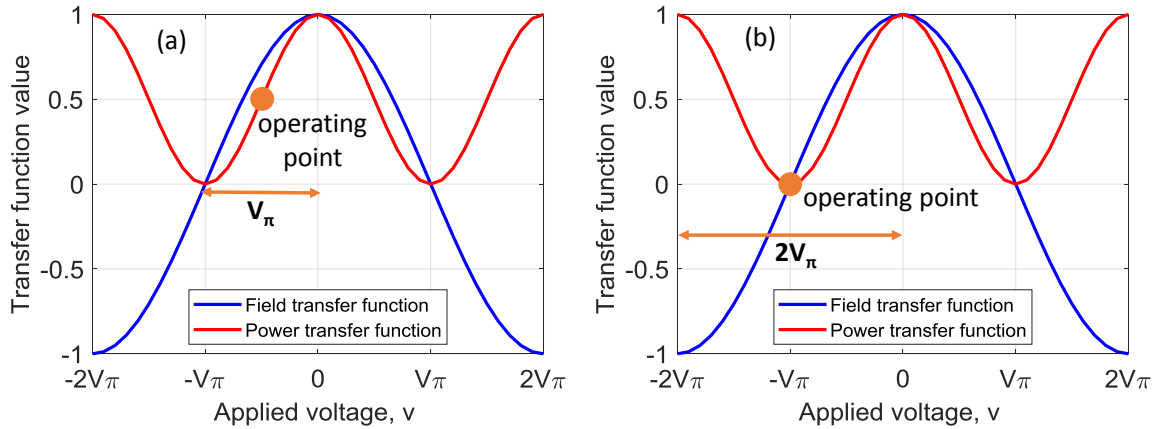
Figure 2. 2. Operation of an ideal MZM in the (a) quadrature point and (b) minimum transmission point

Figure 2. 2(a) and (b) show the plots of the optical field and power transfer functions with two different operation of an ideal MZM: pure amplitude modulation such as in on-off keying operation and at the minimum transmission point with a phase alteration of π such as in binary phase-shift keying operation respectively. Similarly MZMs can be used for phase and intensity modulation in IQ modulator.

2.1.2 Optical IQ modulator

Optical IQ modulation can be realized with Mach-Zehnder type push pull modulators in parallel combination, using a $\dfrac{\pi}{2}$ phase shift between them [27]. A simple schematic of optical IQ modulator is given below in Figure 2. 3.

In Figure 2. 3, an ideal optical IQ modulator is shown, in which two nested MZMs in push-pull operation ($v_1 = v_2$) with additional $\frac{\pi}{2}$ phase difference are used in parallel. The incoming signal is equally split into in-phase (*I*) and quadrature-phase (*Q*) components in the upper and lower arm respectively. In each of the arms, intensity modulation is applied through MZM in push-pull mode at minimum transmission point as described before. The absolute voltages applied in the in-phase and quadrature phase MZMs are $v_I(t)$ and $v_Q(t)$ respectively. The fixed 90 degree phase shift is applied using a phase modulator placed in one of the arms (lower arm in this case), with $-\frac{V_\pi}{2}$ applied voltage. At the output the lights from both the branches are combined to get the output optical field resulting in constellation points to be in the complex IQ plane.
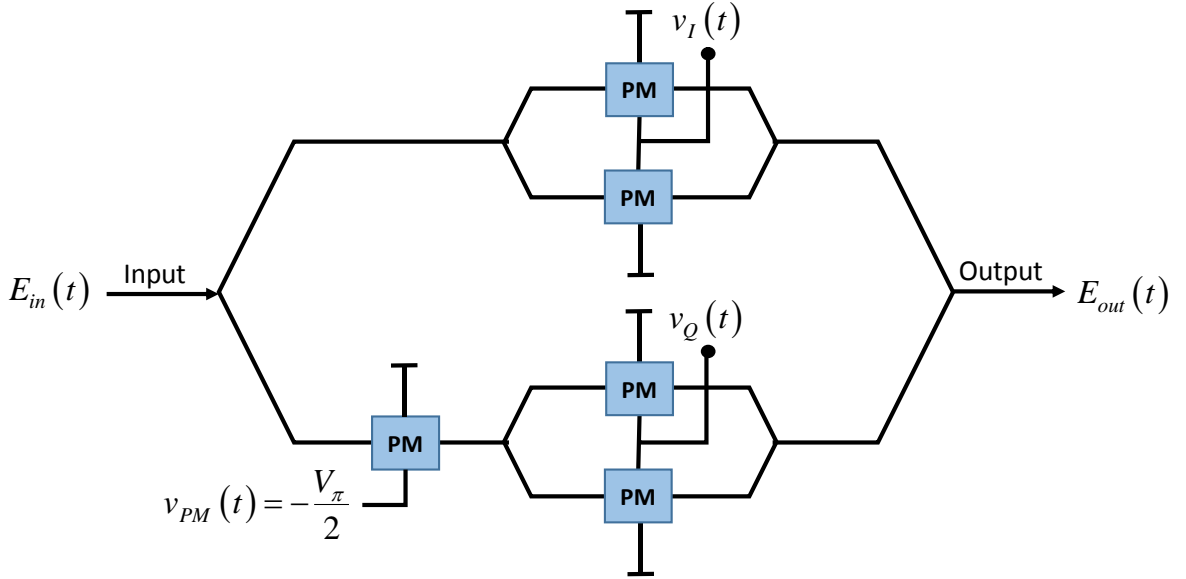
Figure 2. 3. Optical IQ modulator based on nested MZMs in parallel and a phase modulator between them

The field transfer function of the IQ modulator can be expressed as:

$$H(v_I, v_Q) = \frac{1}{2}\cos\left(\frac{\Delta\varphi_I(t)}{2}\right) + j.\frac{1}{2}\cos\left(\frac{\Delta\varphi_Q(t)}{2}\right) = \frac{1}{2}\cos\left(\frac{v_I\pi}{2V_\pi}\right) + j.\frac{1}{2}\cos\left(\frac{v_Q\pi}{2V_\pi}\right) \qquad (2.11)$$

$$\text{where,} \qquad \Delta\varphi_I(t) = \frac{v_I\pi}{2V_\pi} \qquad \text{and} \qquad \Delta\varphi_Q(t) = \frac{v_Q\pi}{2V_\pi}$$

$\Delta\varphi_I(t)$ and $\Delta\varphi_Q(t)$ represent the phase difference in the in-phase and quadrature-phase MZM respectively. The imaginary term j defines the complex plane due to $\dfrac{\pi}{2}$ phase shift in the lower arm. The amplitude (a_{IQ}) and phase (φ_{IQ}) modulated terms in IQ modulation can also be described from Eq. (2.11) as:

$$\begin{cases} a_{IQ} = \dfrac{1}{2}\sqrt{\cos^2\left(\dfrac{v_I \pi}{2V_\pi}\right) + \cos^2\left(\dfrac{v_Q \pi}{2V_\pi}\right)} \\[3mm] \varphi_{IQ} = \arg\left[\cos\left(\dfrac{v_I \pi}{2V_\pi}\right), \cos\left(\dfrac{v_Q \pi}{2V_\pi}\right)\right] \end{cases} \tag{2.12}$$

In Eq. (2.12), arg[I,Q] defines the angle of a complex value from the real and imaginary parts in the range between $-\pi$ and π. The basic IQ operation in a complex plane is shown in Figure 2. 4(a).
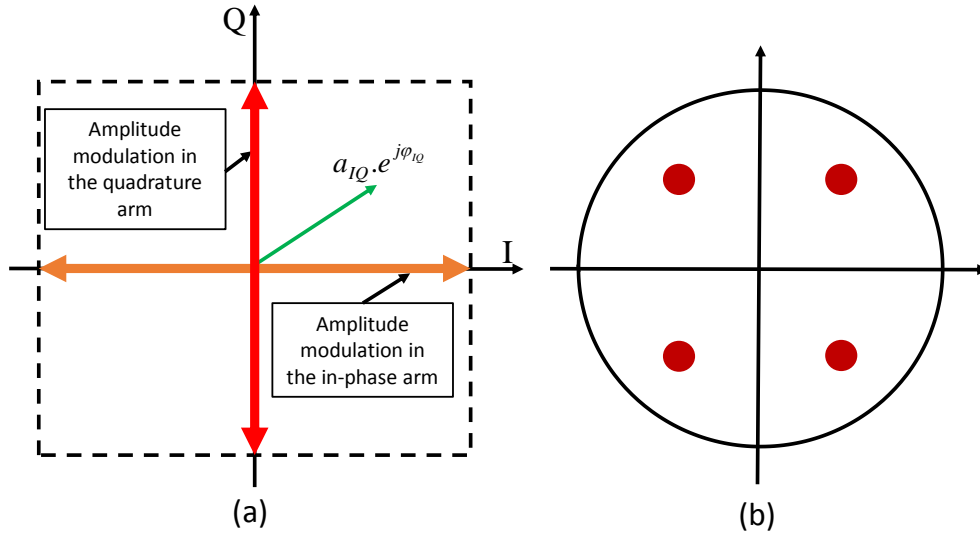
Figure 2. 4. (a) Basic operational principle of IQ modulator and (b) QPSK constellation diagram

Quadrature phase shift keying (QPSK) modulation uses the similar basic IQ modulator and four possible constellation points are achieved in the complex IQ plane. In a similar operational principle shown in Figure 2. 4(a), four possible phase shifts ($\dfrac{\pi}{4}, \dfrac{3\pi}{4}, \dfrac{5\pi}{4}, \dfrac{7\pi}{4}$) can be obtained at the output of the modulator given by $\left(\dfrac{\pm 1 \pm j}{\sqrt{2}}\right)$. The constellation points of QPSK modulation format are shown in Figure 2. 4(b). In QPSK, two bits of information are encoded in one symbol and four constellation points are used in the complex plane. More different types of modulation formats can

be obtained using the same super Mach-Zehnder architecture applying more complex drive voltages at the MZMs, which allows to encode more number bits per symbol.

Another way of increasing the spectral efficiency of a given modulation technique is using polarisation multiplexed carriers. A dual polarisation symbol is the combination of amplitude/phase states and the polarisation states. To generate DP-QPSK modulated signal, a pair of IQ modulators is needed to create X-polarised and Y-polarised QPSK signals, which are then combined at the output to get dual polarised quadrature phase shift keying (DP-QPSK) modulated signal. A polarisation rotator is usually used at the output of one of the IQ modulators to generate Y-polarised QPSK signal. Finally X and Y polarised QPSK modulated signals are combined through a polarisation beam combiner to maintain the orthogonal polarisation at the same signal wavelength [28].

2.2 Coherent Receiver

The coherent receiver is the basic building block of coherent fibre optic communication system and it consists of a coherent detection front-end, analog to digital converter (ADC) and digital signal processing (DSP) block.
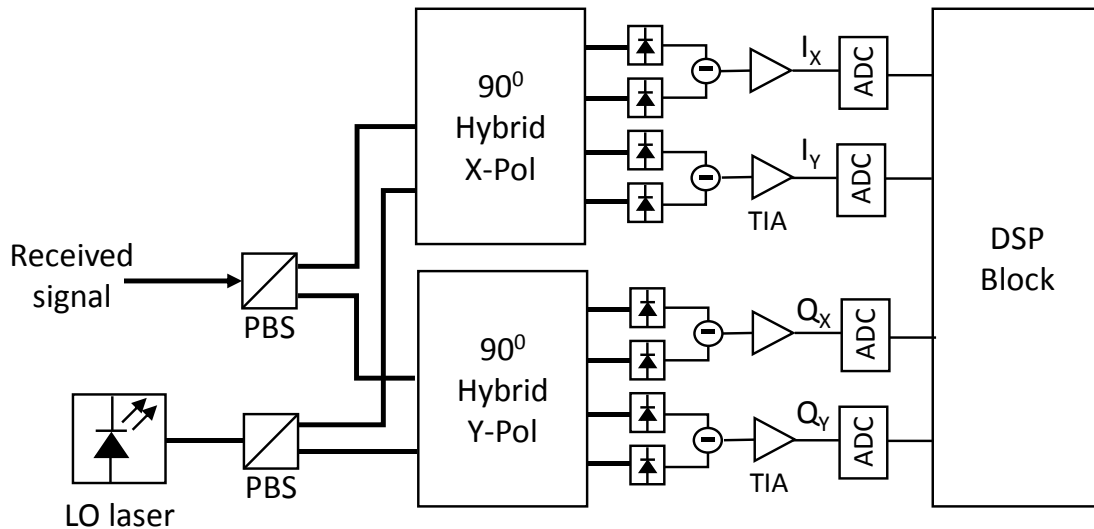
Figure 2. 5. Schematic diagram of a polarisation diverse coherent optical receiver. LO = local oscillator, PBS = polarisation beam splitter, ADC = analog to digital converter, TIA = trans-impedance amplifier

A polarisation diverse digital coherent receiver is shown in Figure 2. 5. A linearly polarised local oscillator laser with narrow linewidth is used to demodulate the received signal. Both the received signal and LO are split into two orthogonal polarisations (X and Y) using two separate polarisation

beam splitters (PBSs) before passing into the 90^0 hybrids which are used to mix signal and LO in order to coherently detect the in-phase (I) and quadrature-phase (Q) component for each polarisation (X and Y). The configuration of an optical hybrid is given below in Figure 2. 6.
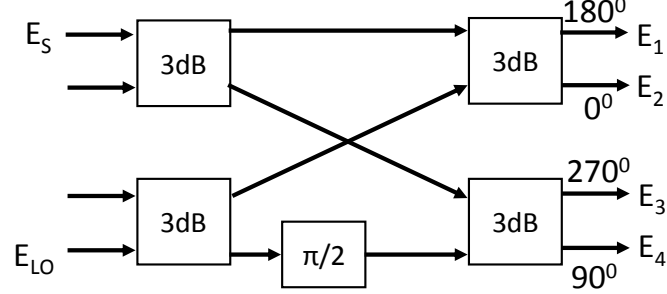
Figure 2. 6. Basic block diagram of a 90^0 hybrid

In Figure 2. 6, a basic diagram of a 90^0 optical hybrid which includes two 3dB (50/50) couplers at the input and two similar beam combiners at the output and also a 90^0 phase shifter. One of the outputs of from LO power splitter undergoes a 90^0 phase shift through a phase shifter. Then the quadrature outputs of the LO are combined with the signal using another pair of 3dB couplers at the output, resulting in four combined (E_1, E_2, E_3 and E_4) optical fields expressed as:

$$E_1 \approx \frac{E_S - E_{LO}}{2}, E_2 \approx \frac{E_S + E_{LO}}{2}, E_3 \approx \frac{E_S - jE_{LO}}{2}, E_4 \approx \frac{E_S + jE_{LO}}{2} \tag{2.13}$$

The outputs from the optical hybrid are then passed into balanced detectors as shown in Figure 2. 5. Two square law photodetectors are used in each balanced detector which cancels out the common dc component. Each optical hybrid provides currents proportional to the in-phase and quadrature-phase components into the receiver. Complete mathematical model can be found in [29]. The output currents from the balanced detectors are amplified using trans-impedance amplifiers (TIAs) before passing into the ADCs.

The ADC converts the analog electrical signal to digital signal through sampling and quantization. In the ADC, a sampler converts a continuous analog signal into a time-discrete analog signal. The sampling rate must be at least twice the bandwidth of the baseband signal to avoid aliasing. The bit resolution of the ADC determines the finite number of discretized levels. Quantization noise is also added in the sampled signal due to the limited bit resolution of the ADCs. Another associated problem of ADC is clipping of large signal due to limited full scale voltage range (FSR). An automatic gain control (AGC) method can be used to avoid the problem of signal clipping and excessive quantization.

Finally, DSP is applied in the signal to get rid of the linear impairments and retrieve the original signal. Basic DSP block includes signal equalization, clock recovery, correction of hybrid imperfections, carrier phase recovery, and chromatic dispersion compensation and so on. Details of each functionality are discussed in [29, 30].

2.3 Recirculating Fibre Loop

In long-haul repeatered transmission systems, a chain of optical amplifiers are used with usually 80~100km span lengths. The long haul transmission system can be emulated using a recirculating fibre loop with few number of amplifier spans in a very useful and flexible way. In a recirculating fibre loop, an input light is sent over a fixed short distance multiple times to study the long-haul fibre optic transmission systems. Recirculating loop helps to investigate different transmission impairments (i.e. noise, nonlinearity, polarisation mode dispersion (PMD) etc.) on the signal quality [31]. The other major advantage of using recirculating loop is the cost efficiency compared with a full systems. A simple design of a recirculating loop may even consist of a single optical amplifier and associated fibre length.
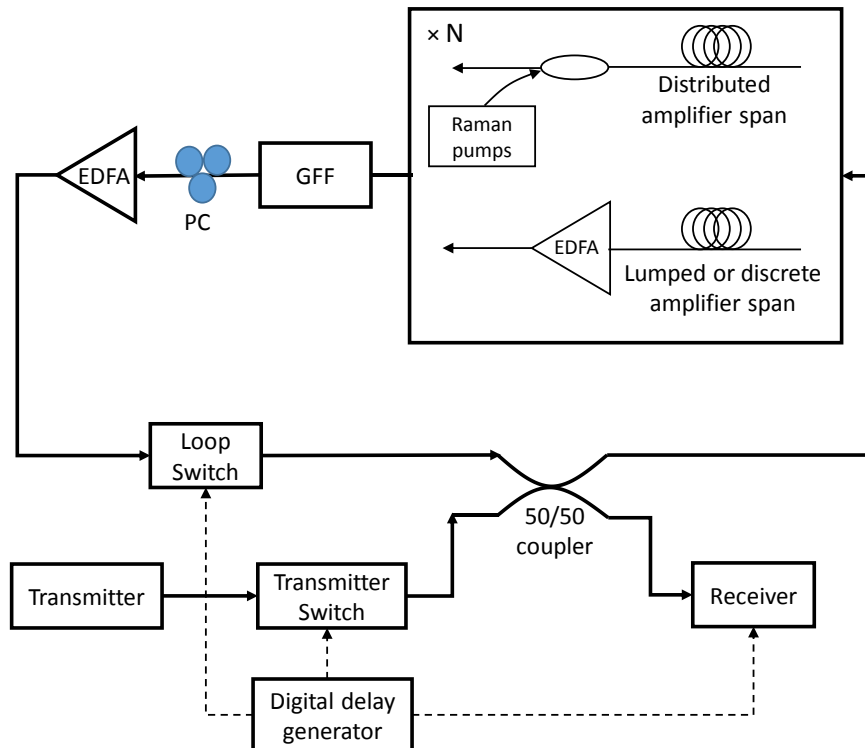
Figure 2. 7. A simple recirculating loop setup (GFF = gain flattening filter, PC = polarisation controller)

The schematic diagram of a typical single span recirculating loop is shown in Figure 2. 7. Signal from the transmitter is fed into the loop using a transmitter switch which works with the gated signal from a digital pulse generator know as digital delay generator (DDG). The transmitter switch allows signal burst to pass into the loop and controls the loop fill time. The length of the signal burst should be such that it exactly matches with the fill time, otherwise unfilled section may result in more ASE noise generation. On the other hand in case of overfilling the loop, the incoming signal from the transmitter will interfere with the signal passing through the loop and cause signal performance degradation [32]. Moreover, a fast response time switch is required to avoid feeding the input light into the loop during transition from on to off position. In addition to that, the switch should have low insertion loss and low polarisation dependence. An acousto-optic modulator (AOM) can be used as the switch which has high extinction ration (60-70dB) to avoid light to pass into the loop when switch is at off position and high polarisation diversity [33].

After passing through the input switch at the input, the signal is then coupled into the loop using a 3dB or 50/50 coupler. The other half of the signal is passed into the receiver simultaneously. A coherent detection technique is usually used in long-haul coherent WDM transmission system. The receiver oscilloscope is also triggered from the same DDG to capture the data after desired number of recirculation.

Along the recirculating loop path, specified number of fibre span with associated amplification scheme such as distributed Raman amplification [21], or discrete (or lumped) amplification (i.e. EDFA) [34] are used. Signals are amplified along the transmission span in case of distributed amplification whereas in case of discrete or lumped amplification, amplifiers are placed in discrete positions along the total transmission link to amplify the signals. The amplifier span can be single to any integer multiple (N). At the amplifier input the signal power is usually low due to the losses from the input switch and 50/50 coupler. The low input signal power is insignificant to cause any pump depletion especially in case of Raman amplified systems such as distributed Raman amplification. A very good design of amplifier is required in terms of noise figure, gain flatness etc., otherwise these will be magnified in each recirculation and cause huge penalty in long-haul transmission performance measurement.

A gain flattening filter (GFF) is also required to equalize the gain variation across the signal bandwidth after each recirculation. Unlike in-line transmission system, a recirculating loop has additional passive losses from additional coupler, GFF, AOM and so on. An additional EDFA is usually used at the end of the loop to compensate the loop losses and keep the input signal power

into the span same in each recirculation. To monitor the input and output optical powers, 1% tap coupler can be used at the loop output. The received light from the loop is detected by a slow-speed photo-detector to convert into electrical signal and then monitored using a low speed oscilloscope [20, 32, 35].

All the components in a recirculating loop are required to have minimal polarisation sensitivity to avoid any kind of polarisation dependent gain, which may be accumulated over many round trip times and become significant in long distance transmission [36]. A polarisation controller (PC) can be used to control the power in polarisation states. A loop synchronous polarisation scrambler is another solution, but additional passive insertion loss may impact the noise performance of the loop [37]. The noise figure of respective amplifier has to be low to maintain very good ASE noise performance.

Once the required distance has been propagated by the signal, the recirculation must be stopped and signal must be disconnected from the loop. A second AOM is usually used as the loop switch which is gated synchronously with the transmitter AOM/switch to either pass or block the signal. But using AOM in the loop has disadvantages such as: increase of loop loss and signal undergoes a small frequency shift (typically ~80MHz) every time it passes the device [33]. More details regarding the timing setup in the delay generator for controlling the transmitter and loop switches and trigger the measurement cycle in the receiver are given in [20, 32].

2.4   Transmission Impairments

As signal propagates along the fibre optic transmission line, it undergoes different linear and nonlinear impairments. Linear impairments such as chromatic dispersion, polarisation mode dispersion dominate over nonlinearity induced penalties when the propagating signal power is low. In contrast with high signal power, potential Kerr induced nonlinear penalties degrade the system performance [38]. The generalized signal propagation along the single mode fibre can be expressed as [39]:

$$\frac{\partial A}{\partial z} = -\frac{\alpha}{2} A - \frac{j}{2} \beta_2 \frac{\partial^2 A}{\partial T^2} + j\gamma |A|^2 A \qquad (2.14)$$

Eq. (2.14) is also known as the nonlinear Schrödinger equation (NLSE), where A represents the slowly varying amplitude of the pulse envelope propagating along the fibre and T is the time measured in a frame of reference moving with the pulse with group velocity $v_g \left(T = t - \frac{z}{v_g} \right)$. z and

42

α are the distance along the fibre and fibre attenuation coefficient respectively. The group velocity dispersion (GVD) and Kerr nonlinearity coefficient are given by β_2 and γ respectively. The three terms on the right hand side of Eq. (2.14) defines the fibre losses, dispersion and nonlinearities on pulse propagation respectively.

2.4.1 Attenuation in optical fibre

Fibre loss is one of the important system design parameters which determines the maximum transmission reach of propagating signal before getting undistinguishable from the noise level. Low loss fibres are desirable to use for reducing the signal attenuation during propagation. The propagation of a signal with average power P_S, along distance z can be described as following:

$$\frac{dP_S}{dz} = -\alpha_S P_S$$

(2.15)

where, α_S is the fibre attenuation coefficient. The signal power at a distance $z=L$ can be defined by solving the partial differential Eq. (2.15) as:

$$P_S(L) = P_0 e^{-\alpha_S L}$$

(2.16)

where, P_0 is the input signal power. The attenuation coefficient is usually expressed in dB/km as:

$$\alpha_S(dB/km) = -\frac{10}{L} \log_{10}\left(\frac{P_S(L)}{P_0}\right)$$

(2.17)

The most significant fibre loss mechanism consists of intrinsic (infrared absorption, ultraviolet absorption and Rayleigh scattering) and extrinsic (fibre impurities: OH ions and metallic impurities of fibre curvature) loss factors [3]. The presence of OH ions causes the extrinsic loss in silica fibre. The residual water vapor in the silica fibres contributes to vibrational absorptions near 0.95μm, 1.24μm and 1.39μm and results in high loss. In modern silica core fibre, the OH absorption peak near 1.39μm is reduced to almost zero such as in dry fibre, zero water peak fibre.

Infrared and ultraviolet absorptions represent the intrinsic material absorption and correspond to electronic and vibrational resonances associated with specific molecules respectively. The material absorption contributes to 0.03 dB/km attenuation loss in silica based fibre in the wavelength range from 1.3 to 1.6μm [3].

The fundamental loss mechanism due to Rayleigh scattering is occurred because of the microscopic density fluctuations which cause random variations of refractive index along the fibre in a scale

smaller than the incident optical wavelength λ. The scattering loss in silica fibre from Rayleigh scattering can be written as [40]:

$$\alpha_R = \frac{C_R}{\lambda^4} \tag{2.18}$$

where, C_R is the Rayleigh scattering coefficient varying from 0.7~0.9 (dB/km)-μm^4. In silica fibre, α_R corresponds to the Rayleigh scattering loss of 0.12~0.16 dB/km around 1.55μm. In addition to that, loss due to waveguide imperfection including Mie scattering, macro and micro-bending losses also contribute to insignificant losses in silica fibre [3].

2.4.2 Fibre chromatic dispersion

Fibre chromatic dispersion is one of the most significant performance limiting factors on propagating signals along the optical fibres. When optical pulse propagates along a single mode fibre, different spectral components travel at different speeds due to the impact of chromatic dispersion. The frequency dependent group velocity causes temporal broadening of pulse, which is known as group velocity dispersion (GVD). GVD contributes to signal distortion through inter symbol interference (ISI) and limits the overall transmission reach of WDM system. The speed of different spectral components can be defined as $\frac{c}{n_g(\omega)}$, where ω is the frequency, c is the speed of light in and $n_g(\omega) = n + \frac{dn}{d\omega}$ is the frequency dependent group refractive index. If we consider a pulse with central frequency ω is received at the receiver after propagating along a transmission fibre with length L and the time delay $T = \frac{L}{v_g}$, then the group velocity v_g can be expressed as:

$$v_g = \left(\frac{d\beta}{d\omega} \right)^{-1} \tag{2.19}$$

where, β is frequency dependent propagation constant which can be expanded in a Taylor series [3]:

$$\beta(\omega) = \beta_0 + \beta_1(\omega - \omega_0) + \frac{1}{2}\beta_2(\omega - \omega_0)^2 + \frac{1}{6}\beta_3(\omega - \omega_0)^3 ... \tag{2.20}$$

$$\text{where } \beta_m = \left(\frac{d^m\beta}{d\omega^m} \right)_{\omega=\omega_0} \quad (m = 0,1,2,...) \tag{2.21}$$

44

β_1 corresponds to the inverse of group velocity as described in Eq. (2.19). β_2 and β_3 are known as second- and third- order dispersion parameters which dominates the pulse broadening in optical fibres. Now the spectral broadening of a pulse with pulse width $\Delta\omega$ can be expressed as:

$$\Delta T = \frac{dT}{d\omega}\Delta\omega = \frac{d}{d\omega}\left(\frac{L}{v_g}\right)\Delta\omega = L\frac{d^2\beta}{d\omega^2}\Delta\omega = L\beta_2\Delta\omega \qquad (2.22)$$

where Eqs. (2.19) and (2.21) are used and β_2 is the GVD parameter which mainly determines the broadening of optical pulse inside the fibre. The frequency spread ($\Delta\omega$) can also be described in terms of range of wavelengths as:

$$\Delta\omega = \left(-\frac{2\pi c}{\lambda^2}\right)\Delta\lambda \qquad (2.23)$$

Now the delay spread can be represented in terms of wavelength spread ($\Delta\lambda$):

$$\Delta T = \frac{d}{d\lambda}\left(\frac{L}{v_g}\right)\Delta\lambda = LD\Delta\lambda \qquad (2.24)$$

$$\text{where } D = \frac{d}{d\lambda}\left(\frac{1}{v_g}\right) = \left(-\frac{2\pi c}{\lambda^2}\right)\beta_2 \qquad (2.25)$$

where, D is the dispersion parameter which is defined in ps/(km-nm) unit. In any fibre D varies with wavelengths and becomes completely zero at a wavelength known as *zero-dispersion wavelength* (λ_{ZD}). Near zero-dispersion wavelength the linear change of dispersion with respect to wavelength is known as dispersion slope (*S*) at λ_{ZD} and related to dispersion as: $D = S(\lambda_{ZD} - \lambda)$. Higher order i.e. third order dispersion also increases pulse broadening but has very less impact compared with β_2. The third order dispersion parameter (β_3) is related to the dispersion slope (*S*) as [41]:

$$S = \left(\frac{2\pi c}{\lambda^2}\right)^2 \beta_3 \qquad (2.26)$$

The characteristics of different fibres vary with respect to λ_{ZD}, *D* and *S* parameters. The impact of dispersion induced penalty can be eliminated in the DSP block of the coherent receiver.

2.4.3 Polarisation mode dispersion

Polarisation mode dispersion (PMD) is another linear impairment in optical fibres, which is caused due to the random birefringence along the fibre because of the inhomoginities in the fibre design and imperfection in the cylindrical geometry. Due to PMD, orthogonal polarisations travel with slightly different phases and group velocities, resulting in PMD induced pulse broadening. The stretched pulse due to the time delay (ΔT) between the two polarisation components travelling in slightly different group velocities, overlaps with neighboring time slot and causes inter symbol interference (ISI). The time delay is given as [3, 40]:

$$\Delta T = \left| T_x - T_y \right| = \left| \frac{L}{v_{gx}} - \frac{L}{v_{gy}} \right| = L \left| \beta_{1x} - \beta_{1y} \right| = L\left(\Delta\beta_1\right) \tag{2.27}$$

where, x and y define the two orthogonal polarisation states. The group velocity mismatch between two orthogonal polarisation states is represented by $\Delta\beta_1$. The impact of PMD is relatively smaller than GVD, however PMD may cause serious degradation in high-bit rate data transmission over long-distance operating near zero-dispersion wavelength [41]. In digital coherent systems, the slowly varying PMD induced pulse broadening and state of polarisation can be corrected by implementing a digital multiple input multiple output (MIMO) adaptive filter [42].

2.4.4 Kerr induced nonlinearities in optical fibres

Fibre nonlinearity has the most significant impact on the transmission performance of high capacity coherent WDM systems. The nonlinearities can be described as two different types: intra-channel and inter-channel nonlinearities. The very basic type of nonlinearity is the self-phase modulation (SPM), which occurs when the signal intensity modulates the refractive index and in turn its own phase known as nonlinear phase shift (NPS). SPM induces spectral broadening of optical pulses during propagation through the fibre [39]. In a WDM transmission system, phase modulation can be occurred by the intensity of other adjacent channels with different frequencies, which is known as cross-phase modulation (XPM). XPM induces nonlinear coupling of adjacent overlapping pulses which causes inter-channel crosstalk in WDM systems. It also produces amplitude and timing jitter [43, 44]. In addition to that, four-wave mixing (FWM) can also occur if three frequency components (ω_1, ω_2 and ω_3) interact with each other within a phase matched condition to generate a fourth frequency component $\omega_4 = \omega_1 \pm \omega_2 \pm \omega_3$. In the FWM process, photon energy is transferred to a new frequency component. The crosstalk between the signals and the newly generated FWM products, and the depletion of signal energy leads to performance degradation of WDM systems.

Fibre nonlinearity induced penalty can be somehow compensated digitally by digital back propagation (DBP) technique using inverse NLSE [45, 46]. But it is still not an obvious solution for high bandwidth transmission systems and has very high computational complexity and also impractical for real-time system implementation. An optical way of compensating the fibre nonlinearities mainly due to signal-signal interactions is optical phase conjugation (OPC) [47, 48]. For example, in a mid-link OPC based transmission system, a phase conjugator is placed at the middle of the transmission link to invert the dispersion term (β_2) and nonlinearity coefficient term (γ) of the signal after half of transmission, so that both dispersion and nonlinearities can be cancelled out during propagation along the other half of the transmission line and a clean signal is received at the receiver [38]. But perfect symmetry in the signal power profiles before and after the mid-link OPC is required to get maximum efficiency of nonlinearity compensation. Even with perfect OPC based transmission system, residual nonlinearity due to signal-noise and noise-noise interactions may still degrade the system performances [48].

2.5   Performance Characterisation Parameters

Different figure of merits are used to describe the performance of digital coherent transmission systems. Here we present a brief overview of few of those parameters.

Bit error rate (BER) is calculated from the ratio of the detected bit errors to the total number of bits over a certain time interval. If additive white Gaussian noise (AWGN) is considered with zero mean and variance dependent on the signal amplitude, the Q-function can be given by the integral of the tail of a zero-mean unitary-variance Gaussian distribution beyond a given decision threshold (*x*) and expressed in terms of the complementary error function:

$$Q(x) = \frac{1}{2}\text{erfc}\left(\frac{x}{\sqrt{2}}\right) \tag{2.28}$$

Another performance criteria is the ratio of signal power to noise power and can be expressed in terms of electrical *signal-to-noise ratio* (SNR) and *optical signal-to-noise ratio* (OSNR). SNR is expressed in the electrical domain with noise and signal power are measured within the same bandwidth. Whereas, OSNR is measured considering the total signal power over a specified noise bandwidth (i.e. 0.1nm). SNR can also be expressed in terms of the ratio of energy per bit (in Joules) to noise power spectral density (in W/Hz) ($\frac{E_b}{N_0}$) as:

$$SNR = \frac{E_b}{N_0} \cdot \frac{f_b}{B} \tag{2.29}$$

where, f_b and B are the data rate in bits/s and signal bandwidth in Hz. The performance of different signals independent of their respective bandwidth can be defined by the E_b/N_0.

The Q-factor is also a performance measurement metric of binary signals which can be defined using SNR as:

$$Q = \frac{(\mu_1 - \mu_0)}{(\sigma_1 - \sigma_0)} = \sqrt{SNR} \tag{2.30}$$

where, $\mu_{1,0}$ and $\sigma_{1,0}$ are the mean value and standard deviation of marks and spaces respectively. For non-binary signals, an effective Q factor (Q_{eff}) can be related to the measured BER using the complementary function as[49]:

$$BER = \frac{1}{2}\text{erfc}\left(\frac{Q_{eff}}{\sqrt{2}}\right) \tag{2.31}$$

$$Q_{eff}(dB) = 20\log_{10}\left[\sqrt{2} \times \text{erfcinv}(2 \times BER)\right] \tag{2.32}$$

For binary system limited by AWGN and negligible ISI, Q_{eff} and Q factors are considered to be equal.

Error vector magnitude (EVM) is another performance metric which is defined as the root-mean-square (RMS) value of the difference between the measured symbols and ideal symbols [50]. EVM also describes the SNR performance of quadrature amplitude modulation (QAM) signals. EVM can be expressed by comparing the N symbols before and after the transmission as:

$$EVM = \sqrt{\frac{\frac{1}{N}\sum_{i=1}^{N}\left|S_i^r - S_i^t\right|^2}{\frac{1}{N}\sum_{i=1}^{N}\left|S_i^t\right|^2}} \approx \sqrt{\frac{1}{SNR}} \tag{2.33}$$

where, S_i^r and S_i^t are the ith received and transmitted symbol vectors. The relationship between EVM and BER in an AWGN channel can be expressed as below for large m-QAM (m>>2) constellations considering raised cosine pulses [50, 51]:

$$BER = \frac{4\left(1 - m^{-1/2}\right)}{\log_2(m)}Q\left(\sqrt{\frac{3}{(m-1)EVM^2}}\right) \tag{2.34}$$

48

CHAPTER 3

OPTICAL AMPLIFICATION TECHNIQUES

The intrinsic loss characteristic of optical fibre introduces attenuation to the signal during propagation along the transmission line. So amplification of the signal is required for repeatered transmission systems at certain repeater distances. Optical amplification have many advantages such as: energy efficiency, colorlessness, transparency to WDM signals, bitrate, modulation formats and protocols etc and is preferred over previously deployed conventional electrical amplification through regeneration process.

The innovation of new state-of art fibres with very low loss in the conventional transmission windows (i.e. C, L band) has significantly improved the reach of modern data transmission system and advanced amplifier design. Optical amplification is one of the key enabling technologies of the modern data communication networks, which allows petabits of data transmission over few hundreds kilometers to trans-oceanic distances.

The basic performance parameters of any optical amplifier are determined by the gain and the operation range of input and output powers. Gain determines the amplification factor of the input signal and ranges usually between 10~30dB depending on the application and feature. Optical amplifier can be designed with a fixed pre-set gain or a range of operating gain values. Moreover, the operating range of input and output powers is another important characteristic. Optical amplifiers for wide bandwidth application are usually designed to have high output power. Maximum output power characteristic can also be termed as saturated output power. While single channel optical amplifier can operate over large dynamic gain range, WDM optical amplifiers are usually designed to maintain minimum gain variation across the specified gain bandwidth. A flat gain across the amplification band is required over different number of WDM channel counts, otherwise accumulated gain variation across different channels will be very high in a very long amplifier chain.

In the real-time data traffic network with optical add-drop multiplexer (OADMs), the dynamic change in the input number of channels to the amplifier may cause fluctuations of the noise

performance. As the bandwidth demand is increasing with the exponential growth of internet data traffic, the particular choice of optical amplifier in today's fibre optic transmission system is also determined by the gain-bandwidth property. So, the important features of optical amplifiers are:

- high gain
- high power conversion efficiency
- low noise
- low crosstalk
- high saturated output power
- polarisation insensitivity
- broad spectral bandwidth
- very low coupling losses
- low cost

Optical amplifiers can be categorized into many different categories depending on the application and technologies. Here we will focus on the amplifiers used in fibre optical transmission systems such as doped (i.e. erbium) fibre amplifier, Raman amplifier, semiconductor amplifier etc. Different characteristics and design issues of Raman amplifiers will be discussed in details including a brief overview of other common types of amplifiers..

3.1 Erbium Doped Fibre Amplifiers

Erbium doped fibre amplifier (EDFA) is the most widely used optical amplifier in currently deployed transmission system. It is a fibre amplifier where a silica core fibre doped with erbium ions (Er^{3+}), is used as gain medium. Er^{3+} has the emission spectrum in C band which is happened to be the low loss window of modern telecommunication fibre.
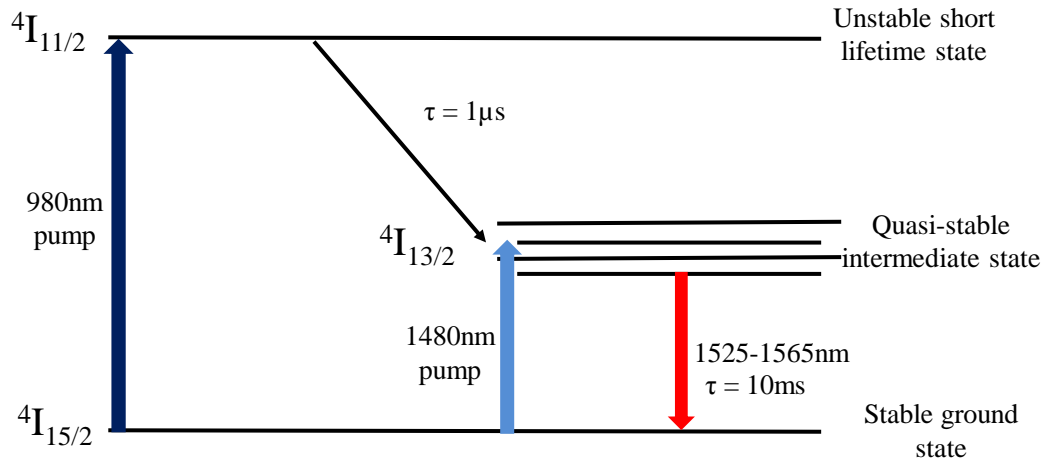
Figure 3. 1. Energy level transition of Er^{3+} in EDF with the presence of pump wavelength

The EDFA is usually pumped with suitably chosen pump wavelength around 980nm or 1480nm. The whole process is summarized in Figure 3. 1. When erbium dope fibre (EDF) is pumped with 980nm pump, electrons from ground energy state is excited to an unstable energy state with short life time ($\sim$1µs), before decaying to a quasi-stable state with longer life time ($\sim$10ms). Whereas, 1480nm pump directly excites Er^{3+} to the quasi-stable energy state. The longer life time provides high population inversion from ground state to the quasi-stable state allowing stimulated amplification. From quasi-stable energy state Er^{3+} ion decays back to the stable ground state by emitting new photon in the 1525~1565nm signal band. A stimulated decaying process is occurred with the presence of already existed light in signal band, resulting in signal amplification.

3.1.1 Basic design of EDFA

The very basic EDFA design consists of a suitable pump wavelength (980nm or 1480nm), a short piece of EDF typically about 10~30m, a pump/signal combiner known as WDM coupler. A semiconductor laser diode is usually used as pump source. The choice of the pump wavelength is very crucial for the noise performance of the amplifier. The emission cross-section is equal to zero at 980nm, which is not the case around 1480nm. Broadly speaking, EDFAs pumped with 980nm pump performs better both in terms of noise figure and pump power efficiency compared with 1480nm pump because of higher absorption efficiency [52].

The direction of pump beam is also important to modify the performance of EDFA. The pumping configuration can be implemented three different ways with respect to the signal propagation direction: forward (co-propagating), backward (counter propagating) and bidirectional (co and counter propagating simultaneously). Furthermore, an additional pair of isolators is used at the

input and output of the amplifier to avoid any kind of lasing in the EDF and isolate the pump light from the signal at the output of the amplifier as shown in Figure 3. 2.
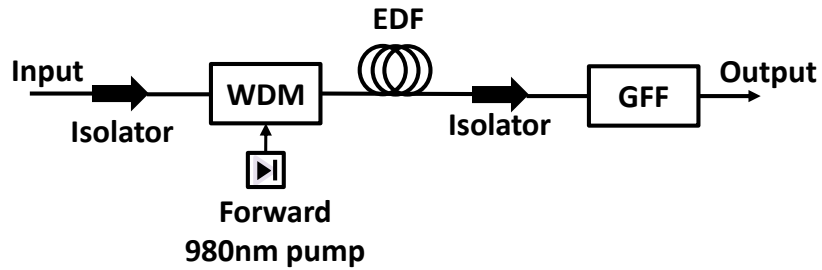
Figure 3. 2. Schematic diagram of a single stage EDFA forward pumped with a 980nm pump

Figure 3. 2 shows a very basic single stage EDFA design, in which forward pumping is used with 980nm pump. For multi-channel WDM application a gain flattening filter (GFF) is required just before the output end to flatten the gain or power variation across the bandwidth. GFF applies a fixed opposite attenuation profile to the signal band compared with the EDFA output in order to achieve a combined flat output. In the most basic design, a 980nm pump is used in forward pumping configuration with improved noise performance. However, simultaneous pumping with both 980nm and 1480nm pump has been also investigated at different inversion levels. At low inversion level, 980nm pumping allows best noise figure, whereas pumping with 1480nm pumps provides best pump power efficiency [52]. Moreover, cascaded multi-stage EDFA with two or more number of pumps can be used to optimise more than one performance parameters and to provide better gain flatness across the gain bandwidth [53-55].

Dynamically configured variable gain EDFA is required to support different span lengths in transmission link. Most single channel amplifier operates over large dynamic range, however for WDM channels, a proper design is required to achieve both desired gain and minimum gain variation across different channels. Inclusion of variable optical attenuator (VOA) either at the input or at the output of a single stage amplifier provides uniform attenuation at all the channels but at the cost of high noise figure and required pump power respectively. A better solution is achieved by placing the VOA in between two gain stages pumped by a single pump as shown in Figure 3. 3.
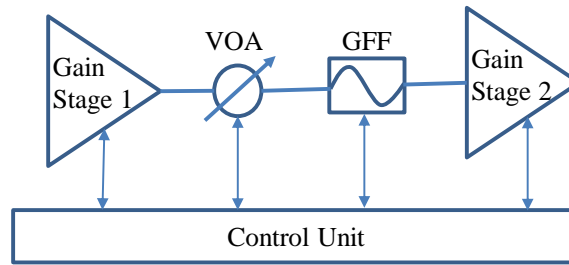
Figure 3. 3. Basic design of a variable gain EDFA for WDM application

Figure 3. 3 shows a variable gain dual-stage EDFA with a pre-amplifier stage-1, booster amplifier stage-2 and including a mid-stage VOA and GFF. The same pump can be shared in two stages. The control unit monitors the output power from the 1st gain stage and sets the attenuation of VOA to control the total gain of the amplifier. Advanced control unit can be designed in a feed forward loop mode where automatic pump power adjustment can be made with sudden change in input signal power for fast suppression of transients in the amplifier. In this design scheme, careful design of EDF length and pump power in each stage allows very good noise figure performance over a range of gain values at a cost of slight increase in pump powers compared with fixed gain EDFA. Dual stage EDFA with mid-stage dispersion compensating module (DCM) can also be designed to compensate the chromatic dispersion of the transmission line [56]. In this design, the first stage is usually used as a variable gain pre-amplifier and the second stage as fixed booster amplifier. But this dual stage design with mid stage DCM has become unpopular in modern coherent transmission systems, because chromatic dispersion induced penalty is corrected at the receiver by applying advanced DSP.

Typically, EDFA can achieve amplification of about 20 to 30dB with ~10m EDF length. The available pump power determines the maximum available output power, typical EDFA saturated output power varies between 17~20dBm. The gain bandwidth of typical EDFA is about 35nm (~4THz) around 1550nm which is much wider than that of electrical regenerators. Moreover amplification in L band is also possible with EDFA [57, 58]. However one of the main issues with extended band EDFAs is the discontinuous gain bandwidth i.e. a 5-8nn gap in amplification bandwidth around 1565~1570nm is required to have C+L band EDFAs. Additional passive components are required to split and re-combine the signals before and after separate amplification in C and L band respectively.

Another fundamental problem of EDFA is the amplified spontaneous emission (ASE) noise which is always associated with the stimulated emission. The accumulated noise in a chain of EDFAs

degrades the output signal to noise ratio (SNR) and may saturate the amplifiers. Careful optimization of amplifier lengths and pump powers can produce almost ideal optical amplifier with 3dB quantum limited noise figure performance even in high gain amplifiers [59, 60]. A complete model of signal power, gain and associated noise performance is derived in [61-63].

3.2 Other Rare Earth and Bismuth Doped Fibre Amplifiers

The amplification band of EDFAs are limited to C and mostly up to L band. But the exponential growth of bandwidth demand is increasing the demands of designing wideband transmission systems. The advent of modern single mode fibres with very low loss profile in telecommunication windows and recent advances in the design optical sources at different wavelength bands have also made it interesting to explore other bands for signal amplification beyond Er^{3+} emission bands, using other rare earth (RE) materials such as: bismuth (Bi), thulium (Tm), holmium (Ho), praseodymium (Pr) and so on.

Recently Bi-doped fibres have been shown as a promising choice in the development of fibre laser and amplifiers due to their very wide luminescence properties from 1150-1800nm in different glass materials (i.e. aluminosilicate, phosphosilicate and germanosilicate) [64, 65]. Wideband amplification over 40nm in the O-band (1320-1360nm) with flat gain of about 25dB and noise figure 4-6dB has been reported with Bi-doped phosphosilicate fibres [66]. Commercial Raman pump laser diode at 1240nm with reasonable pump power less that 500mW has been used for the amplification which makes it even more promising for future commercial use. The challenges in designing improved Bi-doped fibre amplifiers are temperature dependence causing unknown near infrared radiation in fibre fabrication process, excited state absorption and unsaturable losses [67].

In addition to that, thulium doped fibre amplifiers (TDFA) have been demonstrated to provide amplification with high gain and low noise in the wavelength range between 1660 and 2050nm [68-70]. The amplification beyond 2000nm is somehow difficult with TDFAs due to the decreasing emission cross-section of thulium [71]. Recently another RE material holmium (Ho) doped fibre amplifiers (HDFAs) have been demonstrated to obtain optical amplification beyond 2µm (2050-2130nm) to provide high gain above 15dB with low noise figure below 10dB [72]. However noise performances of HDFAs are mainly affected by high insertion loss from passive components operating at that region and lower average inversion level. So, achievable extended bandwidth beyond 2100nm depends on the appropriate pump sources at particular wavelengths and minimum coupling losses from the passive components [73]. Although RE-doped fibre amplifier are still not

commercially available and not implemented yet in real fibre optic transmission systems, however the gain, bandwidth and noise performances of these types of amplifiers are very promising and attractive for next generation, high capacity wideband transmission systems.

3.3   Semiconductor Optical Amplifiers

Semiconductor optical amplifiers (SOAs) are quite different from the silica based optical amplifiers. It uses semiconductor as gain medium in a waveguide and works similarly like a conventional semiconductor laser without any optical feedback to avoid lasing. The principle of light amplification in SOA is based on the recombination of electrons and holes at the transmission of *p-n* structure of the semiconductor [74]. Unlike other optical amplifiers, SOAs are pumped electronically without requiring a separate pump laser source. SOAs are compact in size and are typically packaged in "butterfly" packages. So significant characteristics of SOAs are small size and the direct electrical pumping.

But it has many other drawbacks which stall it widespread application in modern WDM coherent transmission systems. As it is not a fibre device, the coupling of light from and into the device is difficult, thus it introduces high coupling losses resulting in high noise figure performance. Very low reflections from cleaved end facets are required to design SOAs with very high gain (~30dB) and low gain ripple, otherwise amplifier bandwidth will be determined by the cavity resonances rather than the gain spectrum itself. A common solution is to use anti-reflection coating at the end facets and design travelling wave (TW) type SOAs by suppressing the reflections below 10^{-4}, which is difficult to obtain by using only the anti-reflection coating.

In particular SOAs have low gain (<15dB) and low saturated output power (<13dBm). In SOA, gain depends on the carrier population and injection current (typical currents are ~100mA). Moreover, with appropriate composition and design, SOA gain can be achieved over very wide bandwidth from 1200 to 1650nm (though specific semiconductor device has limited bandwidth up to ~80nm for a given bandgap) [75].

An important characteristic of SOA is very short life time of injected carriers in the order 100ps. The fast response time introduces inter-channel crosstalk due to the cross gain modulation in WDM channel operation [76, 77]. The gain saturation in one channel affects the carrier population through stimulated recombination and thereby modifies the response of other channels. Operating the amplifier well below the saturation may reduce the cross saturation through inter-channel crosstalk but the relatively limited saturation output power of SOAs (of the order of 10mW) makes

it difficult in WDM systems. Moreover, the stimulated recombination affects the carrier number and introduces nonlinear four-wave mixing effects. The requirement of high output saturation power for WDM application can be achieved by gain-clamped SOA with improve linearity [78-80]. The inter-channel crosstalk can be avoided by the 'linear' property of these gain-clamed SOAs having power independent characteristics [81].

Similar to other amplifiers, spontaneous emission noise associated with the stimulated process increases the noise figure of the amplifier. Noise figure of SOAs are determined by the emission due to spontaneous emission and also by the non-resonant internal losses (i.e. free carrier absorption or scattering loss), which reduces the effective available gain. Moreover, there are residual facet reflectivities which degrade the noise figure by adding losses to the input signal and via multi-path interference. The noise figure of SOAs are typically 3dB more than that of EDFAs varying between 6~8dB.

Early SOAs showed strong polarisation sensitivity which is the result of gain difference in transverse-electric (TE) and transverse-magnetic (TM) modes in the semiconductor waveguide structure. However, polarisation sensitivity has been reduced down to < 1dB in current SOAs [82, 83].

In summary, the major drawbacks of SOAs are polarisation sensitivity, inter-channel crosstalk in WDM system and high coupling losses. Although the drawbacks have been reduced by using different approaches, however the resultant performances are still significantly worse than EDFAs. So far the impact of SOAs in WDM transmission systems has been very limited. However, they can be used as booster amplifier in single channel configuration without requiring high gain or output power. Moreover, the application of SOAs is not only limited to amplification but also in wavelength conversion, fast optical switching, optical detection and so on [84].

Recently a novel design of ultra-wideband SOA has been demonstrated for the first time in high capacity (115Tb/s) coherent WDM transmission over 100nm (S+C+L bands) with transmission reach up to 100km [18], which has brought forward a renewed interest in the research community for further application of SOAs in short-haul high capacity transmission systems.

3.4   Fibre Optic Parametric Amplifiers

Fibre optic parametric amplifier (FOPA) is a four-wave mixing process in silica fibre involving one or two pump photon(s), a signal and one idler photon. A third order Kerr nonlinearity (the

nonlinear refractive index) leads to the signal amplification. A silica based highly nonlinear fibre (HNLF) with reasonably high nonlinear coefficient (γ = ~10W^{-1}km^{-1}) is used as the nonlinear gain medium. Reasonably short length of HNLF and high pump powers are usually used in FOPA. If one or two pump waves with frequencies ω_{P1} and ω_{P2} serve as pumps and a co-propagating signal with frequency ω_S is injected into the fibre, optical parametric process generates an idler at frequency ω_i. The idler spectrum is the mirror image and complex conjugate of the signal with respect to the centre frequency $\omega_C = (\omega_{P1} + \omega_{P2})/2$ as shown in Figure 3. 4(a) and (b) for two pumps and one pump respectively [85]. In single pump case, two photons at the same pump frequency (ω_P) are considered in the four photon mixing process.
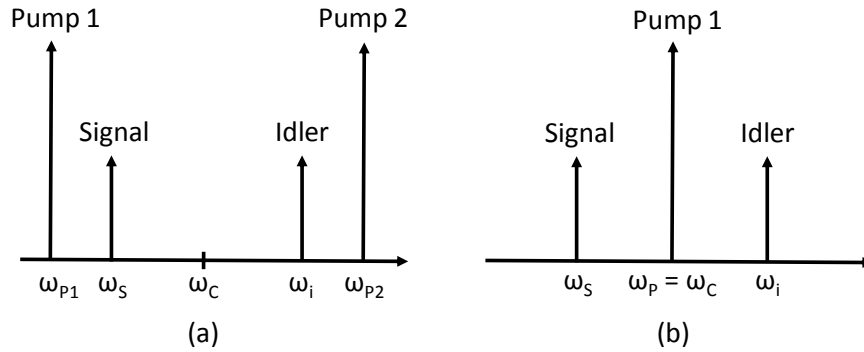
Figure 3. 4. Output spectral of FOPA process: (a) two pump version and (b) one pump process [85]

In Figure 3. 4(a) and (b), two and single pump based FOPA processes are shown respectively. The FOPA gain and gain bandwidth largely depends on the zero-dispersion wavelength (ZDW) characteristic of the fibre being used in parametric process, ideally which should be as close as possible to the pump frequency ($ZDW \approx \omega_C$) to obtain 2nd order dispersion value at pump frequency to be zero as $\beta^{(2)}(\omega_C) \approx 0$. The fourth order dispersion co-efficient, $\beta^{(4)}(\omega_C)$ also plays an important role in determining the gain spectrum of FOPA, as the gain bandwidth scales like

$\left[\dfrac{\gamma P_0}{\beta^{(4)}(\omega_C)} \right]^{1/4}$ [86], where P_0 is the input pump power. So HNLF with high nonlinear co-efficient

(γ) and high $\beta^{(4)}$ value are desirable for high gain over large bandwidth FOPA design. Most of the FOPA design can be divided into two main modes of operation: phase-insensitive amplifier (PIA) and phase-sensitive amplifier (PSA) [87].

In PIA, only pump and signal beams are injected into the amplifier. Idler is created in the four-wave mixing process, with optical phase according to the phase of the signal. There is no need to control the phase of any interacting beams, as parametric gain in this case is independent of the relative phase of the signal with respect to the pump(s). The operational principle is very much like an EDFA which is also a phase-insensitive amplifier. The noise figure performance can also be obtained as similar to EDFA.

The design of PSA requires the injection of signal, high power pump and additional idler beam into the amplifier. In general, signal and idler amplitudes are about the same. The pump and idler interact between them and create gain for signal with a particular optical phase property. As the gain is dependent on the relative phase of the waves, some means of phase control mechanism (i.e. phase locked loop, phase modulator etc.) are required to maintain the phase matching condition along the amplifier span. The noise figure of PSA can be less than 3dB unlike other optical amplifiers [88-90]. However, four-wave mixing efficiency depends on the polarisation property of interacting waves. So pump beam has to be depolarised through some polarisation scrambler or polarisation multiplexing. The requirement of high pump powers also imposes serious limitation introducing poor power conversion efficiency. The bandwidth increases with increasing the pump power and bandwidth over 200nm has been demonstrated in pulsed pumped optical parametric amplifier using high pump power in only 20m of HNLF [91].

In summary, FOPA has the potential of achieving very high gain, high output power, good noise and bandwidth performance. But the development of FOPA is far from real system implementation due to some major drawbacks.

Stimulated Brillouin scattering (SBS) introduces serious problem in the gain stability of FOPA when pump power is increased above a threshold limit. Phase modulation of pump can be used to broaden the pump spectrum and increase the SBS threshold but additional noise is introduced by this technique because of the transfer of phase into signal by the parametric gain process which is undesirable in optical communication [85].

The shape of gain spectrum depends on the random spatial modulation of the dispersion parameters which may vary from spool to spool even with identical fibre due to the lack of longitudinal uniformity. So novel fibre design with tailored dispersion profile is required to get flat gain over wide gain bandwidth [92]. Moreover, in broadband FOPA, contribution of Raman gain also distorts the gain flatness and increases noise figure. So a careful design is required for broadband FOPA based transmission systems.

The performance of FOPA with polarisation division multiplexed (PDM) higher order modulation formats are not stable because of strong gain sensitivity with different state of polarisations along the fibre. The variation of gain imposes serious degradation in system performance. Different polarisation diversity schemes have been adopted to get rid of the polarisation issues but each of these schemes have their own disadvantages [93-95].

Recently there has been many efforts to design FOPA with broad gain bandwidth > 100nm and very low gain ripple in the conventional low loss window of single mode fibre [96, 97]. Although the pump power efficiency and polarisation sensitivity are still questionable for WDM data transmission, however in a recent experiment polarisation division multiplexed DWDM data transmission has been demonstrated for the first time in both in-line and re-circulating loop experiment showing a record transmission distance up to ~605km with 15dB net gain polarisation insensitive (PI)-FOPA. These results show key advances of FOPA design for realizing in in-line transmission system with better noise performance than conventional EDFAs.

3.5   Raman Amplifiers

Raman amplification is an inelastic scattering process caused by the interaction between pump photon and molecule where a new photon is created at the signal frequency which is down shifted in frequency than the pump frequency. This process is known as stimulated Raman scattering (SRS) where energy is transferred from pump to signal and optical phonon is created due to energy absorption by the material. Energy of different vibrational states is a material property and that's why Raman gain spectrum created by SRS varies from material to material. The new signal photon is also called the Stokes wave which grows rapidly inside the medium as energy gradually transfers from intense pump wave. The newly generated Stokes waves propagate both co-propagating and counter-propagating directions with the incident pump beam [39]. The basic process can be understood by the energy state diagram given in Figure 3. 5 below:
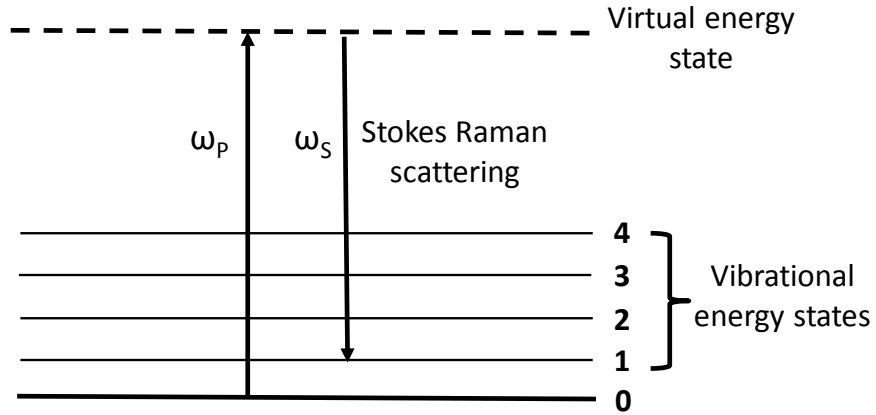
Figure 3. 5. Raman scattering process

In Figure 3. 5, an incident pump photon (ω_P) on a medium excites a molecule up to a virtual state.

The molecule rapidly decays to a lower energy state emitting a signal photon (ω_S) in the process.

The Raman process is very fast, almost instantaneous unlike EDFA. The energy difference between

the pump and signal photons is dissipated by the molecular vibration of the host material [98]. The

Stokes shift ($\omega_P - \omega_S$) and Raman gain spectrum shape are determined by the vibrational energy of

the molecules. So with a proper choice of pump frequency, Raman gain can be achieved at any

signal wavelength, limited only by the transparency of the material. Raman gain is also

independent of the pump direction as phase matching is automatically fulfilled. A simple SRS

process in Raman amplifier using a standard single mode fibre (SSMF) and a pump is shown in

Figure 3. 6.
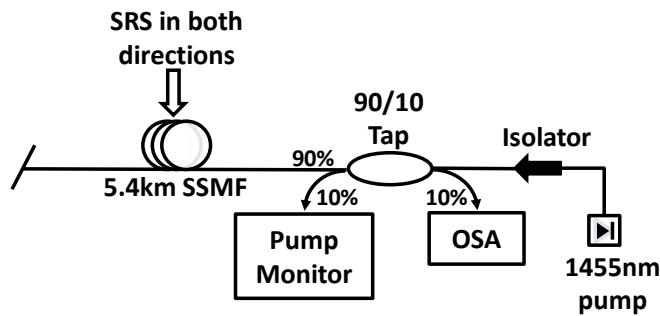
Figure 3. 6. Schematic diagram of a basic SRS process

An example of SRS spectrum generation process in Raman amplifier is shown in Figure 3. 6,

where a 5.4km standard single mode fibre (SSMF) was pumped by a 1455nm Raman fibre laser

source. The pump was coupled into the fibre through a 2-by-2 90/10 coupler and no input signal

was used to be amplified. The pump power fed into the fibre was 1W and was monitored in the forward 10% monitor port. SRS was created in both directions at the presence of enough pump power along the fibre. Backward propagating SRS components were measured through the other 10% port using an optical spectrum analyser (OSA). The gain bandwidth of Raman amplification is usually about 40 THz and the full width at half maximum (FWHM) of Raman gain spectrum is about 6THz. The measured peak Raman gain in the obtained SRS spectrum was about 100nm (13.2THz in frequency) away from the 1455nm pump around 1555nm as shown in Figure 3. 7.
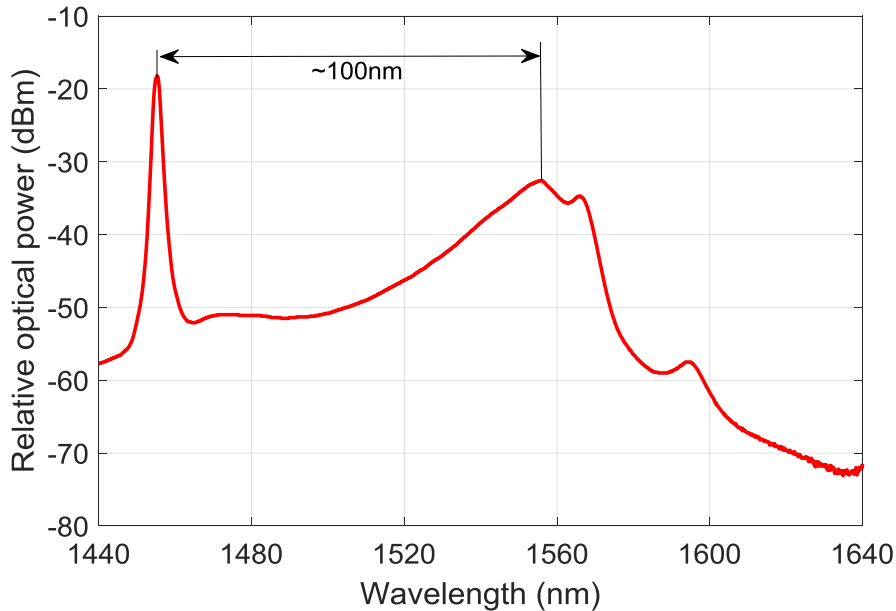
Figure 3. 7. ASE spectrum of a Raman amplifier with 5.4km SSMF backward pumped by a 1455nm pump source

The bandwidth of Raman amplifier is usually narrower than that of intrinsic Raman gain, but extended gain bandwidth can be obtained by combining amplification spectra from multiple pumps. By proper choice of pump wavelengths and careful optimization, gain bandwidth beyond ~10THz with overall gain ripple 0.5dB has been demonstrated with more than 10 first order pumps in silica fibre [99]. In order to obtain broadband gain spectrum with multiple first order (14xx) Raman pumps, we experimentally designed a distributed Raman amplifier consisting of an 80km SSMF span which was backward pumped by different combination of maximum five first order Raman pumps : 1425nm, 1444nm, 1462nm, 1476nm and 1508nm. At the input, broadband signal was used combining ASE spectra from C and L band EDFAs using a 3dB coupler, with a flat bandwidth nearly 85nm (1525~1610nm). Using all five first order pumps, 16.5dB Raman on-off gain was obtained at the end of the amplifier to maintain 0dB net loss with 1.5dB gain ripple across 85nm signal bandwidth as shown in Figure 3. 8.
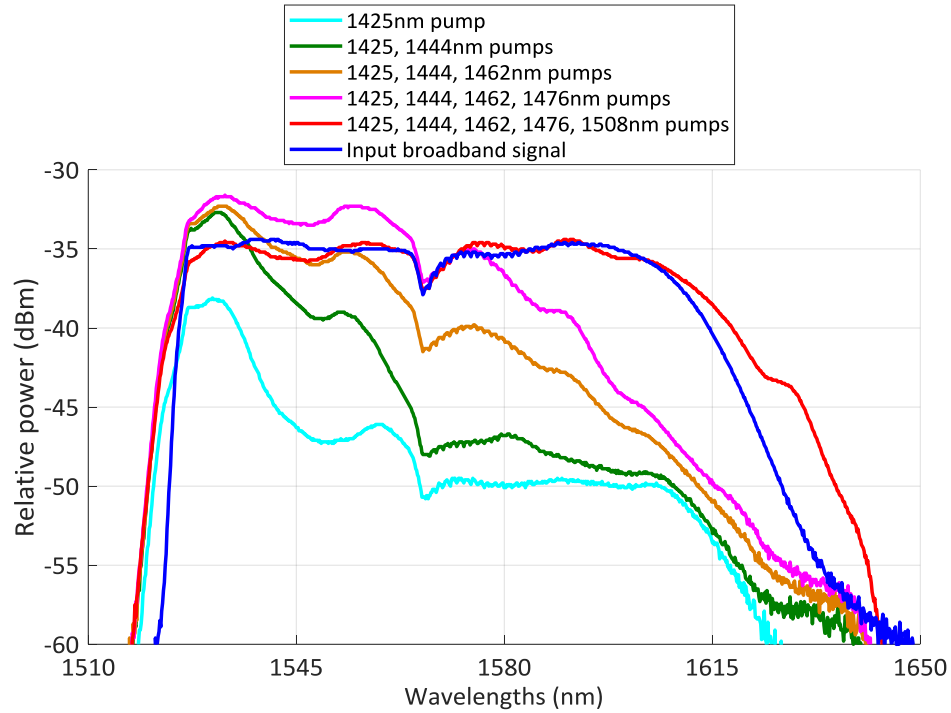
Figure 3. 8. Input and output broadband Raman amplification gain spectra with different pump combinations

In Figure 3. 8, the dip in signal power around 1565~1573nm was due the combined ASE gain spectra from C and L band EDFAs. As it can be seen that, gradual inclusion of longer wavelength pumps increased the bandwidth. In 5 pumps combination, pump power was transferred from shortest 1425nm pump to longest 1508nm pump and finally a flat gain output spectrum was obtained with proper pump power optimization. Similar broadband discrete Raman amplifier using other gain fibres such as dispersion compensating firbe (DCF), highly nonlinear fibre (HNLF) and so on is also possible. More details on the simulation and experimental results will be discussed in chapter 7.

Raman gain is polarisation dependent [100]. Maximum and minimum (almost zero) gain are achieved when both pump and signal are co-polarised and orthogonally-polarised respectively. So polarisation dependence of Raman effect has a big impact on Raman gain spectrum. In conventional fibre over long length, the state of polarisation varies randomly, which may introduce random signal gain fluctuations named as polarisation dependent gain (PDG) [101]. Depolarised pumps are usually used in case of Raman amplification to avoid any PDG but in this case Raman gain efficiency is reduced by half of the maximum.

So Raman amplifiers are quite different from the EDFA, without requiring a specially fabricated gain fibre doped with Er^{3+} ions.

The types of Raman amplifiers can be divided into distributed and discrete Raman amplifiers depending on their application and choice of fibre types.

3.5.1 Distributed Raman amplification

Distributed Raman amplification is a special type of optical amplification where the signal is amplified along the transmission fibre. The intrinsic loss of fibre is counter balanced at every point in an ideal distributed amplifier. As distributed amplification occurs inside within the transmission fibre, no additional special fibre is needed as gain medium and that makes it more attractive choice than others.

In mid 1980s, successful long haul transmission experiments over thousands of kilometers using distributed Raman amplification were carried out by Mollenauer and co-workers [102]. But surge of EDFAs with higher pump power conversion efficiency took over the place of Raman amplifier in early nineties. Then again after the availability of high power Raman fibre laser, the benefits of distributed Raman amplification were demonstrated in many high capacity-long haul undersea [103, 104] and terrestrial transmission systems [103]. Since then the use of distributed amplification in long haul and ultra-long haul transmission system has become popular and much studied research topic.

One of the most important benefits of distributed Raman amplification is the improvement of SNR. SNR improvement is achieved by amplifying the signal along the transmission fibre unlike discrete amplifiers (i.e. EDFA) where signals is attenuated first along the transmission fibre before getting amplified in discrete points. As a result, SNR does not drop as much as it would have in discretely amplified transmission system. The benefit of improved SNR allows increased distance between repeaters and extends the overall transmission reach of long-haul transmission systems. High capacity transmission systems using higher order modulation formats require high SNR and distributed amplification is the better choice for allowing higher capacity and extended reach than conventional discrete amplifier counterpart.

Broadband gain can be obtained from distributed Raman amplification by combining gain spectrum of multiple pump laser diodes at suitable wavelengths and powers. Although 3dB gain spectrum of each pump is only few nm but superposition of similar spectra from multiple pumps selected efficiently with optimum power level can produce very wide and flat gain bandwidth [105, 106].

3.5.1.1 Higher order pumped distributed Raman amplifiers

In distributed Raman amplification, higher order pumping can improve the noise figure performance by distributing the gain further into the amplifier span. In this pumping scheme, primary pump is usually chosen to be two or more Stokes shifts away from the signal band. For example, in dual order Raman pumping, a 2nd order pump at 1366nm and a 1st order pump at 1455nm can be combined together to amplify the signal in C band. Here, 1st order 1455nm pump is used as a seed with low pump power (~20mW) to transfer the gain from the primary 2nd order pump with high pump power. Third order Raman pumping is also available in which primary pump is usually three Stokes shifts away from the signal. Third order pumping has been demonstrated in unrepeatered transmission systems for their superior gain performance in very long span lengths [107, 108].
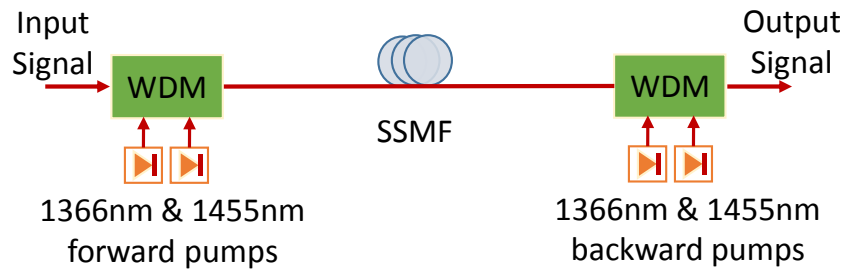
Figure 3. 9. Dual order bidirectional distributed Raman amplifier design

A standard bidirectional dual order pumped distributed Raman amplifier with SSMF span is shown in Figure 3. 9, where 1366nm and 1455nm pumps are used in a dual order combination. Here, the main gain contribution comes from the primary high power 1366nm pump which allows further penetration of distributed signal gain into the span and reduces the overall signal power variation (SPV). Here 1455nm pump is used at low pump power (~20mW) to increase the gain efficiency from two Stokes shifted 1366nm pump to signal around 1550nm. The same amplifier can be used as 1st order bidirectional distributed Raman amplifier by removing the 1366nm pumps. In that case, 1455nm acts as the primary pump to provide gain to the signals in C band.
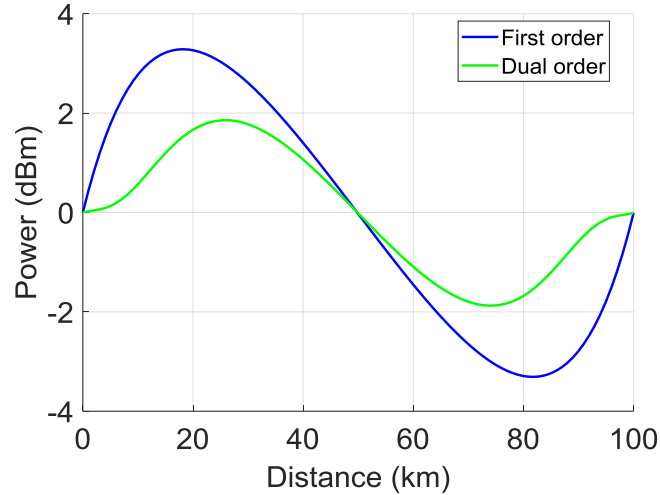
Figure 3. 10. Comparison of SPVs between first and dual order bidirectional distributed Raman amplifiers.

The comparison of SPVs at 1550nm in a symmetrically pumped 100km SSMF based distributed Raman amplifier with dual and first order pumping is shown in Figure 3. 10. Due to the benefit of improved gain distribution along the span in bidirectional dual order pumping, the SPV is reduced by ~2.9dB compared with 1st order bidirectional pumping. The improved optical signal to noise ratio (OSNR) resulted from reduced SPV allows improved transmission performance of high capacity WDM systems. But additional challenges comes with bidirectional Raman pumping such as pump noise transfer, pump saturation etc. which will be discussed in later sections.

3.5.1.2 *Ultra-long Raman fibre laser based distributed Raman amplifiers*

Ultra-long Raman fibre laser (URFL) based distributed Raman amplifier is an alternative higher order pumping scheme using only a single Raman pump laser source as higher order pump. The intermediated lower order pump(s) are created in a long cavity fibre laser within the amplifier span. In 2nd order URFL amplifier, the primary pump is usually chosen to be two Stokes shifted away from the signal band i.e. 1366nm pump. The intermediate 1st order pump near 1455nm is created by feeding back the Stokes shifted light using high reflectivity fibre Bragg gratings (FBGs) acting like mirrors [15, 109].
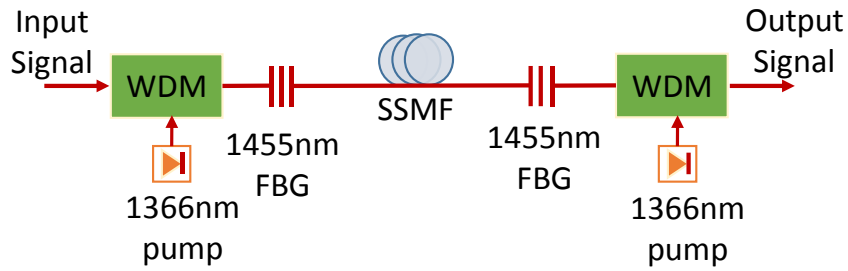
Figure 3. 11. Schematic diagram of URFL based distributed Raman amplifier

In Figure 3. 11, an URFL based distributed Raman amplifier is shown using SSMF span, in which 1366nm pumps are used as primary sources in both forward and backward direction. When 1366nm pump is propagated along the SSMF, Stokes shifted Raman scattered lights are created in both directions from the SRS effects around 1455nm and reflected back into the span by the end high reflectivity (>95%) FBGs. Eventually a Fabry-Perot (FP) laser cavity is created as soon as SRS overcomes the fibre loss and effectively creates a gain medium at 1455nm using the transmission fibre as the laser resonator. Finally amplification of signals is achieved by the 2nd order 1366nm pump via the cavity generated fibre laser at 1455nm. The properties of the cavity can be optimized by changing the FBG wavelengths, bandwidth and position. URFL based amplifier is different from the conventional dual order pumped distributed amplifier, because it requires only 2nd order pumps and a pair of passive FBGs. But relatively high 1366nm pump power is required to overcome the lasing threshold at 1st order pump wavelength (1455nm). One of the main benefits of using this pumping configuration is to have quasi-lossless signal power profile along the amplifier span with improved OSNR performance because of the nearly constant 1st order lasing power along the amplifier span [14]. If we consider symmetric bidirectional pumping with equal 1366nm pump power from each direction, then the OSNR improvement from forward pumping mainly depends on the strength of front FBG reflectivity. Let us consider a 100km SSMF based URFL bidirectional amplifier with variable input reflectivity (from 10~99%) and fixed high 99% output end reflectivity. The total pump power required to get 0dB net loss of signal at the output of the amplifier is split equally between forward and backward 1366nm pumps. The simulated signal power profiles and total pump powers required are shown in Figure 3. 12(a) and (b) respectively using the parameters given in [15]. As the input reflectivity levels were increased from 10% to 99%, the SPVs were also reduced (Figure 3. 12 (a)) and the required total pump powers were also reduced by ~300mW (Figure 3. 12 (b)). So URFL based distributed Raman amplifier with high reflectivity (>95%) FBGs at both ends simultaneously improves the SPV and pump power efficiency.
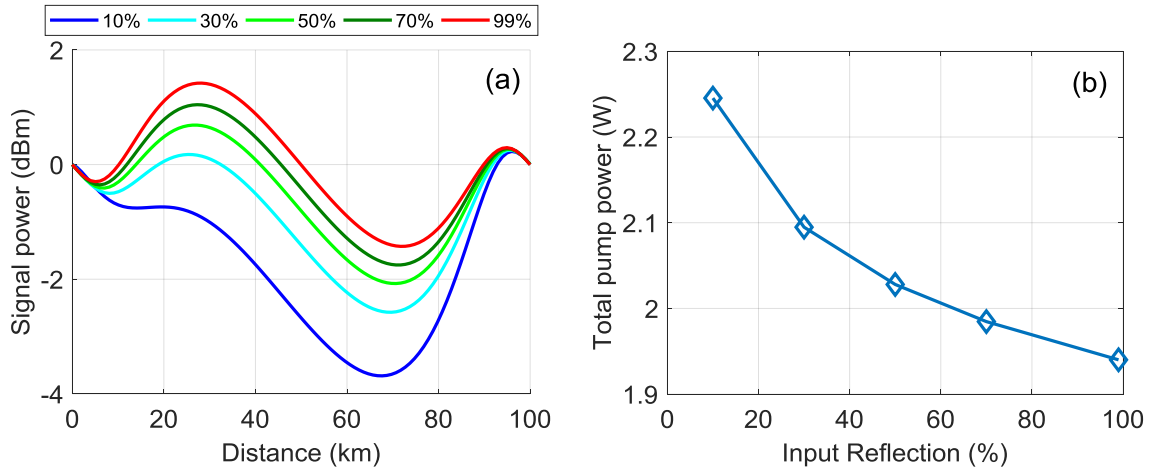
Figure 3. 12. In a bidirectional pumped URFL with variable input FBG reflections: (a) signal power variation (SPV) and (b) total pump power required

3.5.2 Discrete Raman amplification

Discrete or lumped Raman amplifiers are basically similar to EDFA as the amplification is provided at discrete points at transmission line using separate gain fibre and pump power is confined only within this unit to provide net gain. Different wavelength bands (S band, L band etc.) of silica fibre can be used for signal transmission using such discrete Raman amplifier choosing Raman pumps accordingly. A basic schematic diagram of a discrete Raman amplifier using a Raman gain fibre and backward pumping is shown in Figure 3. 13 (a).
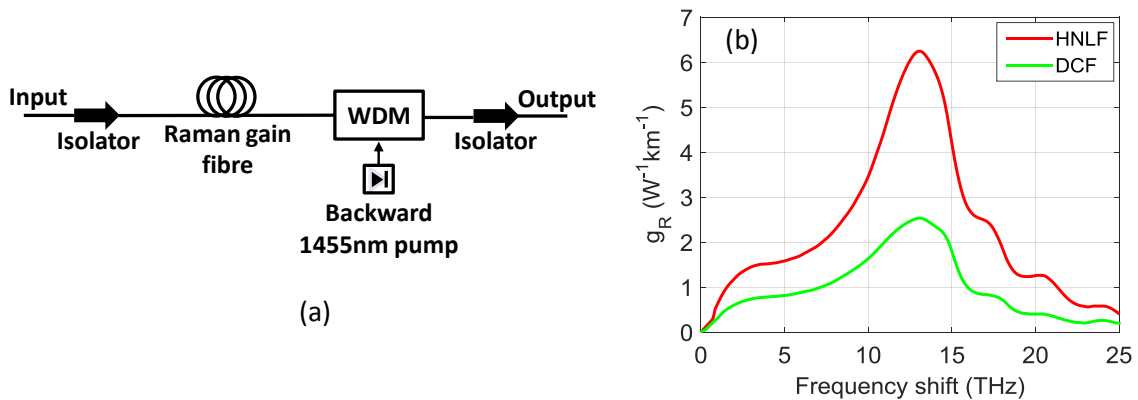
Figure 3. 13. A schematic diagram of a simple discrete Raman amplifier and (b) Raman gain coefficient of highly nonlinear fibre (HNLF) [110] and dispersion compensating fibre (DCF) [111]

Figure 3. 13(b) shows the Raman gain coefficient of two conventional Raman gain fibres HNLF [110] and DCF [111] with peak values of 6.3W^{-1}km^{-1} and 2.53W^{-1}km^{-1} respectively. The

67

corresponding pump wavelengths for HNLF and DCF were 1450nm and 1453nm respectively. Gain fibres with higher Raman gain coefficient, reasonable attenuation coefficient value (usually 0.5~0.8dB/km) and narrow core diameter are usually chosen for discrete Raman amplification. Dispersion shifted fibre (DSF), DCF, HNLF are preferred in the literatures so far for their higher net Raman gain properties compared with conventional transmission fibre i.e. SSMF [112, 113]. The point of using Raman gain fibre with higher Raman gain efficiency is to allow use of short length fibre (usually <10km) in the amplifier to get similar net gain from the discrete amplifier. But among those, DCFs have been used mostly because of their simultaneous advantages of dispersion compensation and Raman gain [112]. The wideband lossless application and dispersion compensation of DCF using multiple pump laser diodes was demonstrated by Y. Emori and co-workers [114]. All Raman transmission experiments have also been carried out incorporating distributed Raman amplifier and dispersion compensating Raman amplification (DCRA) [115, 116]. All Raman broadband systems are very cost effective because less numbers of passive components are required for system setup.

Discrete Raman amplifiers have many benefits over the commonly used EDFA including arbitrary gain bandwidth, flexible controlling of gain spectrum and so on. As the amplification is provided in a lumped device and high pump power does not propagate along the transmission fibre, discrete Raman amplifier has safer laser operation compared with distributed Raman amplification.

There are some additional challenges in case of using different gain fibres in discrete Raman amplifiers. For example DCF will have additional dispersion in the system which will have pronounce effect in selecting proper transmission span lengths in case of dispersion compensated systems. Present transmission systems use coherent technology where dispersion effects are managed at the receiver using DSP. So total dispersion map has to be remodeled in the DSP for additional dispersion provided by DCF or similar high dispersive fibres as gain medium. Moreover, Raman gain fibres usually have high nonlinear coefficients which give rise to additional Kerr induced intra-channel and inter-channel crosstalk and degrade the system performance. So improved nonlinearity compensation technique has to be considered in discrete Raman amplifiers. More details will be discussed in chapter 7.

Forward, backward and bidirectional pumping scheme can also be used in the design of discrete Raman amplifier. Forward and bidirectional pumping schemes are usually used to improve the noise performance of the amplifier. However increased nonlinearity from higher path average

power and increased intensity noise transfer from pump may degrade the system performance, which will be discussed in next section.
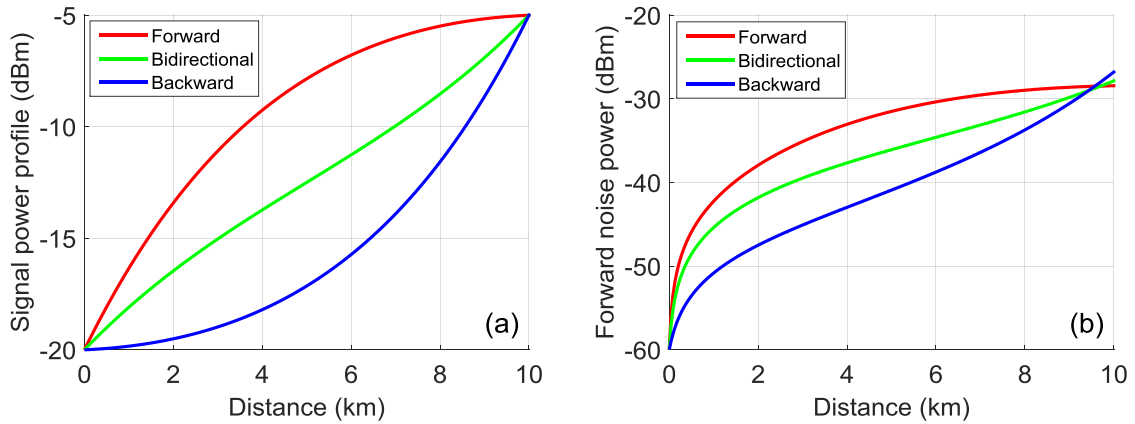
Figure 3. 14. (a) Signal power profiles and (b) total forward propagating noise for different pumping schemes in a 10km DCF based discrete Raman amplifier using a single 1455nm pump and 1550nm signal

The simulated signal power profiles and forward propagating total noise (combined amplified spontaneous emission and double Rayleigh scattering noise) along a 10km long DCF based discrete Raman amplifier are shown in Figure 3. 14(a) and (b) respectively. The simulation parameters used for discrete Raman amplifier design will be given in chapter 7. The path average powers along the amplifier span are much higher in bidirectional and forward pumping than that of backward pumping as shown in Figure 3. 14(a), which gives additional penalty from self-phase modulation induced nonlinear phase shift [39]. The benefit of improved noise performance from forward gain contributions can be observed from the forward propagating total noise profiles in Figure 3. 14(b), which shows ~1.5dB and 1dB reduced output noise levels compared with backward only pumping in case of forward only and bidirectional pumping respectively.

Broadband discrete Raman gain is also possible by combining multiple pumps at optimized pump wavelengths and powers and that will be discussed in details in chapter 7.

3.5.3 Performance limiting factors in Raman amplifiers

The important performance limiting factors of Raman amplifier include amplified spontaneous emission (ASE) noise, relative intensity noise (RIN) due to the fast gain dynamics, double Rayleigh scattering (DRS) induced multi-path interference (MPI), Kerr nonlinearities and so on. Each of these challenging factors will be discussed briefly here in the following sections.

3.5.3.1 Spontaneous Raman scattering

The spontaneous Raman scattering is inherently associated with stimulated Raman scattering process and induce additional noise to the amplified signal [117, 118]. The spontaneous Raman scattering appears as a noise in the signal band because of the random phases associated with the all spontaneously generated photons. Unlike EDFA, the associated noise depends on the phonon population in the vibrational states, which in turn depends on the temperature. ASE noise degrades the SNR of the signal amplified by Raman amplifier and the amount of degradation can be quantified through noise figure, which is described as [63, 101, 119]:

$$NF = \frac{SNR_{IN}}{SNR_{OUT}}$$ (3.1)

where, SNR_{IN} and SNR_{OUT} are the electrical signal to noise ratio of input and output signal respectively, calculated from the electrical current converted from optical signal power. If an ideal detector is considered, which is limited only by the shot noise then input electrical SNR is defined as:

$$SNR_{IN} = \frac{\langle I_{IN} \rangle^2}{\sigma_{shot}^2} = \frac{\langle R_d P_{IN} \rangle^2}{\sigma_{shot}^2}$$ (3.2)

where, I_{IN} is the input signal current and $R_d = \dfrac{q}{h\nu}$ is the responsivity of the receiver with 100% quantum efficiency ($\eta = 100\%$). σ_{shot}^2 is the variance of the input shot noise over the receiver bandwidth B_e, which can be defined as:

$$\sigma_{shot}^2 = 2q(R_d P_{IN})B_e = 2h\nu R_d^2 P_{IN} B_e$$ (3.3)

where, P_{IN} is the input signal power, q is the electron charge, h is the Plank's constant and ν represents the signal frequency. So the input SNR can now be expressed as:

$$SNR_{IN} = \frac{R_d^2 P_{IN}^2}{2h\nu R_d^2 P_{IN} B_e} = \frac{P_{IN}}{2h\nu B_e}$$ (3.4)

ASE noise has to be included in the amplified output signal for the calculation of output electrical SNR. If all noise sources are included, the detector current is defined as:

$$I_{OUT} = R_d G_L P_{IN} + I_{SIG-ASE} + I_{ASE-ASE} + I_{shot} + I_T$$ (3.5)

where, I_{OUT} is the output current and G_L defines the net gain. The shot and thermal noise induced current fluctuations are also included in the output current and are defined by I_{shot} and I_T respectively. The ASE noise can be separated into two polarisation parts: co-polarised with the signal and orthogonally polarised with the signal. Only the co-polarised part has the beating contribution with the signal. The current fluctuations resulting from signal-ASE and ASE-ASE beating are represented by $I_{SIG-ASE}$ and $I_{ASE-ASE}$ respectively [120]. The output noise variance can be calculated from the respective current component and defined as:

$$\sigma_{OUT}^2 = \sigma_{SIG-ASE}^2 + \sigma_{ASE-ASE}^2 + G_L \sigma_{shot}^2 + \sigma_T^2 \tag{3.6}$$

The thermal noise variance is usually given by [121]:

$$\sigma_T^2 = \frac{4K_B T B_e}{R_L} \tag{3.7}$$

where, K_B, is the Boltzmann's constant, T is the absolute temperature, B_e is the electrical bandwidth of the photodetector and R_L is the load resistor in the optical receiver.

In Eq. (3.6), the thermal noise contribution (σ_T^2) is relatively small and can be neglected. The ASE-ASE beat noise ($\sigma_{ASE-ASE}^2$) is also very small compared to SIG-ASE beat noise ($\sigma_{SIG-ASE}^2$) and can be further reduced with the implementation of a narrowband optical filter [101].

$$\sigma_{SIG-ASE}^2 = 4R_d^2 G_L P_{IN} S_{ASE} B_e \tag{3.8}$$

where, $\sigma_{SIG-ASE}^2$ represent the SIG-ASE beat noise and S_{ASE} is the ASE spectral density, which definition is given in [101] as:

$$S_{ASE} = n_{sp} h \nu g_R G_L \int_0^L \frac{P_p(z)}{G(z)} dz \tag{3.9}$$

where, n_{sp} is the spontaneous-scattering factor and $h\nu$ is the photon energy. The Raman gain coefficient is given by g_R and L is the length of the amplifier span. The pump power along the amplifier span length z is given by P_p. The total ASE noise power considering an ideal filter $H_f(\nu)$ placed at the output of the amplifier can be expressed as:

$$P_{ASE} = 2\int_{-\infty}^{+\infty} S_{ASE}H_f(v)dv = 2S_{ASE}B_e \tag{3.10}$$

where, B_e corresponds to the bandwidth of the optical filter. The factor 2 in the equation stands for the two polarisation mode of the fibre. So, the SIG-ASE beat noise term from Eq. (3.6) can now be simplified as:

$$\sigma_{SIG-ASE}^2 = 2R_d^2 G_L P_{IN} P_{ASE} \tag{3.11}$$

The output electrical SNR of the amplified signal can be approximated by:

$$SNR_{OUT} = \frac{(R_d G_L P_{IN})^2}{G_L \sigma_{shot}^2 + \sigma_{SIG-ASE}^2} = \frac{(R_d G_L P_{IN})^2}{2G_L hv R_d^2 P_{IN} B_e + 2R_d^2 G_L P_{IN} P_{ASE}} \tag{3.12}$$

Now, the noise figure can be expressed using the Eq. (3.4) and Eq. (3.12):

$$NF = \frac{P_{ASE}}{G_L hv B_e} + \frac{1}{G_L} \tag{3.13}$$

The noise figure in Eq. (3.13) shows that it depends on the output ASE noise power, net gain and reference optical bandwidth of the noise. Here P_{ASE} represents the total ASE noise power in both polarisation states. Eq. (3.13) can also be expressed in terms with pump power and Raman gain co-efficient using the ASE noise power definition described in Eq. (3.9) and (3.10) as:

$$NF = 2n_{sp}g_R \int_0^L \frac{P_P(z)}{G(z)}dz + \frac{1}{G_L} \tag{3.14}$$

From Eq. (3.14) it can be seen that, noise figure in Raman amplifier depends on the pumping configuration [101]. The pump power along z can be very different depending on the pumping schemes. In general, forward pumping provides maximum SNR and minimum noise figure because most of the Raman gain is concentrated at the input end where the pump power is very high. The ASE noise generated at the input end also faces attenuation along the span and at the output the level becomes even lower than that of backward only pumping scheme.

Distributed Raman amplifier uses the transmission fibre itself as gain medium. So a localized lumped pre-amplifier with similar gain (G_L) and noise figure (NF) can be considered at the end of the transmission fibre as shown in Figure 3. 15.
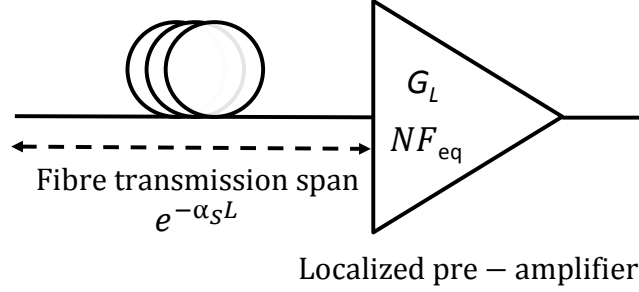
Figure 3. 15. Equivalent noise figure of distributed Raman amplifier

In distributed Raman amplification case, noise figure is usually termed as "effective" or "equivalent" noise figure as expressed as following [101]:

$$NF_{eq} = NF \exp(-\alpha_S L) \tag{3.15}$$

where, α is the attenuation coefficient of the fibre at signal wavelength. In decibel unit:

$$NF_{eq}(dB) = NF(dB) - \alpha_S L \tag{3.16}$$

where, span loss in dB is defined by $\alpha_S L$. So noise figure in distributed Raman amplifier could even be negative depending on the span length, which makes it so attractive for long-haul WDM transmission systems [120, 122]. In a chain of amplifiers, the total noise figure can be calculated as following [119]:

$$NF_{Total} = NF_1 + \frac{NF_2 - 1}{G_1} + \frac{NF_3 - 1}{G_1 G_2} + ... \tag{3.17}$$

where, NF_i and G_i represent the noise figure and net gain of the ith amplifier in the chain in linear units. Eq. (3.17) shows that in a chain of amplifiers with reasonable high gain, total noise figure is determined by the noise performance of 1st amplifier. In distributed amplification, the fibre attenuation is effectively compensated in a distributed manner creating a quasi-lossless medium. Forward pumping amplify both the signal and noise at the input of the span and at the output the generated noise level is attenuated and NF is improved. However, increased average signal power along the span may create Kerr induced nonlinear penalties at the output.

3.5.3.2 *Rayleigh backscattering*

Rayleigh backscattering is another performance limiting factors of Raman amplifiers and it occurs in all types of fibres [101]. Due to the inhomogeneity in the fibre core design, a portion of light travelling along the fibre is reflected back to the opposite direction. The backward propagating

reflected light can be reflected again and propagated in the same direction as the signal. This double reflected signal is called double Rayleigh scattering (DRS) which gets further amplified along the amplifier span and introduces Rayleigh induced noise in the signal band. The DRS of the signal propagates in the same direction as signal and creates in-band crosstalk with almost similar spectral properties as signal. In distributed Raman amplifier, Rayleigh scattered signal gets multiples reflections along the amplifier span, which are subsequently amplified and finally introduces penalty at the output of the amplifier, which is also referred as multipath interference (MPI) noise [120]. The DRS induced MPI noise sets an upper limit to the maximum achievable gain from the amplifier span before the additional penalty dominates the performance. The process of signal, Rayleigh and double Rayleigh scattered lights in a Raman amplifier can be described by the following set of equations (details of numerical modelling are given in chapter 4):

$$\frac{dP_S}{dz} = -\alpha_S P_S + g_R P_S P_P \tag{3.18}$$

$$\frac{dP_{RS}}{dz} = \alpha_S P_{RS} - g_R P_{RS} P_P - kP_S \tag{3.19}$$

$$\frac{dP_{DRS}}{dz} = -\alpha_S P_{DRS} + g_R P_{RS} P_P + kP_{RS} \tag{3.20}$$

Eqs. (3.18)-(3.20) describe the propagation of forward propagating signal, backward propagating Rayleigh scattering (RS) and forward propagating double Rayleigh scattering (DRS) signal components respectively. The power of pump, signal, RS and DRS components are given by P_P, P_S, P_{RS} and P_{DRS} respectively. α_S and g_R are the attenuation co-efficient of signal and Raman gain coefficient of pump at signal frequency. The amount of backscattering power is denoted by the coupling coefficient or capture factor k, which has different values for different fibre types. The value of k in SSMF and DCF are $4.3\sim6.4\times10^{-5}$ km^{-1} and $6\sim7.1\times10^{-4}$ km^{-1} respectively [15, 123].

In discrete Raman amplifier, special Raman gain fibre with high Raman gain efficiency are usually chosen for better pump conversion efficiency over short length of fibre. The corresponding coupling coefficients due to Rayleigh backscattering and Raman gain coefficients are also reasonably very high than standard transmission fibre with low loss profile (i.e. SSMF). For this reason, DRS induced MPI noise becomes significantly important in discrete Raman amplifier with very high gain levels.
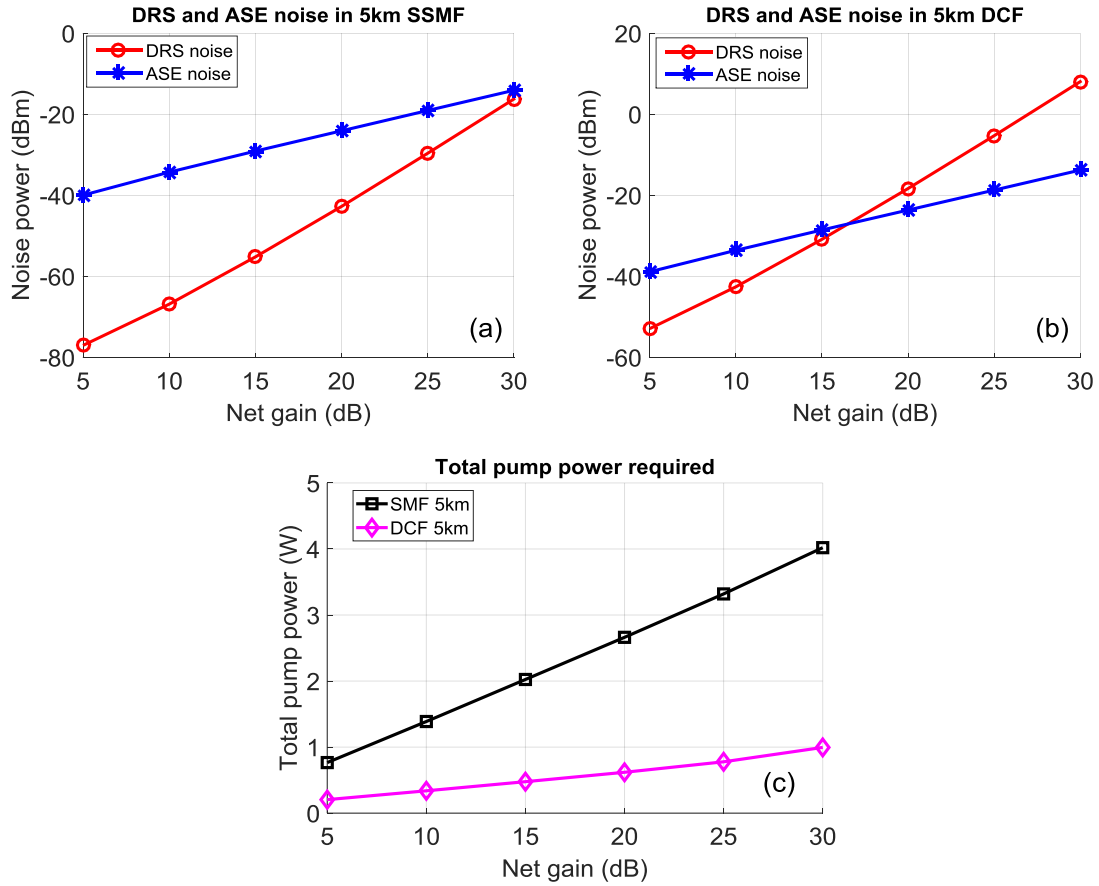
Figure 3. 16. ASE and DRS noise power comparison for different net gain levels in a 5km amplifier span of (a) SSMF and (b) DCF; and (c) total pump power required in numerical simulation for corresponding fibre type

The DRS and ASE noise with increasing net gain levels in 5km SSMF and DCF are shown in Figure 3. 16(a) and (b) respectively. Backward pumping with 1455nm pump and signal at 1550nm is considered with -10dBm power in both the cases. The fibre attenuation coefficients at pump and signal wavelengths are 0.3dB/km and 0.2dB/km for SSMF and 0.8dB/km and 0.5dB/km for DCF respectively. The peak Raman gain coefficients at 1550nm signal wavelength of SSMF and DCF are $0.43W^{-1}km^{-1}$ and $2.6W^{-1}km^{-1}$. In SSMF 5km, DRS noise levels are very low and remain substantially lower than ASE noise level up to net gain of 25dB. Whereas, DRS noise dominates over ASE noise and increases rapidly beyond 15dB net gain in case of DCF 5km due to high coupling coefficient (7.1×10^{-4} km^{-1}) than that of SSMF (4.3×10^{-5} km^{-1}). DRS induced noise becomes more serious when the span length of the amplifier is increased due to increased amount of multipoint reflected signals co-propagating with the signal and distributed gain along the longer span length before fibre attenuation loss dominates over the amplified backscattered signal power. Interestingly, the ASE noise power increases slowly with higher net gain levels and remains similar

75

in both SSMF and DCF fibres with same length and net gain levels. The total pump power required to obtain particular net gain levels for both SMF and DCF are also shown in Figure 3. 16(c). The required pump power is much higher than that of DCF due to having smaller Raman gain coefficient. For example to get 30dB signal net gain, an additional 3W pump power is required in case of SMF compared with DCF.
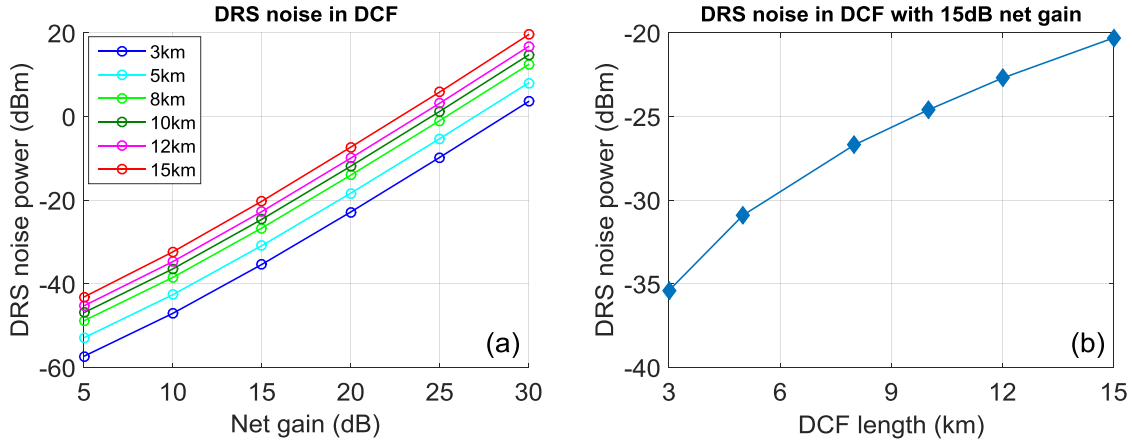
Figure 3. 17. (a) DRS noise vs. net gain for different amplifier span lengths and (b) DRS noise vs. span lengths at fixed 15dB net gain in DCF based discrete Raman amplifier

In Figure 3. 17(a), it is shown that DRS noise increases with increasing net gain at different span lengths. At a fixed net gain level, the increase in DRS noise can be as large as 15dB when DCF length increases from 3km to 15km as shown in Figure 3. 17(b).

3.5.3.3   *Relative intensity noise*

One of the major challenges of Raman amplifier is the relative intensity noise (RIN) transfer from pump to signal, which may counter balance the noise performance benefits of Raman amplifier if not designed properly. Any intensity fluctuations in the pump laser source is transferred to the signal due to the extremely fast stimulated Raman scattering process in the order of femto-seconds [22, 124]. The Raman gain depends exponentially on the pump power, so any fluctuations of pump power will result in larger fluctuations in the amplified signal power. However, the strength of this pump to signal noise transfer depends on many factors such as: pumping direction, amplifier length and the walk-off parameter between the pump and signal frequency determined by the dispersion parameter of the fibre [101]. The intensity fluctuation in a pump laser is usually defined by the ratio between the variance of intensity fluctuations and average power and called as RIN. It represents the spectrum of the intensity or power fluctuations and expressed as [101]:

$$\frac{\sigma_P^2}{\langle P_P \rangle^2} = \int_0^\infty RIN_P(f) df \qquad (3.21)$$

$$\frac{\sigma_S^2}{\langle P_S(L) \rangle^2} = \int_0^\infty RIN_S(f) df \qquad (3.22)$$

where, the variance of pump and signal power are defined by σ_P^2 and σ_S^2. The average pump and signal power at the end of the amplifier span are also given by $\langle P_P \rangle^2$ and $\langle P_S(L) \rangle^2$ respectively. The increase in intensity noise level at a particular frequency (f) is defined by the frequency dependent RIN transfer function:

$$H(f) = \frac{RIN_S(f)}{RIN_P(f)} \qquad (3.23)$$

In the calculation of RIN transfer function, it has to be considered that pump and signal travels at different group velocity due to having different wavelength. The group velocity difference or walk-off between the pump and signal is determined by the dispersion (D) parameter of the fibre. Large walk-off value means pump and signal are travelling at different speeds and transfer of intensity fluctuations from pump to signal is less. The pumping configuration with respect to the signal is also very important. In forward pumped Raman amplifier, pump and signal propagate along the fibre in same direction with slightly different group velocities (in low dispersion fibre) allowing the highest overlap of signal and pump time windows. So any fluctuations in the pump power remains in the same temporal window and transfer to the signal. In the fibre with large dispersion, the signal is moved out of the temporal window of noisy pump and experienced with an average gain. The averaging effect is very strong in case of backward pumping where pump and signal are propagating in opposite direction, because of very large relative speed difference. The pump power fluctuations are averaged out and minimum RIN is transferred to the signal. So backward pumping is the best pumping configuration in Raman amplifier even though the noise performance is worse than bidirectional pumping.
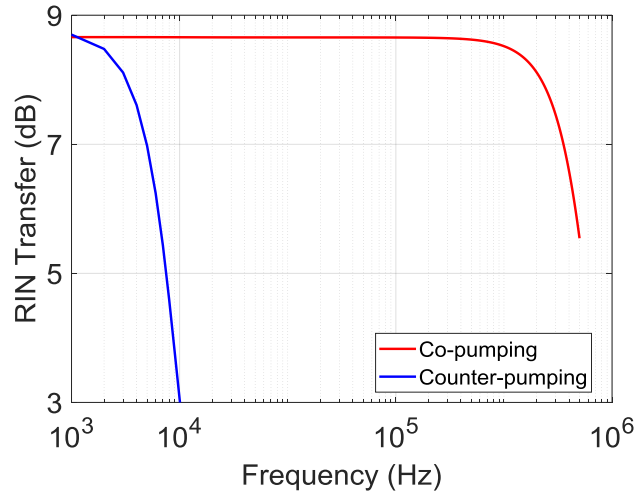
Figure 3. 18. RIN transfer function for co- (forward) and counter- (backward) pumped distributed Raman amplifier with 60km SSMF

Figure 3. 18 shows the calculated RIN transfer function for a distributed Raman amplifier consisted of a 60km SSMF span with 0dB net loss across the span, 1455nm 1st order pump and a signal at 1550nm. Although the absolute values of maximum RIN transfer are similar (8.7dB) for both co- (forward) and counter- (backward) propagating pumping schemes, however the 3dB corner frequency is much higher for co-propagating pumping at ~50MHz than that of counter-propagating scheme at ~7kHz. Details of the numerical simulation of signal RIN in Raman amplifiers are given in section 4.3 of chapter 4.

Efficient pump to signal RIN transfer reduction techniques are required in order to utilize the noise performance benefits in long-haul WDM transmission system. Bidirectional pumping scheme with optimized forward pump power is required to reduce the RIN transfer and improve the OSNR performance in Raman amplified transmission systems.

3.5.3.4 *Polarisation mode dispersion*

Polarisation mode dispersion (PMD) also has significant impacts on Raman gain. Raman gain is polarisation sensitive and maximum gain is achieved when both signals and pumps are co-polarised and maintain their state of polarisation (SOP) during propagation. However due to residual birefringence of silica fibre, SOP changes randomly and cause PMD. In most of the cases, depolarised pump is used in Raman amplification process and effective Raman gain is considered to be half of the co-polarised gain. PMD increases fluctuations of signal in time domain and average Raman gain is reduced in this process. It has been experimentally shown that increasing

differential group delay (DGD) values due to PMD of silica fibre cause more distortion of signal and Raman gain [125]. Polarisation maintaining fibre (PMF) can be used to maintain the SOP and reduce gain distortion in Raman amplifiers.

3.5.3.5 *Kerr nonlinearities*

Another challenge of using multiple Raman pumps for wideband application is the location of ZDW in between pumps or pump and signals. This will give rise to four wave mixing products due to the nonlinear interaction between pump-pump or pump-signals and FWM sidebands will fall in the signal bands and deplete pump powers. A severe degradation of OSNR will happen in those channels. If ZDW lies close to the longest wavelength pump then there will be more FWM sideband generation in the signal band because of significant phase matching over longer amplification length. R. E. Neuhauser and co-workers demonstrated that FWM sideband products are severe in broadband Raman amplifiers and depend on mainly high pump power of longest wavelength pumps, choice of pump wavelengths, fibre characteristics and pumping directions [126]. Pump-signal FWM was also experimentally described in distributed Raman amplifier and shown up to 2~3 dB Raman gain degradation in case of minimum phase matching [127]. FWM products can be removed by choosing pumps at unequal spacing, deleting affected signal channels which in turns reduces capacity, reducing longest wavelength pump power, modulating pump amplitude, increasing local dispersion in the fibre and so on.

CHAPTER 4

NUMERICAL MODELLING OF RAMAN AMPLIFIERS

Raman amplification in a medium is occurred through a nonlinear process called stimulated Raman scattering (SRS) [39]. SRS was first observed in silica fibre in 1972 by Stolen et al. [128]. In optical fibre SRS has relatively high threshold (~1W) with CW pump beam. Raman amplification can be achieved in any pumping configuration such as: forward, backward and bidirectional because of the isotropic property of SRS effect. Here, we will discuss different Raman amplification techniques by numerically describing the evolution of signal, pump and noise powers along amplifier span using standard average power model.

The numerical model of Raman amplifier used in this chapter has been implemented by the author of this thesis, under the supervision of Dr Juan Diego Ania-Castañón, director IO-CSIC, Madrid, Spain. Useful advices were taken from Giuseppe Rizzelli, Francesca Gallazzi from IO-CSIC and Auro Perego from AIPT. The Raman amplifiers' performance parameters (i.e. noise, gain, signal power evolution etc) modelled in this chapter are also compared and validated with already published results for different Raman pumping schemes in the literatures [15, 129].

4.1   Simple Model with Single Pump and Signal

A typical bidirectional Raman pumping scheme with 1st order 1455nm pumps is shown in Figure 4. 1. The Raman pumps provide gain mainly around 1550nm signals which are propagating in the forward direction through the single mode fibre (SMF).
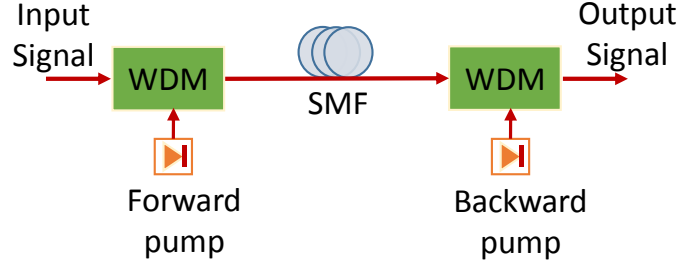
Figure 4. 1. Schematic diagram of typical bidirectional Raman amplifier

In the simplest Raman amplifier model, only fibre attenuation and interaction between pump and signals are taken into account. Under this assumptions, the evolution of pump, P_p and signal, P_s along the longitudinal axis of the fibre z can be expressed by the following equations [101]:

$$\frac{dP_p^{\pm}}{dz} = \mp\alpha_p P_p^{\pm} \mp \frac{\omega_p}{\omega_s} g_R P_s P_p^{\pm} \tag{4.1}$$

$$\frac{dP_s}{dz} = -\alpha_s P_s + g_R\left(P_p^{+} + P_p^{-}\right)P_s \tag{4.2}$$

where P_s and $P_P^{\pm}$ represent the powers of signal, forward (+) and backward (-) propagating pump respectively. α_P and α_s are the corresponding attenuation coefficients at pump and signal frequencies respectively. g_R is the Raman gain coefficient expressed in $W^{-1}km^{-1}$, which is calculated as the ratio between Raman gain coefficient in m/W and effective area of the fibre (A_{eff}) in m^2 at the pump frequency. The pump and signal frequencies are denoted by ω_p and ω_s respectively. This analysis does not include the impact of amplified spontaneous emission (ASE) noise and Rayleigh backscattering. If we consider small signal amplification and no pump depletion, Eq. (4.1) can be simplified as:

For forward propagating pump: $P_p^{+}(z) = P_p(0)\exp[-\alpha_p z]$ (4.3)

For backward propagating pump: $P_p^{-}(z) = P_p(L)\exp[-\alpha_p(L-z)]$ (4.4)

Substituting the pump equation into Eq. (4.2) results in the analytical solution of the signal power at the end of the amplifier span as:

$$P_s(L) = P_s(0)\exp(g_R P_0 L_{eff} - \alpha_s L) \tag{4.5}$$

with P_0 being the input pump power either $P_p(0)$ or $P_p(L)$ or $(P_p(0)+ P_p(L))$ depending on the pumping configuration. L_{eff} represents the effective fibre length and defined as:

$$L_{eff} = \frac{[1-\exp(-\alpha_p L)]}{\alpha_p}$$

(4.6)

Now if we want to include ASE noise and Rayleigh backscattering, the simple model described above can be expanded by introducing two new equations for the forward and backward propagating noise.

$$\frac{dP_p^\pm}{dz} = \mp\alpha_p P_p^\pm \mp \frac{\omega_p}{\omega_s} g_R \left(P_s + n_s^+ + n_s^- + 4h\omega_s\Delta\omega_s \left(1 + \frac{1}{\exp\left(\frac{h(\omega_p-\omega_s)}{K_B T}\right)-1} \right) \right) P_p^\pm$$

(4.7)

$$\frac{dP_s}{dz} = -\alpha_s P_s + g_R\left(P_p^+ + P_p^-\right)P_s$$

(4.8)

$$\frac{dn_s^+}{dz} = -\alpha_s n_s^+ + g_R\left(P_p^+ + P_p^-\right)\left(n_s^+ + 2h\omega_s\Delta\omega_s \left(1 + \frac{1}{\exp\left(\frac{h(\omega_p-\omega_s)}{K_B T}\right)-1} \right) \right) + \varepsilon n_s^-$$

(4.9)

$$\frac{dn_s^-}{dz} = \alpha_s n_s^- - g_R\left(P_p^+ + P_p^-\right)\left(n_s^- + 2h\omega_s\Delta\omega_s \left(1 + \frac{1}{\exp\left(\frac{h(\omega_p-\omega_s)}{K_B T}\right)-1} \right) \right) - \varepsilon\left(n_s^+ + P_s\right)$$

(4.10)

where n_s^+ and n_s^- are the forward and backward propagating noise at the signal frequency (ω_s), $\Delta\omega_s$ is the signal bandwidth, K_B is the Boltzmann's constant, T is the absolute temperature and ε is the Rayleigh backscattering coefficient. The estimation of optical signal to noise ratio (OSNR) at the end of the amplifier is possible with this model by calculating the signal and total noise power separately. The system of ordinary differential equations (ODEs) for Raman amplifiers (Eqs. (4.7)-(4.10)) were solved using MATLAB's default "bvp4c" function which is implemented as boundary value problem with three-stage Lobatto IIIa formula [130]. The step size in the numerical analysis was 100m and the offset accuracy level was set to 10^{-5}.

For example, a bidirectonally pumped distributed Raman amplifier was considered first with 100km long span of standard single mode fibre (SSMF). First order pump at 1455nm and 1550nm signal were considered for the amplifier design. Signal and total pump power were 1mW and 700mW respectively. For SSMF, attenuation coefficients at 1455nm and 1550nm were considered to be 0.19dB/km and 0.27dB/km. Rayleigh backscattering coefficient was 4.3×10^{-5} km^{-1}. Since P_s << P_p, pump depletion was considered to be negligible. The peak Raman gain coefficient for the 1455nm pump was chosen as 0.43W^{-1}km^{-1}. The distribution of power of different forward and backward propagating pump, signal and noise fields are given in Figure 4. 2.
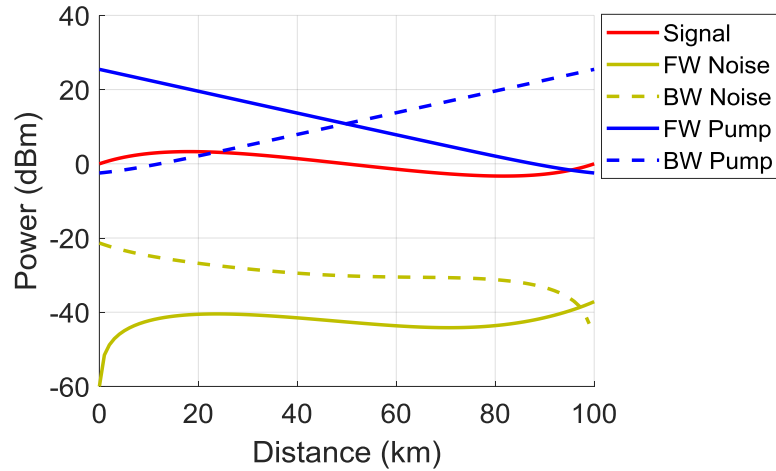
Figure 4. 2. First order bidirectional distributed Raman amplifier: evolution of signal, pump and noise fields (FW = forward, BW = backward)

A symmetric bidirectional pumping was considered in Figure 4. 2 with total pump power divided equally between forward and backward pumps. Total signal power variation (SPV) was 6.6dB over 100km span. The output OSNR (37.2dB) was also calculated at the end of the amplifier span from the total forward propagated noise and output signal power, considering 125GHz of noise bandwidth.

We have also observed how the total noise power at the end of the span could be improved by increasing the input forward pump power. Increasing the forward pump power ratio with respect to the total pump power improves the input end gain and noise performance as shown in Figure 4. 3.
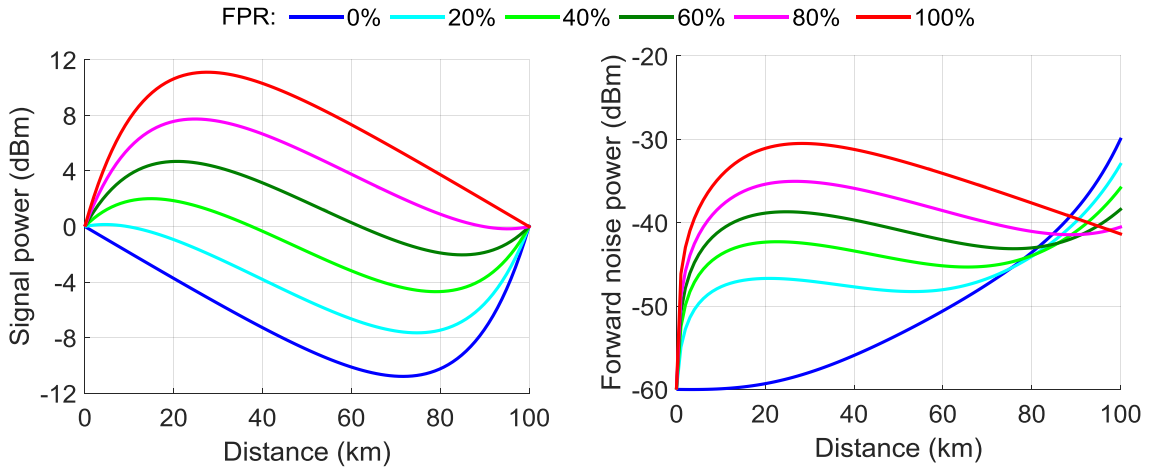
Figure 4. 3. (a) SPVs and (b) evolution of forward propagated noise at increasing forward pump power ratios (FPRs)

In a distributed Raman amplifier (DRA) with 100km SSMF span and 0dB net gain at the output, Figure 4. 3(a) and (b) show how the distribution of signal power and forward propagated ASE noise evolve over the amplifier span respectively. With increasing forward pump power ratios, most of the noise from ASE is generated at the input of the amplifier which then experiences high level of attenuation during propagation along the fibre. Thus the impact of total noise at the end of the span is reduced at higher forward gain levels. The calculated output OSNRs and output noise levels at increasing forward pump power ratios are given in Figure 4. 4.
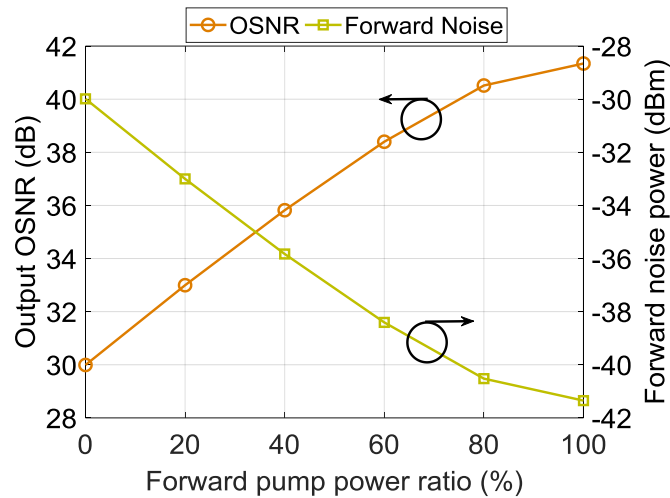
Figure 4. 4. Comparison of output OSNR and output noise power levels at increasing forward pump power ratios

In Figure 4. 4, output OSNR increases and forward propagated noise power decreases with increasing forward pump power (FPP) ratios. An 11dB reduction in output noise level shows a

84

similar level of OSNR improvement when FPP ratio is increased from 0% (backward only) to 100% (forward only).

4.2 Higher Order Distributed Raman Amplification using Ultra-long Raman Fibre Laser

In higher order DRA, Raman gain to the signal is provided from pumps which are usually two (2nd order), three (3rd order) or more Stokes shift away from the signal band. In usual configuration, all the pumps are cascaded together where higher order pump amplify the lower order pump to subsequently amplify the signal. An obvious benefit of using this configuration is to distribute the gain further into the span and improve the signal power distribution along the amplifier span. In dual order pumping configuration, a 2nd order (1366nm) pump and 1st order (1455nm) pump are usually combined together to provide gain in C band signals, in which the main gain contribution comes from the 2nd order pump with high power and 1st order pump acts as a seed with lower power.

Ultra-long Raman fibre laser (URFL) based amplifier is also a higher order distributed Raman amplifiers, where the main contribution comes from a higher order pump (i.e. 1366nm) and intermediated lower order pump(s) (i.e. 1455nm) is generated in a fibre laser cavity using high reflectivity fibre Bragg grating (FBG) at that wavelength(s). In 2nd order bidirectional URFL based amplifier as shown in Figure 4. 5, the intermediated 1st order pump at 1455nm pump is created in Raman fibre laser cavity consisted of a standard single mode fibre (SSMF) and two 99% reflectivity FBGs at each end acting like mirrors.
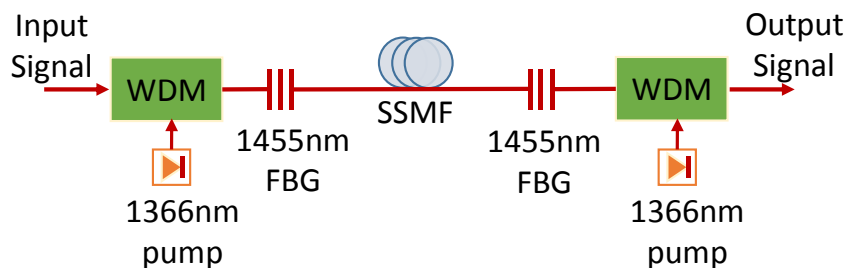
Figure 4. 5. Schematic diagram of a 2nd order bidirectional distributed URFL based amplifier

In Figure 4. 5, the primary 1366nm pump provides Stokes shifted light around 1455nm. The two FBGs at each end and the fibre span forms a cavity, feeding back the first Stokes shifted 1455nm light from the 1366nm pumps. When 1366nm primary pumps have enough power above the

required threshold for the SRS to overcome the fibre attenuation of 1st Stokes, a stable ultra-long cavity laser at secondary pump wavelength (1455nm) is formed across the span from the ASE in the cavity. The 1455nm cavity laser shows very little variation across the span and provides nearly constant gain for the signal in C band. The cavity configurations can be changed for broadband amplification by changing the FBG wavelength and reflectivity properties [131]. The real benefits of using URFL based amplification is to get quasi-lossless transmission and replacement of 1st order pump lasers by the passive FBGs [15]. The numerical model of this type of 2nd order distributed Raman amplifier could be described by the set of ODEs from Eqs. (4.11) – (4.15) [15]:

$$\frac{dP_{P1}^{\pm}}{dz} = \mp \alpha_1 P_{P1}^{\pm} \mp g_1 \frac{\omega_1}{\omega_2} P_{P1}^{\pm} \left(P_{P2}^{+} + P_{P2}^{-} + 4h\omega_2\Delta\omega_2 \left(1 + \frac{1}{\exp\left(\frac{h(\omega_1-\omega_2)}{K_BT}\right)-1} \right) \right) \pm \varepsilon_1 P_{P1}^{\mp} \tag{4.11}$$

$$\frac{dP_{P2}^{\pm}}{dz} = \mp \alpha_2 P_{P2}^{\pm} \pm g_1 \left(P_{P2}^{+} + P_{P2}^{-} + 2h\omega_2\Delta\omega_2 \left(1 + \frac{1}{\exp\left(\frac{h(\omega_1-\omega_2)}{K_BT}\right)-1} \right) \right)\left(P_{P1}^{+} + P_{P1}^{-} \right)$$

$$\mp g_2 \frac{\omega_2}{\omega_S} P_{P2}^{\pm} \left(P_S + N_S^{+} + N_S^{-} + 4h\omega_S\Delta\omega_S \left(1 + \frac{1}{\exp\left(\frac{h(\omega_2-\omega_S)}{K_BT}\right)-1} \right) \right) \pm \varepsilon_2 P_{P2}^{\mp} \tag{4.12}$$

$$\frac{dP_S}{dz} = -\alpha_s P_S + g_2 P_S \left(P_{P2}^{+} + P_{P2}^{-} \right) \tag{4.13}$$

$$\frac{dN_S^{+}}{dz} = -\alpha_S N_S^{+} + g_2 \left(N_S^{+} + 2h\omega_2\Delta\omega_2 \left(1 + \frac{1}{\exp\left(\frac{h(\omega_2-\omega_S)}{K_BT}\right)-1} \right) \right)\left(P_{P2}^{+} + P_{P2}^{-} \right) + \varepsilon_S N_S^{-} \tag{4.14}$$

$$\frac{dN_S^{-}}{dz} = \alpha_S N_S^{-} - g_2 \left(N_S^{-} + 2h\omega_2\Delta\omega_2 \left(1 + \frac{1}{\exp\left(\frac{h(\omega_2-\omega_S)}{K_BT}\right)-1} \right) \right)\left(P_{P2}^{+} + P_{P2}^{-} \right) - \varepsilon_S \left(P_S + N_S^{+} \right) \tag{4.15}$$

where, (+) and (-) superscripts represent the forward and backward propagating fields respectively. The subscripts 1, 2 and S denote the primary 1366nm pump, secondary 1455nm lasing and signal respectively. P_{Pi} *(i=1, 2)* are the respective pump powers, P_S and N_S are the signal and noise power

at signal frequency respectively. The effective bandwidth of the secondary pump and signal are denoted by $\Delta\omega_2$ and $\Delta\omega_S$ respectively. The respective Raman gain coefficients and Rayleigh backscattering coefficients for each pump are given by g_i and ε_i. The frequencies of pump and signal components are represented by ω_i and ω_S respectively. Rest of the parameters are same as described before. The boundary conditions to solve the system of ODEs are given as:

$$P_{P1}^+(0) = P_{P1}^+(L) = P_0 \tag{4.16}$$

$$P_{P2}^+(0) = R_1 P_{P2}^-(0) \tag{4.17}$$

$$P_{P2}^-(L) = R_2 P_{P2}^+(L) \tag{4.18}$$

$$N_S^+(0) = N_0 \tag{4.19}$$

$$N_S^-(L) = 0 \tag{4.20}$$

$$P_S(0) = P_{IN} \tag{4.21}$$

where, L is the length of the amplifier span and R_1 and R_2 are the reflectivity of the input (span length = 0) and output (span length = L) end FBGs respectively. P_0 and P_{IN} represents the input 1366nm pump and signal power respectively. The parameters used in the numerical simulation are summarized in Table 4. 1 [15].

Table 4. 1. Parameters used in the numerical simulation of URFL based distributed Raman amplifiers [15]

Parameter	Symbol	Value	Unit
Signal frequency	ω_S	193.414	THz
Signal bandwidth	$\Delta\omega_S$	125	GHz
Raman gain coefficient at 1366nm	g_1	0.53	$W^{-1}km^{-1}$
Raman gain coefficient at 1455nm	g_2	0.43	$W^{-1}km^{-1}$
Rayleigh scattering coefficient at 1366nm	ε_1	1×10^{-4}	km^{-1}
Rayleigh scattering coefficient at 1455nm	ε_2	6×10^{-5}	km^{-1}
Rayleigh scattering coefficient at 1550nm	ε_S	4.3×10^{-5}	km^{-1}
Pump attenuation at 1366nm	α_1	0.38	dB/km
Pump attenuation at 1455nm	α_2	0.27	dB/km
Signal attenuation at 1550nm	α_S	0.19	dB/km
Plank's constant	h	6.626×10^{-34}	J-s
Boltzmann's constant	K_B	1.38×10^{-23}	J/K
Absolute temperature	T	298	K

The numerical simulation of URFL based dual order distributed Raman amplifier was obtained considering different span lengths and 0dBm input signal power into the span. The effective bandwidth of the generated 1st order lasing at 1455nm was determined by the bandwidth of the FBG, which was considered to be 125GHz. Different features like SPV along the amplifier span, output OSNR and self-phase modulation (SPM) induced nonlinear phase shift (NPS) were characterized in the URFL based distributed Raman amplifier setup. Output OSNR were characterized over 12.5GHz noise bandwidth. OSNR and NPS expressions are given in Eq. (4.22) and (4.23) respectively.

$$OSNR(dB) = 10\log_{10}\left(\frac{P_S(L)}{N_s^+(L)}\right) + 10\log_{10}\left(\frac{B_m}{B_{ref}}\right) \tag{4.22}$$

$$NPS(rad) = \gamma\int_0^L P_S(z)dz \tag{4.23}$$

where, $P_s(L)$ and $N_s^+(L)$ represent the signal and noise power respectively at the end of the amplifier. B_m and B_{ref} denotes the noise equivalent bandwidth (125GHz) and reference optical bandwidth (12.5GHz) respectively. In Eq. (4.23), NPS is calculated by the multiplication of nonlinear coefficient of the SSMF and integral of the signal power profile over the span length (L).
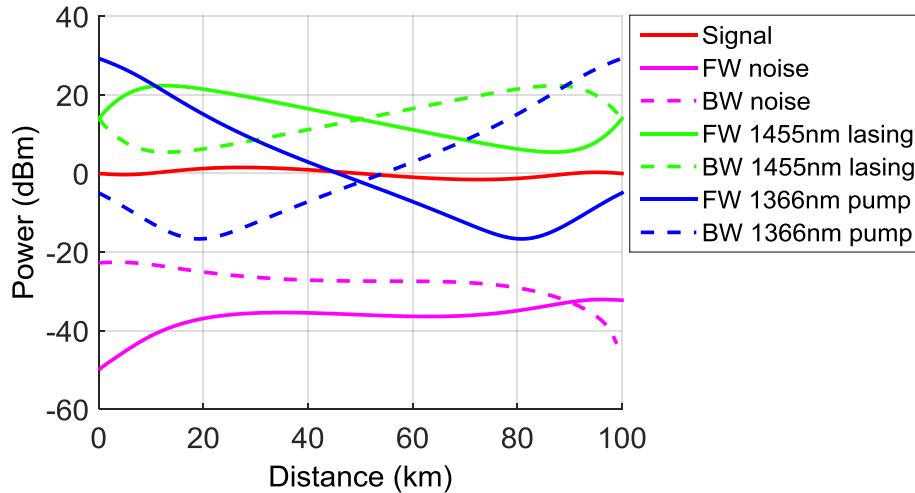
Figure 4. 6. Numerical simulation of distribution of signal, pumps and noise powers along the URFL based 100km bidirectional DRA (FW = forward, BW = backward)

Figure 4. 6 shows the evolution of different field powers in a symmetrically pumped URFL based bidirectional DRA with 100km SSMF span. A total 1.7W of 1366nm pump power is required to maintain 0dB net gain level at the end of the amplifier span. The forward and backward propagating 1st order lasing are first amplified by the 2nd order 1366nm pump and subsequently amplify the 1550nm signal. A quasi-lossless signal power distribution with 3.1dB SPV is observed, which is 3.5dB better than the bidirectional 1st order pumped DRA using symmetric pumping as shown in Figure 4. 2. The output forward noise power at the end of the amplifier span is -37.6dBm which is about 0.4dB lower than that of 1st order bidirectional pumping scheme as shown in Figure 4. 2. So, higher order pumping has better noise performance than 1st order pumped DRA scheme. But the benefit comes at a cost of poor pump to signal power conversion efficiency as high power 2nd order pumps are required to push the gain further into the span. Although it is presumable that, increasing the reflectivity of FBGs improves the 1366nm pump power efficiency, however it does not always ensures the optimum quasi-lossless signal power profile with minimum SPV. So it is possible to reduce the SPV by reducing the FBG reflectivity at both ends without compromising the pump power efficiency too much. In Figure 4. 7, we show the different SPVs and required total pump powers as we vary the FBG reflectivity at both ends in a 100km SSMF URFL span with symmetric bidirectional pumping.
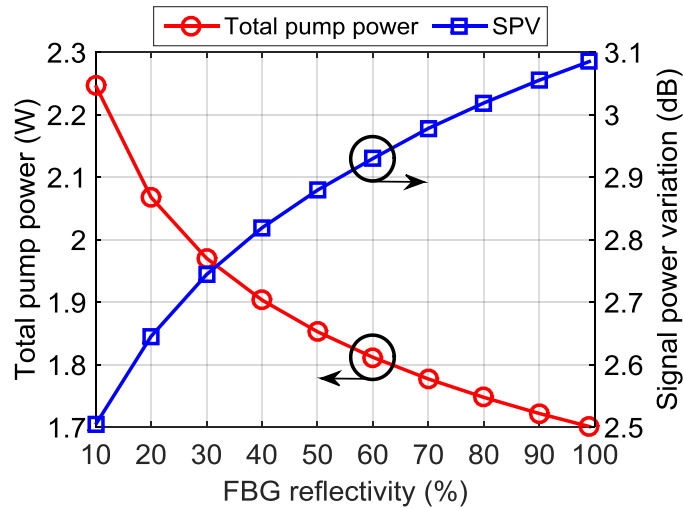
Figure 4. 7. Total pump powers required and SPVs at varying FBG reflectivity in URFL based DRA with 100km span

In URFL with long span length such as 100km, SPV improvement of 0.6dB is possible by reducing the FBG reflectivity from 99% to 10% without compromising the pump power requirement too much. Additional 550mW 1366nm pump power is required at 10% reflectivity. The impact of FBG reflectivity on SPV reduction gets insignificant at very long span lengths i.e. for unrepeatered

transmission with span length over 200km. Whereas, reducing the FBG reflectivity in shorter span lengths increases the SPVs and also shows a rapid increase in the pump power requirements [132]. A detailed characterisation on SPV and required pump power with varying FBG reflectivity and span lengths are presented in [132]. Here, we have also investigated how the total pump power and SPV change with increasing span lengths with fixed 99% FBG reflectivity based URFL configurations as shown in Figure 4. 8.
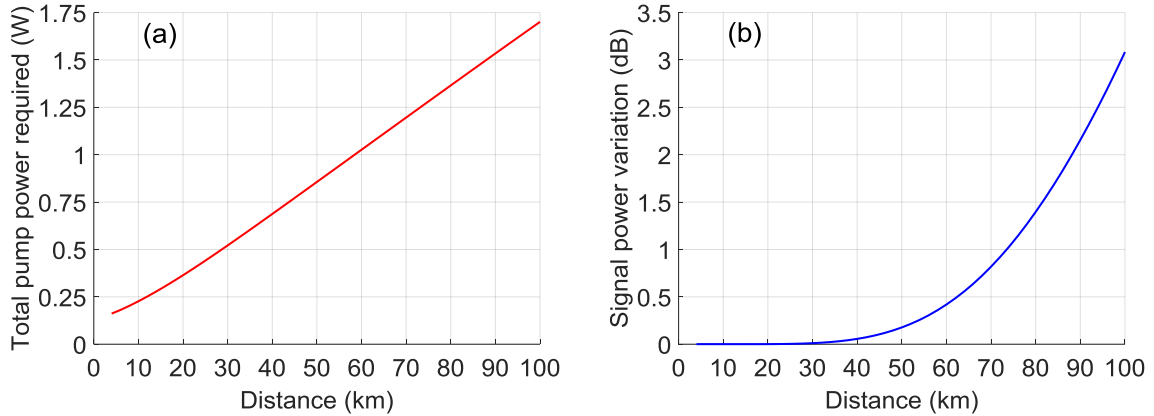
Figure 4. 8. Total pump powers required and SPVs for varying span lengths of URFL based DRA with 99% FBG reflectivity and symmetric pumping

In Figure 4. 8(a) and (b), both total pump power and SPV increase with increasing span length when very high reflectivity (99%) FBGs are used in symmetrically pumped URFL based DRA. So high reflectivity allows both pump efficiency and better signal power excursion in shorter span lengths. This is opposite to the case with longer span lengths (i.e. 100km), in which SPVs are improved with lowering the FBG reflectivity at the cost of reduced pump power efficiency as shown in Figure 4. 7.

Although bidirectional URFL based DRA scheme provides improved OSNR performance by reducing the SPV along the span, however this benefits are counterbalanced by the strong impact of relative intensity noise (RIN) transfer from forward pumps to signal. The detailed transmission performance analysis has been presented by M. Tan et al. in [14], where they have shown that URFL based DRA performance is highly dominated by the RIN transfer and achieved even lower transmission reach compared with conventional dual order backward only pumping with DP-QPSK coherent WDM transmission system. To mitigate the deleterious impact of RIN transfer from forward pumps to signal, a random distributed feedback (rDFB) lasing based DRA scheme has been proposed with dual order bidirectional pumping scheme [133, 134], where input reflectivity

level was reduced closed to zero and transmission performance improvement was achieved. But the benefits comes at a cost of low pump power efficiency due to the lack FBG reflectivity at the 1st order pump wavelength. Here we have also investigated dual order DRA scheme with varying input end FBG reflectivity to determine different characteristics of these type of distributed Raman amplifiers.
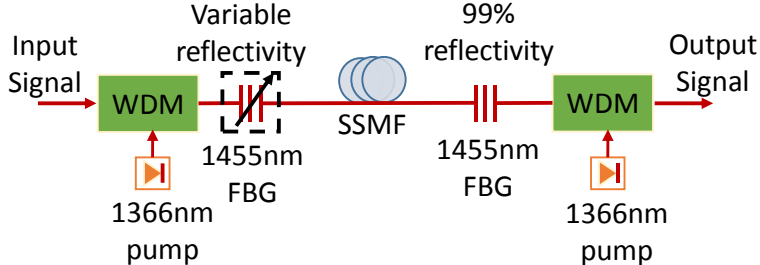
Figure 4. 9. Dual order Raman fibre laser based DRA with variable input reflectivity FBG

In Figure 4. 9, input FBG reflectivity levels are varied from 0 to 99%, whereas the output FBG reflectivity is fixed at 99%. At 0% input reflection, a random DFB laser cavity is formed at 1455nm across the amplifier span [129] in a half-open cavity configuration [135]. At 99% input reflectivity, it acts like URFL based DRA as discussed above. The input signal at 1550nm and 1366nm pump are coupled into the fibre span considering a 3-by-1 WDM coupler. At variable reflectivity levels, the un-reflected part of 1455nm lasing is considered to be dumped through the 14xx port of the input end WDM. Input signal power is 0dBm and total pump power is adjusted to maintain 0dB net gain at the output of the amplifier.
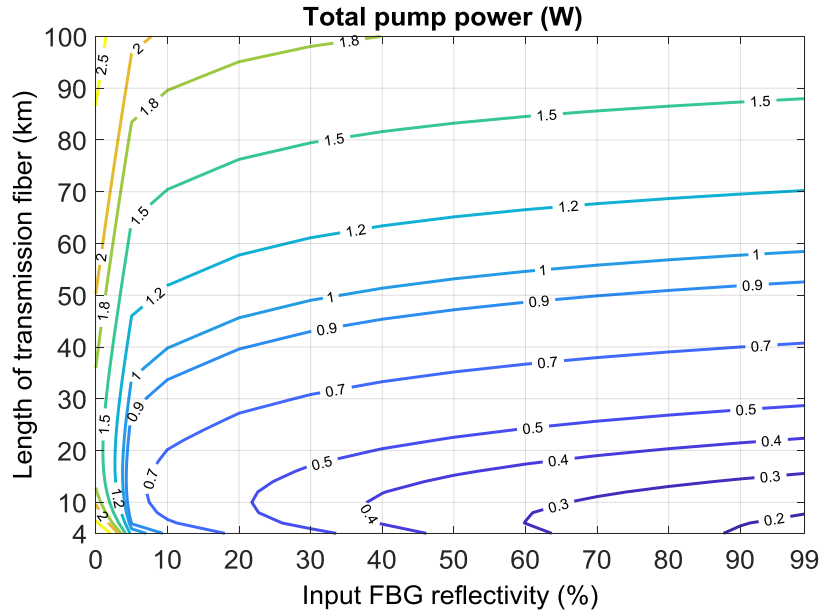
Figure 4. 10. Contour plot of total pump power required at different span lengths and input FBG reflectivity in Raman fibre laser based DRA

The contour plot in Figure 4. 10 shows the total pump power required at different levels of input reflectivity and span lengths with symmetric bidirectional pumping. An additional ~1W total pump power is required if input reflectivity is reduced down to 0% from 99% for almost all the lengths mainly due to the inefficiency of energy conversion from forward 1366nm pump to 1550nm signal in the absence of the intermediate 1st order pump. Inclusion of small input reflection level ~10%, improves the pump power efficiency significantly by reducing the required total pump power by ~500mW. Increasing the input end reflection should also increase the efficiency of forward Stokes at 1455nm and improve OSNR.
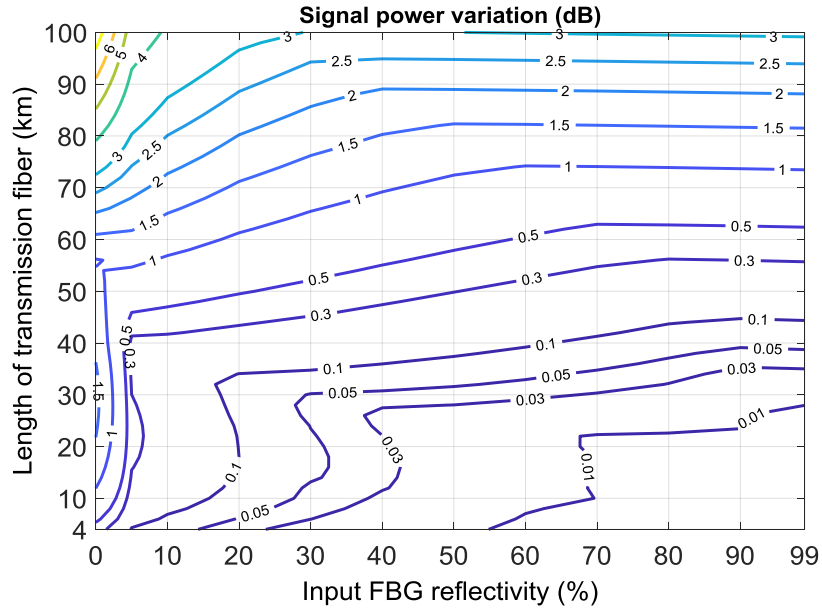
Figure 4. 11. Contour plot of signal power variations (SPVs) at different span lengths and input FBG reflectivity in Raman fibre laser based DRA

In Figure 4. 11, SPV increases with increasing span length at a fixed input reflectivity level. At only 10% input FBG reflection, very small SPV < 0.5dB can be achieved allowing span length up to 45km. Longer span lengths >80km introduces SPVs >1.5dB irrespective of the input reflection levels. If we allow 1dB SPV, realistic distributed span lengths up to ~65km can be considered with only 30% input FBG reflection level and symmetric bidirectional pumping. So smaller lengths of Raman spans are better choice in terms of minimum SPV and quasi-lossless signal power distribution.

Output OSNR (dB)/0.1nm
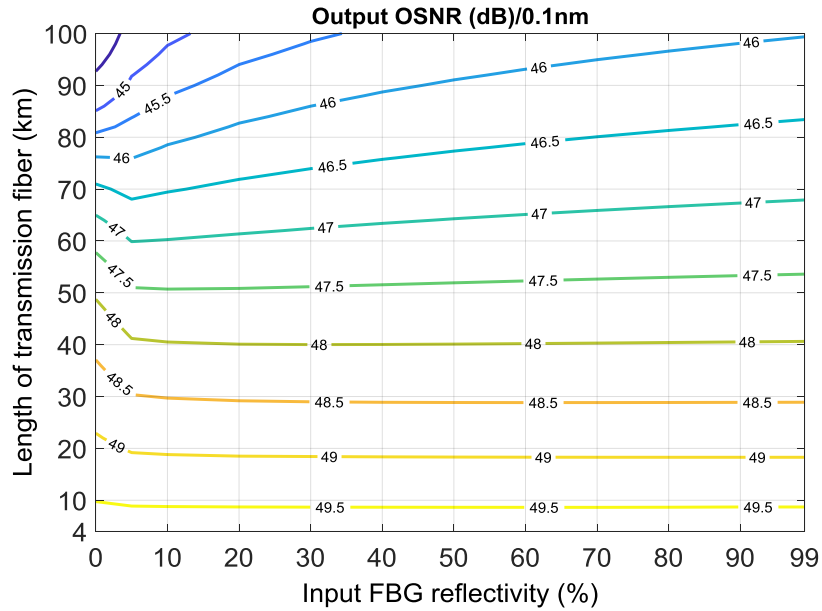
Figure 4. 12. Contour plot of output OSNR for different input reflectivity and transmission span lengths in a Raman fibre laser based DRA with symmetric bidirectional pumping

Figure 4. 12 shows the characteristics of output OSNR at different input FBG reflectivity and span lengths. The reduction of SPVs with increasing input reflectivity levels or in smaller span lengths as shown in Figure 4. 11, provides improved output OSNR in the amplifier. In Figure 4. 12, the best output OSNR is achieved at span lengths below 10km without even requiring any input FBG reflection, because the 1st order laser created by the backward 1366nm pump and output FBG is enough to maintain the signal gain almost lossless in such a short cavity ensuring maximum output OSNR. Interestingly with symmetric bidirectional pumping, input FBG reflectivity level comes into act for OSNR improvement for span lengths beyond 50km, whereas below 50km OSNR remains almost similar for input FBG reflection between 10-99% due to similar SPV performances where most of the gain contributions come from backward amplified 1455nm component [136] as shown in Figure 4. 11. Longer span lengths provide worse OSNR performances at fixed input FBG reflectivity but that can be improved by increasing the input end reflections.

So far we have observed that, in a symmetric bidirectional dual order pumping inclusion of input FBG reflection improves the pump power efficiency by reducing the lasing threshold of 1st order fibre laser generation in the cavity. The SPVs are also improved with increasing input reflection, however at shorter span lengths it is not that evident because of the dominant gain contribution from backward pumping.

Here, we also investigate the performance of pure rDFB 1st order lasing based DRA scheme with 0% input FBG reflection, which has the minimum RIN transfer from forward 1366nm pump to signal [21].
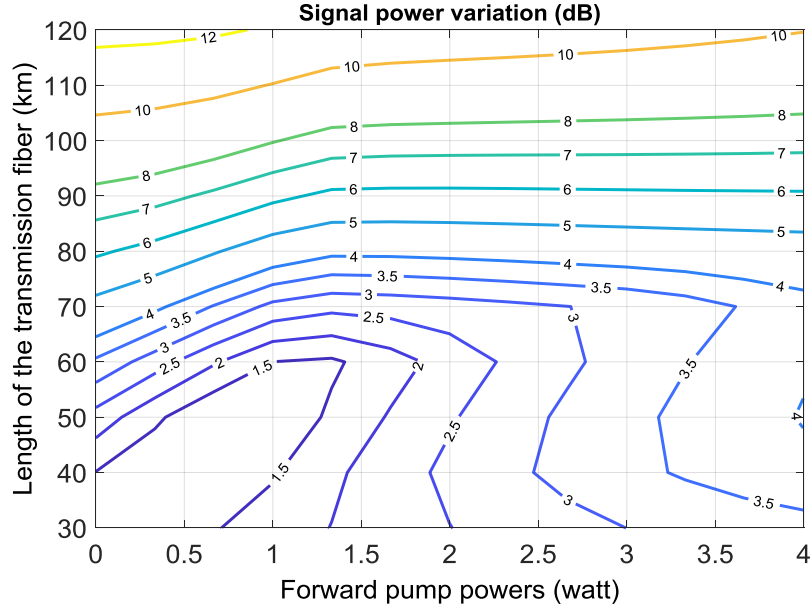
Figure 4. 13. Contour plot of signal power variations (SPVs) at different forward pump powers and span lengths in an rDFB lasing based bidirectional DRA

In Figure 4. 13 with rDFB based bidirectional DRA, SPVs increase with increasing span lengths at a fixed forward pump power. At span lengths <70km, the SPV decreases with increasing forward pump powers up to a certain level, then it starts increasing due to dominant forward gain contributions than backward pumping. There is no significant improvement of SPV with increasing forward pump powers for span lengths over 75km.

We also investigate the nonlinear penalty by calculating the NPS as described in Eq. (4.23). For a specific fibre as SSMF in this case, NPS depends on the signal power profile along the amplifier span. Figure 4. 14 shows the NPS values calculated from the signal power profiles at varying forward pump power levels at different span lengths. Here NPS values determine the level of SPM induced nonlinear penalty caused at different forward pump power levels. As expected, NPS increases with increasing forward pump powers at a fixed span length due to higher average signal power across the amplifier span, which can also described by the signal power profiles given in Figure 4. 15(a). On the other hand, NPS decreases with increasing span lengths beyond 60km at

fixed forward pump power, due to smaller average signal power across the span as shown in Figure 4. 15(b).
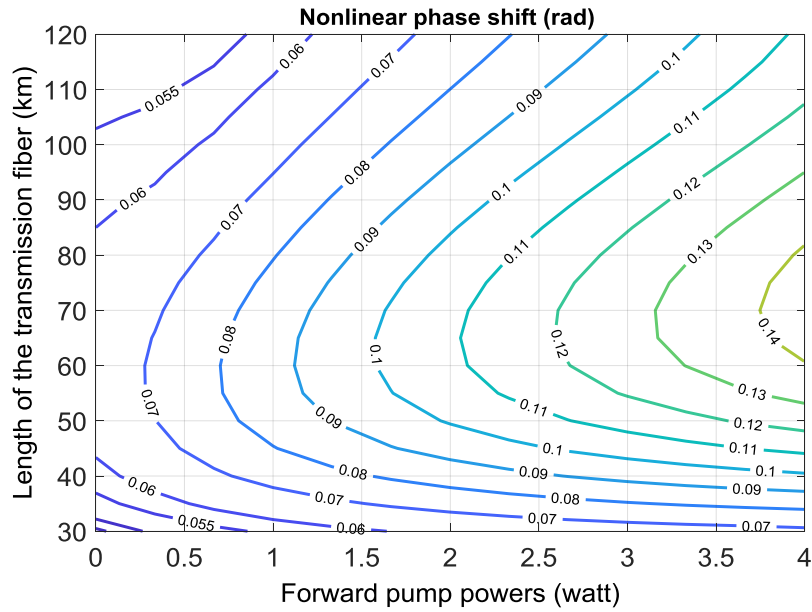
Figure 4. 14. Contour plot of nonlinear phase shift at varying forward pump powers and span lengths in an rDFB lasing based DRA
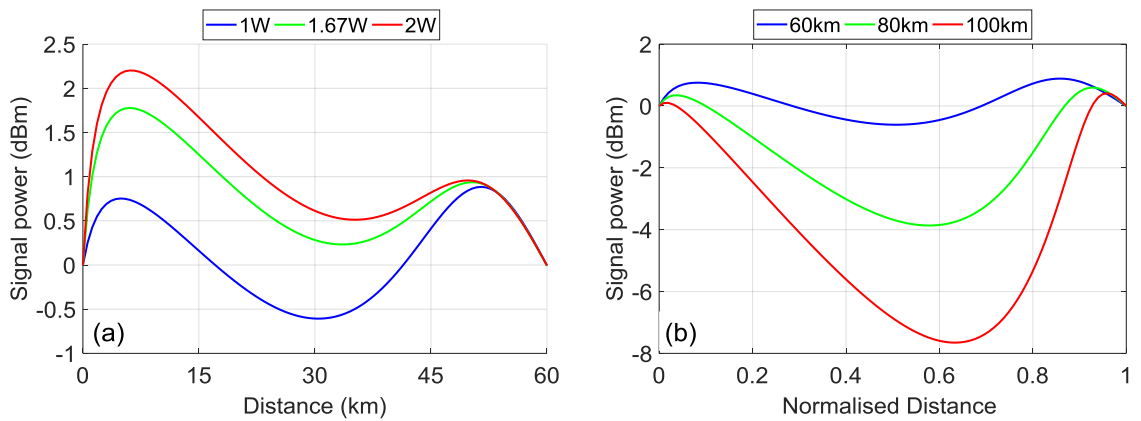
Figure 4. 15. (a) Distribution of signal power at different forward pump powers in 60km span length and (b) SPVs at different span lengths with 1W forward pump power

In order to investigate the impact of the forward pump powers in determining the SPV and corresponding NPS, the SPVs at varying forward pump powers with fixed 60km span length and varying span lengths at fixed 1W forward pump power are given in Figure 4. 15(a) and (b) respectively. When increasing forward pump powers dominates the forward gain over backward as

shown in Figure 4. 15(a), NPS increases due to higher average signal power. On the other hand, NPS decreases with increasing span lengths at fixed pump power due to lower average signal power along the span.

4.3   Numerical Modelling of RIN Transfer

In Raman amplifier, any fluctuations in the pump power will transfer to the signal providing additional intensity fluctuations in the signal power, which becomes a new source of noise known as relative intensity noise (RIN). If the output power of a laser source is defined by the following expression:

$$P(t) = P_0 + \Delta P(t) \tag{4.24}$$

where, P_0 and $\Delta P(t)$ represent the constant average power and random fluctuations of power with zero mean respectively. Then the relative fluctuation in the laser is represented by:

$$\delta P(t) = \frac{\Delta P(t)}{P_0} \tag{4.25}$$

Then the RIN can be expressed by the time-averaged mean square of the relative fluctuations:

$$RIN = \left\langle \delta P^2(t) \right\rangle = \frac{\left\langle \Delta P^2(t) \right\rangle}{P_0^2} \tag{4.26}$$

So RIN is defined by the ratio of the time-averaged mean square of the random fluctuations to the average power squared [137]. In case of Raman fibre laser, a second order 1366nm pump is used and a 1st order fibre laser is generated in the cavity. The main gain contribution comes from the high power higher order 1366nm pump. So, the RIN transfer from pump to signal is defined as [138]:

$$H_{2ndOrder}(\omega) = \left| \frac{RIN_S(\omega)}{RIN_{P1}^+(\omega)} \right| \tag{4.27}$$

where, $RIN_S(\omega)$ and $RIN_{P1}^+(\omega)$ represent the signal RIN level and pump RIN of 1366nm pump at different pump modulation frequency ω respectively, which are calculated following the Eq. (4.26). In Eq. (4.26), the average power in the denominator can be calculated from the power obtained at the end of the amplifier following the solutions from the system of ODEs described in Eqs. (4.11) – (4.15) with proper boundary conditions defined in Eqs. (4.16) – (4.21). For the determination of average intensity fluctuation for each spectral component considered in the

amplifier design, additional ODEs related to the evolution of RIN from primary pump and 1st Stokes or secondary pump propagating both in forward and backward direction and signal are needed to be defined and solved numerically with other average power equations for signal, pump and noise in Eqs. (4.11) – (4.15) [22, 139].

$$\frac{dn_1^{\pm}}{dz} = -id_1^{\pm}\omega n_1^{\pm} \mp \alpha_1 n_1^{\pm} \mp g_1 \frac{\omega_1}{\omega_2} P_{P1}^{\pm}\left(n_2^+ + n_2^-\right) \mp g_1 \frac{\omega_1}{\omega_2}\left(P_{P2}^+ + P_{P2}^-\right)n_1^{\pm} \pm \varepsilon_1 n_1^{\mp}$$ (4.28)

$$\frac{dn_2^{\pm}}{dz} = \left\{ \begin{array}{l} -id_2^{\pm}\omega n_2^{\pm} \mp \alpha_2 n_2^{\pm} \pm \varepsilon_2 n_2^{\mp} \\[2mm] \pm g_1 \frac{\omega_1}{\omega_2} P_{P2}^{\pm}\left(n_1^+ + n_1^-\right) \pm g_1 \frac{\omega_1}{\omega_2}\left(P_{P1}^+ + P_{P1}^-\right)n_2^{\pm} \\[2mm] \mp g_2 \frac{\omega_2}{\omega_S} P_{P2}^{\pm} n_S \mp g_2 \frac{\omega_2}{\omega_S} n_2^{\pm} P_S \end{array} \right\}$$ (4.29)

$$\frac{dn_S}{dz} = -\alpha_S n_S + g_2 P_S\left(n_2^+ + n_2^-\right) + g_2 n_S\left(P_2^+ + P_2^-\right) + \varepsilon_S n_S^-$$ (4.30)

where, $n_i^{\pm}$ ($i=1,2$) and n_S represent the forward (+) and backward (-) spectral density of amplitude noise of pump (s) and the forward propagating signal respectively. Subscripts 1 and 2 are for 2nd order 1366nm and 1st order 1455nm cavity laser respectively. The term $d_i^{\pm} = \dfrac{1}{v_{gS}} - \dfrac{1}{v_{gi}}$ denotes the effect of the relative propagation speed of different spectral components. v_{gS} and $v_{gi}(i=1,2)$ represent the group velocity of signal and corresponding pump respectively. The other parameters remain same as described before in Eqs. (4.11) – (4.15). The boundary conditions include the cavity design parameters and described as [138, 140]:

$$n_1^+(0) = n_{10}$$ (4.31)
$$n_1^-(0) = n_{20}$$ (4.32)
$$n_2^+(0) = R_1 n_2^-(0)$$ (4.33)
$$n_2^-(L) = R_2 n_2^+(L)$$ (4.34)
$$n_S(0) = 0$$ (4.35)

where, R_1 and R_2 represent the FBG reflectivity in the forward and backward end respectively and L is the amplifier span length. The above system of equations and boundary conditions represent a dual order bidirectional Raman amplifier. However similar mathematical approach can be applied to any design of Raman amplifier including higher order pumping with proper considerations of required boundary conditions. Same boundary value problem (BVP) approach can be applied to

solve the ODEs and corresponding RIN of signal, pump and RIN transfer. The example of RIN transfer function for forward and backward 1st order pumped DRAs are shown in Figure 3. 18.

4.4   Conclusions

In this chapter, we have described how to numerically model different Raman amplification schemes using a system of ODEs based on simple average power model. All the important impacts in the amplification process such as: attenuation, energy transfer among different frequency components, ASE noise and Rayleigh scattering have been considered in the complete model. Advanced higher order DRA schemes have also been discussed with proper boundary conditions. Here we have also reported different characteristics of advanced Raman amplification techniques through proper numerical simulation which are very beneficial to predict the power conversion efficiency, noise and nonlinear performances in the Raman amplified system design. URFL based 100km bidirectional DRA can provide quasi-lossless signal power distribution along the amplifier span and shows more that 3dB better SPV than first order bidirectional DRA. A variable input reflectivity based dual order bidirectional DRA is also presented and SPV up to 1dB has been shown numerically with a span length of 65km. Finally, a brief overview on RIN modelling is also given which may be used for characterizing signal RIN performances with different pumping schemes.

CHAPTER 5

RIN PERFORMANCE CHARACTERISATION IN RAMAN FIBRE LASER BASED DISTRIBUTED AMPLIFIERS

In this chapter, experimental investigation of the different features such as: relative intensity noise (RIN) of the amplified signal and intra-cavity 1st order lasing, lasing mode structures and signal power distribution of 2nd order Raman fibre laser (RFL) based distributed amplifiers will be discussed in details. The benefits of ultra-long Raman fibre laser (URFL) based distributed Raman amplification (DRA) in quasi-lossless signal transmission and optical signal to noise ratio (OSNR) improvement have already been discussed both analytically [15, 141, 142] and experimentally [14, 143, 144] in previous literatures. The main problem of using this amplification scheme is the high RIN transfer from forward propagating pumps to signal [14]. One solution of mitigating the RIN transfer to the signal could be using a random distributed feedback (rDFB) lasing based DRA in a half-open RFL cavity without any reflection from the input end [21, 133]. But this benefit comes at a cost of high 2nd order pump power required to provide gain from the input end in order to maintain low signal power variation (SPV) along the amplifier span. Providing a low Fresnel reflection (~4%) from a flat (FC-PC) connector at the input end increases the pump power efficiency in a semi-random DFB lasing cavity along the amplifier span compared with the rDFB pumping scheme. But RIN transfer can still dominate the performance at high forward pump powers [21]. Here Raman fibre laser based DRA schemes both with rDFB (no input reflection) and semi-rDFB cavity with different low level reflections from the input end will be investigated at different amplifier span lengths. The impact of front end reflections on signal RIN, OSNR and overall transmission performance in a 30GBaud DP-QPSK coherent system are experimentally analyzed in RFL based distributed amplifiers.

In this chapter, experimental characterisation of random and semi-random DFB laser based DRA schemes at different span lengths were carried out in collaboration with Dr Mingming Tan at AIPT.

The experimental results on variable input FBG reflectivity based Raman fibre laser based distributed amplifiers using an 83km span were carried out together with Giuseppe Rizzelli during his academic secondment at AIPT. A standard RIN measurement setup was built using the facilities at AIPT to characterise the signal and pump RIN profiles. The signal power profiles along the amplifier span were measured using a modified optical time domain reflectometer (OTDR) technique available at AIPT laboratory. Dr Mingming Tan and Dr Paul Harper helped to build the recirculating loop based long-haul coherent transmission setup. The coherent transmission experiment using different distributed Raman pumping schemes used in this chapter was carried out by the author of this thesis. The digital signal processing (DSP) codes used for offline processing of signals were developed by AIPT researchers. The results presented in this chapter are related to the following publications:

1. G. Rizzelli, **M. A. Iqbal**, F. Gallazzi, P. Rosa, M. Tan, J. D. Ania-Castañón, L. Krzczanowicz, P. Corredera, I. D. Phillips, W. Forysiak, and P. Harper, "Impact of input FBG reflectivity and forward pump power on RIN transfer in ultralong Raman laser amplifiers," Opt. Express 24(25), 29170-29175 (2016).

2. M. Tan, P. Rosa, S. T. Le, **Md. A. Iqbal**, I. D. Phillips, and P. Harper, "Transmission performance improvement using random DFB laser based Raman amplification and bidirectional second-order pumping," Opt. Express 24(3), 2215-2221 (2016).

3. M. Tan, **M. A. Iqbal**, S. K. Turitsyn and P. Harper, "Mitigating RIN-penalty to enhance the transmission performance in distributed Raman amplification system," in Proc. OECC and PGC 2017, paper oral 3-2T-3 (invited).

4. M. Tan, P. Rosa, **M. A. Iqbal**, S. T. Le, I. D. Philips, S. K. Turitsyn and P. Harper., "Raman fibre laser based amplification in long-haul/unrepeatered coherent transmission systems," in Proc. ICTON 2017, paper We.C5.5 (invited).

5. G. Rizzelli, **M. A. Iqbal**, P. Rosa, M. Tan, L. Krzczanowicz, I. Phillips, W. Forysiak, J. D. Ania-Castañón, and P. Harper, "Impact of front-FBG reflectivity in Raman fiber laser based amplification," in Proc. CLEO 2016, paper SF1F.6.

6. G. Rizzellli, **M. A. Iqbal**, F. Gallazzi, P. Rosa, M. Tan, P. Corredera, J. D. Ania-Castañón and P. Harper, "FBG reflectivity impact on RIN in ultralong laser amplifiers," in Proc. ECOC 2016, paper CLEO 5.3.

7. M. Tan, P. Rosa, **M. A. Iqbal**, I. Phillips, J. Nuño, J. D. Ania-Castanon, and P. harper, "RIN Mitigation in second-order pumped Raman fibre laser based amplification," in Proc. ACP 2015, OSA Technical Digest (online) (Optical Society of America), paper AM2E.6.

5.1 Random and Semi-random Distributed Feedback Laser Based Distributed Raman Amplifiers

5.1.1 Experimental setup

The dual order bidirectional URFL based DRA includes one high reflectivity FBG centred at ~1455nm and a 2nd order Raman pump (1365nm) at each end. A first order Raman fibre laser with strong Fabry-Perot cavity is created in between the two high reflectivity mirror-like FBGs along the span. Whereas, the rDFB lasing based Raman amplifier was generated in a half-open cavity [135, 145], omitting the front high reflectivity FBG as shown in Figure 5. 1(a) [146]. A semi-rDFB was created using a small (~4%) broadband Fresnel reflection at the input as depicted in Figure 5. 1(b).
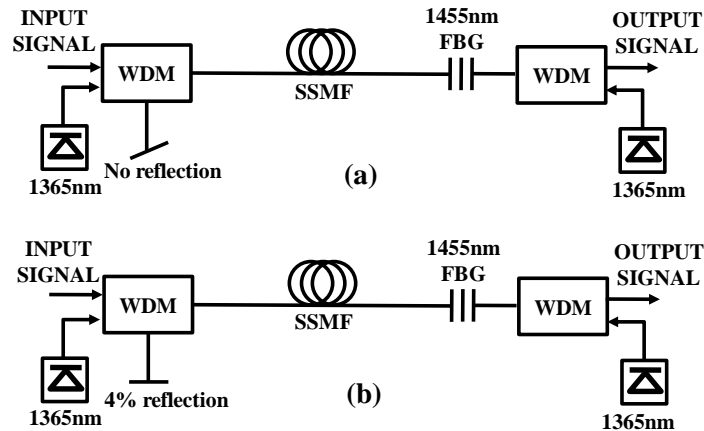
Figure 5. 1. Distributed Raman amplifier (DRA) scheme with: (a) a random DFB laser cavity without any input reflection using an angle connector (b) a semi-random DFB laser cavity with 4% input reflection from a flat (FC-PC) connector

In both bidirectional DRA schemes shown in Figure 5. 1, backward pumping is formed by a 2nd order 1365nm Raman fibre laser with -125dB/Hz RIN level and a high reflectivity (95%) FBG centred at ~1455nm with 0.5nm 3dB bandwidth [21, 133, 147]. The inclusion of the FBG created a distributed random lasing at 1455nm using the Rayleigh backscattering and feedback from the output end FBG. A commercial 3×1 bidirectional wavelength division multiplexing (WDM) coupler was used at each end to combine a 2nd order 1365nm Raman pump with the signal. The third port of the WDM coupler corresponded for the wavelength band 1420~1480nm. The forward

1365nm pump amplify the 1455nm lasing at the input end which subsequently amplify the signal around 1550nm. In Figure 5. 1(a), the use of angled (APC) connector at the 1455nm port of the 3×1 input WDM ensures no reflection (0%) at first order wavelengths from the input end and creates an rDFB laser cavity with no Fabry-Perot like dominant mode structures. In Figure 5. 1(b), a flat-cleaved (FC-PC) connector was used in place of the APC connector which introduced about 4% front-end reflectivity and also improved the forward 1365nm pump power efficiency for an equal forward gain contribution. The broadband reflections at first order pump wavelengths were limited between 1420-1480nm by the input WDM. Further OSNR improvement and better pump efficiency are possible by increasing the input end reflections with enhanced gain efficiency. But at the same time RIN transfer from forward pump(s) to signal are increased significantly. For example, a front FBG with high reflectivity (95%) creates a closed Fabry-Perot cavity which maintains a quasi-lossless signal power profiles [15] but the OSNR improvement is hugely dominated by the associated signal RIN penalty [14]. The impact of using variable input reflectivity in the dual order bidirectional RFL amplifiers will be discussed in the next section. In this section, different features of these two schemes are investigated at four different span lengths 20km, 40km, 62km and 83km and at different forward pump powers (FPPs): 250mW, 500mW, 750mW and 1W.

5.1.2 RIN characterisation

Figure 5. 2 shows the RIN measurement technique using an ultra-low noise photo-receiver and RF spectrum analyser [148, 149]. A DC blocker was used to get rid of the low frequency DC components. The setup allowed RIN measurement ranging from 166kHz to 100MHz. A CW laser centred at 1545.32nm and with low RIN (-145dB/Hz) was used for signal RIN measurement after one span of corresponding amplifier scheme.
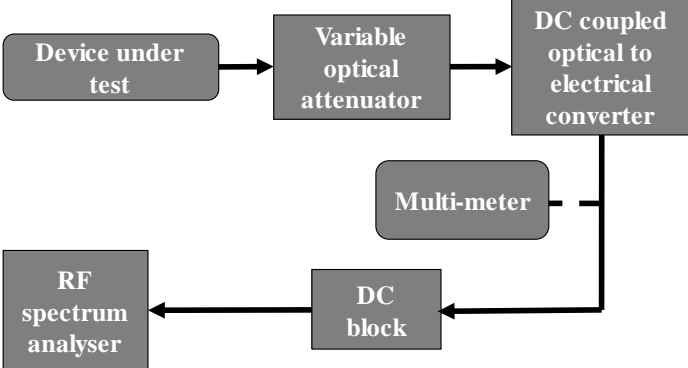
Figure 5. 2. RIN measurement setup

We measured and compared the signal RIN and the 1st order Raman fibre laser RIN which was generated in an rDFB or semi-rDFB lasing cavity as shown in Figure 5. 1(a) and (b) respectively at different span lengths. In these 2nd order DRA schemes, RIN from forward 1365nm 2nd order pump is first transferred to the intra-cavity 1st order Raman fibre laser then to the signal. So any increase in the forward propagated intra-cavity 1st order laser RIN level also transfers additional RIN to the signal. In the characterisation, signal RIN, forward propagated lasing RIN and lasing mode structures were measured and compared at different lengths for both 0% and 4% input reflections with increasing forward 1365nm pump powers. The pump powers used for the experimental characterisation of rDFB and semi-rDFB based distributed Raman amplifiers are given below.

Table 5. 1. Pump powers used in the characterisation of RFL based DRA at different span lengths and 0% input reflection (FW = forward, BW = backward)

| FW 1365nm (mW) | 20km | | 40km | | 62km | | 83km | |
	BW 1365nm (mW)	FW pump ratio (%)	BW 1365nm (mW)	FW pump ratio (%)	BW 1365nm (mW)	FW pump ratio (%)	BW 1365nm (mW)	FW pump ratio (%)
0	1130	0	1060	0	1140	0	1220	0
250	970	20.5	980	20.4	1090	18.7	1190	17.4
500	820	38	910	35.5	1060	32.1	1170	30
750	680	52.5	880	47.5	1000	42.9	1140	39.7
1000	530	65.4	770	56.5	960	51	1110	47.4

Table 5. 2. Pump powers used in the characterisation of RFL based DRA at different span lengths and 4% input reflection (FW = forward, BW = backward)

| FW 1365nm (mW) | 20km | | 40km | | 62km | | 83km | |
	BW 1365nm (mW)	FW pump ratio (%)	BW 1365nm (mW)	FW pump ratio (%)	BW 1365nm (mW)	FW pump ratio (%)	BW 1365nm (mW)	FW pump ratio (%)
0	770	0	930	0	1110	0	1220	0
250	560	31	750	25	1000	25	1150	17.9
500	350	58.8	580	46.3	860	36.8	1100	31.3
750	150	83.3	420	64.1	720	51	970	43.6
1000	0	100	210	82.7	570	63.7	760	56.8

Table 5. 1 and Table 5. 2 show the pump powers used and the forward pump ratio (FPR) for different span lengths. The same forward pump powers were used at different amplifier lengths, whereas backward 1365nm pump powers were optimized for each forward pump power level to maintain zero net gain at the output of the amplifier. The required backward pump powers to maintain 0dB net Raman gain at the end of the span were decreased as the forward pump power levels were increased at 250mW step from 0mW to 1000mW. Moreover, due to the inclusion of

4% input reflection (Table 5. 2), the forward pump ratio (FPR) were higher than that of no input reflection (0%) in rDFB scheme.
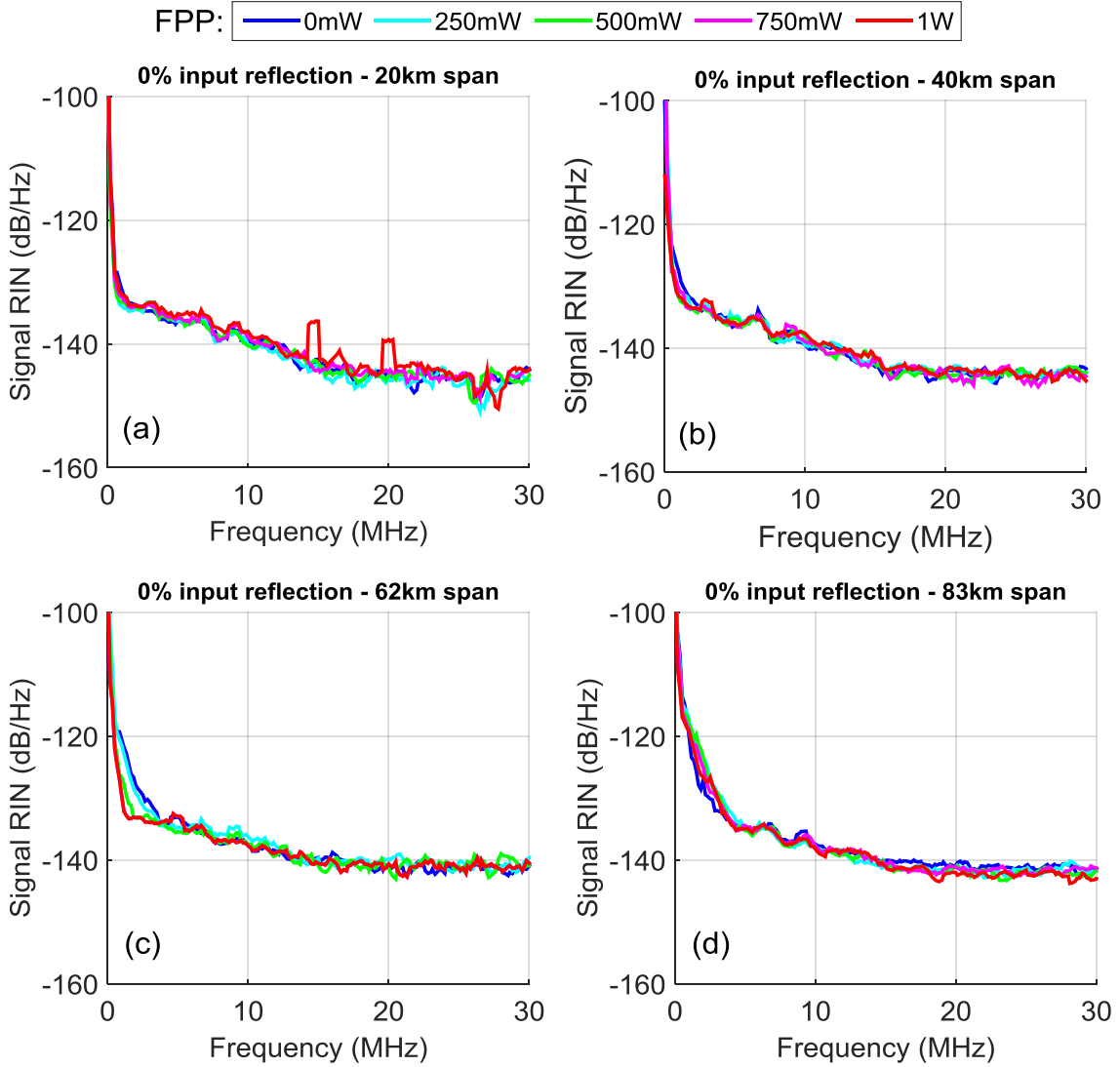
Figure 5. 3. Signal RIN comparison at 0% input reflection at increasing forward pump powers (FPPs) for different span lengths (a) 20km; (b) 40km; (c) 62km; and (d) 83km

Figure 5. 3 shows the signal RIN performance at different span lengths with 0% input reflection in the rDFB laser based Raman amplifiers. There was no increase in the signal RIN level which suggest that there was negligible RIN transfer from the forward 1365nm pump power to the signal even for very high FW pump powers at any span length. This is because the minimization of input reflectivity at first order pump wavelengths led to the inefficiency of the Stokes shifted power transfer from 2nd order 1365nm pump to signal around 1550nm which are two Stokes shifted away from the 1365nm pump and thus subsequent RIN transfer was also reduced.

105
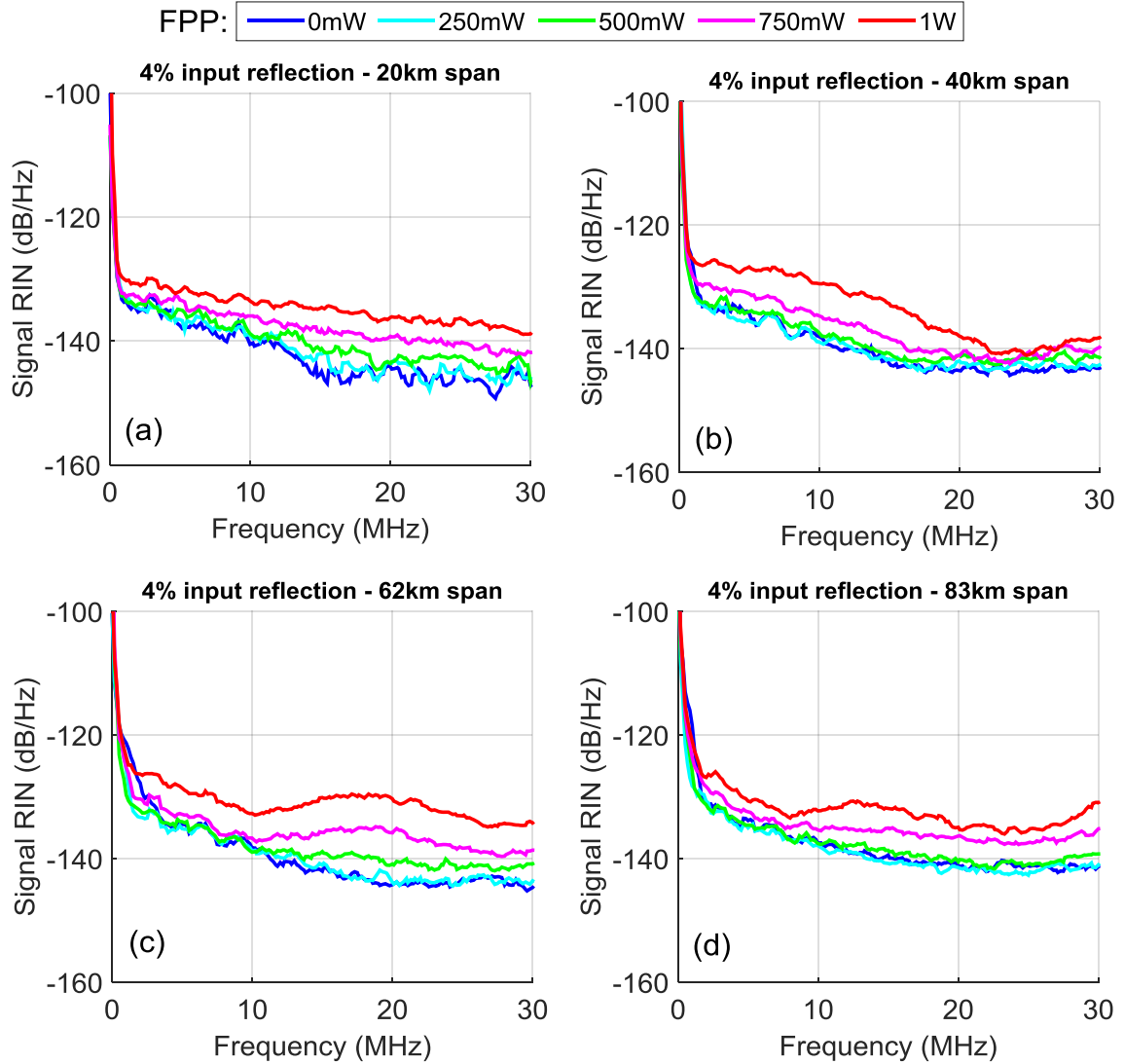
Figure 5. 4. Signal RIN comparison at 4% input reflection at increasing FPPs for different span lengths: (a) 20km; (b) 40km; (c) 62km; and (d) 83km

At 4% Fresnel reflection from the input end, a significant signal RIN level increase was observed above 500mW of forward 1365nm pump power in all four span lengths as shown in Figure 5. 4(a)-(d). At the output of the amplifier, backward 1365nm pump first generated Raman scattered light around 1455nm. A random laser was then created with the feedback from high reflectivity FBG and Rayleigh backscattering from the fibre using the generated 1455nm light as seed. The 2nd order 1365nm FW pump amplified the weakly reflected and forward propagated 1455nm lasing near the input end and and subsequently provided gain to the signal. Thus, transfer of RIN from 1365nm forward pump to signal was occurred via 1455nm laser due to the presence of input reflection.
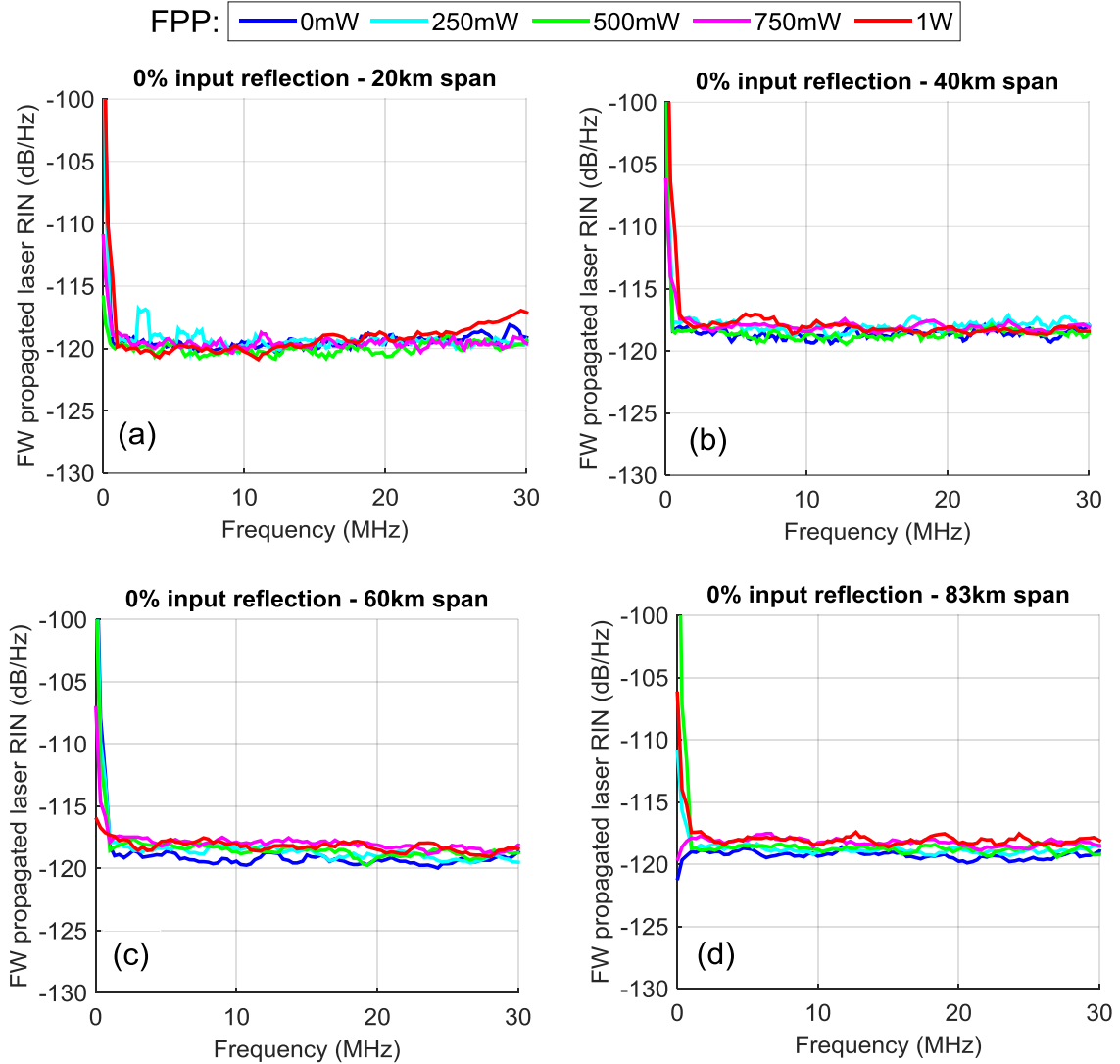
Figure 5. 5. Forward propagated intra-cavity 1st order Raman fibre laser RIN with 0% input reflection at increasing FPPs for different span lengths: (a) 20km; (b) 40km; (c) 62km; and (d) 83km

We also measured the 1st order intra-cavity laser RIN both for rDFB and semi-rDFB laser based DRAs. At 0% input reflection, there was no transfer of RIN from forward 1365nm pump and the forward propagated lasing RIN did not increase and showed similar RIN level (about -120dB/Hz) with increasing FPPs in all four span lengths as shown in Figure 5. 5 (a)-(d). As the lasing RIN levels were same for all the FPPs at 0% input reflection, the signal RIN also showed similar performances. On the other hand, the RIN transfer from 1365nm forward pump to the intra-cavity first order laser was expected to be higher at 4% input reflection compared with no reflection, due to the presence of weakly reflected 1455nm lasing from the input end flat connector. The increasing signal RIN penalty with high FPP at 4% input reflection (Figure 5. 4) could also be

107

described by the RIN characteristics of forward propagated 1st order lasing generated inside the cavity.
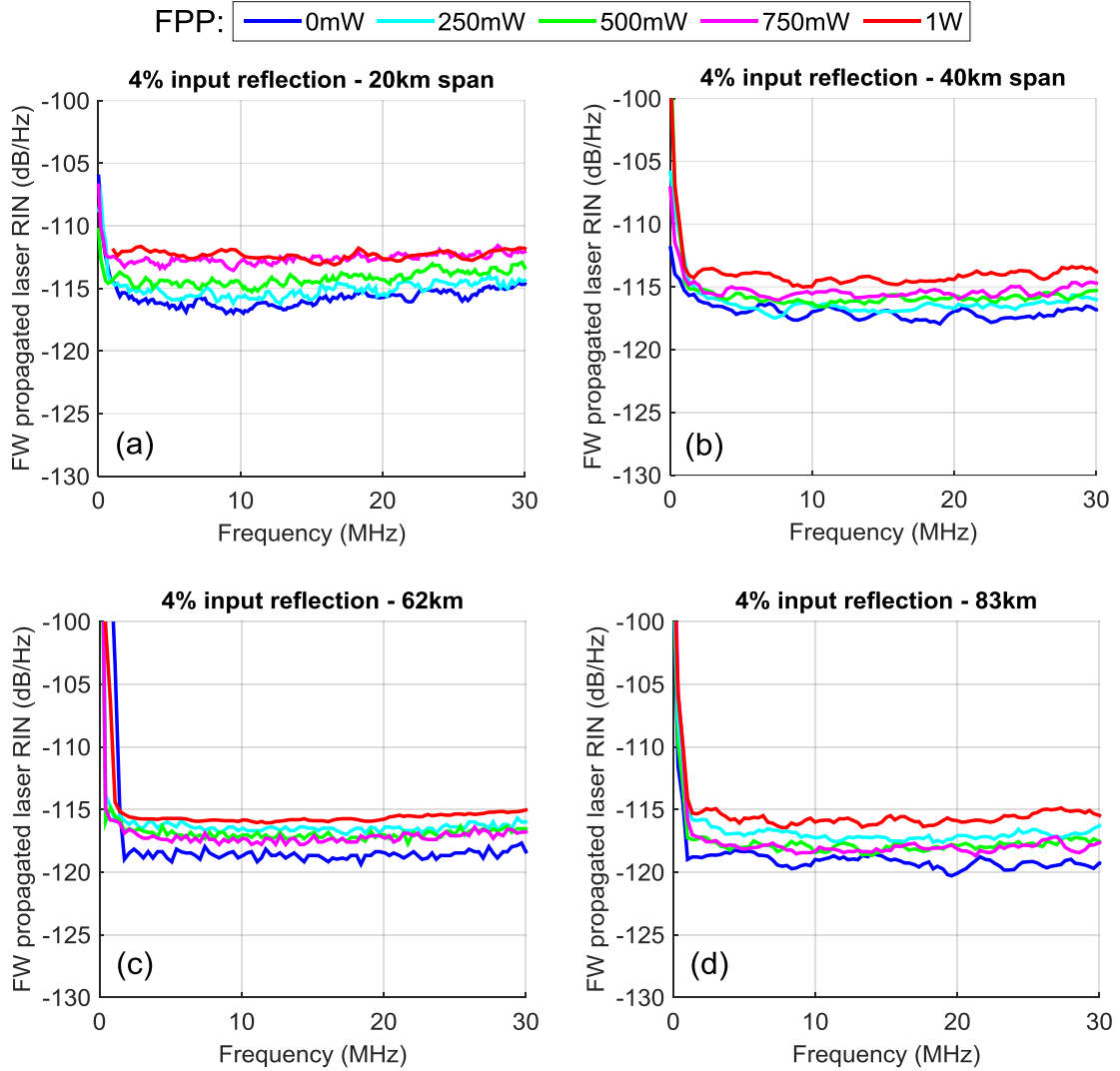
Figure 5. 6. Forward propagated intra-cavity 1st order Raman fibre laser RIN with 4% input reflection at increasing FPPs for different span lengths: (a) 20km; (b) 40km; (c) 62km; and (d) 83km

Figure 5. 6 shows the measured RIN of the intra-cavity FW propagated 1st order lasing at 4% input reflection and with different span lengths. A clear increase in RIN level was observed with increasing forward 1365nm pump powers for all the amplifier span lengths. The RIN level increase up to 3~4dB with 1W forward 1365nm pump power was obtained at 4% input reflection.

5.1.3 Intra-cavity RF lasing structure

We also investigated the intra-cavity radio frequency (RF) lasing structures of 1st order rDFB and semi-rDFB laser in dual order bidirectional distributed amplification consisted of 0% and 4% input reflection respectively with different cavity lengths.
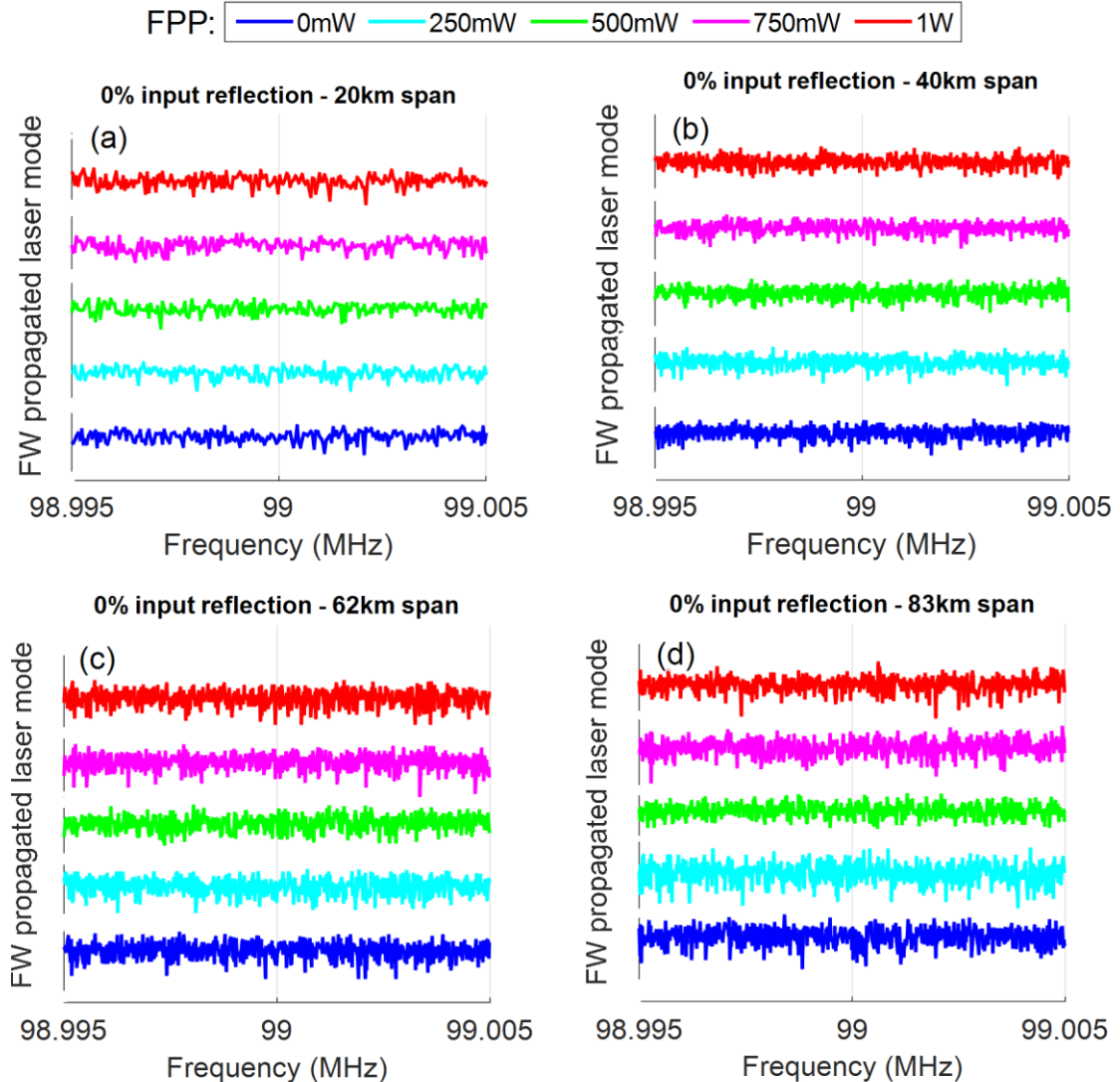
Figure 5. 7. Forward propagated 1st order lasing mode structure with 0% input reflection at increasing FPPs for different cavity lengths: (a) 20km; (b) 40km; (c) 62km; and (d) 83km (Y-axis not in scale)

The intra-cavity forward (FW) propagated 1st order laser mode structures at different span length and with 0% input reflections are shown in Figure 5. 7(a)-(d). The 1st order lasing mode structures were essentially the electrical spectrum measured using the RF-spectrum analyser setup shown in Figure 5. 2. Due to the absence of input reflection, no Fabry-Perot cavity was formed and a random

DFB fibre laser at 1455nm was generated using the output end FBG and Rayleigh backscattering from the fibre span as soon as the resonant mode reached the lasing threshold. No dominant cavity mode structure in the forward propagated lasing was observed for all span lengths.
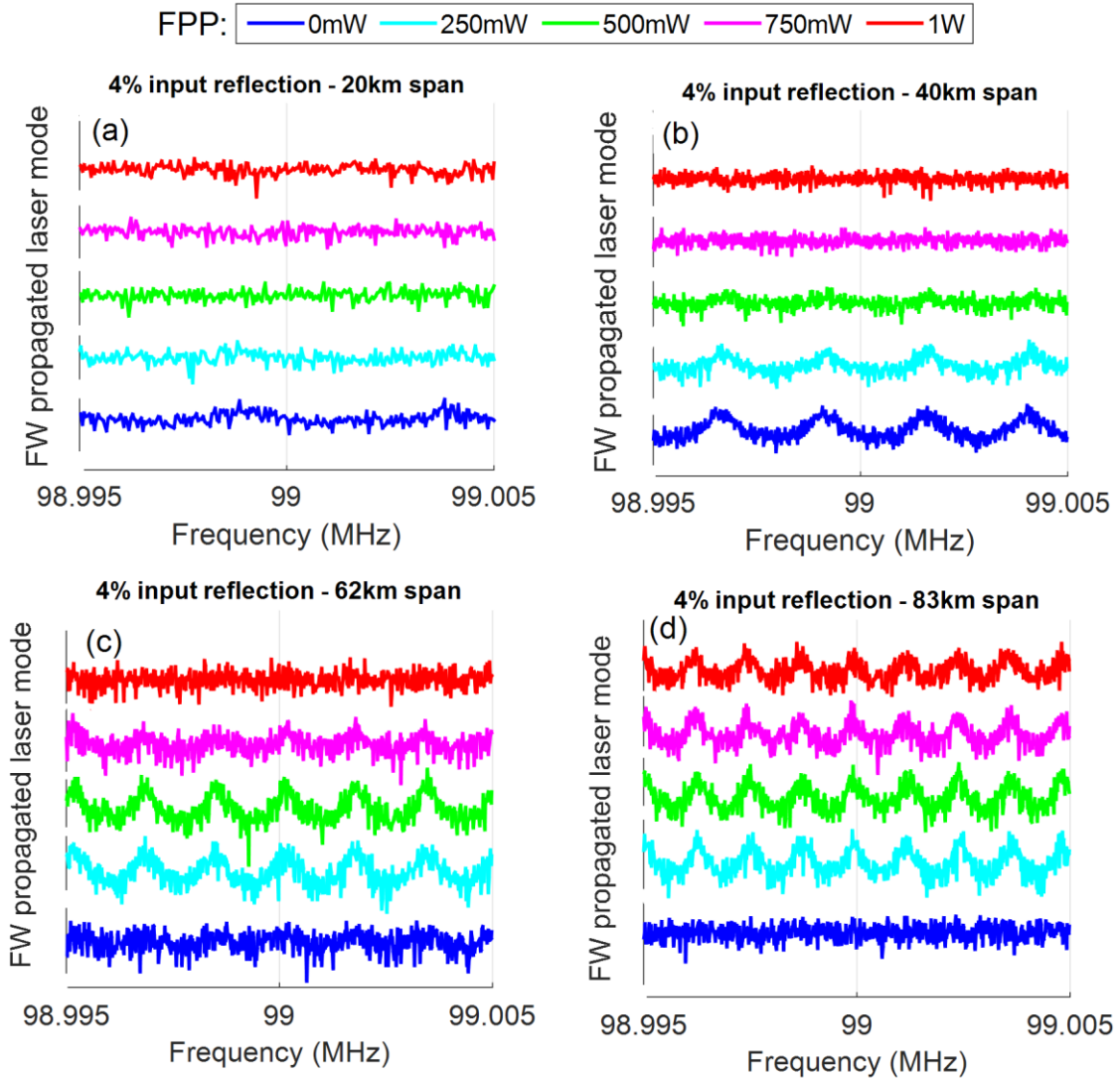
Figure 5. 8. Forward propagated 1st order lasing mode structure with 4% input reflection at increasing FPPs for different cavity lengths: (a) 20km; (b) 40km; (c) 60km; and (d) 80km

Figure 5. 8 shows intra-cavity forward propagating 1st order lasing mode structures at 4% broadband input Fresnel reflection for different amplifier lengths. A completely random DFB or weak Fabry-Perot laser mentioned as semi-rDFB laser was created depending on the span length and forward pump power level. In shorter cavity lengths up to 40km a very weak Fabry-Perot mode structures were seen at backward only pumping and FPP up to 250mW. The main lasing in the cavity was created by the contribution from high backward 1365nm pump power and feedback

from output FBG. Being a short cavity, a weak reflection from front end flat connector was also dominant and a weak Fabry-Perot cavity-like structure was observed for forward propagated 1st order laser. When backward 1365nm pump power were decreased due to increasing FPPs, the Fabry-Perot modes were disappeared due the absence of higher input reflection level to provide enough feedback at 1st order lasing wavelength.

For backward only pumping in a long span (cavity) length over 60km, a pure rDFB lasing is created within a cavity formed by the FBG in one end and Rayleigh backscattering from the fibre itself as distributed mirror. However with increasing FPPs, strong Fabry-Perot modes with 1.2kHz mode spacing were formed to generate an ultra-long Fabry-Perot cavity along the amplifier span even with only 4% input reflection. At 1W of forward 1365nm pump power the mode structures disappeared for 62km cavity length due to the absence of high reflection from the input end and weakly generated lasing at the output end. However in 83km span, the presence of enough amplified Rayleigh backscattered 1st order lasing from the input end maintained 83km ultra-long Fabry-Perot cavity for all bidirectional pumping schemes. Overall, in the presence of a very low Fresnel reflection at the input end, the ultra-long distributed Raman fibre laser based amplifier becomes a Fabry-Perot cavity with bidirectional pumping scheme. Fabry-Perot cavity was created along the whole amplifier span and increased the efficiency of RIN transfer from forward pumps to signal and degraded the signal RIN performance. A comparison of signal RIN levels from Figure 5. 4, at different span lengths with fixed 500mW forward pump power is shown in Figure 5. 9.
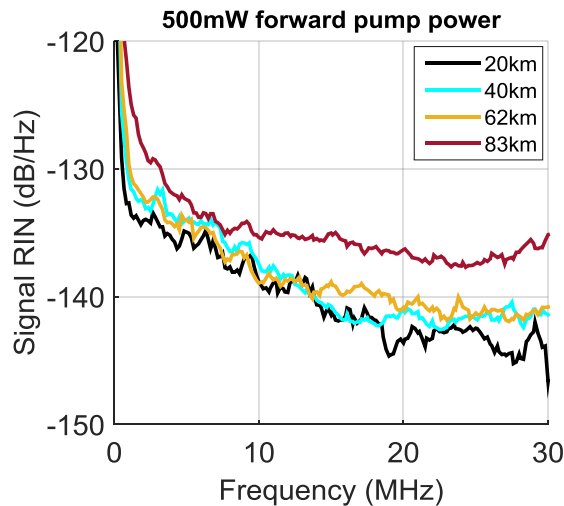
Figure 5. 9. Comparison of signal RIN levels at different span lengths with fixed 500mW forward pump power in an 83km RFL based distributed Raman amplifier with 4% input reflection from flat connector

Figure 5. 9 shows that, using 500mW forward pump power and only 4% input reflection from flat connector increased the signal RIN level at longer span lengths due to the presence of strong Fabry-Perot cavity like mode structures along the span as shown in Figure 5. 8.

So far we have showed that at longer span length of the amplifier, more distributed Rayleigh backscattering generates Fabry-Perot cavity like mode structures along the amplifier at increasing forward pump power even with a very small input reflection from a flat end connector. Fabry-Perot cavity remains along the entire cavity and helps the transfer of RIN from higher order 1365nm forward pump to signal. Whereas random lasing based cavity is formed in between the output end 95% reflectivity FBG and distributed Rayleigh backscattering from the fibre and remains strong within the last 20~30km. At 0% input reflection, no cavity like structure was formed even at high forward pump powers and no increase in the RIN level of signal or forward propagating lasing was observed.

5.2 Investigation of RIN with Variable Input Reflectivity Raman Fibre Laser Based Amplification

In this section, variable input reflection levels were used by changing the reflectivity of the input FBG. We explored different lasing regimes of the amplifier at a fixed span length of 83km and demonstrated how these different lasing regimes contributed to the RIN transfer mainly from forward pumps to signal at different pump power levels [150-152]. Figure 5. 10 shows the Raman fibre laser based amplifier configuration including a variable reflectivity FBG at the input end. The input FBG reflectivity levels were varied from 7% to 95%.
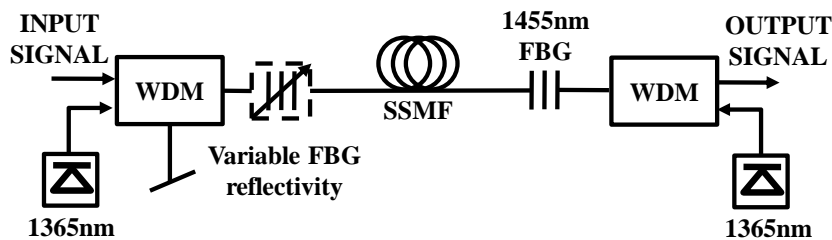
Figure 5. 10. Raman fibre laser based distributed Raman amplification with 83km SSMF span and variable input FBG reflectivity

112

5.2.1 RIN characterisation

The signal RIN levels were measured for different input reflection levels with increasing forward pump powers (ratios). The characterisation of signal RIN at fixed 10% input FBG reflectivity and increasing forward 1365nm pump powers (ratios) is illustrated in Figure 5. 11. The forward pump powers (FPPs) used including forward pump ratios (FPRs) are also given in Table 5. 3. At 10% input reflection, an increasing trend in signal RIN level was observed with increasing FPP (FPR) with a sharp rise beyond 745mW (40%). Although similar RIN levels were obtained up to 40% FPR, however at 100% FPR a significant ~10dB increase in RIN level was obtained due to very high RIN transfer from forward 1365nm pump.
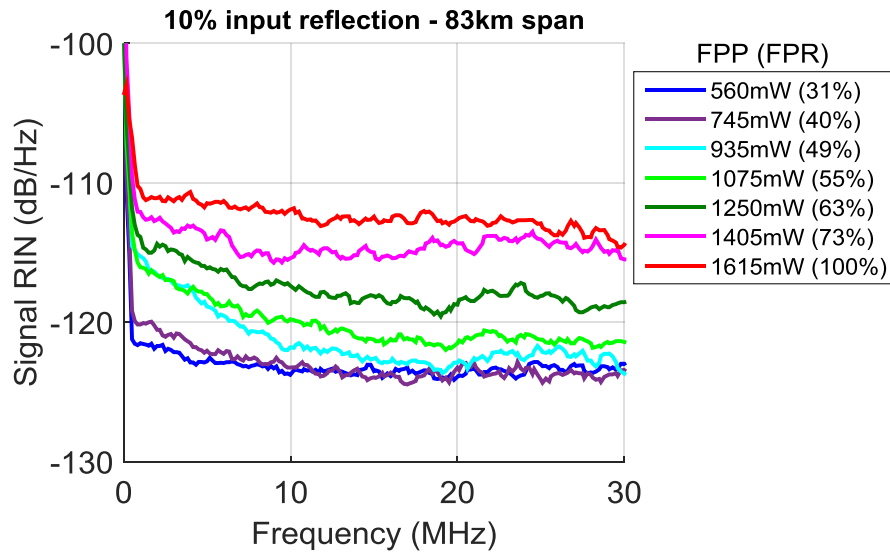
Figure 5. 11. Comparison of signal RIN at different forward pump powers (ratios) in an 83km RFL based DRA with an input FBG at 10% reflection (FPP = forward pump power, FPR = forward pump ratio)

Table 5. 3. Forward pump powers (ratios) used in the characterisation of a RFL based DRA with 10% input FBG reflection

Forward 1365nm pump power (mW)	Backward 1365nm pump power (mW)	Forward 1365nm pump power ratio (%)
560	1250	31
745	1120	40
935	980	49
1075	880	55
1250	730	63
1405	520	73
1615	0	100

Additionally comparison of signal RIN performance at fixed forward pump powers of 745mW and 1075mW are also shown in Figure 5. 12(a) and (b) respectively. In both cases, 0% input reflection from angle connector showed the lowest signal RIN. Sharp increase in signal RIN levels were observed at higher input reflection levels. Although flat connector gave only ~4% input reflection, however higher signal RIN level was observed than 7% input FBG reflection due to the broadband reflections over 60nm from 1420~1480nm which added additional stochastic fluctuations in the signal intensity level and increased the RIN. Whereas 7% input FBG reflection was limited to only 0.6nm 3dB bandwidth of the FBG centred at 1455nm and showed lower signal RIN level up to 745mW forward 1365nm pump power due to inefficient energy transfer from 1365nm pump to signal. At higher 1365nm forward pump power (1075mW) forward pump, both flat and 7% FBG reflection from the input end showed similar RIN performance.
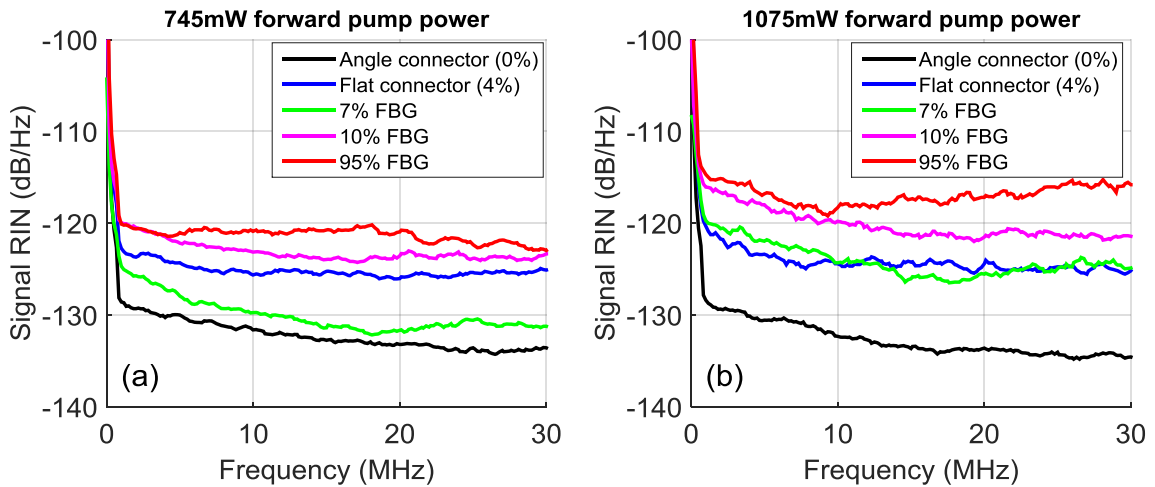
Figure 5. 12. Signal RIN comparison at different input FBG reflectivity levels with fixed (a) 745mW and (b) 1075mW forward pump powers

The signal RIN characteristics in an 83km RFL based distributed Raman amplifier at different input reflection levels could also be described by the 1st order intra-cavity forward propagating laser mode structures at 745mW FPP in different input reflection levels as shown in Figure 5. 13.
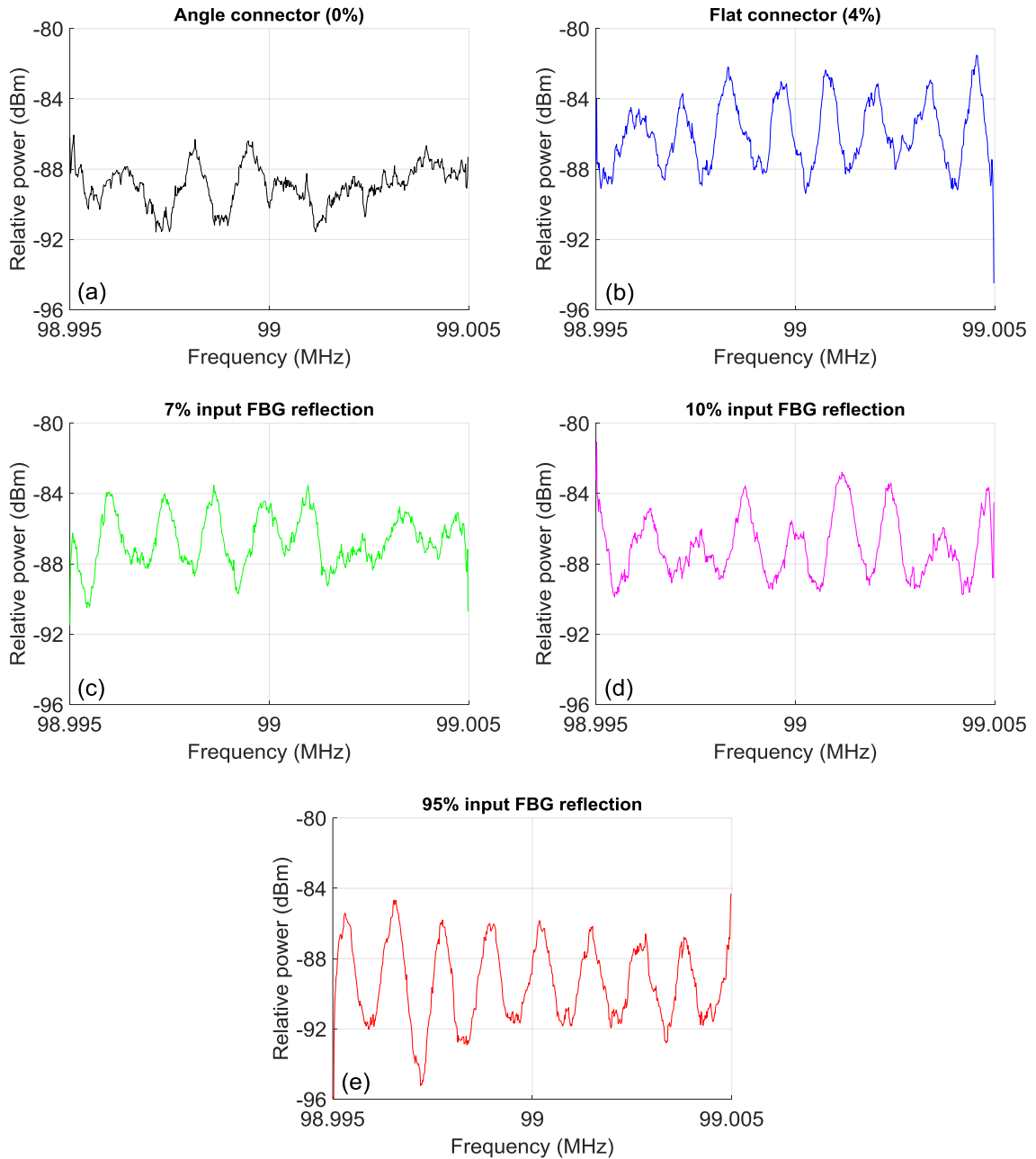
Figure 5. 13. Forward propagated intra-cavity lasing mode structure with 745mW FPP and variable input reflectivity

In Figure 5. 13(a), there was not well defined mode structure at 0% input reflection, confirming the formation of random lasing with Rayleigh backscattering feedback in the forward direction and inefficiency of seeded forward 1st order Stokes. The absence of 1455nm seed at 0% input reflection reduced the RIN transfer from higher order 1365nm pump to signal and maintained lowest signal RIN level as shown in Figure 5. 12. The dominant mode structures started appearing with increasing input reflections. In Figure 5. 13(b-d), gradual building up of Fabry-Perot like mode

structures was observed even with low input reflection levels from 4% to 10%. Figure 5. 13(e) shows a strong Fabry-Perot cavity with equal mode spacing of ~1.2kHz along the 83km distributed amplifier with 95% input FBG reflection allowing high RIN transfer from forward pumps to signal as shown in Figure 5. 12(a).
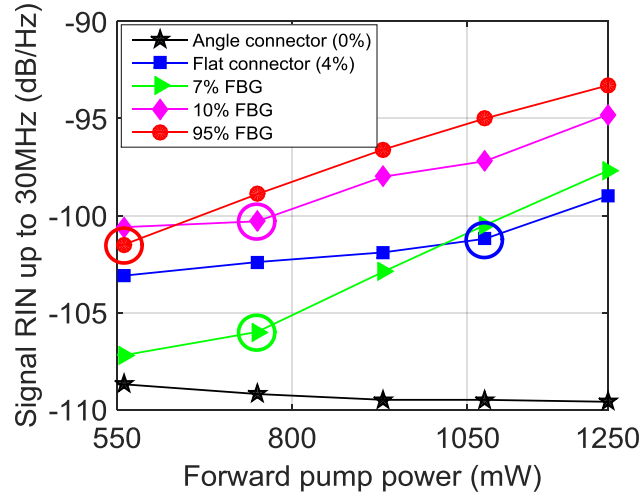
Figure 5. 14. Integrated signal RIN between 500 kHz and 30 MHz for increasing forward pump powers and with different input reflection levels (inflection points are in circles)

The signal RIN increases as we increase the forward pump powers with the presence of some input reflection even at very small level (i.e. 4~10%). The interesting point would be to investigate the inflection point beyond which there was a sharp increase in signal RIN at each input reflection level discussed above. In order to do that, we measured the signal RIN for increasing forward pump powers and integrated the total RIN from 500kHz to 30MHz modulation frequencies and then compared the performance at different input reflection levels as shown in Figure 5. 14. The low frequency RIN measurement was limited by the experimental setup, in which low frequencies were cut-off to avoid high DC components. In Figure 5. 14, the inflection points beyond which integral of signal RIN increased by more than 2dB were shifted towards higher FPPs for low input reflection levels. Input reflection from 95% reflectivity FBG showed a sharp increase in signal RIN at increasing forward pump power and inflection point was observed at only 560mW. Whereas maximum allowable forward pump power of 1075mW was obtained at ~4% input reflection from a flat connector. Both 7% and 10% input FBG reflectivity showed similar inflection point up to ~750mW. Total integrated signal RIN with flat connector (4%) showed higher level up to 930mW forward 1365nm pump power than 7% input FBG reflection which was due the broadband reflection (1420~1480nm) characteristic of flat connector which induced more stochastic signal

fluctuations in the signal level and caused more signal RIN as shown in Figure 5. 12. More interestingly, lowest signal RIN levels with no significant increase with increasing forward pump powers were observed in case of 0% input reflection from an angle connector.

5.2.2 Characterisation of signal power distribution along the amplifier

In order to evaluate how the signal power profile changes with increasing forward pump power levels, signal power distributions along the amplifier span were measured using a modified optical time domain reflectometer technique (OTDR) [153] as shown in Figure 5. 15. In the pre-built available OTDR setup, a pulsed Fabry-Perot semiconductor laser output at 1550nm was first converted into electrical pulses using a photodetector. The electrical pulses were then used to modulate an external tuneable laser source through an acousto-optic modulator (AOM) setup. Then the tuneable pulsed laser was fed into the amplifier span and back-reflected signals were received and processed by the OTDR to obtain signal power distribution along the span.
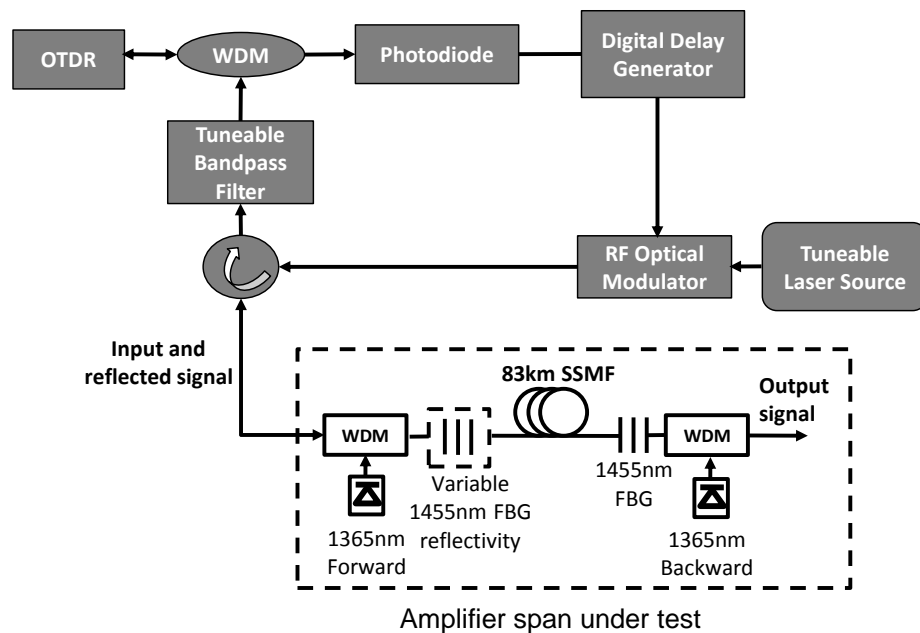
Figure 5. 15. Schematic diagram of the measurement technique of signal power variation along the amplifier span using a modified optical time domain reflectometer technique

In the signal power profile measurement using the above mentioned OTDR technique, the gain distribution along the span was measured using the received power from the Rayleigh backscattering signals which was very low in power and did not occur any pump depletion. In actual gain measurement by real signal, small signal gain was also considered in a non-depleted pump regime. In case of high-power input signal, gain saturation can be different for each

direction, and the lower-powered backward propagating Rayleigh backscattered signal might experience more gain than the forward propagating one, which would introduce some error. But in non-depleted gain measurement, there was no such case of gain saturation and the effective attenuation experienced by the signal in both forward and backward direction was the same as the Rayleigh backscattered signal experienced in its return (backward direction).
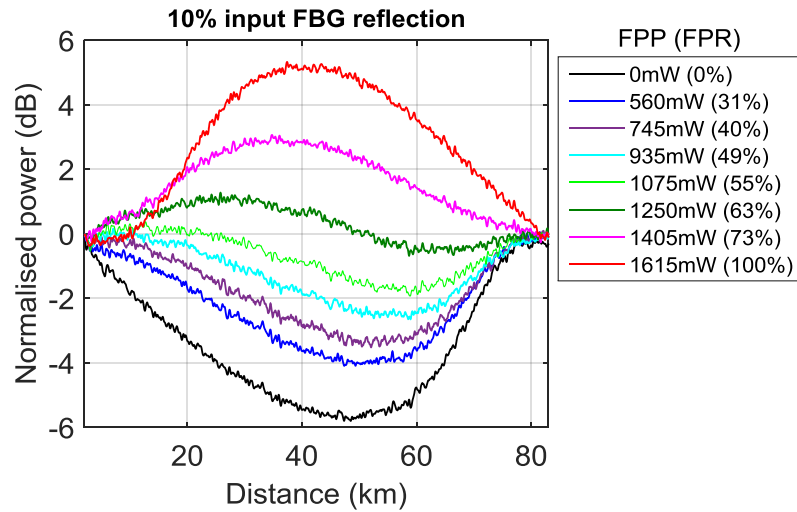
Figure 5. 16. Signal power profiles along 83km SSMF RFL based DRA at 10% input FBG reflection with increasing forward pump powers (ratios). Abbreviations: FPP = forward pump power, FPR = forward pump ratio

Figure 5. 16 shows the SPVs at increasing forward pump powers (ratios) in the RFL based DRA scheme with 10% input reflectivity. The maximum SPV of 5.8dB was obtained at backward only pumping with 0mW FPP. As the forward gain contribution increased with increasing FPP, the SPV decreased up to ~1.9dB at 1250mW and then it increased again due to the superior forward gain contribution than from the backward end.
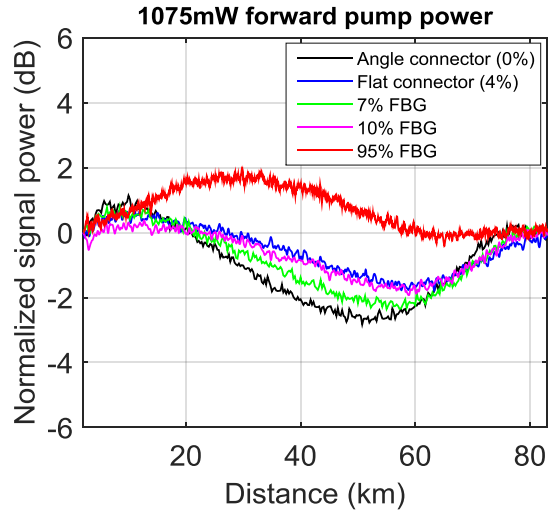
Figure 5. 17. Signal power profiles along the amplifier at 1075mW of forward pump power with different input reflection levels

Figure 5. 17 shows the signal power profiles for a fixed forward 1365nm pump power of 1075mW and different forward input reflection levels in an 83km RFL based distributed Raman amplifier. As expected, at 0% input reflection using an angle connector provided the maximum signal power variation 3.6dB. At increased input reflection levels, the forward gain contributions were improved and reduced signal power distributions along the amplifier span were achieved. Low input reflections (4%~10%) either from flat connector or low reflectivity input FBG provided similar power distributions with 10% showing the smallest SPV (2.1dB). On the other hand, very high 95% input reflectivity formed a closed Fabry-Perot laser cavity and provided almost forward only pumping signal distribution with very 3.1dB SPV at high 1075mW of 1365nm forward pump power.
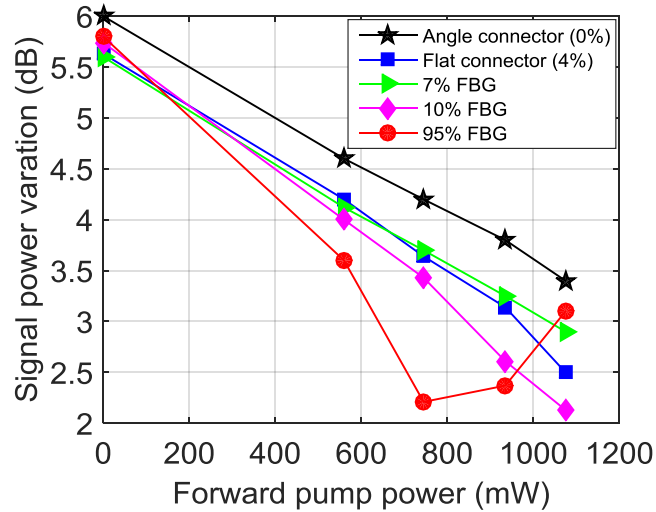
Figure 5. 18. Comparison of SPVs obtained at different input reflection levels for fixed forward pump power levels

We also measured signal power profiles at increasing forward 1365nm pump powers for different input reflection levels in 83km span DRA. Then the actual SVPs achieved by different input reflections at fixed forward pump powers were compared as shown in Figure 5. 18. As expected schemes with lowest (0%) input reflection showed the maximum SPVs among all. At 95% input reflection, the minimum SPV obtained was 2.2dB at ~750mW forward pump power and then SPVs were increased due to the dominant forward gain contribution with increasing pump powers. Flat connector (4%) and 7% input FBG reflection based schemes provided similar trends, while 10% input FBG reflections showed slightly improved SPVs than those due to better forward gain transfer efficiency at the input end. Adding low level input reflection up to 10% improved the forward pump power efficiency substantially compared with 0% input reflection based rDFB laser based scheme. For example at 3.6dB SPV, required FPP was reduced from 1075mW (0%) to 745mW at 10% input FBG reflection with about 31% pump power efficiency compared with rDFB based DRA.

5.2.3 Transmission results

The long-haul coherent transmission experiment was carried out in a recirculating loop setup as shown in Figure 5. 19. A narrow linewidth (100kHz) external cavity laser (ECL) at 1550nm was used as the channel under test (CUT) in the transmitter. The CUT was then QPSK modulated using a Mach-Zehnder IQ modulator. A 30GHz synthesizer was used to apply electrical signal with $2^{31}-1$ PRBS pattern in both I and Q with 18bits relative delay between them. The 30GBaud QPSK signal was then amplified by a polarisation maintaining EDFA. The amplified signal was then passed through a polarisation multiplexer (PolMux) with 300 symbols equivalent delay between the

polarisation states to generate dual polarised QPSK (DP-QPSK) 120Gb/s signal at the output of the transmitter. The signal from the transmitter was then input to the recirculating loop through transmitter acousto-optic modulator (Tx AOM).
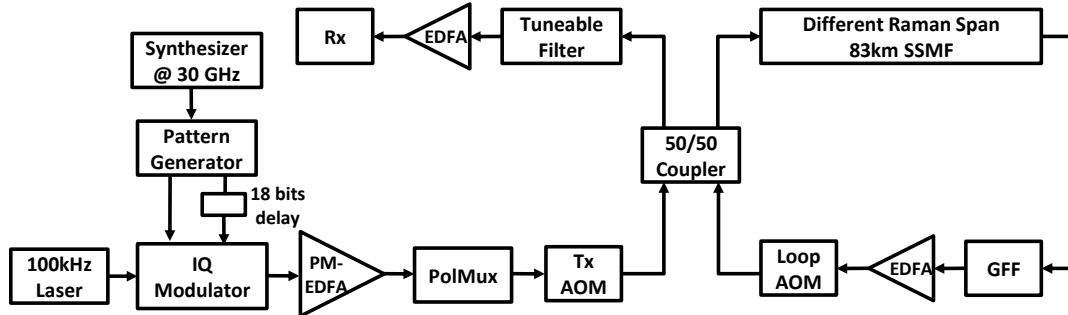
Figure 5. 19. Schematic diagram of the experimental setup for single channel coherent transmission

The transmission span in the recirculating loop is formed by the distributed Raman span with ~83km SSMF with a total loss of 17.6dB including 16.5dB span loss and 1.1dB passive component loss from pump/signal combiners. A dual-stage EDFA is used to compensate the additional 12dB loop losses from gain flattening filter (GFF), 3dB coupler and loop AOM. At the receiver, the received signal is first de-multiplexed using a tuneable bandpass filter and then amplified using an EDFA before passing it to a standard polarisation diverse coherent receiver with 80GSa/s and 36GHz bandwidth oscilloscope. Digital signal processing (DSP) was applied in offline post-processing for linear impairment mitigation and signal recovery. Q factors were measured from actual bit error counting and averaged over 2 million bits.
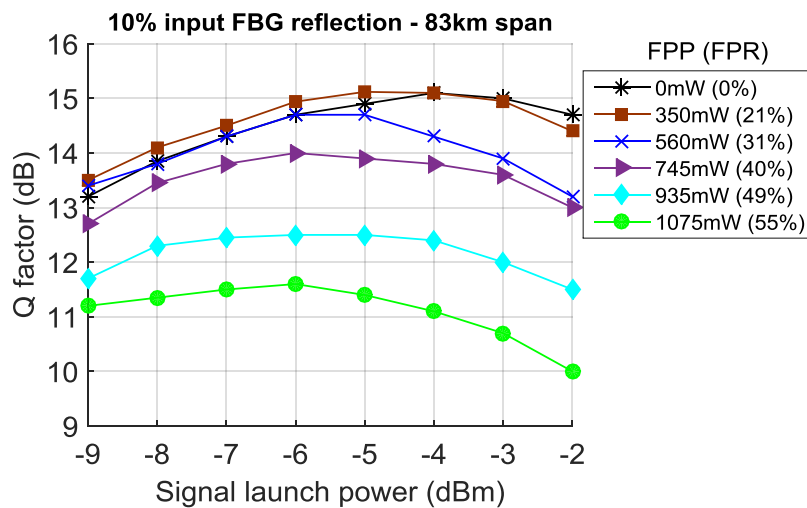
Figure 5. 20. Q factors vs. launch power for RFL based distributed amplification with 10% input FBG reflection and increasing forward pump powers (ratios) measured at 2000km transmission distance

121

Figure 5. 20 shows the Q factors at different launch power levels of the signal (1550nm) with varying forward 1365nm pump powers in RFL based 83km distributed Raman amplifier with 10% input FBG reflection. At 0mW of forward pumping (backward only) case, Q factor of 15.1dB was obtained at -3dBm optimum launch power. At only 350mW FPP, small improvement (0.1dB) of Q factor was observed in the linear regime due to improved OSNR and similar maximum Q factor (15.1dB) was obtained at optimum launch power of -4dBm. Degradation of maximum Q factors were observed with higher FPPs. At 40% forward pump ratio (FPR) with ~750mW forward 1365nm pump power, 1dB degradation of optimum Q factor was observed compared with 0% FPR. The optimum Q factors were reduced down to 12.5dB and 11.6dB at further high FPPs of 935mW and 1075mW respectively. A high degradation of more than 2dB was obtained at FPPs beyond 745mW, which could be described by the inflection point of signal RIN increase as shown in Figure 5. 14. At high FPPs, the optimum launch powers for maximum Q factors were also reduced up to 2dB than backward only pumping level (-3dBm) because of increased nonlinearity from higher path average power of signal as shown in Figure 5. 16. Although increasing FPPs improved the OSNR significantly by reducing the signal power variations (SPVs) as shown in Figure 5. 18, however the increased signal RIN penalty (Figure 5. 14) counterbalanced the OSNR benefit and degraded the transmission performance.

Similar Q factors vs. signal launch powers experiments were carried out at increasing FPPs for other input reflection levels and performances were compared among all the schemes in terms of Q factor penalty. At a fixed input reflection level, Q factor penalties at different FPPs were calculated with respect to backward only pumping with 0mW FPP.
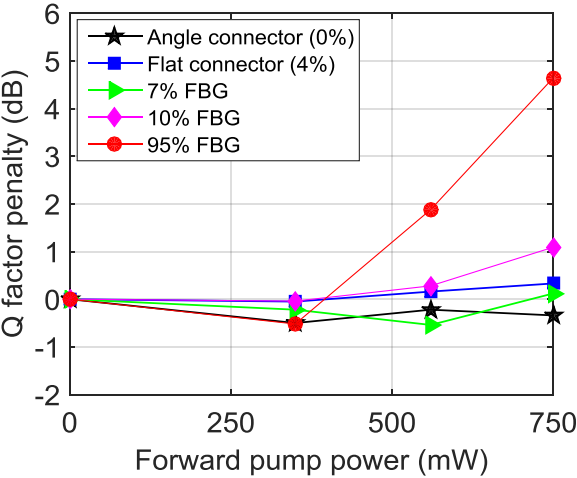
Figure 5. 21. Q factor penalty vs. forward pump powers for RFL based distributed amplifier schemes with different input reflection levels after 2000km transmission distance

Figure 5. 21 shows the Q factor penalty vs. increasing level of forward pump powers. At 0% input reflection from angle connector, there was no signal RIN penalty with increasing FPPs as discussed in the previous section and similarly no Q factor penalty was observed. Moreover, Q factor improvement (shown by negative values of Q factor penalty) up to 0.5dB was achieved at 750mW forward 1365nm pump power. At the highest level of input reflection from 95% FBG, Q factor penalties increased abruptly beyond 350mW forward pump powers with more than 4dB penalty at ~750mW. On the other hand, low input reflections allowed forward pump powers up to 750mW with Q factor penalties reaching up to maximum 1dB at 10% input reflection. So allowing low reflection from the input end improved the signal power variations resulting in improved OSNR and reduced the forward pump power requirement compared with 0% input reflection level or backward only pumping.

5.3   Conclusions

In this chapter, the RIN performances of different RFL based distributed Raman amplifiers have been demonstrated in details experimentally for different amplifier span lengths, input reflectivity and forward pump powers. It has been presented that low input reflection allows lower RIN transfer from 2nd order 1365nm pump to signal due to the lack of 1st order lasing at the input end but at the cost of poor forward pump power efficiency. We report that, at the presence of input reflection, a Fabry-Perot like intra-cavity 1st order laser is created along the whole amplifier and that helps to transfer more stochastic intensity noise from high power and noisy 2nd order forward pump to signal. Whereas at the presence of random lasing cavity at 1st order pump wavelength without any input reflection, there is almost no RIN transfer from pump to signal, which has also been demonstrated by showing no increase in RIN level in the intra-cavity 1st order lasing.

Finally, we have shown through coherent transmission experiment with an 83km distributed RFL based amplifier that, input reflection up to 10% can allow 40% forward pump power to the total pump power, keeping the Q factor penalty up to 1dB due to additional signal RIN penalty. These results give us useful information about how much forward pump powers can be used before signal RIN penalty dominates over the improved OSNR performance of RFL based DRAs.

CHAPTER 6

RIN MITIGATION TECHNIQUES IN DISTRIBUTED RAMAN AMPLIFIERS

In previous chapters different impairments of Raman amplification have been described including the impact of relative intensity noise (RIN) transfer from pump to signal. In chapter 5, it has been discussed that RIN transfer is critical in forward pumping configuration where pump and signal propagate at the same direction [22, 154, 155]. In backward pumping case, the intensity fluctuations from the pump are mostly averaged out and RIN transfer is minimized. Although backward only pumping is preferred in distributed Raman amplification to avoid the problem of RIN transfer from forward pumps to signal, however possible RIN mitigation can still improve the transmission performance significantly [101] in bidirectional and backward pumping schemes.

Here, novel RIN mitigation techniques in distributed Raman amplifiers (DRAs) using an incoherent broadband and low RIN pump will be discussed in details for both backward and bidirectional pumping schemes and also compared with conventional Raman pumping schemes.

In this chapter, the broadband incoherent first order pump based RIN mitigation technique has been proposed by the author. The experimental setup for broadband pump generation using different techniques was carried out by the author. The signal and pump RIN and power profiles at different bidirectional and backward pumping schemes were measured using the available setup at AIPT. Thanks to Dr Atalla El-Taher for his useful advices and helps in the lab to generate high power broadband pump. Dr Mingming Tan helped to build the recirculating loop based long-haul WDM coherent transmission experiment setup. The author is grateful to Dr Paul Harper to directly supervise the project and also to Dr Mingming Tan for his useful comments and helps during experiment. The publications related to this chapter are given below:

1. **M. A. Iqbal**, M. Tan and P. Harper, "On the mitigation of RIN transfer and transmission performance improvement in bidirectional distributed Raman amplifiers," J. Lightwave Technol. 36(13), 2611-2618 (2018).

2. **M. A. Iqbal**, M. Tan and P. Harper, "Enhanced transmission performance using backward-propagated broadband ASE pump," IEEE Photonics Technology Letters, 30(9), 865-868 (2018).

3. **M. A. Iqbal**, M. Tan, and P. Harper, "Transmission performance improvement using broadband incoherent counter-pumped distributed Raman amplification," in Proc. OFC 2018, paper Th1C.2.

4. **M. A. Iqbal**, M. Tan, and P. Harper, "Evaluation of RIN mitigated dual order bidirectional distributed Raman amplification using a broadband first order forward pump," in Proc. ECOC 2017, paper P1.SC1.13.

5. **M. A. Iqbal**, M. Tan, and P. Harper, "Enhanced long-haul transmission using forward propagated broadband first order Raman pump," in Proc. ECOC 2017, paper P2.SC6.25.

6. **M. A. Iqbal**, M. Tan and P. Harper, "RIN reduction technique for dual order forward pumped distributed Raman amplification," in Proc. CLEO/Europe-EQEC 2017, paper CI-2.2.

7. **M. A. Iqbal**, M. Tan, A. El-Taher and P. Harper, "RIN and transmission performance improvement using second order and broadband first order forward Raman pumping," in Proc. OECC and PGC 2017, paper P2-050.

6.1 RIN Mitigation Using a Novel Broadband Pump

RIN transfer from pump to signal not only depends on the RIN level but also on the spectral properties of the pump. Recently the use of smooth profile large bandwidth pseudo-incoherent pump in RIN transfer reduction is demonstrated theoretically [156] showing the reduced transfer of amplitude noise due to the non-degenerate four wave mixing (FWM) process among broadband pump and signal frequencies with random phase variations. We experimentally demonstrate significant signal RIN reduction and OSNR improvement in dual and first order forward pumped bidirectional and backward only pumping using a novel broadband first order source in an 83km long standard single mode fibre (SSMF) based distributed Raman span [157-161]. A detail experimental characterisation of signal RIN and power evolution along the amplifier span are discussed here.

6.1.1 Broadband pump generation techniques and its characteristics

Here, the broadband 1st order forward pump seed was generated by backward pumping a 10km long SSMF with 1365nm pump [162, 163]. The 10km fibre length was used as a compromise between the pump power requirement and 1st order power generation efficiency. The proposed method was simpler and different from the previously reported techniques: manipulating the cavity properties of a semiconductor optical amplifier (SOA) [164] or cascading multiple semiconductor pumps packaged in a fully integrated optical module [165]. The broadband light around 1455nm was generated by the backward 1365nm pump using the Raman scattering property in the fibre, which was then Rayleigh backscattered and re-amplified by the same pump to provide broadband source in an open cavity [145, 159, 160].

We investigated two techniques of broadband pump generation: scheme-1 with no reflection from both ends and scheme-2 allowing 4% Fresnel reflections into the cavity as shown in Figure 6. 1. The choice of 10km SSMF with no reflections ensures a low RIN (~ -132dB/Hz), stable and efficient 1st order seed. Although providing a small Fresnel (~4%) back-reflections in the cavity improves 1365nm pump efficiency but the RIN of the generated 1455nm pump becomes very high (~ -120dB/Hz) and unstable due to unwanted lasing from the double Rayleigh scattered (DRS) feedback [145].
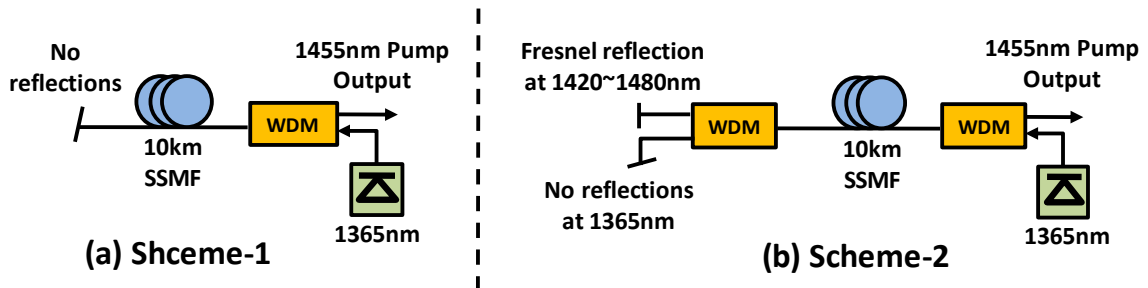
Figure 6. 1. Broadband 1st order (1455nm) pump generation schemes (a) scheme-1: no reflection from both ends and (b) scheme-2: 4% Fresnel reflection into the cavity from far end of the pump

The comparison of pump RIN and spectral properties between these two schemes are presented in Figure 6. 2(a) and (b) respectively. Both the schemes show the similar spectral properties with 3dB bandwidth of about 18nm. Scheme-2 spectrum is bit narrower at the longer wavelengths from the peak due the inclusion of small reflection in the cavity. As there is no reflections from the either end of the span in scheme-1, the generated output power of generated 1455nm seed is very low and remains within 2~3mW using 1365nm pump power up to 4W [163].
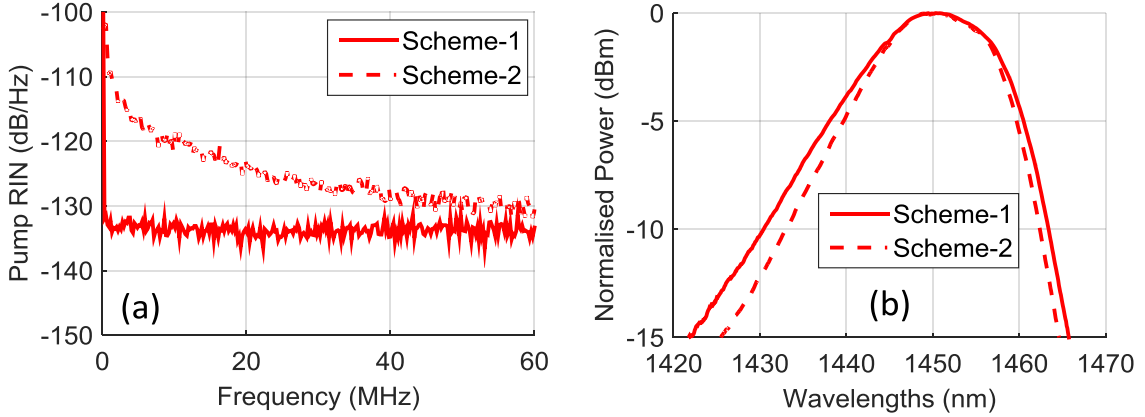
Figure 6. 2. Comparison of broadband 1st order (1455nm) pump (a) RIN and (b) spectral properties

So, a very broad and low RIN 1st order source around 1455nm was possible to generate using scheme-1 which was then used in different distributed pumping schemes for RIN mitigation from higher order pump to signal in the following sections of this chapter.

6.2 RIN Mitigation in Backward Pumped Dual Order Distributed Raman Amplification

Backward pumping is usually preferred in long-haul transmission systems with distributed Raman amplifier (DRA) for avoiding the deleterious effects of RIN transfer from forward propagating pumps. In backward pumping scheme, the signals and the pumps travel in opposite direction, so the RIN evolution is averaged out over the long span length and also has lower cut-off frequency of RIN transfer function [22]. However, the amount of RIN transfer up to 10-100kHz frequencies mainly depends on the RIN level of the backward pump(s) and can still limit the transmission performance. Higher order pumping is also desirable to distribute the gain further into the amplifier span and improve OSNR. So for backward and higher order pumping would provide simultaneous reduction of ASE and signal RIN [166-168].

In this section, we present a dual-order backward pumping scheme which uses an incoherent broadband 1st order pump. This pumping scheme improves the ASE noise performance by distributing the gain further into the amplifier span and suppresses the signal RIN penalty by mitigating the evolution of RIN transfer from higher order 2nd order pump to signal. Here, the dual-order backward pumping consists of a 1365nm 2nd order fibre laser and a broadband 1455nm 1st order seed, generated using Raman and Rayleigh scattering. We show that, the use of inherently depolarised 1st order broadband pump allows improved transmission performance by reducing the

signal RIN penalty compared with conventional 1st order Raman pumps i.e. low RIN semiconductor pumps or random distributed feedback (DFB) based Raman fibre laser (RFL) pump with narrow bandwidth profile. In a 10×120Gb/s DP-QPSK WDM system as shown in Figure 6. 8, our proposed pumping scheme extends the transmission reach up to 7915km with 833km transmission reach improvement compared with conventional Raman pumping schemes. In addition, the use of such broadband pumping can provide a flatter gain spectrum, which reduces the number of pumps required in broadband (i.e. C and L band) transmission.

6.2.1 Characterisation of backward pumped DRA span

We investigated three dual-order counter-pumped DRA schemes with ~83km standard single mode fibre (SSMF) which include a commercially available depolarised 1365nm Raman pump laser from IPG with -125dB/Hz RIN as 2nd order backward pump and different 1st order sources: proposed broadband pump, commercial semiconductor pump and random fibre laser (RFL) pumps shown in Figure 6. 3(a)-(c) respectively.
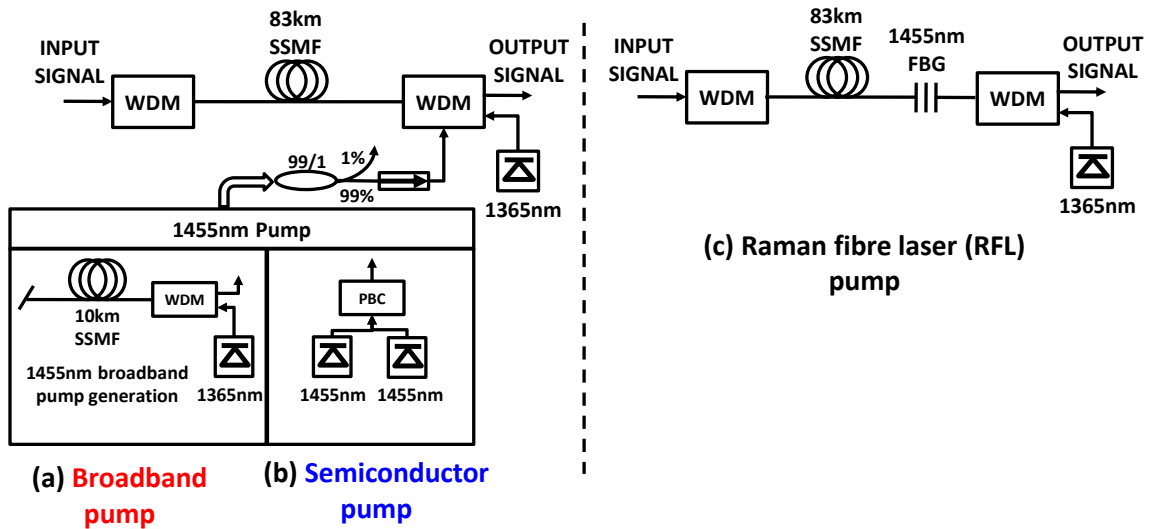
Figure 6. 3. Dual order backward pumped distributed Raman amplification schemes including a 1365nm Raman laser as 2nd order pump and different 1st order sources: (a) proposed broadband pump; (b) semiconductor pump and (c) RFL pump

In Figure 6. 3(a), the broadband 1st order pump seed at 1455nm was generated by backward pumping a separate 10km SSMF by another 2nd order 1365nm pump at ~3.5W power in an open cavity configuration [135, 145]. Here in addition to scheme-1, the generated 1st order seed was then amplified by the residual 1365nm pump in a similar 2nd stage configuration including a 10km TrueWave single mode (TW-SM) fibre to launch 20mW of 1455nm broadband pump into the main amplifier span as shown in Figure 6. 4(a). The generated broadband 1st order pump power with

respect to the 1365nm pump is also shown in Figure 6. 4(b). So, a maximum of 250mW of broadband pump stable output power can be obtained using ~3.8W of 1365nm pump power in a cascaded two stage setup. The lengths of SSMF and TW-SM in the broadband seed generation sections were optimized for efficient generation of stable 1455nm broadband pump power without any parasitic lasing effects caused by excessive Rayleigh scattering in the fibre at very high input pump power. The 3dB bandwidth and RIN level of the pump were measured as about 12nm and -132dB/Hz respectively.
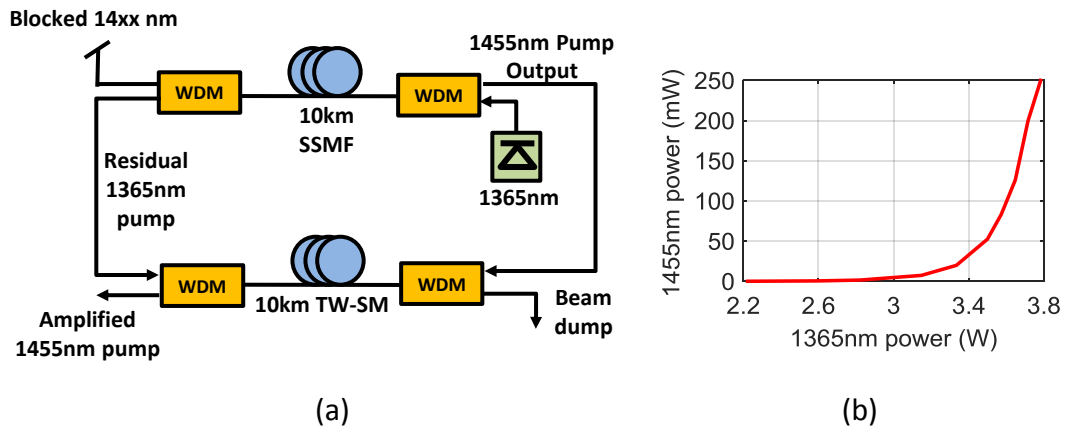
Figure 6. 4. (a) Broadband 1st order pump generation using an amplified 2nd stage (b) broadband 1st order pump power vs. generating 1365nm pump power

In Figure 6. 3(b), two 1455nm semiconductor laser diodes with 0.8nm 3dB bandwidth and -135dB/Hz RIN were depolarised through a polarisation beam combiner (PBC) and used as 1st order pump as depicted. The 1st order pump was combined with the 2nd order 1365nm pump and then to the amplifier span through a 3×1 WDM coupler. An isolator and a 99/1 tap coupler were also used at the 1455nm pump output to restrict the back-propagated pumps and monitor the input power into the span respectively. Fixed 20mW and 1W powers of 1st and 2nd order backward pumps were used respectively in both the cases of broadband and semiconductor pump to maintain 0dB net loss across the ~83km Raman span.

Figure 6. 3(c) shows a RFL based dual order pumping including a 1365nm pump and a high reflectivity (95%) fibre Bragg grating (FBG) centred at 1455nm with 95% reflectivity and 0.6nm 3dB bandwidth. The RFL at 1455nm was formed in a distributed cavity created by the Rayleigh scattering and feedback from the FBG [135]. A 1365nm pump power of 1.1W was required to overcome the lasing threshold and maintain 16.5dB Raman on-off gain. An additional 100mW pump power was required to overcome the random lasing threshold in the ~83km span compared

with other 1st order pumped schemes. The generated lasing at 1455nm has a 3dB bandwidth of ~0.6nm due to some spectral broadening resulted from the thermal effect at the high power of 1365nm [169, 170] and very high RIN level of -115dB/Hz. Here, the FBG based scheme gave a cost-effective solution by replacing a pump laser at 1455nm at the cost of 100mW extra power of 1365nm Raman pump laser. The pump RIN and spectral properties of these three different types of 1st order sources are given in Figure 6. 5 and Figure 6. 6 respectively.
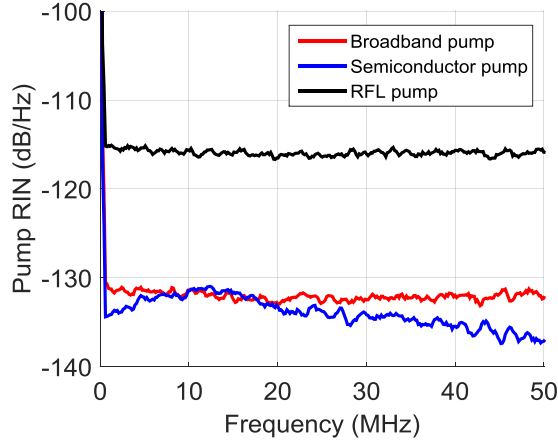
Figure 6. 5. Comparison of the RIN levels of three different 1st order pump sources

As expected the RFL pump and semiconductor laser has the highest (-115dB/Hz) and the lowest (-135dB/Hz) RIN levels respectively. Broadband pump shows much lower RIN than RFL but slightly higher average RIN than semiconductor pump at -132dB/Hz. According to these pump RIN levels, much less RIN transfer is expected in the proposed dual order backward pumping with the broadband 1st order seed.
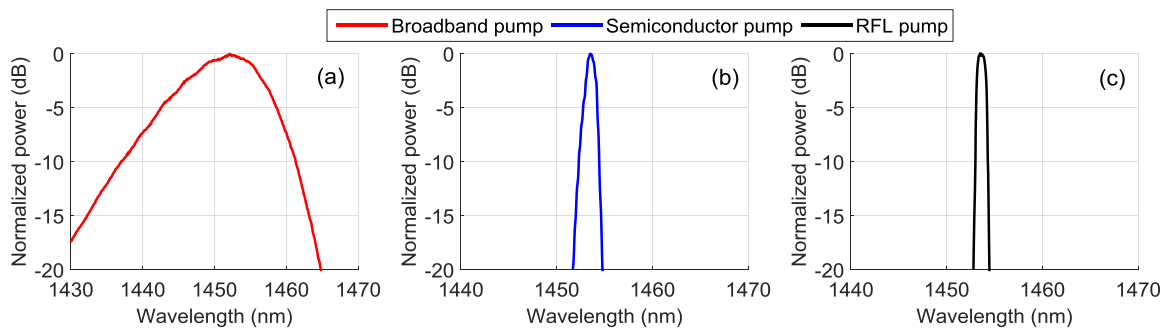
Figure 6. 6. Pump spectra of different 1st order sources: (a) broadband pump; (b) semiconductor laser diode and (c) Raman fibre laser (RFL) pump

Figure 6. 6 shows the spectral properties of different 1st order pumps. Broadband pump shows much wider 3dB bandwidth (>10 times) than those of semiconductor pump and RFL pump with 0.8 and 0.6nm 3dB bandwidth respectively.

In backward pumped DRA, the RIN transfer can be observed mainly in the low frequency regime (10 to 100kHz). In the experimental setup, RIN measurement was possible from 166kHz to 100MHz, which limited us to measure signal RIN in low frequencies and observe significant change in signal RIN levels in different schemes discussed here. In order to verify the impact of RIN transfer in all the schemes, we maintained similar signal power profiles for all to ensure equal ASE noise performance. So that, any improvement in transmission experiment corresponded to the improved signal RIN performance. The signal power profiles were measured at 194THz (1545.32nm) signal using a modified optical time domain reflectometer technique [153], as discussed in chapter 5. The pump powers used here provided similar profiles with 5.8~6dB SPVs across all three backward pumped DRA schemes as shown in Figure 6. 7.
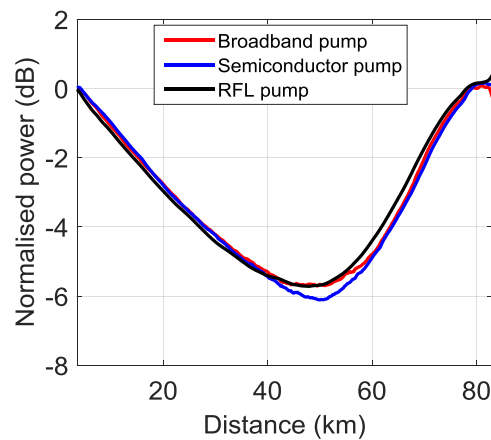
Figure 6. 7. Signal power profiles along the amplifier span for different 1st order pumped dual order backward pumped DRA schemes

In the dual order backward pumped DRAs, the main RIN transfer to the signal comes from the high RIN 1365nm fibre laser because the 1455nm seed pumps were really low powered at 10~20mW. So the highest RIN transfer is expected from RFL pumped scheme with both the high RIN 1st and 2nd order pumps. Semiconductor pumps based scheme has the lowest 1st order pump RIN as shown in Figure 6. 5, however narrow bandwidth profile still allows some RIN transfer from 2nd order 1365nm pump to signal. The broadband incoherent 1st order pump also has similar RIN as semiconductor pump, but RIN from higher order pump gets distributed over the wide bandwidth of

131

1st order pump and averaged out due to the non-degenerate four-wave mixing effects [156, 164], which subsequently ensures the lowest overall RIN transfer to the signal.

6.2.2 Transmission results

The coherent transmission experiment was performed in a recirculating loop setup as shown in Figure 6. 8. Ten DFB lasers from 194.3THz (1542.94nm) to 193.4THz (1550.12nm) with 100GHz spacing were multiplexed using an arrayed waveguide grating (AWG) to form the WDM grid. The output of the multiplexed signal was then combined with a 100kHz linewidth (LW) external cavity laser (ECL) used as "channels under test (CUT)". During each measurement, the particular DFB laser was switched off and replaced by the CUT. The continuous wave (CW) signal channels were then QPSK modulated using a Mach-Zehnder I-Q modulator. The applied electrical signal from a pulse pattern generator (PPG) was 30Gb/s, 2^{31}-1 word length, normal and inverse pseudo random binary sequences (PRBS) patterns with a relative delay of 18bits. The output 10×30GBaud QPSK signals were then amplified using a polarisation maintaining EDFA (PM-EDFA) and polarisation multiplexed through a polarisation multiplexing (POLMUX) emulator with a relative delay of 300symbols (~2ns) between the two polarisation states to generate 10×120Gb/s DP-QPSK signals at the input of the loop.
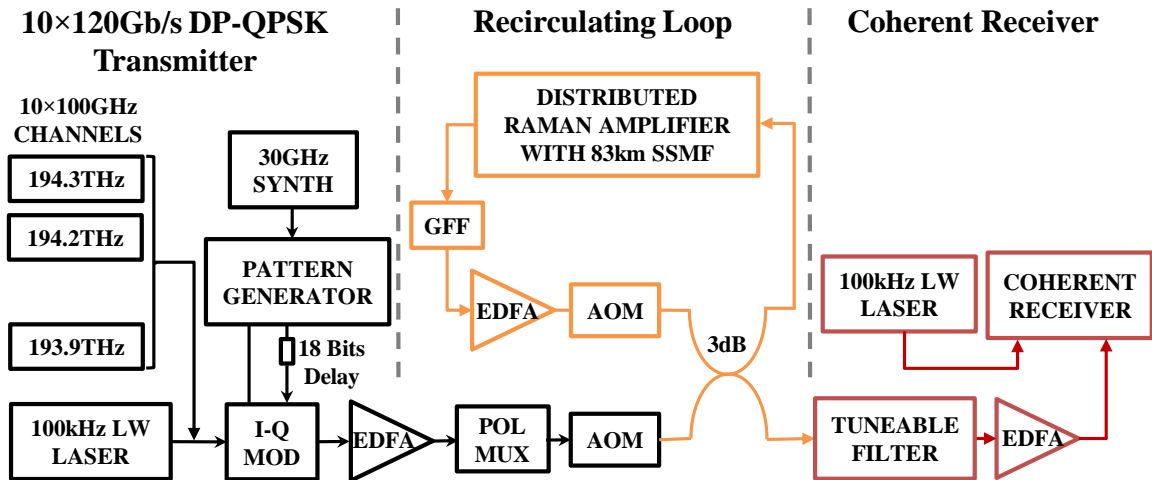
Figure 6. 8. Schematic diagram of long-haul coherent WDM transmission system in a recirculating loop setup. Abbreviations: SYNTH = synthesizer, POLMUX = polarisation multiplexer, LW = linewidth, GFF = gain flattening filter and AOM = acousto-optic modulator

The transmission span in the recirculating loop was formed by the distributed Raman span with ~83km SSMF with a total loss of 17.6dB including 16.5dB span loss and 1.1dB passive component loss from pump/signal combiners. A dual-stage EDFA was used to compensate the additional 12dB

loop losses from gain flattening filter (GFF), 3dB coupler and acousto-optic modulator (AOM). At the receiver, the received signal is first de-multiplexed using a tuneable bandpass filter and then amplified using an EDFA before passing it to a standard polarisation diverse coherent receiver with 80GSa/s and 36GHz bandwidth oscilloscope. Digital signal processing (DSP) was applied in offline post-processing for linear impairment mitigation and signal recovery. Q factors were measured from actual bit error counting and averaged over 2 million bits. A HD-FEC limit of 8.5dB Q factor was considered for performance measurement.

First of all, in order to compare the transmission performance of different dual order backward pumped DRA schemes, maximum Q factor at optimum launch power was determined through a launch power per channel sweep and then at the optimum launch power, respective maximum distance was obtained for all the schemes.
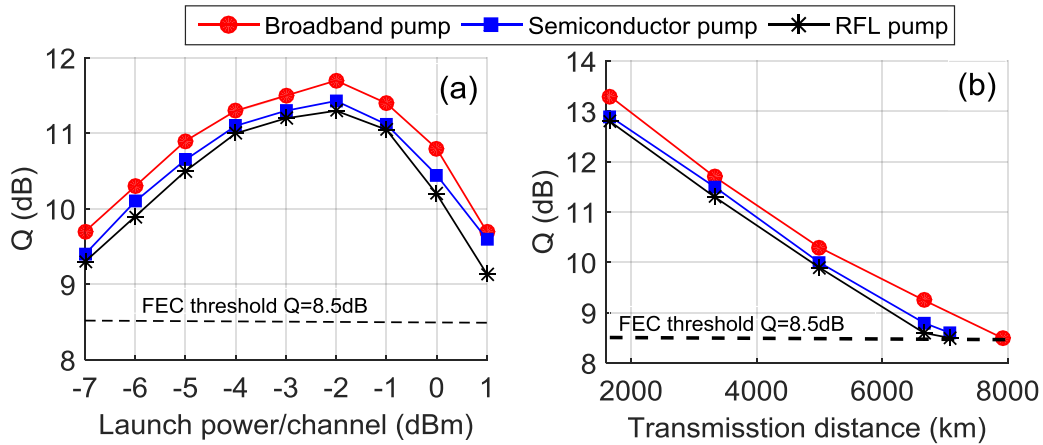
Figure 6. 9. Transmission performance comparisons among three different dual order backward pumped schemes: (a) Q factors vs. launch power per channel at 3333km and (b) Q factors vs. transmission distance at the optimum launch power measured at 194THz (1545.32nm) signal

Figure 6. 9(a) and (b) show the Q factors versus signal launch power per channel and Q factors versus transmission distance at optimum launch power respectively measured for the middle WDM signal at 194THz (1545.32nm) in three different dual-order counter-pumped schemes. The proposed broadband 1st order pumped scheme shows the maximum Q factor of 11.7dB at optimum launch power per channel (-2dBm) with an improvement of 0.3dB and 0.4dB compared to conventional semiconductor laser and RFL pumped schemes respectively. As all the schemes have similar signal power profiles as shown in Figure 6. 7, a similar noise performance was expected and an equal optimal launch power of -2dBm for all the schemes was also observed in Figure 6. 9(a). However, a similar Q factor enhancement in both linear and nonlinear regime proves the

resulted improvement, due to the mitigation of signal RIN penalty in case of broadband pump. The RFL based scheme shows the worst Q factor of 11.3dB at optimum launch power due to the highest signal RIN penalty, whereas semiconductor pump performs slightly better (0.1dB) than RFL pump. In Figure 6. 9(b), the proposed broadband pumped scheme provided maximum transmission distance up to 7915km with 833km reach extension compared with similarly performed (~7082km) other conventional pump sources considering an HD-FEC threshold of Q = 8.5dB. Q factors and received spectra at the maximum transmission distances for all the Raman pumping configurations are also shown in Figure 6. 10.
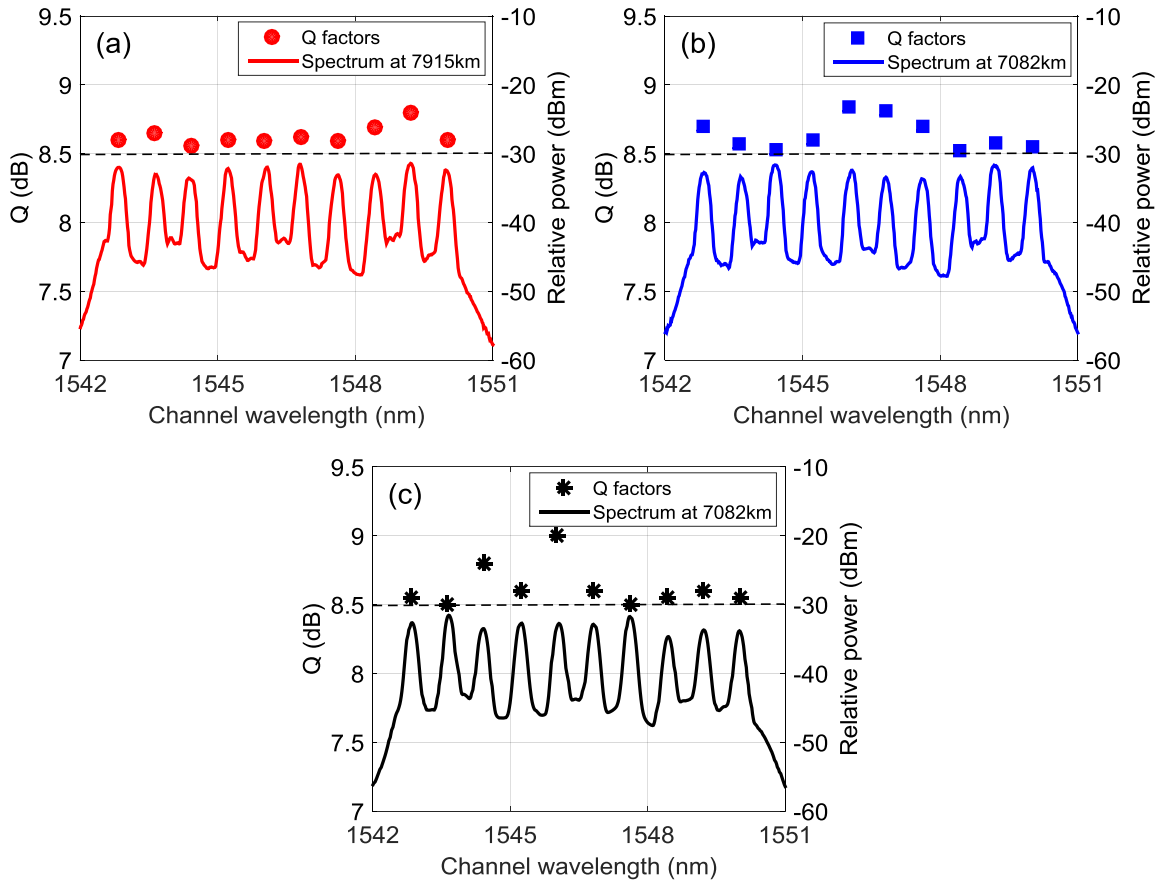
Figure 6. 10. Q factors and received spectra at maximum transmission distance for corresponding dual order backward pumping scheme with different 1st order sources: (a) broadband pump; (b) semiconductor pump and (c) RFL pump

So we can conclude that, using only a 20mW incoherent broadband seed in a dual-order backward pumped DRA can significantly reduce the RIN transfer from higher order pumps to signal. This allows a minimum of 833km transmission reach extension compared with conventional dual order Raman backward pumping schemes based on widely deployed low RIN semiconductor laser and

cost-effective FBG assisted random DFB fibre laser. Such broadband pump can provide flatter and wider gain spectrum which is also useful and cost-effective for broadband transmission.

6.3 RIN Mitigation in Dual Order Forward Pumped Bidirectional DRA

Using bidirectional DRA in long haul, high-capacity DWDM transmission systems improves OSNR compared to lumped amplification due to lower ASE noise and better SPV along the transmission span [171]. Dual-order forward pumping can distribute the gain more evenly further into the span compared with 1st order improving OSNR but that comes with a penalty of poor pump efficiency [133] and RIN transfer to signal from high power 2nd order pump laser [172].

In dual order bidirectional DRA, 2nd order pump acts as the primary source of gain and RIN, whereas 1st order pump works like a seed with very low power. RIN transfer from primary higher order pump to signal not only depends on the pump RIN of the 1st order seed but also on the spectral property. Recently the use of smooth profile, broad bandwidth pseudo-incoherent pump in RIN transfer reduction is demonstrated theoretically [156] showing the reduced transfer of amplitude noise due to the non-degenerate four wave mixing (FWM) process among broadband pump and signal frequencies with random phase variations. However to our knowledge, long-haul WDM coherent transmission performance using a RIN mitigated bidirectional distributed DRA with broadband forward pump is not well documented. An experimental demonstration has been reported for a single channel coherent transmission system, but the performance benefits were not clearly established with conventional backward only pumping and other pump sources [49].

In this section, we demonstrate an efficient use of an inherently depolarised broadband and low RIN 1st order pump with much wider 3dB bandwidth (~18nm) than conventional pump sources, for significant signal RIN mitigation up to a level comparable to backward only pumping in dual order forward pumped bidirectional DRAs. In dual order forward Raman pumping, stochastic amplitude fluctuations from high power and high RIN 2nd order pump is transferred and distributed over the random phases of broadband 1st order seed. Eventually the intensity noise evolution is averaged out over the wide bandwidth of the low RIN pump and subsequent RIN transfer to the signal is mitigated. We also optimize the forward 2nd order 1365nm pump powers for the maximum signal RIN reduction with best transmission performance. The transmission performance improvement due to the benefit of improved OSNR from forward pumping are also presented and compared with conventional low RIN pumps. We report more than 10dB signal RIN reduction and transmission

reach extension of a 10×120Gb/s coherent WDM transmission system up to minimum of 1250km compared with low RIN 1st order semiconductor pump based dual order forward pumping.

6.3.1 Characterisation of dual order forward pumped bidirectional DRA

The configuration of dual order forward pumped bidirectional DRA are shown in Figure 6. 11. An 83km SSMF amplifier span was backward pumped by a 2nd order (1365nm) Raman fibre laser. A high reflectivity (95%) fibre Bragg grating (FBG) with centre wavelength at 1455nm and 3dB bandwidth of 0.6nm was used at the output of the span to provide feedback at the 1st order pumping wavelength. Dual order forward pumping consisted of a 2nd order 1365nm pump combined with the broadband 1st order pump at 1455nm which was generated using the technique described in Figure 6. 1(a) (scheme-1).
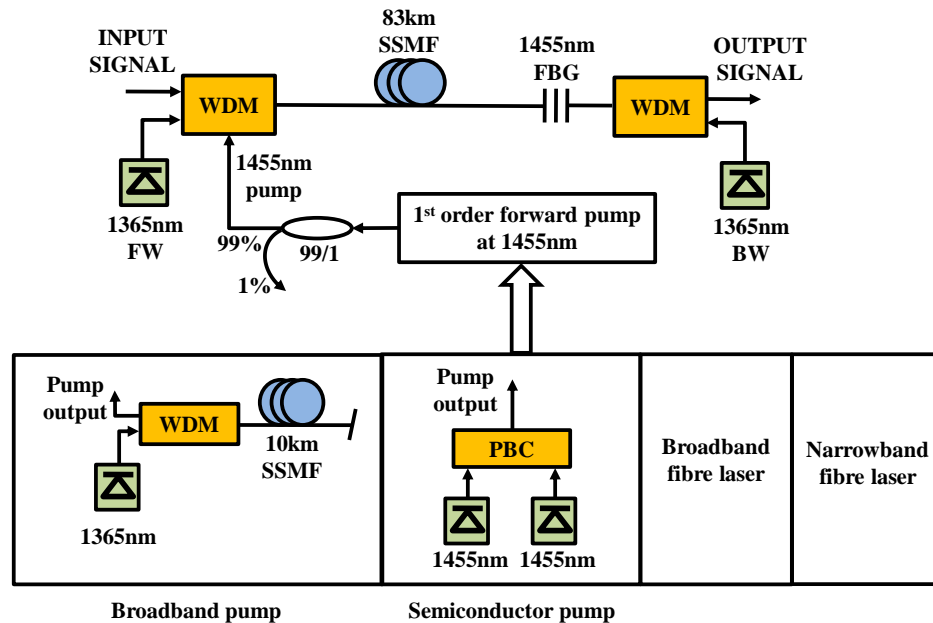
Figure 6. 11. Bidirectional distributed Raman amplifier with 83km SSMF span and proposed dual forward pumping schemes (FW = forward, BW = backward)

The broadband 1st order forward pump was inserted into the amplifier span (~83km) through an bidirectional WDM which allowed the amplified 1455nm light from the 83km transmission span to be reflected back into the seed generation span (10km SSMF) and to be further amplified. Finally, stable ~20mW broadband pump was maintained into the transmission span using ~3.5W of 1365nm pump in the seed generating section and monitored through a 99/1 tap.
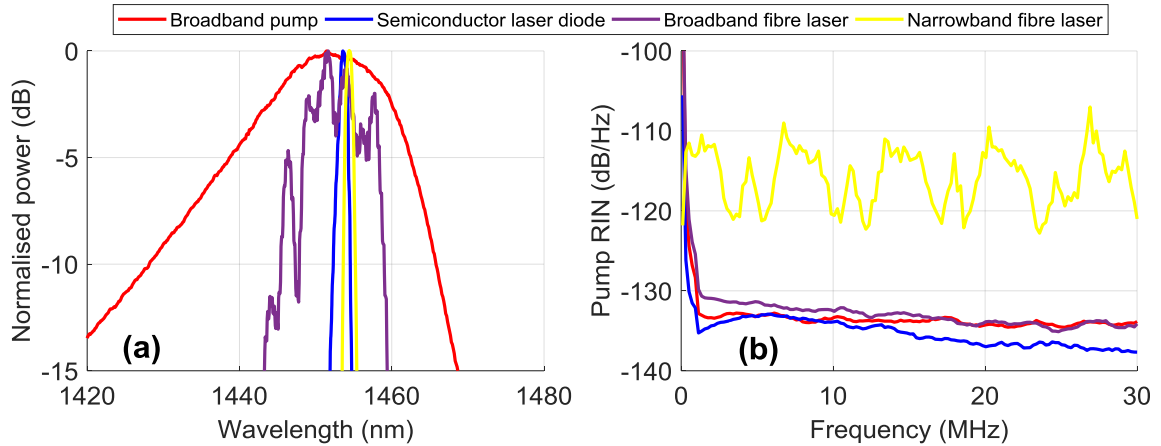
Figure 6. 12. Comparison of spectral properties and RIN profiles of different 1st order pump sources used in dual order forward pumped bidirectional DRA schemes

The broadband pump had much wider 3dB bandwidth (~18nm) than conventional 1st order pump sources and low RIN level (-132dB/Hz) as shown in Figure 6. 12(a) and (b) respectively. For performance comparison, widely deployed conventional 1st order semiconductor laser diodes at 1455nm with ~0.8nm 3dB bandwidth and -135dB/Hz RIN were used. The pumps were depolarised through a polarisation beam combiner (PBC). In addition, a commercial broadband fibre laser with low RIN (-130dB/Hz) and reasonably wide (~8nm) bandwidth and also a narrowband fibre laser with high RIN (-113dB/Hz) and narrow bandwidth (~0.5nm) were used for performance comparison with the proposed broadband pump. The maximum output power of the commercial fibre lasers was ~5W and also depolarised.

We first studied the signal RIN and power variation along the amplifier span at 194THz (1545.32nm) signal. The results were then compared with other dual order forward pumping schemes using low RIN conventional 1st order semiconductor laser diode, fibre laser with broad and narrowband spectral profiles and backward only pumping. Fixed 750mW and 20mW forward pump powers were used for 1365nm and 1455nm sources respectively for the comparison. Also the signal RIN performances were optimized for different pump powers of forward 1365nm which was the primary source of RIN transfer to the signal. Then the benefit of OSNR improvement using dual order forward pumping with minimal RIN penalty is demonstrated through WDM coherent transmission experiment.
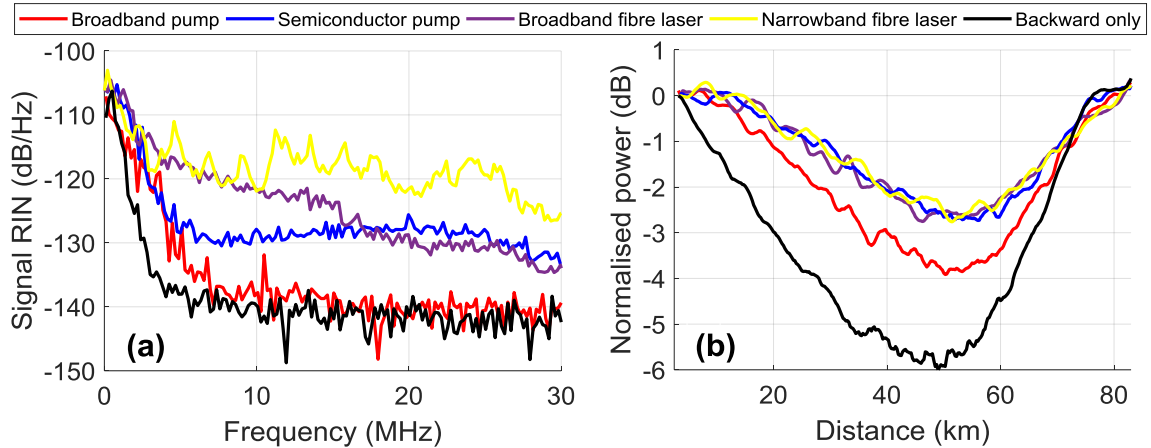
Figure 6. 13. Comparison of (a) signal RIN and (b) signal power profiles along the amplifier span length among different dual order forward pumped bidirectional DRAs with broadband and narrowband forward 1st order pump seed and backward only pumping

In Figure 6. 13(a), signal RIN were measured with fixed 2nd and 1st order forward pump powers of 750mW and 20mW respectively. Backward 1365nm pump powers were varied between 1 and 1.2W in order to maintain 0dB net gain across 83km SSMF span in each scheme. The signal RIN from backward only pumping was the lowest and baseline for minimum signal RIN. Dual order forward pumping with broadband 1st order source shows the lowest signal RIN compared with other commercial 1st order pumped schemes. The 1st order broadband seed distributes the transferred RIN from higher order noisy 1365nm pump over the random phases of its wide bandwidth. The overall noise evolution to signal is then averaged out and mitigated significantly. Semiconductor pump shows more than 10dB signal RIN level increase than broadband 1455nm seed below 25MHz despite having the lowest pump RIN profile, whereas both broadband and narrowband fibre lasers show even worse results due to the higher pump RIN levels as shown in Figure 6. 12(b).

The SPVs along a single span amplifier for different schemes are shown in Figure 6. 13(b). As expected backward only pumping has the highest SPV of ~6dB. Broadband 1st order pumped scheme shows 4dB SPV which is 2dB better than worst performed backward only pumping. In bidirectional dual order pumping schemes, broadband 1st order pumped scheme has 1dB more SPV than other conventional sources which is mainly due to the poorer power spectral density.

So far the performance characterisation have been carried out for fixed forward pump powers of 2nd and 1st order pumps at 750mW and 20mW respectively. A clear benefit of broadband 1st order pumped bidirectional dual order DRA has been established over the conventional narrowband

138

pump sources due to significant RIN transfer mitigation from forward pumps. Then a further characterisation have been carried out to optimize the performance of broadband 1st order forward pumped scheme for maximum signal RIN mitigation with improved OSNR. To do so, we carried out signal RIN characterisation by varying the forward 2nd order pump power from 300mW to 950mW and at fixed broadband 1455nm forward pump power at 20mW as a seed.
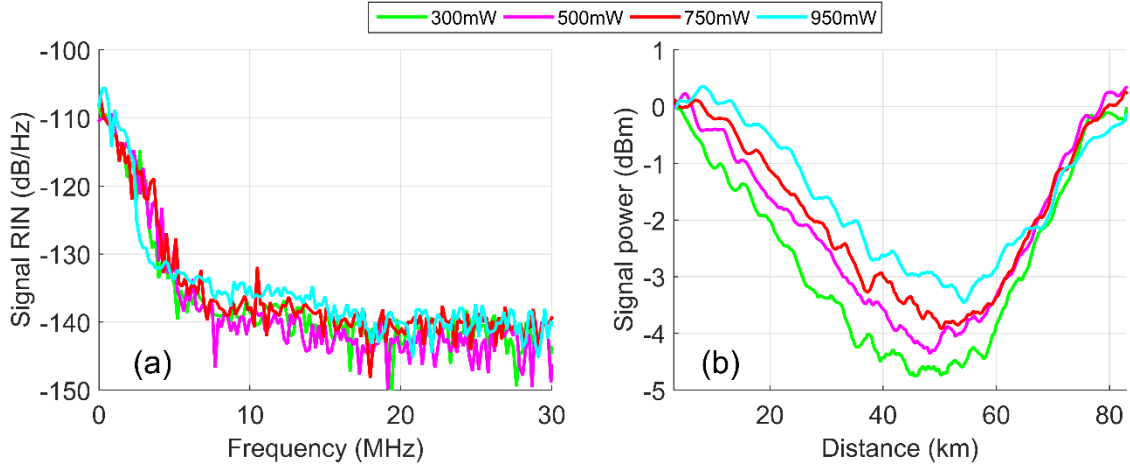
Figure 6. 14. Dual order forward pumped DRA characterisation at fixed 20mW 1st order broadband forward pump and different 2nd order forward pump powers: (a) signal RIN (b) signal power profile along the amplifier span

Table 6. 1. Forward 2nd order pump power ratios used in the characterisation

1365nm forward pump power (mW)	1455nm forward pump power (mW)	1365nm backward pump power (mW)	Total pump power (mW)	1365nm forward pump power ratio (%)
300	20	1230	1550	19.4
500	20	1200	1720	29.1
750	20	1150	1920	39.1
950	20	1096	2066	46

Figure 6. 14(a) and (b) show the signal RIN and power evolution along the span at varying forward 1365nm pump powers. The primary forward 1365nm pump powers and ratios with respect to the total pump power are given in Table 6. 1. The integral of signal RIN up to 20MHz for 300mW, 500mW and 750mW power of forward 1365nm pump give almost similar results ~ -101.2dB/Hz with only 0.5dB variation. Whereas, a clear increase in signal RIN level below 20MHz can be seen at 950mW, which gives about -98.8dB/Hz integral RIN up to 20MHz and that is more than 2dB higher than that of other forward pump powers considered here. Figure 6. 14(b) shows that, SPVs

139

were reduced from 4.8dB to 3dB as forward 1365nm pump power (ratio) was increased from 300mW (19.4%) to 950mW (46%). So increasing the forward 1365nm pump power to 950mW improved the SPV by 1.8dB, however significant signal RIN level increase would deteriorate the transmission performance which will be discussed in the next section.

6.3.2 Transmission performance

Long-haul coherent transmission experiments with 10×120Gb/s DP-QPSK WDM system have been carried in a recirculating loop as shown in Figure 6. 8, in order to compare the transmission performances with backward only pumping and other bidirectional pumping schemes. Firstly, we compared the performance of the proposed broadband 1st order pumped dual order bidirectional DRA scheme at different forward 1365nm pump powers to determine the best transmission performance and optimum pump powers. Then performances were compared with other conventional 1st order forward pump sources at fixed pump power combinations.
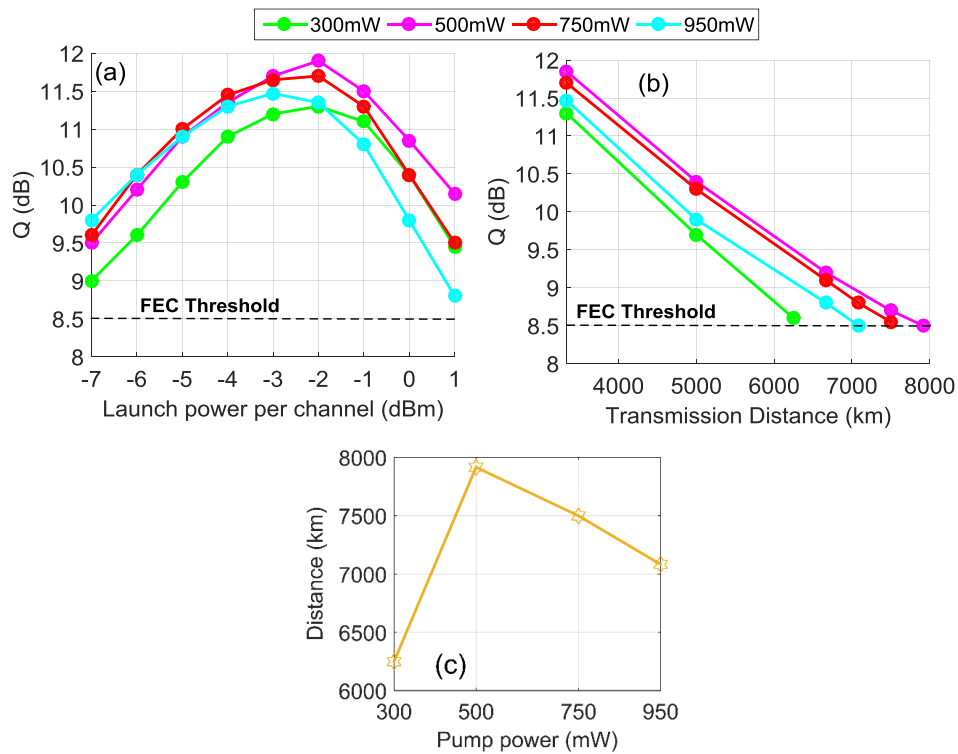
Figure 6. 15. Transmission performance characterisation of dual order forward pump bidirectional DRA: (a) Q factors vs. launch power per channel (b) Q factors vs. transmission distance and (c) maximum transmission reach at different forward 1365nm 2nd order pump powers

Figure 6. 15(a) shows the Q factors versus launch power per channel at 3333km transmission distance with varying forward 1365nm pump powers. We achieved maximum Q factor of 11.9dB

at 500mW of 1365nm forward pump power which is ~29% of the total power as shown in Table 6. 1. The maximum transmission distance was also extended up to 7915km at this pump power as shown in Figure 6. 15(b). Increasing the 1365nm pump power (ratio) up to 750mW (~39%) degraded the maximum Q factor by 0.2dB and reach by 420km due to additional signal RIN penalty. Increasing forward 1365nm pump power (ratio) further up to 950mW (46%) improved the OSNR by reducing the SPV to 3dB (Figure 6. 14(b)) but transmission reach was degraded to 7082km due to the increase in signal RIN. On the other hand, forward pump power reduction to 300mW resulted in the poorest OSNR and lowest reach up to 6225km. It can be seen from Table 6. 1 that, ~39% of the total pump power could be used in forward pumps without significant RIN penalty which extended the maximum transmission reach up to 7915km. The maximum distances at different forward 1365nm pump powers are also depicted in Figure 6. 15(c) which shows the reach improvement up to 7915km with 500mW then it deteriorated due to increased signal RIN penalty at 750mW and 950mW pump powers.

Then we compared the transmission performance of proposed broadband 1st order pumped scheme with other three conventional 1st order sources with fixed 750mW and 20mW of forward 1365nm and 1455nm pump powers in order to validate the improved signal RIN performance from the characterisation shown in Figure 6. 13.
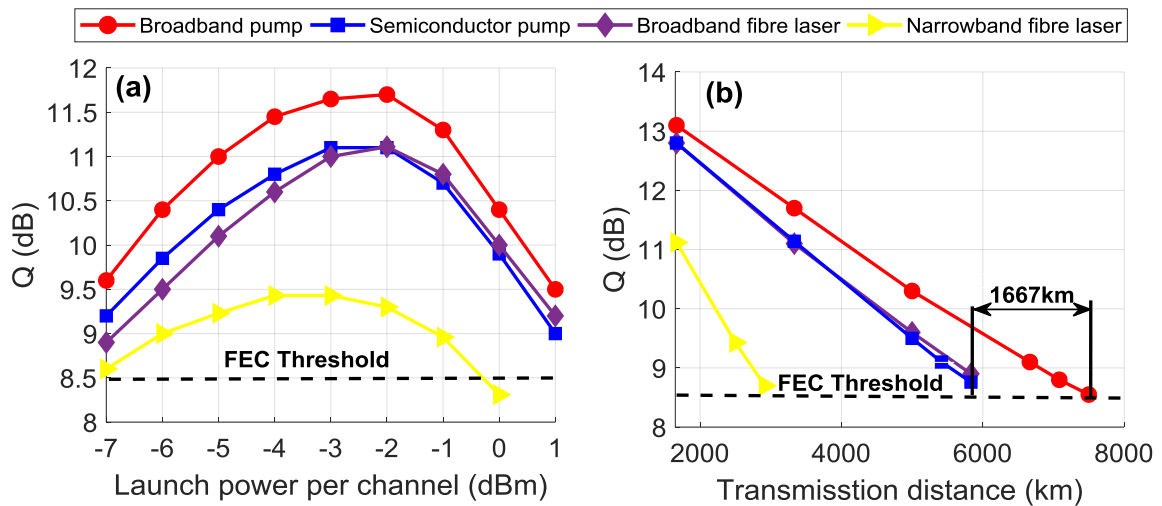
Figure 6. 16. Transmission performance comparison at fixed 750mW and 20mW of 2nd and 1st order forward pump powers respectively with different 1st order forward pump sources: (a) Q factors vs. signal launch power per channel at 3333km and (b) Q factors vs. transmission reach at optimum launch power

In Figure 6. 16(a) and (b), dual order forward pumping with 1st order semiconductor laser diode and broadband fibre laser produces similar results with 11.1dB maximum Q factor and 5832km

transmission reach at optimum launch power. The benefits of reduced signal RIN and improved OSNR with broadband 1st order pumped dual order forward pumping scheme provided a maximum Q factor of 11.7dB and transmission reach up to ~7500km with at least 0.6dB improved Q factor and 1667km enhanced reach respectively compared with conventional narrowband 1st order sources. Narrowband 1st order fibre laser based forward pumping demonstrated the worst performance among all the configurations giving only optimum Q factor of 9.4dB and reach up to 2900km due to highest signal RIN penalty as shown in Figure 6. 13(a).

Then we also measured the Q factor of each WDM signal in the 10 channel WDM grid at maximum transmission distance for different bidirectional pumping scheme. The overall flatness of the gain spectrum at the maximum transmission distance remained reasonably flat within ±1dB and Q factor of each channel was measured above the considered HD-FEC limit of 8.5dB for DP-QPSK modulation format as shown in Figure 6. 17(a)-(d).
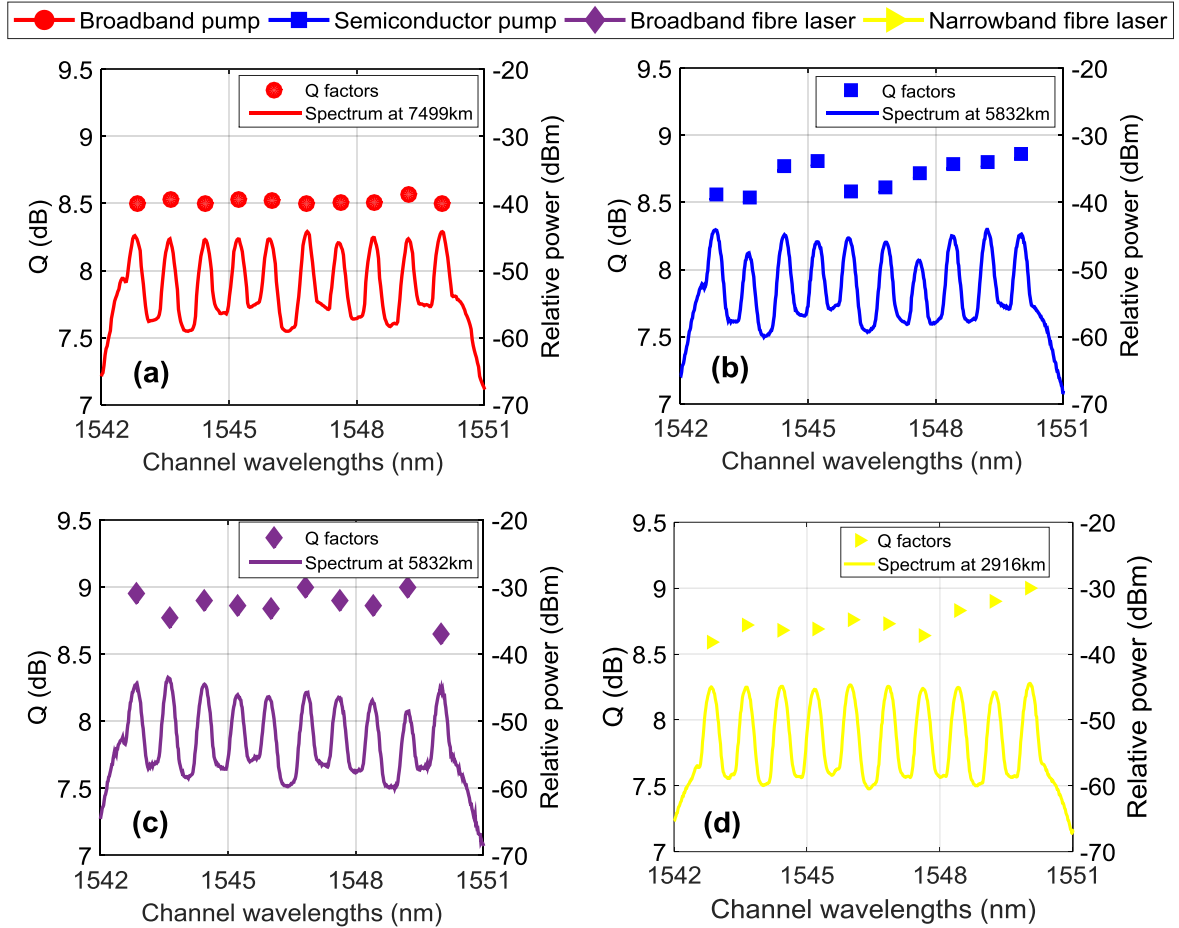
Figure 6. 17. Q factors of WDM signals at maximum transmission distance and corresponding spectrum for bidirectional dual order pumping scheme with different first order sources: (a) proposed broadband pump (b) semiconductor pump (c) broadband fibre laser and (d) narrowband fibre laser

It is clear from above transmission results that, our proposed broadband first order pumped dual order bidirectional DRA scheme performed much better than other conventional sources in RIN mitigation and transmission performance improvement with improved OSNR.

Finally, the transmission performance were also compared with widely deployed low RIN 1st order semiconductor pump at the optimum forward 1365nm pump power of 500mW (as shown in Figure 6. 15) and also with backward dual order pumping only scheme to finally prove the superior RIN performance of the proposed scheme.
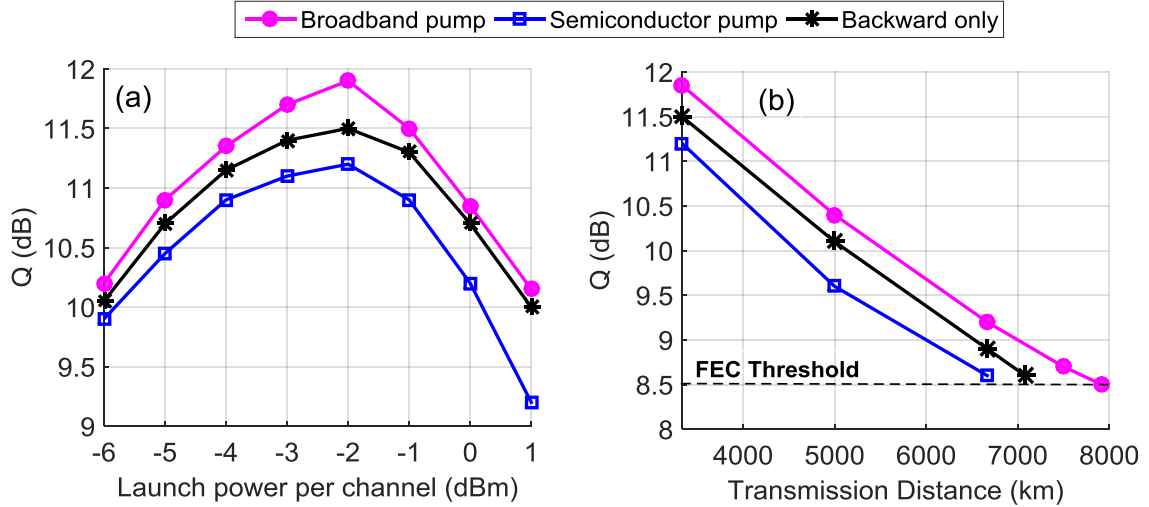
Figure 6. 18. Transmission performance comparison among different dual order forward pumped DRA schemes with 500mW and 20mW forward pump powers of 1365nm and 1455nm pumps respectively: (a) Q factors vs. launch power per channel at 3333km and (b) Q factors vs. transmission distance at optimum launch power

Figure 6. 18 shows the transmission performance comparison among bidirectional pumping schemes with broadband pump, semiconductor pump and conventional Raman fibre lasing based backward only pumping. Optimized forward pump powers for broadband pumped scheme (500mW and 20mW for 1365nm and 1455nm pump respectively) were also used for 1st order semiconductor pumped dual order bidirectional pumping. Backward 1365nm pump power of ~1.3W was required in case of backward only pumping. Broadband pumped scheme provided Q factor improvement of 0.7dB and 0.4dB compared with semiconductor pumped dual order bidirectional and backward only pumping scheme respectively. Improved signal RIN and OSNR performances also allowed the transmission distance up to 7915km with ~1250km and ~830km reach extension compared with semiconductor pumped forward and Raman fibre laser based backward dual order pumping. The summary of the transmission performances are also shown in the following Table 6. 2.

Table 6. 2. Summary of transmission performances among different dual order bidirectional pumping with two different 1st order pump and dual order backward only pumping

Schemes	Q factor at 3333km (dB)	Maximum distance (km)
Broadband pump	7915	11.9
Semiconductor laser diode	6665	11.2
Backward only pumping	7082	11.5

144

6.4 RIN Mitigation Using First Order Forward Pumped Distributed Raman Amplification

First order forward pumped bidirectional Raman amplification is also an attractive choice for distributed amplification considering the fact that it does not need high power, higher order Raman pumps because of the direct gain contribution to the signals from just single Stokes shifted pumps. But higher signal power variation and direct RIN transfer from forward propagating pumps may counterbalance the benefits of energy efficiency. In the previous section broadband 1st order pump seed has been successfully used for significant RIN reduction from higher order forward pump and subsequent transmission performance compared with conventional Raman pumps in a dual order bidirectional pumping. In this section we demonstrate the impact of broadband pump in RIN transfer when used as a primary source for forward pumping at higher power in bidirectional 1st order forward pumped distributed Raman amplification.

6.4.1 Characterisation of 1st order forward pumped bidirectional DRA

The 1st order forward pumped bidirectional DRA scheme consisted of an 83km SSMF span as shown in Figure 6. 19.
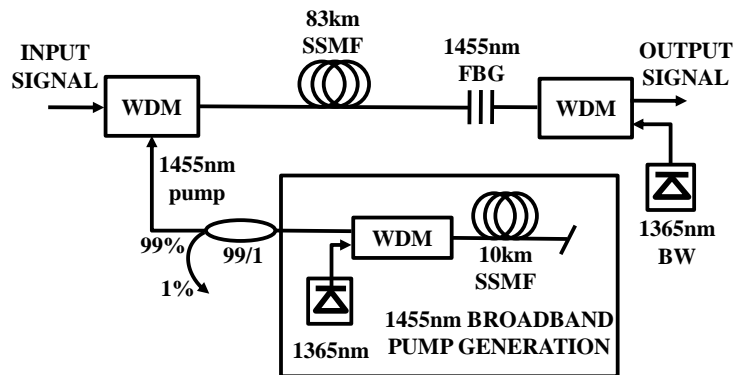
Figure 6. 19. First order forward pumped bidirectional distributed Raman amplifier span

In Figure 6. 19, the backward pumping is consisted of a 1365nm 2nd order Raman fibre laser and FBG at 1455nm with 95% reflectivity and 0.6nm bandwidth to provide feedback for lasing at 1st order pump wavelength. The forward pumping is formed by only the broadband pump without requiring the 2nd order pump. The broadband pump was generated by separately pumping a 10km SSMF using a 1365nm pump as described in Figure 6. 1(a). Here we used different pump powers (30~250mW) of forward broadband pump to characterize the OSNR and signal RIN performances

at different levels. In order to have enough output power, the generated 1455nm seed pump was amplified by the residual 1365nm pump power from the separate seed generation span, in a similar 2nd stage consisted of a 10km TW single mode fibre which has better Raman gain co-efficient ($\sim 0.6 W^{-1}km^{-1}$) than SSMF and the method has already been shown in Figure 6. 4. In all the cases, backward 1365nm pump powers of the main transmission span were optimized to ensure 0dB signal net gain from the output of the amplifier at different forward pump powers. Full characterisation of signal RIN, power variation and finally transmission experiments were carried out and the results obtained have been compared with conventional backward only pumping and other commercial narrowband Raman pumps: low RIN semiconductor lasers and high RIN fibre laser. Two semiconductor laser diodes (0.8nm 3dB bandwidth and -135dB/Hz RIN), depolarised through a PBC and a commercially depolarised narrowband (0.5nm 3dB bandwidth) Raman fibre laser with high RIN (-113dB/Hz) at 1455nm were used as other 1st order sources to compare the performances with broadband pump.
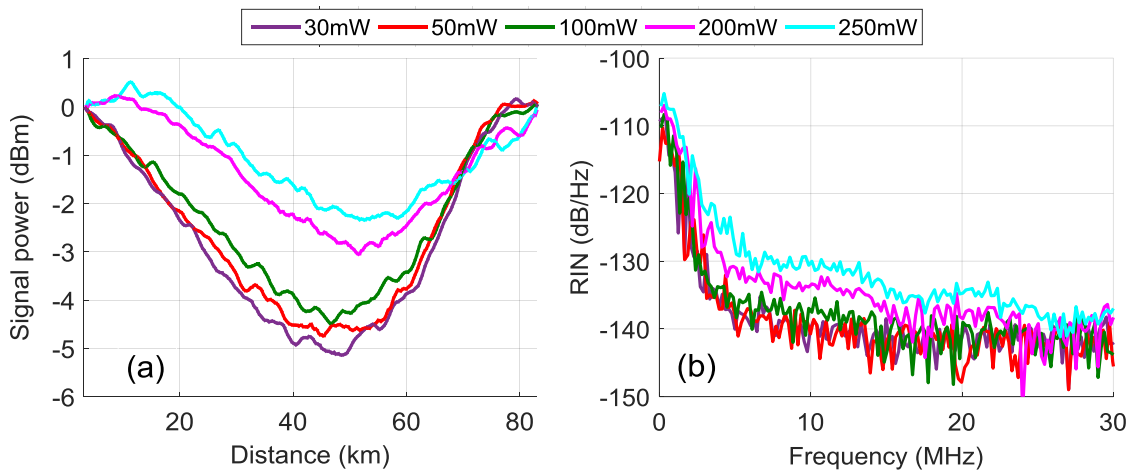
Figure 6. 20. (a) Signal power variations (SPVs) and (b) signal RIN performance at different powers of 1st order broadband pump

The signal power variations (SPVs) and RIN with increasing forward 1st order broadband pump powers are shown in Figure 6. 20(a) and (b). As expected, increasing forward pump powers improved the signal power distribution along the span. The minimum (2.5dB) and maximum (5.1dB) SPVs were achieved at 250mW and 30mW power respectively. A gradual increase in signal RIN level was observed with forward pump power at 100mW and beyond.

6.4.2 Transmission results

The impact of improved OSNR with increasing forward pump powers and associated RIN penalty have been verified through the long-haul transmission experiment in a re-circulating loop setup with 10×120Gb/s DP-QPSK WDM system as shown in Figure 6. 8.
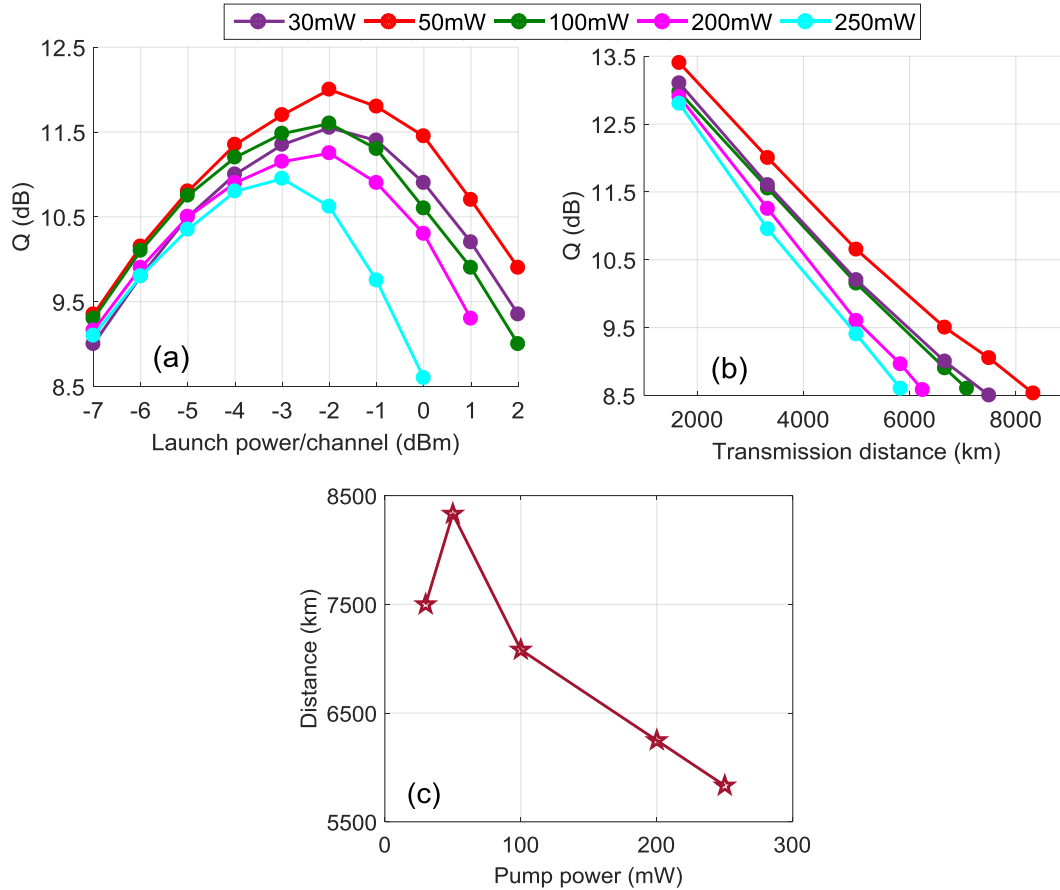
Figure 6. 21. Transmission performance comparisons for 1st order broadband pumped bidirectional DRA at different powers of forward pump measured at 1545.32nm signal: (a) Q factors vs. launch power per channel at 3333km; (b) Q factors vs. transmission distance at corresponding optimum launch powers and (c) maximum transmission reach vs. 1st order forward pump powers

In Figure 6. 21(a) and (b), forward pumping with 50mW broadband 1455nm source provided the best balance between OSNR and signal RIN penalty resulting in maximum optimum Q factor of 12dB and maximum reach up to 8332km respectively. Although forward pumping with 30mW pump power showed lowest signal RIN but transmission performance was limited due to poor OSNR. A summary of maximum transmission distances reached at different broadband forward pump powers are also given in Figure 6. 21(c) and maximum reach (8330km) at 50mW is also

shown here. Transmission performances were significantly dominated by signal RIN with forward pump powers above 100mW. So for an 83km SSMF DRA span, 50mW power of broadband 1st order source provides an optimum trade-off between SPV and signal RIN to achieve the best transmission performance.

A comparison of SPV and RIN with conventional Raman sources (semiconductor laser and Raman fibre laser) as first order forward pumps with 50mW power and backward only pumping is also shown in Figure 6. 22.
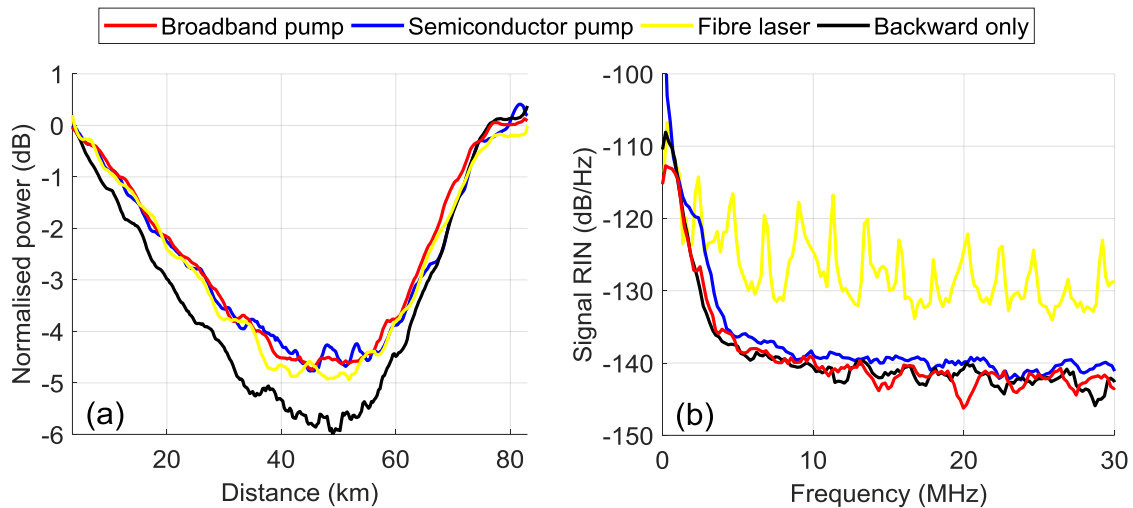
Figure 6. 22. Comparisons of (a) SPVs and (b) signal RIN for different Raman pump sources as 1st order forward pumps in different bidirectional DRA schemes

Signal power profiles along the transmission span measured using a modified OTDR technique are shown in Figure 6. 22(a). Backward pumping only scheme resulted in the largest SPV of ~6dB. In a bi-directionally pumped setup, signal power variation was reduced to ~4.7 dB using only 50mW forward pump power for all the forward pump types.

As the RIN transferred to the signal can result in a significant long-haul transmission penalty, the RIN of the signal at the span output were experimentally measured for all the pumping schemes and are shown in Figure 6. 22(b). The signal RIN (red) using broadband forward pump was similar to backward only pumping only (black) at all frequencies, which indicates low RIN-induced transmission penalty. In comparison, the signal RIN using forward-propagated semiconductor laser (blue) dramatically increased in the low frequency range below 3MHz. This low frequency increase may not cause any penalty in unrepeatered system [173], but can be a limiting factor after a high number of spans in repeatered systems. Using the high RIN fibre laser pump (brown) resulted in up

to 20dB increase in the signal RIN over the entire frequency range, which may result in the severe degradation on the transmission performance. Transmission performances are compared in Figure 6. 23 in order to prove the benefit of proposed distributed pumping scheme.
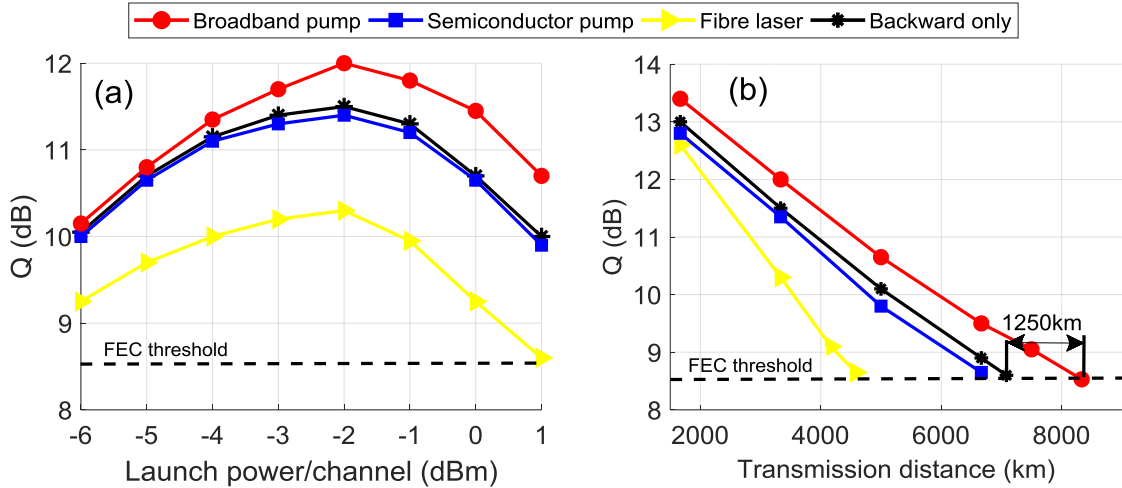
Figure 6. 23. Transmission performance comparison among different conventional 1st order Raman pumps based bidirectional DRA schemes and backward only pumping: (a) Q factors vs. launch power per channel at 3333km and (b) Q factors vs. transmission distance at optimum launch power measured for the middle WDM signal at 1545.32nm

Figure 6. 23 shows the transmission performance comparison among different bidirectional and backward only pumping schemes. For backward pumping only, the maximum reach was 7082km and the maximum Q factor at 3333km was 11.5dB. Using 50mW broadband pump, the maximum reach was improved to ~8330km. The benefit of improved OSNR and minimum signal RIN penalty resulted in 0.5dB improved Q factor at optimum launch power and 1250km transmission reach enhancement with respect to backward only pumping. With conventional semiconductor laser forward pumping, the reach was decreased to 6665 km, and the optimum Q factor at 3333 km was only 11.3dB. As expected from the signal RIN in Figure 6. 22(b), the performance with forward propagated semiconductor laser started to degrade more severely after more recirculation. When using the narrowband Raman fibre laser as the forward pump, due to the high RIN of the fibre laser and narrow bandwidth, the transmission performance was the worst, giving the maximum reach of 4583 km and only 10.3 dB Q factor at 3333 km.
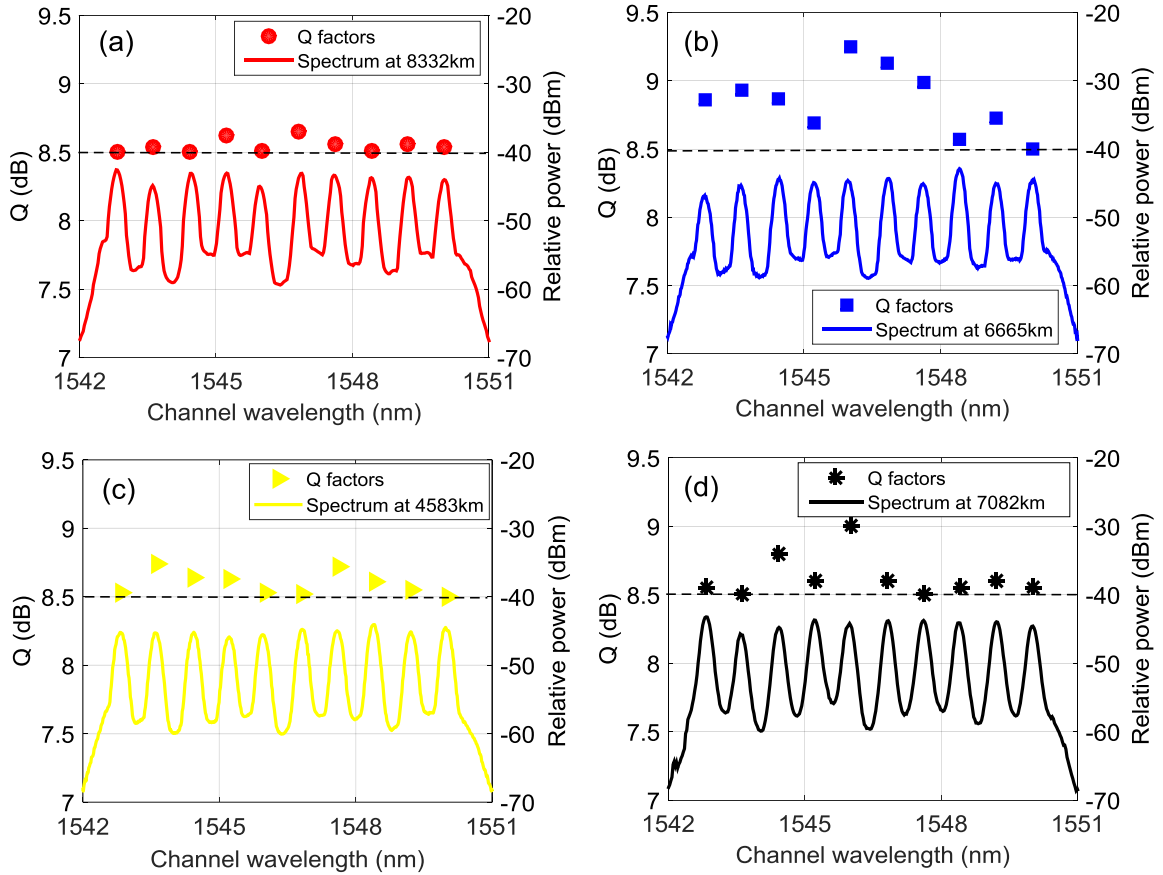
Figure 6. 24. Q factors and received spectra measured at the maximum transmission reach for different pumping schemes: (a) broadband forward pump at 8332km; (b) semiconductor laser diode at 6665km; (c) narrowband fibre laser at 4583km and (d) backward only pumping at 7082km

Figure 6. 24 shows Q factors and the received spectra at maximum transmission distances for the backward only pumping scheme and the other three bidirectional pumping schemes. All channels were above the FEC threshold (Q = 8.5dB at 3.8×10^{-3} in bit error rate).

First order forward pumping with low RIN broadband pump showed better performance than dual order forward pumping by mitigating the signal RIN comparable to backward only pumping and increased the transmission reach by 1250km. To enable the use of first order forward propagated pump in DRA for long-haul transmission, the pump should essentially have sufficiently low RIN level (i.e. < -135 dB/Hz). More importantly, a pump with very broadband 3dB bandwidth (i.e. >10 nm) can prevent the RIN transfer, allowing the benefit of ASE noise reduction to be used in long-haul transmission systems. Here, we have demonstrated a novel broadband low-RIN forward-propagated Raman pumped amplification technique which can reduce the RIN and ASE noise simultaneously. Moreover, this technique gives the best transmission performance and requires

150

only 50mW first order pump power, effectively extending the reach of 10×120Gb/s DP-QPSK long-haul transmission by a minimum of 25%, compared with other commercially available narrowband Raman pumps.

6.5   Conclusions

In this chapter, we report an efficient use of an inherently depolarised broadband 1st order pump with much wider 3dB bandwidth (>10nm) than conventional pump sources, for simultaneous signal RIN mitigation and OSNR improvement. Transmission reach enhancement up to 7915km with ~830km extended reach was achieved in dual order backward pumped DRA compared with other conventional backward only pumping schemes. Significant signal RIN reduction (>10dB) was also demonstrated in dual order forward pumped DRA.

Maximum transmission reach up to 7915km was also achieved with dual order forward pumping with 1st order broadband pump with a substantial reach extension of 1250km compared with widely deployed 1st order semiconductor pumped scheme. Although significant transmission performance improvement was possible with dual order bidirectional pumping, however this scheme may not be an attractive solution for real system implementation because of the additional complexity and energy requirement coming from additional forward pump modules.

Moreover, signal RIN mitigation to a level comparable to backward only pumping in 1st order forward pumped bidirectional DRA was demonstrated with the proposed broadband pump. In bidirectional pumping with only broadband 1st order forward pump at 50mW provides the lowest RIN transfer from forward pump and best transmission distance up to 8330km with 1250km and 1667km extended reach compared with backward only and low RIN semiconductor first order pumped bidirectional pumping schemes.

CHAPTER 7

BROADBAND RAMAN AMPLIFICATION TECHNIQUES

The benefits of Raman amplification with improved optical signal to noise ratio (OSNR) and broad bandwidth have been discussed in chapter 3. In this chapter the novel design methods of both broadband distributed and discrete Raman amplifiers will be discussed in details. We demonstrate novel bidirectional distributed Raman pumping schemes in order to improve the overall noise performance by improving the fundamental issue of noise figure tilt in backward only pumping including multiple pumps. Moreover, we also propose efficient dual stage broadband discrete Raman amplification scheme with high gain, high output power, low noise and low nonlinear penalty.

In this chapter, the numerical modelling of broadband Raman amplifiers was extended from the model presented in chapter 4. The pumping module including multiple first order pumps was developed by the author. The channelized supercontinuum source for broadband distributed Raman gain characterisation shown in section 7.2.1.2 was developed by Dr Atalla El-Taher. The experimental noise figure and gain characterisation were carried out in collaboration with Dr Mingming Tan and Dr Lukasz Krzczanowicz from AIPT. Dr Ian Philips helped to build the broadband recirculating loop for long-haul coherent experiment with broadband Raman amplifiers shown in section 7.3.3. The numerical model for dual stage broadband discrete Raman amplifiers was developed by the author. Dr Paul Harper and Dr Wladek Forysiak helped by supervising and providing useful advices through the process. The results demonstrated in this chapter are related to the following publication list:

1. **M. A. Iqbal**, M. Tan, L. Krzczanowicz, A. El-Taher, W. Forysiak, P. Harper and J. D. Ania-Castañón, "Noise and transmission performance improvement of broadband distributed Raman amplifier using bidirectional Raman pumping with dual order co-pumps," Opt. Express 25(22), 27543-27550 (2017).

2. L. Krzczanowicz, **M. A. Iqbal**, I. D. Philips, M. Tan, P. Skvortcov, P. Harper, and W. Forysiak, "Low transmission penalty dual-stage broadband discrete Raman amplifier," Opt. Express 26(5), 7091-7097 (2018).

3. **M. A. Iqbal**, M. Tan, L. Krzczanowicz, P. Skvortcov, A. El-Taher, I. D. Philips, W. Forysiak, J. D. Ania-Castañón, and P. Harper, "Performance characterisation of high gain, high output power and low noise cascaded broadband discrete Raman amplifiers", in Proc. ICTON 2017, paper We.D5.4.

4. **M. A. Iqbal**, G. R. Martella, F. Gallazzi, Mingming Tan, P. Harper and J. D. Ania-Castañón, "Performance improvement of broadband distributed Raman amplifier using bidirectional pumping with first and dual order forward pumps," in Proc. ICTON 2016, paper Tu.P.30.

5. **M. A. Iqbal**, M. Tan, L. Krzczanowicz, G. Rizzelli Martella, F. Gallazzi, A. El-Taher, W. Forysiak, P. Harper, and J. D. Ania-Castanon, "Noise performance improvement of broadband distributed Raman amplifier using dual order bidirectional pumping," in Proc. ACP 2016, OSA Technical Digest (online), paper AF4G.2.

6. L. Krzczanowicz, **M. A. Iqbal**, I. Phillips, M. Tan, P. Skvortcov, P. Harper, and W. Forysiak, "Low penalty, dual stage, broadband discrete Raman amplifier for high capacity WDM/metro networks," in Proc. OFC 2018, paper W3D.3.

7.1   Design of Broadband Raman Amplifiers

In Raman amplifier, the signal gain bandwidth is usually defined by the pump frequency and the material. In standard single mode fibre (SSMF), the peak signal gain occurs about 13.2THz downshifted from the pump. So wisely choosing multiple pump frequencies will result in combined broad gain bandwidth. The Raman amplifier designs with gain bandwidth up to 100nm have already been discussed in previous literatures [174-176]. Gain ripple over the whole amplification bandwidth is also another important design parameter of broadband Raman amplifier. Overall gain ripple can be minimized within 1dB by increasing the number of asymmetrically spaced pumps [177].

7.1.1 Numerical modelling of multi-pump broadband amplifier

A standard steady state numerical model [15, 174, 177-180] can be used to numerically simulate the evolution of WDM signals and pumps in the amplifier. This standard average power model includes all important effects such as: stimulated and spontaneous Raman scattering, pump

depletion, ASE and double Rayleigh scattering (DRS) noise, energy transfer due to pump-pump, pump-signal and signal-signal interactions from either directions. The power evolution of any signal or pump frequency (ν) can be described by Eq. (7.1).

$$\frac{dP_\nu^\pm}{dz} = \pm \left\{ \begin{array}{l} -\alpha_\nu P_\nu^\pm + \varepsilon_\nu P_\nu^\mp \\[2ex] +P_\nu^\pm \left[\begin{array}{l} \displaystyle\sum_{\mu>\nu} \frac{g_{\mu\nu}}{A_\mu}\left(P_\mu^+ + P_\mu^-\right) \\[3ex] -\displaystyle\sum_{\mu<\nu} \frac{\nu}{\mu}\frac{g_{\nu\mu}}{A_\mu}\left(P_\mu^+ + P_\mu^-\right) - 4h\nu\sum_{\mu<\nu}\frac{g_{\nu\mu}}{A_\mu}\left(1 + \frac{1}{e^{\frac{h(\nu-\mu)}{kT}}-1}\right)\Delta\mu \end{array} \right] \\[6ex] +2h\nu\Delta\nu\displaystyle\sum_{\mu>\nu}\frac{g_{\mu\nu}}{A_\mu}\left(P_\mu^+ + P_\mu^-\right)\left(1 + \frac{1}{e^{\frac{h(\mu-\nu)}{kT}}-1}\right) \end{array} \right\} \qquad (7.1)$$

where $P_\nu^\pm$ represents the average power within the frequency interval $\Delta\nu$ either forward (+) or backward (-) direction at centre frequency ν. The attenuation and double Rayleigh scattering (DRS) coefficients at centre frequency ν are given by α_ν and ε_ν. The Raman gain coefficient at frequency ν with respect to pump at frequency μ, Plank's constant, Boltzmann's constant and absolute temperature are represented by $g_{\mu\nu}$, h, κ and T respectively. A_μ is the effective area of the fibre at pump frequency μ. Two polarisation modes of the fibre and ASE noise generation in both direction were considered in the model.

Equation (7.1) represents the average power model of a particular signal or pump frequency along the amplifier span. $P_\nu^\pm$ includes both the powers of noise and signal within the frequency interval $\Delta\nu$ without any distinction between them. Here, the 1st and 2nd terms denote the attenuation loss and double Rayleigh backscattering component propagating in the signal direction of the frequency component respectively. The gain from other higher frequency components is represented by the 3rd term. The depletion from lower frequency components and ASE noise generated in lower frequency bands are given by the 4th and 5th terms. The 6th term represents the total ASE noise generated. To note that, the backward propagating signal (P_ν^-) is generated from the ASE and Rayleigh backscattering at all frequencies. So all the equations corresponding to backward and forward propagating components have to be solved simultaneously to obtain solution at each position of z along the span.

Moreover the noise contribution at frequency v can also be calculated separately from the signal, as described by the following Eqs. (7.2) - (7.3).

$$\frac{dN_v^+}{dz} = -\alpha_v N_v^+ + \varepsilon_v N_v^-$$

$$+ N_v^+ \sum_{\mu > v} \frac{g_{\mu v}}{A_\mu} \left(P_\mu^+ + P_\mu^- \right) + 2hv\Delta v \sum_{\mu > v} \frac{g_{\mu v}}{A_\mu} \left(P_\mu^+ + P_\mu^- \right) \left(1 + \frac{1}{e^{\frac{h(\mu - v)}{kT}} - 1} \right) \tag{7.2}$$

$$\frac{dN_v^-}{dz} = \alpha_v N_v^- - \varepsilon_v \left(N_v^+ + P_v^+ \right)$$

$$- N_v^- \sum_{\mu > v} \frac{g_{\mu v}}{A_\mu} \left(P_\mu^+ + P_\mu^- \right) - 2hv\Delta v \sum_{\mu > v} \frac{g_{\mu v}}{A_\mu} \left(P_\mu^+ + P_\mu^- \right) \left(1 + \frac{1}{e^{\frac{h(\mu - v)}{kT}} - 1} \right) \tag{7.3}$$

where P_v^+ and $N_v^\pm$ represent the forward propagating average signal power and noise power either forward (+) or backward (-) direction at signal frequency v respectively. In the amplifier simulation for gain and noise performance calculation, the above equations were solved numerically considering room temperature, frequency dependent attenuation profile and normalized Raman gain spectra of SSMF considering depolarised pumps.

In distributed Raman amplifier, gain is distributed along the span which is essentially the transmission fibre. So noise figure calculation is done considering a localized pre-amplifier at the end of the amplifier with equivalent Raman on-off gain [120, 181], as discussed in chapter 3. The NF has been termed as equivalent noise figure (ENF) in case of distributed Raman amplifier. A noise bandwidth of 125GHz has been used for the ENF calculation according to the Eqs. (7.4)-(7.5).

$$ENF = \frac{P_{ASE}}{E_{ph} B_0 G} + \frac{1}{G} \tag{7.4}$$

$$ENF(dB) = 10\log 10 (ENF) \tag{7.5}$$

where P_{ASE} and E_{ph} are the ASE noise power and photon energy at frequency v. The on-off gain and reference optical bandwidth are given by G and B_0 respectively. Flat gain profile over wide bandwidth was obtained by optimizing the pump powers. Pump power optimization mainly depends on Raman gain coefficient, signal and pump polarisation, fiber attenuation loss at pump frequency, pump depletion etc [177].

7.1.1.1 Optimization of broadband gain spectrum

In multi-pumped broadband Raman amplifier design, energy is transferred from short wavelength pumps to longer wavelength pumps as well to signals. So proper amplifier design requires both the optimization of pump wavelengths and pump powers to obtain target Raman gain level with minimum gain variation across the bandwidth. Increasing the number of pumps reduces the gain variation and less than 1dB variation across the bandwidth has been reported over almost 100nm covering C and L band [177].

To numerically simulate a broadband Raman amplifier according to Eq. (7.1) with optimized gain flatness, here we consider a backward pumped distributed Raman amplifier with 61.5km SSMF span as shown in Figure 7. 1. Six first order pumps (1425, 1444, 1462, 1476, 1491 and 1508nm) were considered to obtain 90nm (1530-1620nm) gain bandwidth with 0dB target net gain at the output. The pump wavelengths were chosen from the available pumps for the experimental setup. The available pump powers in the experimental setup allowed us to obtain maximum flat Raman on-off gain of about 12.5~13dB over 70~90nm, which is enough to compensate the fibre loss of 61.5km SSMF. That is why we have chosen a consistent DRA span length of 61.5km both in numerical and experimental characterisation in this chapter.
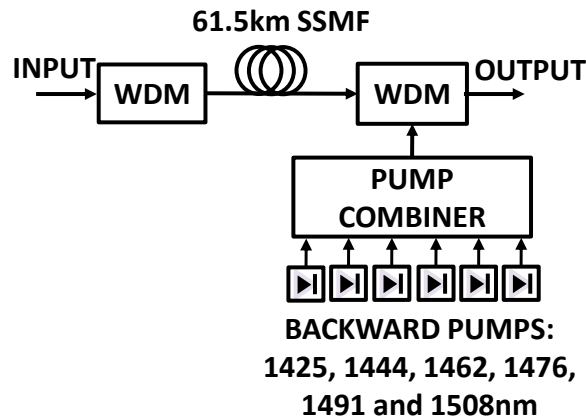
Figure 7. 1. Schematic diagram of backward pumped broadband distributed Raman amplifier with six cascaded first order pumps

In Figure 7. 1, input WDM signals from 1530nm to 1620nm were considered with -10dBm power per channel. All forward and backward propagating components were considered at each signal and pump frequency according to Eq. (7.1) to numerically simulate the system of ODEs for the amplifier. The pump powers were optimized to obtain 0dB average net gain over the 90nm bandwidth with ~1dB gain variation.

There have been many studies for the automatic optimization of gain profile of broadband Raman amplifiers [182-188]. A multi-objective parameter optimization approach with genetic algorithm was used to obtain the optimum pump powers required for target goals. MATLAB's optimization tool box, which implements evolutionary mulit-objective optimization, is used to obtain optimum pump powers [189, 190]. All the noise terms including ASE and DRS in Eq. (7.1) were not included during the gain profile optimization to make the process faster and due to the very insignificant impact of generated noise power in the signal gain profile optimization. We considered two objective functions: (i) the difference between the target net gain and average net gain across the bandwidth and (ii) the gain ripple, which were minimized using the multi-objective optimization tool box. The solver gave many combinations of the two optimized objective functions with a given pump wavelengths set. The lower and upper bound of each pump wavelength were chosen to be 0mW and 350mW respectively. The best solution of the objective functions was chosen and the corresponding pump powers were used for further characterisations (i.e. OSNR, NF etc.) using the full numerical model including the noise terms.
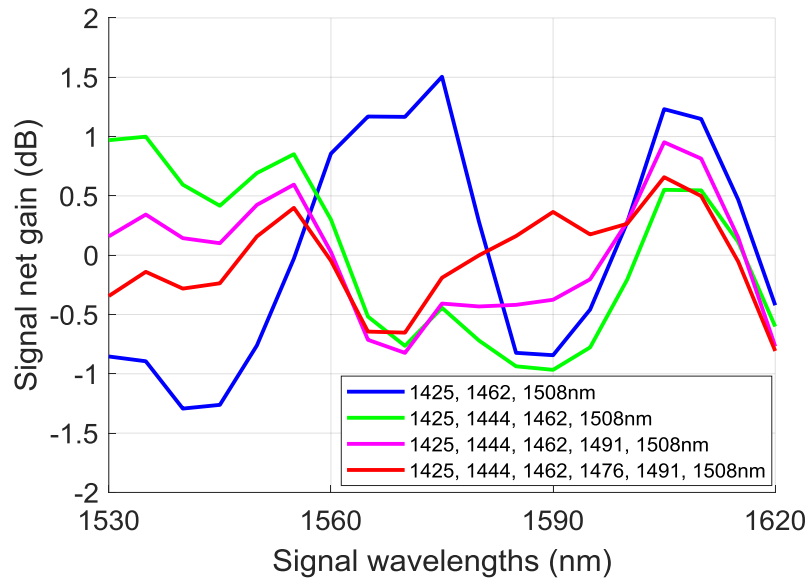
Figure 7. 2. Comparison of numerically simulated of 90nm broad DRA with different number of backward pumps

Figure 7. 2 shows the net gain comparison with different number of backward pumps and optimized pump powers in each case. The gain ripple was about 1.5dB with six pumps, however it increased to 2.5dB with only 3 pumps (1425, 1462 and 1508nm) as shown in Table 7. 1.

Table 7. 1. Pump powers obtained from the optimization toolbox

Scheme	1425nm (mW)	1444nm (mW)	1462nm (mW)	1476m (mW)	1491nm (mW)	1508nm (mW)	Gain ripple (dB)
3 pumps	314	-	254	-	-	150	2.5
4 pumps	277	212	140	-	-	114	1.93
5 pumps	250	243	135	-	20	125	1.8
6 pumps	270	255	110	37	15	112	1.5

In the gain profile optimization steps, the target net gain for 61.5km SSMF span was kept fixed at 0dB. Table 7. 1 shows the one of the best possible pump power combinations that was obtained from the optimization toolbox. Only 20 generations were considered to optimize the pump powers and nearly optimized objective functions were obtained within this limit as shown in Figure 7. 3.
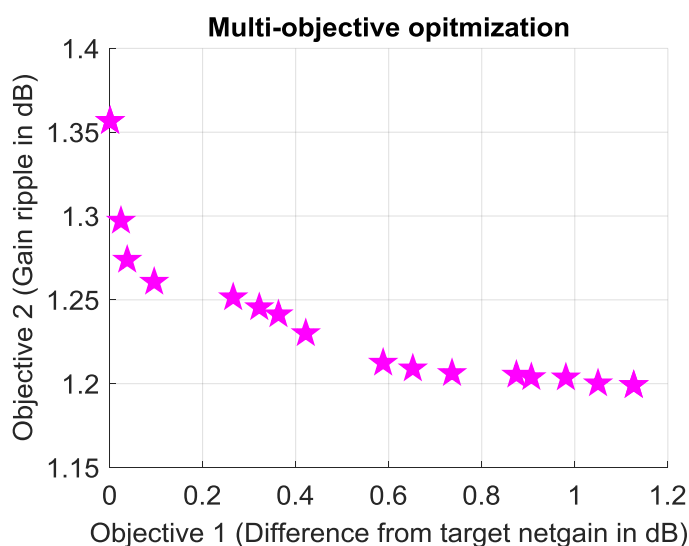
Figure 7. 3. Multi-objective optimization of the two objective functions in six backward pump combinations

Figure 7. 3 shows different combinations of optimized objective functions from the MATLAB toolbox, used to obtain optimum power powers for flat gain over 90nm using only six backward pumps. The Raman gain coefficient spectra of different pumps and fibre attenuation of SSMF used in the optimization process are also illustrated in Figure 7. 4 (a) and (b) respectively.
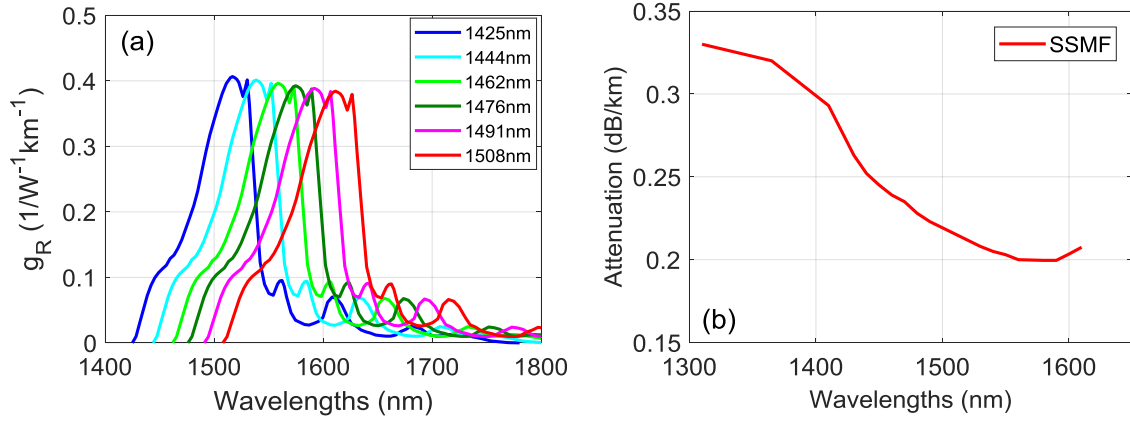
Figure 7. 4. (a) Raman gain coefficient spectra and (b) attenuation coefficient of SSMF used in the numerical simulations for broadband gain optimization

In Figure 7. 4(a), peak Raman gain spectra of the different pump wavelengths were calculated from the reference Raman gain spectrum of 1455nm pump. The calibration factor was chosen to be $\left(\dfrac{\lambda_{ref}}{\lambda_P}\right)$, multiplied by the reference Raman gain coefficient of 1455nm pump with peak Raman gain coefficient of 0.4 $W^{-1}km^{-1}$ [191]. The fibre attenuation coefficients of a SSMF were measured using a tuneable CW laser source as shown in Figure 7. 4(b). So in the numerical modelling, frequency dependent Raman gain and fibre attenuation coefficients were considered in order to ensure a complete model for the Raman amplifier design.

7.1.2 Experimental design of broadband Raman pump module

Here we experimentally develop broadband distributed Raman amplifier with Raman pump module consisted of maximum six first order pumps between 1425nm and 1508nm. Broadband gain up to 100nm was possible using the chosen pump set. Two pumps at each pump wavelength were combined through a polarisation beam combiner (PBC) in order to depolarize and obtain high enough output power. The depolarised pumps were then combined with each other through cascaded filter wavelength division multiplexer (FWDM) setup to build the whole pump module. The combination of Raman pumps in cascaded stages is shown in the Figure 7. 5 . First order semiconductor laser diodes at 14xx nm wavelengths with maximum output power 250~300mW were used as Raman pumps. Each pump was controlled by a multi-channel pump laser diode controller consisting of both current and temperature control units. Figure 7. 5 shows the pump module setup where polarisation combined pumps were cascaded through multiple passive FWDM components. During the experiment we had six first order Raman pumps available at 1425nm,

1444nm, 1462nm, 1476nm, 1491nm and 1508nm, which were combined through the developed pump combiner module. An isolator polarisation beam combiner and depolarizer (IPBCD) was used for the 1425nm pump for depolarisation. The final broadband FWDM combines all the cascaded pumps and broadband C+L band signals. The insertion loss of the FWDM varied between 0.4 and 0.8dB in the setup. The available pump powers for different pumps at the output of the WDM pump combiner module are listed in Table 7. 2.
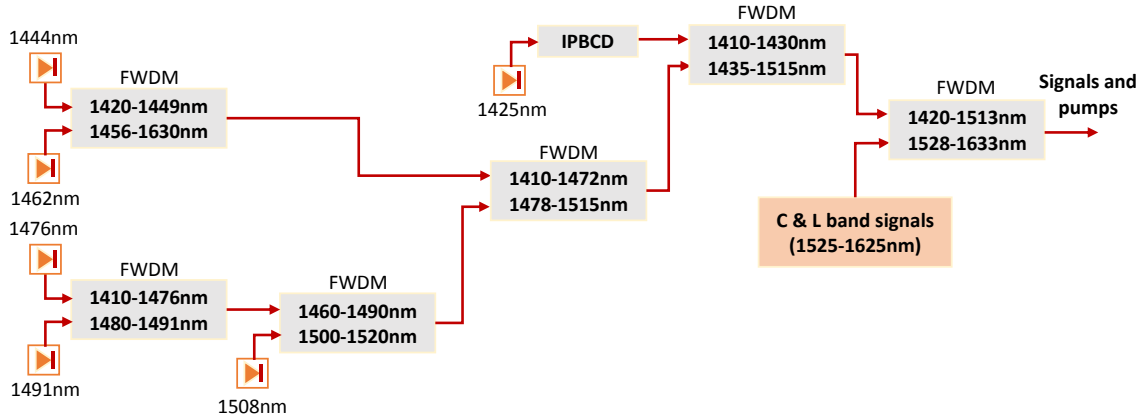
Figure 7. 5. Broadband Raman pump module setup

Table 7. 2. Maximum available output pump power of each pump

Pump wavelength (nm)	Available max pump power (mW)	Available pump power (dBm)	Insertion loss (dB)	Max output power (dBm)	Max output power (mW)
1425	486.3	26.87	0.55	26.32	**428.6**
1444	439.4	26.43	1.45	24.98	**314.8**
1462	437.3	26.41	1.41	25	**316.3**
1476	499.22	26.98	2.64	24.34	**271.7**
1491	463.23	26.66	1.93	24.73	**297.2**
1508	416.3	26.19	1.50	24.69	**294.5**

A list of pump wavelength specific total insertion loss through different passive components are given in Table 7. 2. The highest insertion loss was 2.64dB for 1476nm pump as it passed through five FWDM stages and also remained in the high loss roll-off region of the 3rd FWDM. Pump powers in each polarisation at the same wavelength were kept at equal level in order to avoid any power dependent polarisation crosstalk effect. Maximum and minimum power powers of ~429mW and ~272mW were obtained from 1425nm and 1476nm pumps respectively.

160
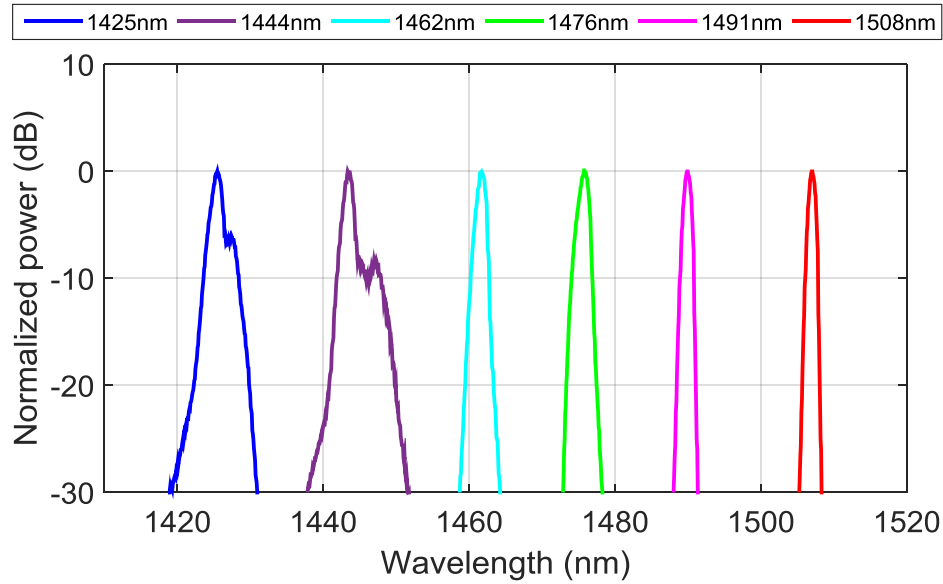
Figure 7. 6. Comparison of Raman pump spectra

Figure 7. 6 shows the pump spectra of six first order pumps used in the Raman pump module. The 3dB bandwidth of each pump laser diode was about 0.8nm.

7.2   Broadband Distributed Raman Amplification

The Raman pump module was used to design broadband distributed Raman amplifier with different SSMF span lengths. In Figure 7. 7, an 80km SSMF fibre was used as the distributed amplifier span and the Raman pumps were used individually or in combination to pump in backward direction without any input signal to characterize the broadband gain spectrum with minimum gain ripple. The Raman pumps were combined using the pump combiner setup as shown in Figure 7. 5.
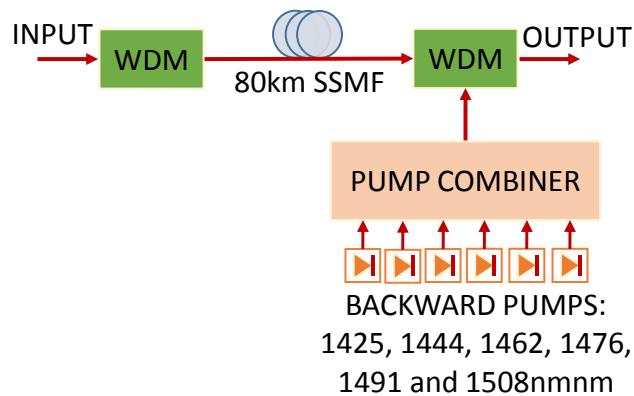
Figure 7. 7. Schematic of an 80km SSMF span based backward pumped broadband distributed Raman amplifier
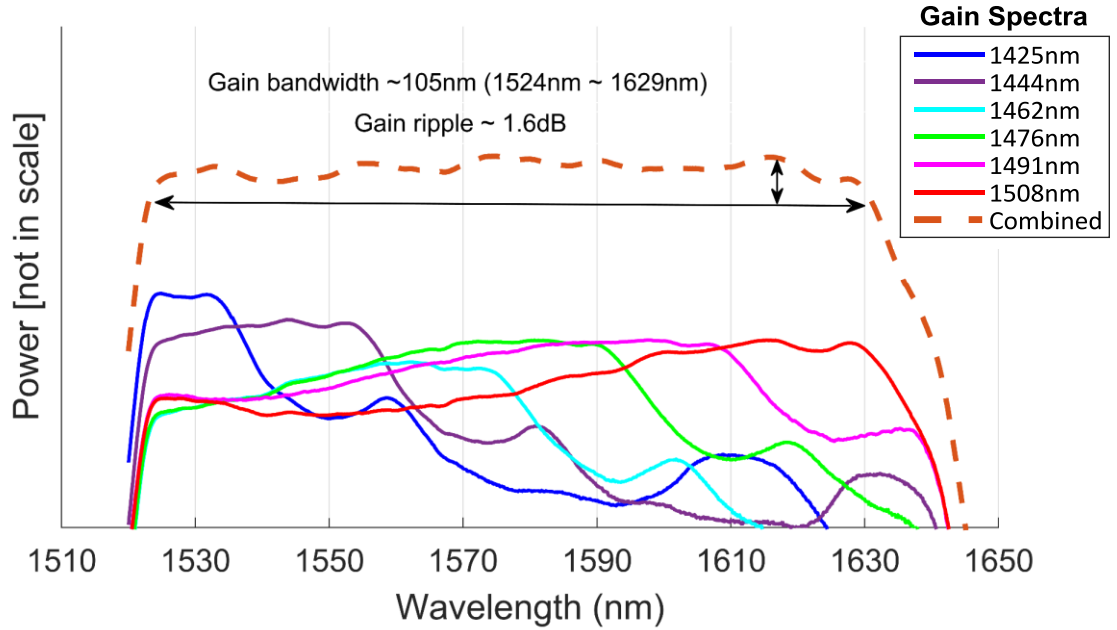
Figure 7. 8. Comparison of ASE gain spectra of individual pump and combined pumps obtained by pumping an 80km SSMF span in backward direction

ASE gain spectrum for each pump and combined broadband gain spectrum were measured in the signal propagation (forward) direction as shown in Figure 7. 8. The ASE gain spectra of 1425nm and 1444nm pump are quite flat and which are due to the fact of having additional gain contribution from the extra side lobe in the pump itself as shown in Figure 7. 6. The cascaded broadband gain bandwidth was extended from 1524nm up to 1629nm with only 1.6dB gain variation. We also verified the ASE gain bandwidth properties using only five Raman pumps (1425nm, 1444nm, 1462nm, 1476nm and 1508nm), which provided 2dB lower average gain and ~1nm reduced gain bandwidth than that of six pumps combination. Similar gain flatness of 1.6dB was also obtained by optimizing the pump power combinations.

162
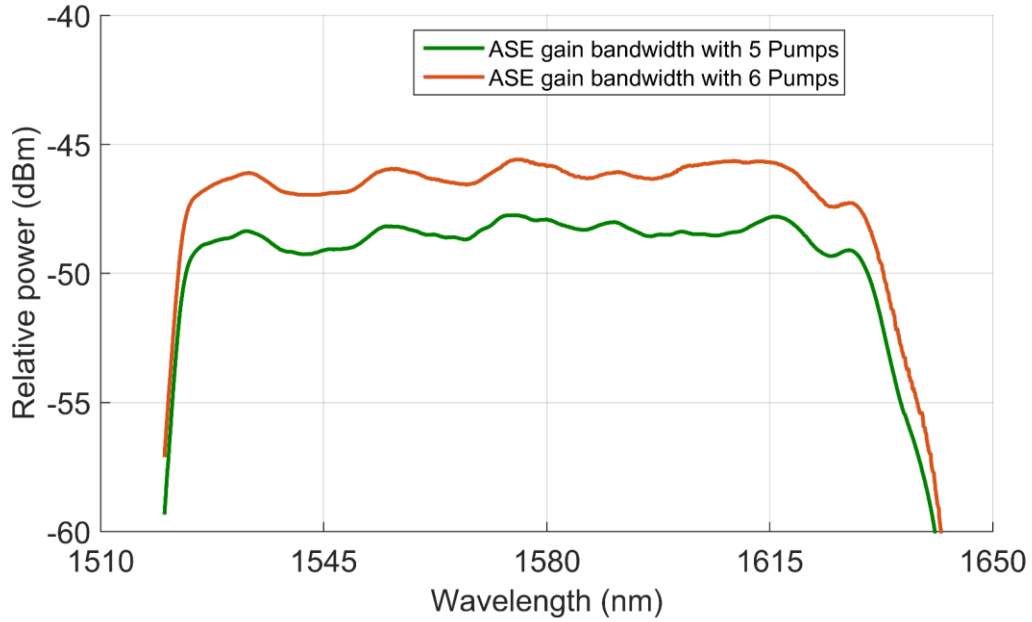
Figure 7. 9. Comparison of broadband pump spectra using 5 pumps and 6 pumps combination for backward pumping an 80km SSMF span without input signal

A comparison of ASE gain spectra between 5 pumps and 6 pumps combination is given in Figure 7. 9. It can be seen that adding 6th pump at 1491nm wavelength provided additional gain flatness in longer wavelength signal band. Pump powers used in those two cases are listed in Table 7. 3. About 154mW additional total power was required in case of 6 pumps combination.

Table 7. 3. Pump powers used for ASE gain bandwidth over 100nm with two different backward pump combinations

5 pumps combination			6 pumps combination		
Pump wavelengths (nm)	Pump power (dBm)	Pump power (mW)	Pump wavelengths (nm)	Pump power (dBm)	Pump power (mW)
1425	25	316.22	1425	25.62	364.75
1444	23.24	210.86	1444	24.4	275.42
1462	21.16	130.62	1462	22.33	171.00
1476	22.3	169.82	1476	21.23	132.74
1508	22.47	176.60	1491	16.87	48.64
			1508	22.08	161.43
Total	**30.02**	**1004.12**	**Total**	**30.62**	**1153.98**

The actual gain performance with input signal was also measured using broadband source. A 75nm (1525nm~1600nm) broadband flat profile source was generated combining the ASE outputs from C and L band EDFAs. The total input signal power was -10dBm over 75nm which was very small to cause any pump depletion. The input and output spectra from an 80km broadband distributed

amplifier with 5 backward pumps (1425nm, 1444nm, 1462nm, 1476nm and 1508nm) are shown in Figure 7. 10.
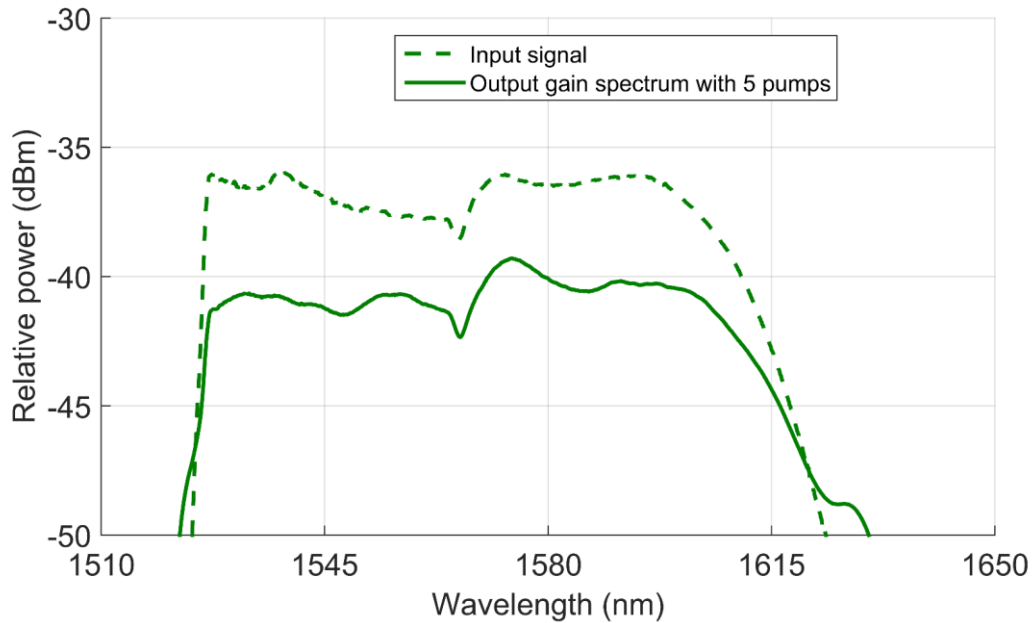
Figure 7. 10. Input and output signal spectra from an 80km SSMF based distributed Raman amplifier using backward only pumping with 5 Raman pumps

From Figure 7. 10 it can be seen that, using 5 pumps it was not possible to get 0dB net gain from 80km amplifier span with a flat (< 2dB ripple) gain profile from the available maximum pump powers, which was mainly due to the energy transfer from lower wavelength pump to higher one. So higher pump powers are needed from lower wavelength pumps to obtain 16.5dB on-off gain to completely compensate the loss from 80km SSMF and input-output WDM couplers. So the pump powers available from the Raman pump module were used to compensate lower lengths of span length up to 62km SSMF based distributed amplifier.

7.2.1.1 *Noise performance improvement using bidirectional broadband distributed Raman amplification*

In broadband DRA, multiple pumps are used to broaden the amplification bandwidth and generate a spectrally flat gain profile. Whilst forward pumping allows the effective increase of signal launch power into the fibre, backward only pumping is preferred in multi-wavelength pumped distributed Raman amplifiers to reduce pump to signal relative intensity noise (RIN) transfer [22, 154] and reduce gain saturation effects. However, in backward only pumped broadband DRA, low wavelength signals suffer more from the thermally generated ASE noise, due to being close to the

longer wavelength pumps. This causes the problem of NF tilt or OSNR variation across the amplifier's bandwidth. Due to this NF tilt in backward pumped systems, overall transmission performance is mainly limited by the ASE-limited low wavelength signals.

One of the potential solutions to this problem is to use a bidirectional pumping scheme with low wavelength 1st order pumps set as forward pumps [192] to improve OSNR in the low wavelengths signal band. However, the noise performance improvement in this case can be counter balanced by the negative impact of RIN transfer from the 1st order forward pumps which are only one Stokes shift away from the signals. Recently, we have experimentally showed that, in a 1st order forward pumped bidirectional DRA, the performance benefits due to OSNR improvement is counteracted by the direct pump to signal RIN transfer which degrades transmission performance when compared to pure backward pumping [133]. It has also been shown [13] that dual order backward pumping including a 2nd order pump cascaded with multiple 1st order pumps improves overall OSNR and NF tilt because of the better gain distribution property of higher order pumping. However, this benefit comes at the cost of reduced pump efficiency which reflects in the requirement of high pump power (>1W) of primary 2nd order pump to push the distributed gain further into the span from the output end and amplify the signal before it gets attenuated close to noise level. Hence, the improved noise performance of the amplifier can be hindered by its poor energy efficiency.

In this chapter, different bidirectional pumping configuration are investigated numerically using Eqs. (7.1) - (7.3) and performances were compared in terms of ENF according to Eqs. (7.4) - (7.5) among those schemes and conventional backward only pumping. Finally the best performed schemes were investigated experimentally for ASE noise and signal RIN performance. Performances were then also compared in terms of long-haul coherent WDM transmission experiment results.
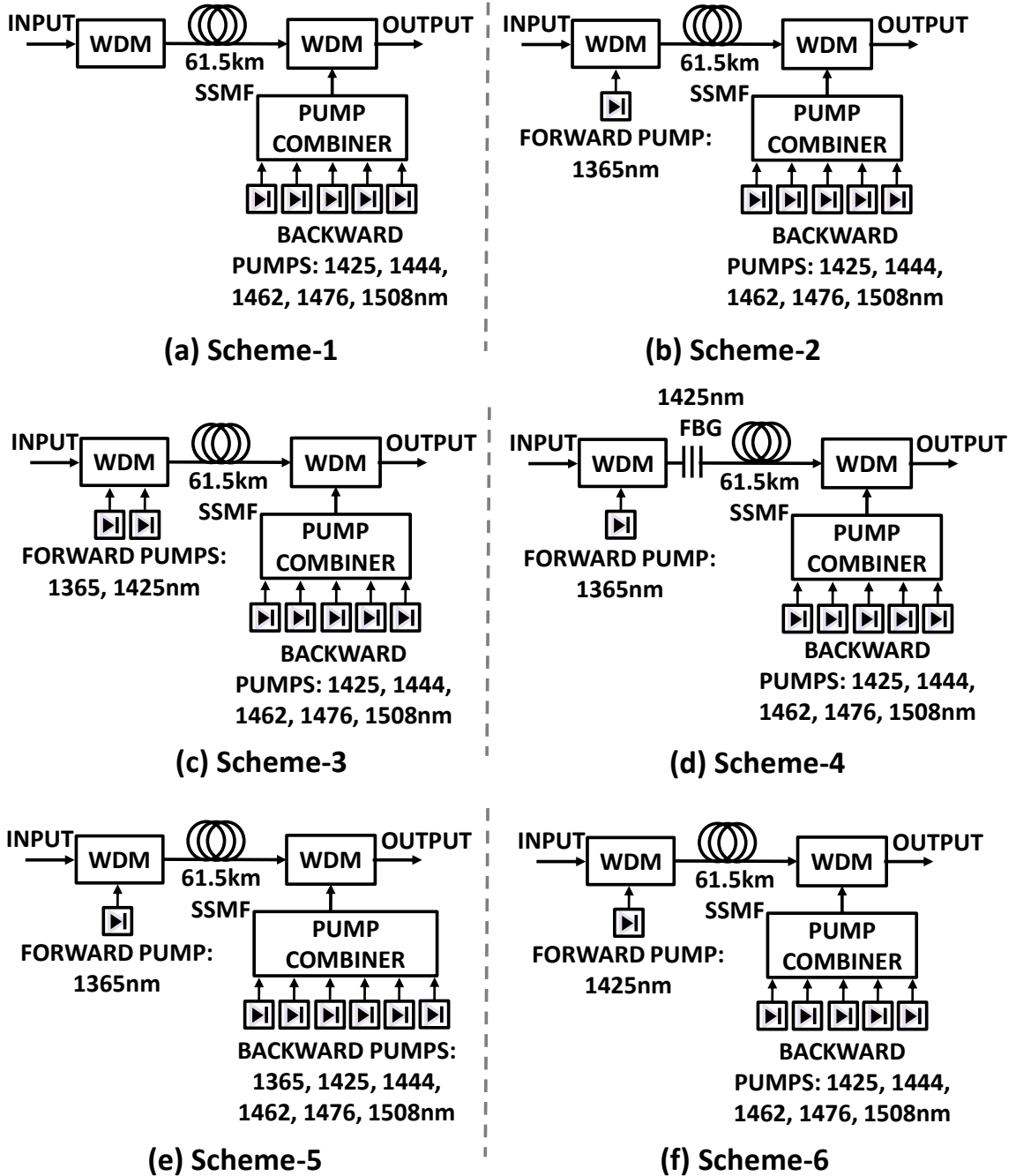
Figure 7. 11. Schematic diagram of different bidirectional broadband distributed Raman amplification schemes: (a) scheme-1 - backward only; (b) scheme-2 – forward pumping with 2nd order 1365nm pump; (c) scheme-3 – forward pumping with 2nd and 1st order 1365nm and 1425nm pumps respectively; (d) scheme-4 – forward pumping with 2nd order 1365nm pump and a 99% reflectivity FBG at 1425nm at input end replacing the 1425nm pump; (e) scheme-5 – forward pumping with 2nd order 1365nm pump and additional 1365nm backward pump; and (f) forward pumping with 1st order 1425nm pump

In Figure 7. 11, a 70nm bandwidth distributed Raman amplifier in a 61.5km SSMF span and with six different pumping schemes is shown. In all the schemes the backward pump module was consisted of five 1st order pumps (1425nm, 1444nm, 1462nm, 1476nm and 1508nm) except scheme-5 where an additional 2nd order 1365nm pump was added with other 1st order pump wavelengths.

Scheme-1 is shown in Figure 7. 11(a), which represents the conventional backward only pumping. To improve the OSNR performance in lower signal wavelengths different forward pumping schemes-2 to scheme-6 have been proposed as shown in Figure 7. 11(b) to Figure 7. 11(f) respectively.

A 2nd order 1365nm pump was used as forward pump in scheme-2. As there was no first order seed at the input of the amplifier span, Stokes shifted energy transfer from forward pump to signal was also inefficient. To improve the forward pumping efficiency, a 1st order seed was included with the 2nd order 1365nm for forward pumping in scheme-3.

In Figure 7. 11(d), scheme-4 used a combination of 1365nm 2nd order pump and 1st order fibre Bragg grating (FBG) with 99% reflectivity and 0.6nm 3dB bandwidth centred at 1425nm at the input end. A random distributed fibre laser at 1425nm is created at the input when the resonant mode overcome the lasing threshold in a distributed cavity formed by the Rayleigh scattering from the fibre and feedback from the FBG [135, 145]. The Raman 1st order pump module was used for backward pumping.

As higher order pumping can distribute the gain further into the span, bidirectional 1365nm pumps were used in scheme-5 as shown in Figure 7. 11(e). Forward pumping consisted of 1365nm pump only, whereas a 1365nm pump was included with the other 1st order Raman pump module in backward pumping.

Figure 7. 11(f) shows schme-6, in which a conventional bidirectional pumping scheme was used with lowest wavelength 1st order pump (1425nm) in the backward pump module used as forward pump to provide direct gain to the lower wavelength signal. Although, this bidirectional pumping scheme was the simplest requiring only a 1st order pump in forward direction, however the direct RIN transfer from one Stokes shifted pump to signal may counterbalance the OSNR improvement and simplicity of the design.

For performance comparison, first of all the average on-off Raman gain of each scheme was maintained at 11.8~12dB in order to compensate the span loss of 61.5km SSMF. Then signal

167

power distribution along the span, output OSNR, equivalent NF and forward propagating ASE noise profiles were simulated and compared among all.
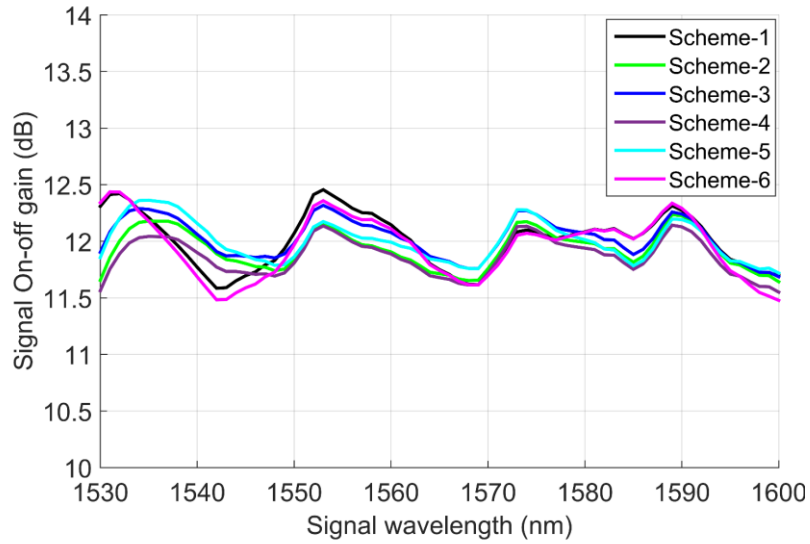
Figure 7. 12. Comparison of Raman on-off gain for different broadband distributed pumping schemes

The average Raman on-off gain over the 70nm bandwidth was kept fixed at 11.8~12dB in all the schemes discussed above as shown in Figure 7. 12. The gain ripple was kept below 1dB by optimizing the backward pump powers in each scheme.

Table 7. 4. Pump power used in the numerical simulation for different pumping schemes (FW = forward and BW = backward)

Pumps (nm)	Scheme-1	Scheme-2		Scheme-3		Scheme-4		Scheme-5		Scheme-6	
	BW (mW)	FW (mW)	BW (mW)	FW (mW)	BW (mW)	FW (mW)	BW (mW)	FW (mW)	BW (mW)	FW (mW)	BW (mW)
1365	-	550	-	450	-	480	-	320	320	-	-
1425	350	-	130	20	94	-	130	-	85	80	230
1444	210	-	110	-	118	-	116	-	45	-	215
1462	115	-	100	-	110	-	105	-	45	-	115
1476	75	-	90	-	90	-	88	-	70	-	95
1508	85	-	145	-	166	-	145	-	135	-	103
Total	835	550	575	470	578	480	584	320	700	80	758

168

The pump powers used in different schemes are given below in Table 7. 4. Forward 2nd order 1365nm and 1st order 1425nm pump powers were limited up to 550mW and 80mW in the simulation in order to have similar signal power distribution along the amplifier span. In scheme-2, maximum 550mW forward 1365nm pump power was needed to get similar signal power profiles to others because of the lack of forward 1st order seed. The required 1365nm forward pump power was reduced down to 450mW in the presence of forward 1425nm seed with only 20mW in scheme-3. In scheme-4, Additional 30mW forward 1365nm was required when 1st order 1425nm seed was replaced by a high reflectivity input end FBG at 1425nm due to high lasing threshold of random distributed feedback lasing. The gain contribution form 2nd order pump was distributed bidirectionally in scheme-5 by using 320mW in either direction. Finally only 80mW forward 1425nm pump power was used in scheme-6.
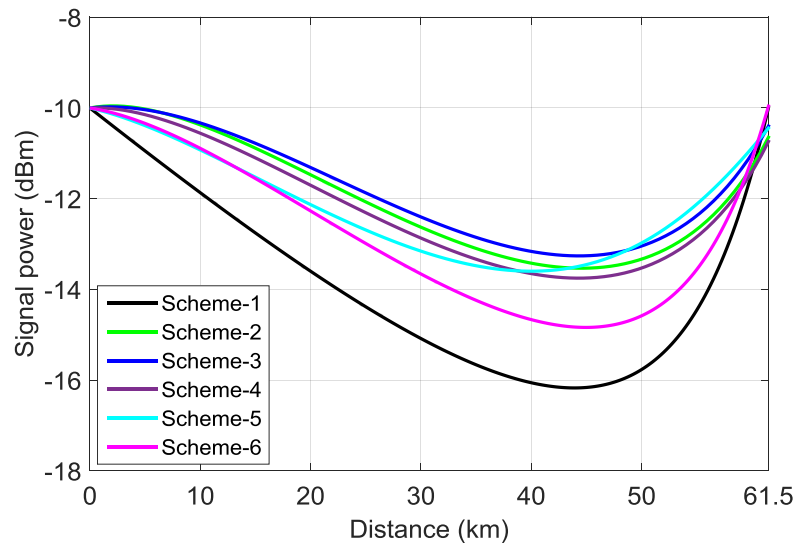
Figure 7. 13. Comparison of signal power profiles among different distributed Raman pumping schemes

Figure 7. 13 shows the numerically simulated SPVs at the lowest wavelength signal 1530nm for different pumping schemes. In the simulation, 1nm spaced WDM signals over 70nm bandwidth from 1530nm to 1600nm were considered with -10dBm signal power per channel. Low signal power levels were considered to ensure negligible pump depletion. The backward only pumped scheme-1 showed the highest SPV of 6.2dB due to the absence of any forward pumping. All the bidirectional pumping with forward 1365nm pump provided similar SPVs varied between 3.3dB and 3.75dB. Scheme-3 with forward 1365nm and 1425nm pumps provided the lowest SPV of 3.3dB. The differences in signal power levels at the end of the span among different schemes were due to having different Raman on-off gain levels at 1530nm as shown in Figure 7. 12.

169
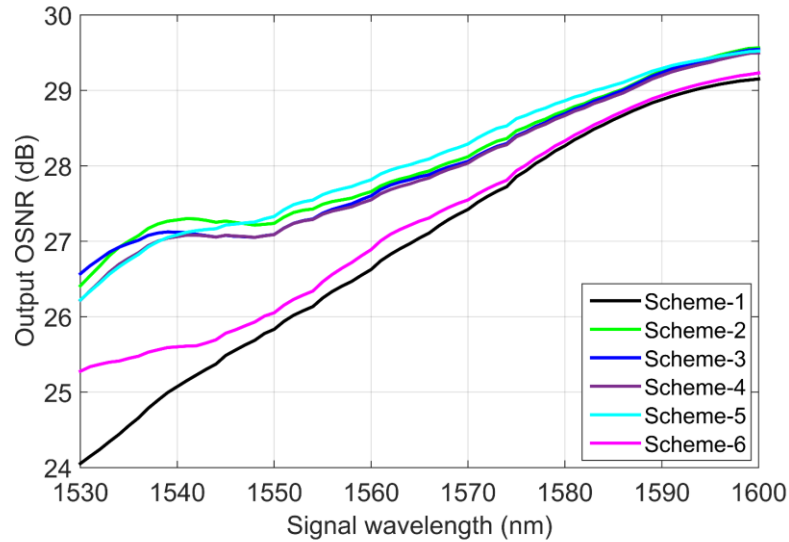
Figure 7. 14. Comparison of simulated output OSNR calculated at 1530nm for different distributed amplifier schemes

Figure 7. 14 shows the output OSNR at signal wavelengths for different pumping schemes. As expected, low signal wavelengths showed the lower OSNR than high wavelength signals due to the impact of more thermally generated ASE noise. Backward only pumping showed the lowest output OSNR in all wavelengths than other bidirectional schemes. Using forward pumping improved the OSNR in the low wavelength bands. All the bidirectional pumping schemes including 1365nm forward pump showed similar OSNR performances. Scheme-3 had the maximum OSNR at the lowest 1530nm signal among all which was due to having the lowest ASE noise contribution and minimum SPV (3.3dB) as shown Figure 7. 13. First order 1425nm forward pumped scheme-6 had better OSNR than backward only pumping scheme-1 but showed lower OSNR performance than other dual order bidirectional pumping schemes. The OSNR performances could also be explained by the forward propagating ASE noise level at the end of the amplifier span.

A comparison of simulated forward propagated ASE noise profiles at 1530nm is shown in Figure 7. 15. In scheme-1, the lowest wavelength signal 1530nm experienced the highest ASE noise level of -34dBm at the end of the 61.5km span. The ASE noise levels were reduced by using different bidirectional pumping schemes which was represented in the OSNR benefit compared with backward only pumping as shown in Figure 7. 14. Minimum of ~1.3dB improvement was achieve in 1st order 1425nm forward pumped scheme-6. An improvement of 2.7dB was also obtained from scheme-5 which used higher order 1365nm pump in both direction but at the cost of an additional high power pump. About 3dB reduced ASE noise level was observed in other 1365nm forward pumped schemes 2, 3 and 4.

170
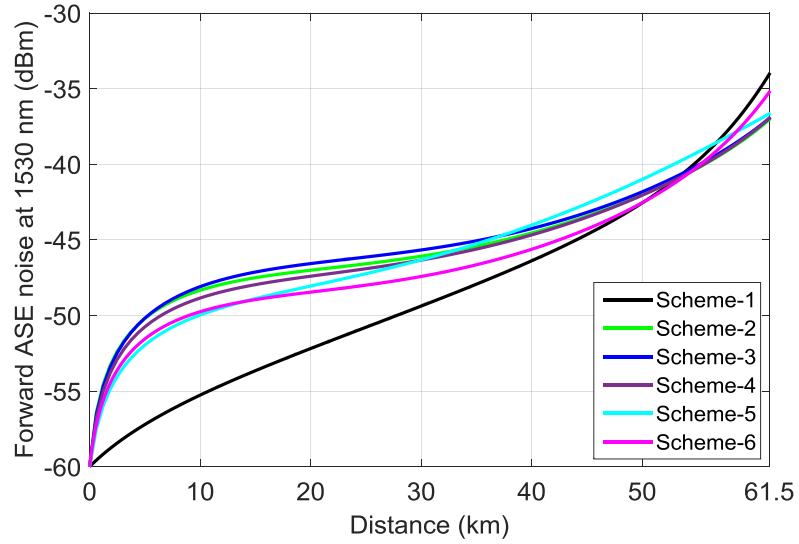
Figure 7. 15. Comparison of simulated forward propagating ASE noise profiles at 1530nm for different distributed
amplifier pumping schemes

From Table 7. 4 it can be seen that, scheme-3 has better pump power efficiency for using lower
1365nm pump power (450mW), whereas additional 100mW and 30mW pump powers were
required due to the absence of 1st order input seed and high 1st order lasing threshold in scheme-2
and 4 respectively.
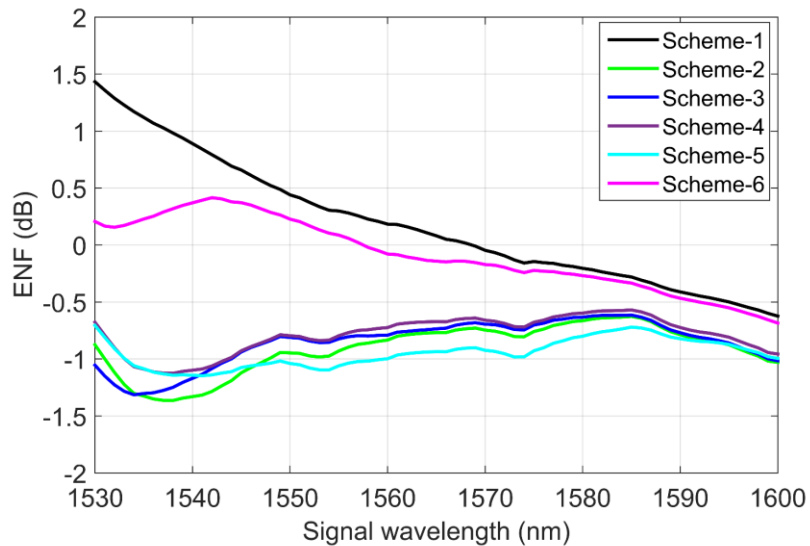
Figure 7. 16. Comparison of equivalent NF over the amplifier bandwidth for different distributed amplifier schemes

The equivalent NF (ENF) performances of 1nm spaced signals over 70nm (1530-1600nm)
amplification bandwidth for different pumping schemes are shown in Figure 7. 16. As expected

171

from the OSNR and ASE noise performances, scheme-3 showed the lowest ENF (-1.1dB) at 1530nm with 2.5dB noise figure improvement compared with backward only pumped scheme-1. The other forward 1365nm pumped scheme-2, 4, and 5 also showed similar ENF performance over the signal gain bandwidth. Scheme-6 showed the smallest ENF improvement (~0.7dB) compared with scheme-1 because of higher SPV and ASE noise power at the end of the span than other bidirectional pumping schemes.

So from the characterisation of signal power distribution, ASE noise power and ENF, it can be concluded that, in a 61.5km long and 70nm wide bidirectional distributed Raman amplifier, noise performance can be significantly improved by using dual order forward pumping including a 2nd order 1365nm pump and a 1st order 1425nm seed (scheme-3) with superior pump power efficiency than similar dual order bidirectional pumping schemes-2, 4 and 5. First order forward pumped scheme-6 would not be a preferred choice due to poor gain distribution capability further into the span than 2nd order pumping and also direct RIN transfer from forward pump to only one Stokes shifted signal [133].

7.2.1.2 *Experimental characterisation*

The noise figure performance improvement in broadband DRA using bidirectional Raman pumping with dual order forward pumps were also characterized experimentally and performance benefits were justified through long-haul coherent WDM transmission experiments [193]. Here, we demonstrate a low noise bidirectional broadband distributed Raman pumping scheme combining dual order forward propagated pumps without increasing the signal RIN level. The noise performance improvement is compared experimentally and numerically with conventional backward only pumping and bidirectional pumping with only 2nd order forward pump for a 70nm bandwidth and 61.5km DRA.
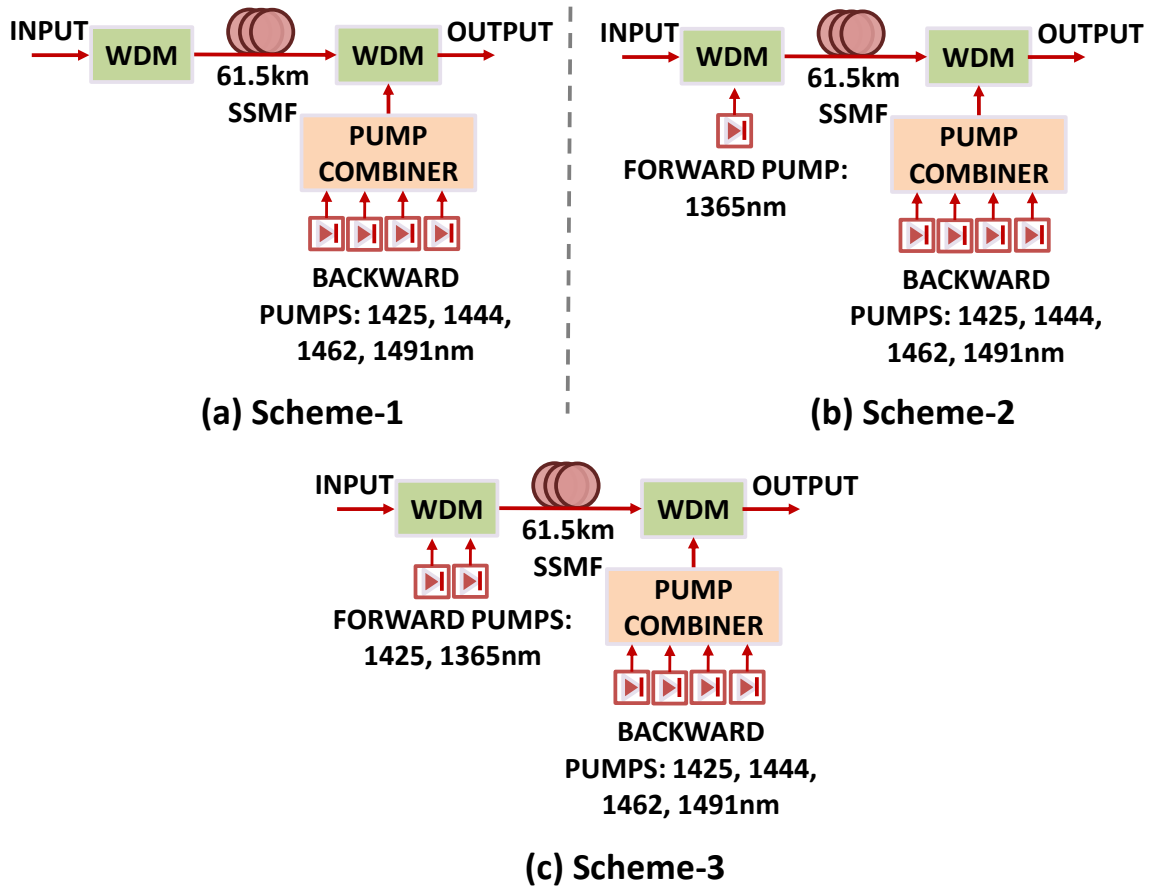
Figure 7. 17. Schematic diagrams of three broadband Raman pumping schemes (a) Scheme-1: backward-pumping only (b) Scheme-2: bidirectional pumping with only 2nd order forward pump and (c) Scheme-3: bidirectional pumping with 1365nm pump and 1425nm pump seed from the input end at 21mW (scheme-3(a)) and 49mW (scheme-3(b)) respectively

We have experimentally investigated conventional backward only pumping and two different types of dual order bidirectional pumping schemes as discussed in the last section and are shown in Figure 7. 17. Four 1st order pump wavelengths (1425nm, 1444nm, 1462nm and 1491nm) were used as backward pumps in all the schemes. In the numerical characterisation of last section, 1508nm was used instead of 1491nm pump which allowed < 1dB gain ripple across 70nm amplification bandwidth. But the 1508nm pump was not available during experimental characterisation and we chose four first order pumps instead of five in the backward pump module including 1491nm as the longest wavelength pump. The choice of pumps gave a flat gain variation (~ ±0.75dB) over a 70nm signal bandwidth (1530nm to 1600nm) for a 61.5km amplifier span of SSMF. Commercial semiconductor laser diodes with maximum output power of 300mW were used as 1st order pumps. Two laser diodes at each wavelength were combined through a PBC to avoid any polarisation dependent gain and then combined subsequently with other 1st order pumps through a cascaded

WDM pump combiner (Figure 7. 5) to form the backward pumping module. Scheme-1 refers to the backward pumping only with above mentioned four 1st order pumps as shown in Figure 7. 17(a). Scheme-2 in Figure 7. 17(b) shows bidirectional pumping with the same backward pump module and forward pumping by only 2nd order pump at 1365nm. A highly depolarised Raman fibre laser with reasonably high RIN (~ -120dB/Hz) and maximum output power of ~ 5W was used as the 2nd order forward pump.

Our proposed bidirectional dual order pumping scheme (scheme-3) consists of 2nd order (1365nm) and 1st order (1425nm) forward pumps as shown in Figure 7. 17(c). The 1425nm pump acts as a seed which first gets amplified by the 1365nm 2nd order forward pump and then finally amplifies the lower wavelength signals in order to improve the ASE noise performance of the amplifier in that region. A commercially available semiconductor laser diode was depolarised thorough an isolator-PBC-deploarizer (IPBCD) and used as 1st order forward pump seed with only 20~50mW power. Two different pump powers, 21mW and 49mW, have been used for the 1425nm forward pump seed, denoted as scheme-3(a) and scheme-3(b) respectively, whereas a constant 216mW power was used for the 1365nm forward pump in both bidirectional pumping schemes to allow a fair comparison in terms of RIN transfer from the 2nd order forward pump to the signal. The particular choice of forward pump powers gave the best trade-off between gain flatness and ASE noise generation.
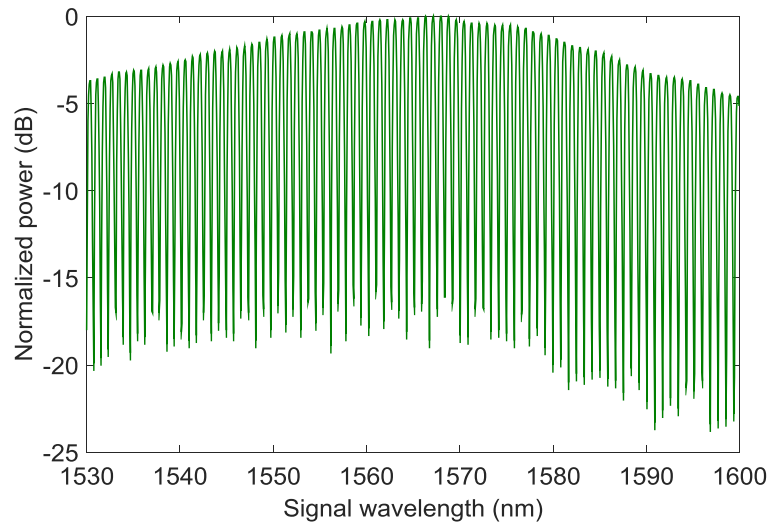
Figure 7. 18. 100GHz channelized supercontinuum source for broadband gain characterisation

In the experiment, the broadband gain performance of the amplifier was characterized using 100GHz channelized spectral shaping of a supercontinuum source [194]. This source gave an

output power of 12dBm over the full 1530-1600nm range of the amplifier with 4dB power variation as shown in of Figure 7. 18. The average signal power per channel of the broadband spectral shaped supercontinuum source was -8dBm and no pump depletion was observed at this power level. The signal power evolution along the span was measured for 1530nm signal following a modified standard OTDR technique [153]. The ASE noise performance has been investigated both experimentally and numerically and a comparison of the schemes is presented in terms of optical NF improvement. Here, 1530nm signal is chosen for characterisation, which is the lowest wavelength in the amplification bandwidth and suffers most from thermally generated ASE noise.

Similar to numerical characterisation, average on-off Raman gain over 70nm bandwidth was maintained at ~12.6dB for all the schemes by optimizing the backward pump powers as shown in Figure 7. 19. The 12.6dB average on-off gain was considered to compensate the 61.5km SSMF span loss and WDM coupler losses at each end. The overall gain ripple of the amplifier was ±0.75dB. Table 7. 5 shows the pump powers used in each scheme. It can be seen that total backward pump powers requirement decreases as more gain contribution comes from the forward pumps. Numerical simulations were carried out with the pump wavelengths and associated experimental pump powers. The simulation results also showed a close match with experimental measurements but are not shown here in order to maintain clarity.
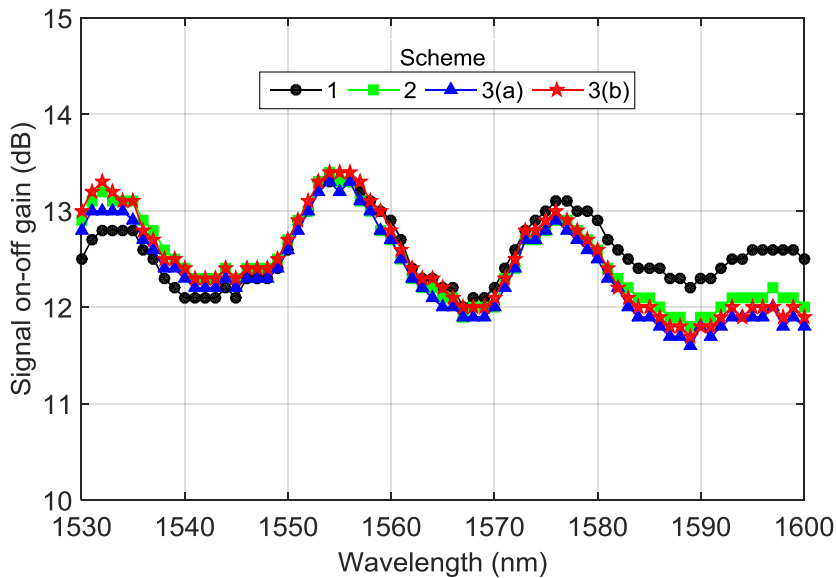
Figure 7. 19. Measured on-off Raman gain characterisation in order to maintain 0dB net gain at the output of the amplifier span for different pumping schemes

Table 7. 5. Pump power required for the experimental characterisation

Pumps (nm)	Scheme-1		Scheme-2		Scheme-3(a)		Scheme-3(b)	
	FW (mW)	BW (mW)	FW (mW)	BW (mW)	FW (mW)	BW (mW)	FW (mW)	BW (mW)
1365	-	-	216	-	216	-	216	-
1425	-	254	-	204	21	163	49	131
1444	-	183	-	181	-	181	-	183
1462	-	117	-	121	-	130	-	136
1491	-	164	-	156	-	164	-	172
Total	-	718	216	665	237	638	265	622

The measured and simulated signal power profiles at 1530nm are shown in Figure 7. 20. Simulation results are marked with dashed lines which closely match the measurements (solid lines) and confirm the SPV improvement with dual order forward pumping schemes. Backward pumping only scheme-1 showed the worst SPV of ~5.2dB. SPV improvements of 1.4dB and 2dB compared with scheme-1 were achieved by scheme-2 and scheme-3(a) respectively. Increasing the 1425nm forward pump seed power from 21mW to 49mW provided additional 0.3dB improvement in scheme-3(b).
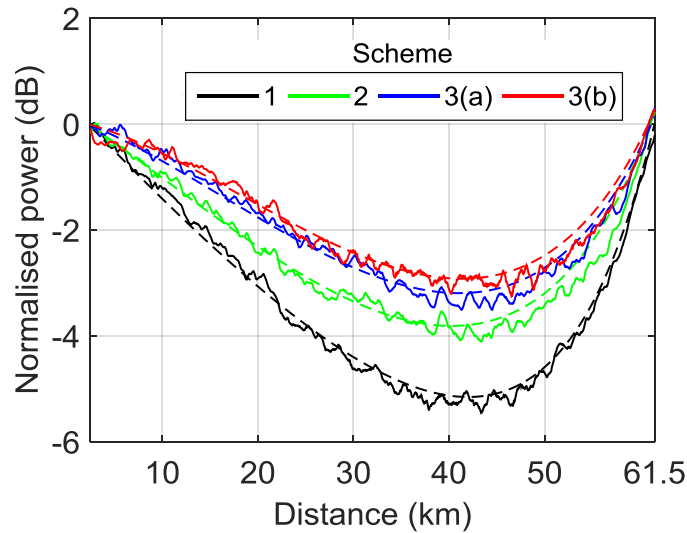
Figure 7. 20. Signal power profiles along the amplifier span for different distributed Raman pumping schemes. Solid and dashed lines represent the experimental and numerically simulated results respectively

Then the performances of different bidirectional pumping schemes are compared with respect to ENF improvement with respect to backward only pumping (scheme-1) as shown in Figure 7. 21.

ENFs were measured every 10nm across the signal bandwidth using a -6dBm tunable CW laser source with the same pump powers shown in Table 7. 5.
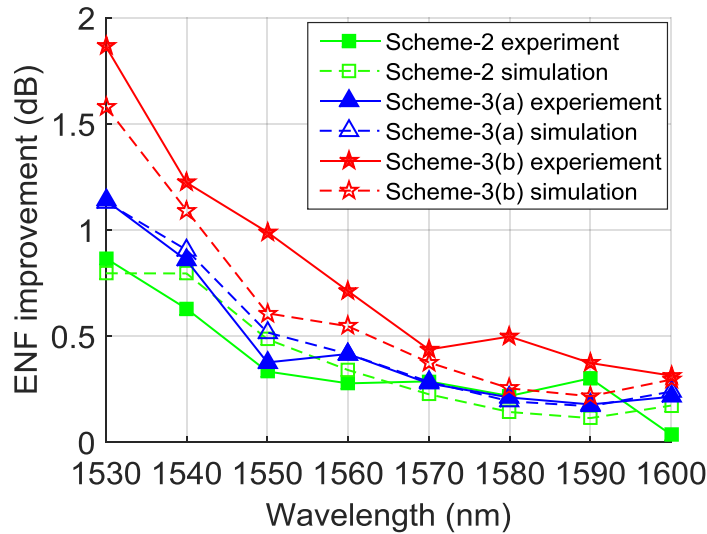
Figure 7. 21. Measured and simulated equivalent NF improvement for scheme-2 and 3 compared with scheme-1

In Figure 7. 21, simulation results show a good agreement with measurements. As expected, higher ENF improvements were obtained at shorter signal wavelengths with bidirectional pumping schemes 2 and 3. ENF improvements decrease at longer wavelengths because gain contribution from forward pumps are weak in that region. Scheme-3(a) shows 1.2dB maximum measured ENF improvement at 1530nm, which is 0.3dB better than that of scheme-2 because of improved SPV and reduced ASE noise as shown in Figure 7. 20. Additional 0.7dB improvement is also shown with scheme-3(b) as the 1425nm forward pump seed power is increased to 49mW.
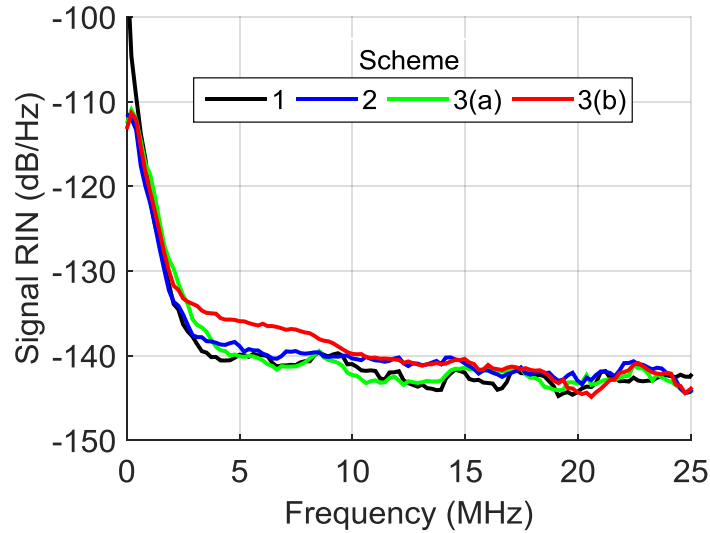
Figure 7. 22. Measured signal RIN at 1530nm for different pumping

The measured RIN performance at 1530nm signal is shown in Figure 7. 22. In scheme-2, the power of the 1365nm 2nd order forward pump has been limited to 216mW, which is insufficient to spontaneously generate forward propagating Stokes light that would transfer RIN efficiently to the signal and thus signal RIN remains at the level comparable with backward pumping only (scheme-1). Scheme-3(a) also does not show any increment in signal RIN level because RIN transfer from higher order 1365nm pump to low power 1425nm forward pump is low, since maximum gain from the 1365nm pump will occur for the 1444 and 1462nm backward components, due to the characteristic Raman frequency shift of about 13THz. There is a slight increase in signal RIN level below 10MHz in scheme-3(b) because of relatively high forward gain contribution from higher power (49mW) of 1425nm forward pump.

One of the important thing of the proposed dual order forward pumped bidirectional distributed Raman amplification scheme-3 is the proper choice of forward pump wavelengths which provide gain in the low signal wavelength regions with no to very little increase of signal RIN. Moreover a flatter noise figure profile was achieved by providing very low gain in the longer wavelength signal band without any signal RIN penalty.
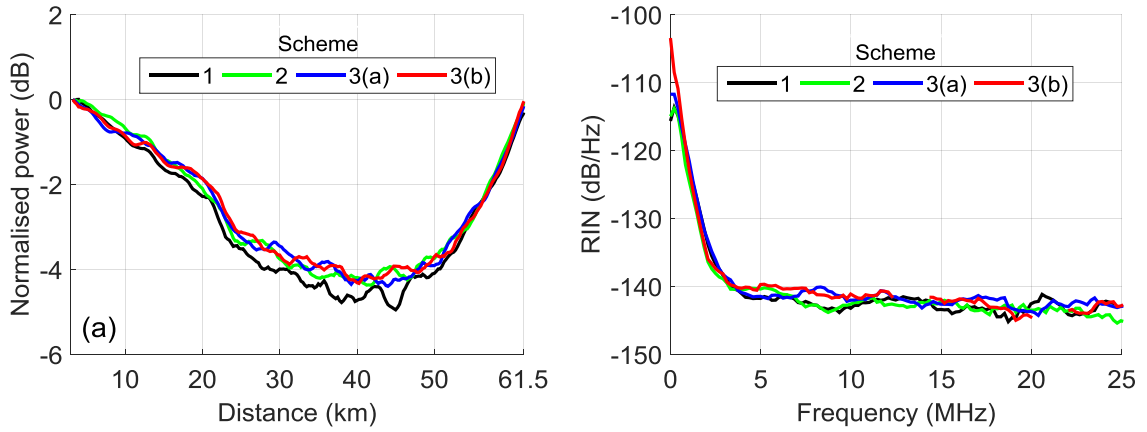
Figure 7. 23. (a) Signal power distributions along the amplifier and (b) signal RIN measured at 1545.32nm signal for different Raman pumping schemes

The measured SPVs and signal RIN performances at 1545.32nm are also shown in Figure 7. 23(a) and (b) respectively to verify the OSNR and RIN performances at other wavelength band of the amplifier. A small SPV improvement of 0.5dB and negligible increase in RIN were observed compared with backward only pumping (scheme-1). Despite having similar power profiles at 1545.32nm, NF improvement from 0.5 to 1dB across different bidirectional pumping schemes can be seen from Figure 7. 21, which mainly come from the overall ASE noise reduction.
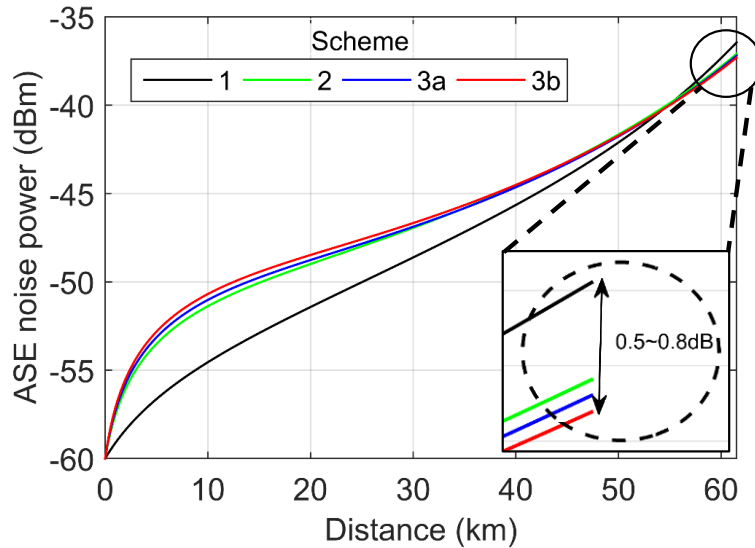
Figure 7. 24. Simulated forward propagated ASE noise profiles for different pumping schemes

In Figure 7. 24, the simulated ASE noise power evolution at 1545.32nm signal using the same pump powers used for overall Raman gain characterisation as given in Table 7. 5. At the end of the

179

amplifier span, a reduction from 0.5 to 0.8dB can be observed in scheme-2, 3(a) and 3(b) respectively and that attributed to the different ENF improvements at 1545.32nm signal as shown in Figure 7. 21. This verifies the benefit of proposed bidirectional pumping scheme in OSNR improvement over the entire amplifier bandwidth without increasing the signal RIN penalty.

7.2.1.3 *Transmission results*

In the previous sections, the noise performance improvement with the proposed dual order forward pumped bidirectional distributed pumping scheme has been shown numerically and experimentally through signal power distribution and noise figure characterisation. It has also been observed that, maximum ENF improvement was achieved at the lowest signal wavelength. In our experimental transmission performance evaluation setup, L-band equipment was not available to test the full bandwidth. However as the aim of this work was to reduce the overall ENF tilt by improving the OSNR of low signal wavelengths, some evaluation can be done using only the C band and measuring the improvement in the low wavelength channels compared with backward only pumping. So transmission results were measured at 1530.33nm signal in a WDM coherent transmission setup. Performances of all other WDM channels were also measured at maximum transmission reach.

A re-circulating loop setup was used as shown in Figure 7. 25. A 13 channel WDM grid was considered, consisting of three 150GHz spaced channels (195.6~195.9THz) in the lowest amplification band and other ten 100GHz spaced channels from 193.4~194.3THz. A 100kHz linewidth tunable laser as "channel under test (CUT)" was combined with the grid. The WDM signals were QPSK modulated at 30GBaud using 2^{31}-1 PRBS data pattern with 18bits relative delay between I and Q. The modulated signals were then amplified by a PM-EDFA and polarisation multiplexed with a 300 symbols equivalent delay line in between two polarisation states. The 13×120Gb/s DP-QPSK signals were launched into the re-circulating loop through an acousto-optic modulator (AOM). The distributed Raman amplifier span consists of a 61.5km SSMF with 12dB loss and 1.1dB loss from pump signal combiner pair from both ends. The gain fluctuation in amplified output signals after the Raman link was equalized using a gain flattening filter (GFF). The 12dB additional loop specific loss from GFF, 3dB coupler and AOM was compensated using a dual stage EDFA at the end of the loop. At the receiver, output signal is first de-multiplexed using a narrowband band pass filter and then amplified by an EDFA. A polarisation diverse coherent receiver with 80GSa/s, 36GHz bandwidth oscilloscope was used to capture the signal. Offline digital signal processing (DSP) was applied to process the data and calculate Q factors from measured bit-error rates averaged over 2 million bits.
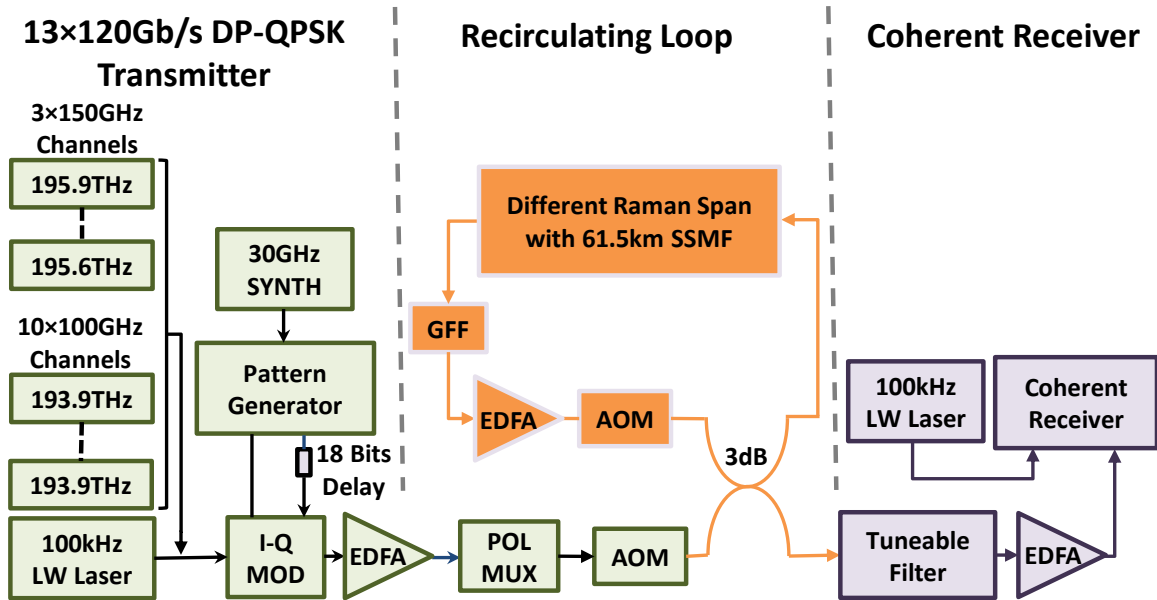
Figure 7. 25. Re-circulating loop setup for coherent WDM transmission with broadband distributed Raman amplified span (Abbreviations: SYNTH = synthesizer, MOD = modulator, LW = linewidth, POLMUX = polarisation multiplexer)

At first, maximum Q factor at optimum signal launch power per channel was determined and then Q factors at different transmission distances were obtained for the optimum signal launch power.
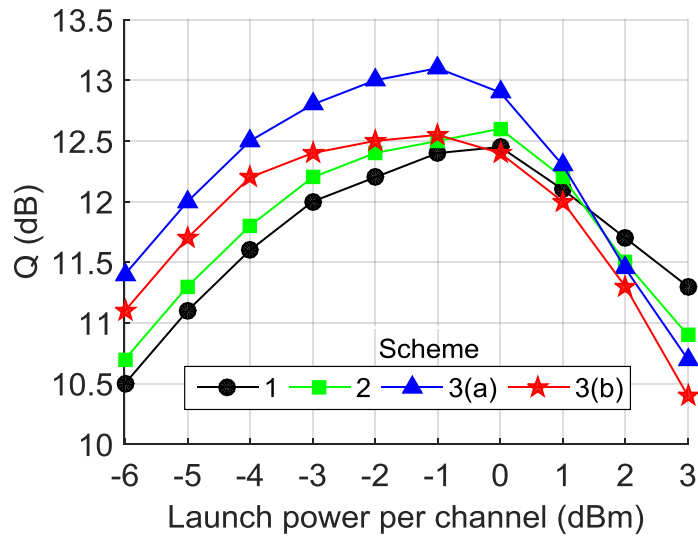
Figure 7. 26. Q factors versus launch power per channel measured at 1530.33nm signal

Figure 7. 26 shows the experimentally measured Q factors versus different launch powers per channel at 1845km transmission distance (30 recirculation) for 195.9THz (1530.33nm) signal in different Raman pumping schemes as described in Figure 7. 17. The maximum Q factor for backward only pumping (scheme-1) was 12.4dB at optimum launch power per channel of 0dBm

when signal RIN penalty is considered to be negligible. A small Q factor improvement of ~0.2dB was observed in scheme-2. In our proposed dual order forward pumping scheme-3(a), Q factor improvement was measured as ~0.7dB and optimum launch power was minimized to -1dBm compared with scheme-1 due to additional nonlinearity from higher average signal power along the span. The improvement comes from the improved ENF and no signal RIN penalty. But increasing 1425nm forward pump power to 49mW in scheme-3(b), the maximum Q-factor was reduced down to 12.5dB due to the additional RIN penalty from forward pumps although ENF improvement was the highest (~1.8dB) compared with scheme-1 as shown in Figure 7. 21. At the optimum launch powers per channel (-1 and 0dBm) for different pumping schemes, total launched signal powers into the span were calculated as 10.2 and 11.2dBm. Insignificant pump depletion could be expected at these higher power per channel levels and above, but it remains the same for all the bidirectional pumping schemes discussed here and will not affect the general conclusion of overall noise performance improvement without increasing the signal RIN penalty [14, 134].
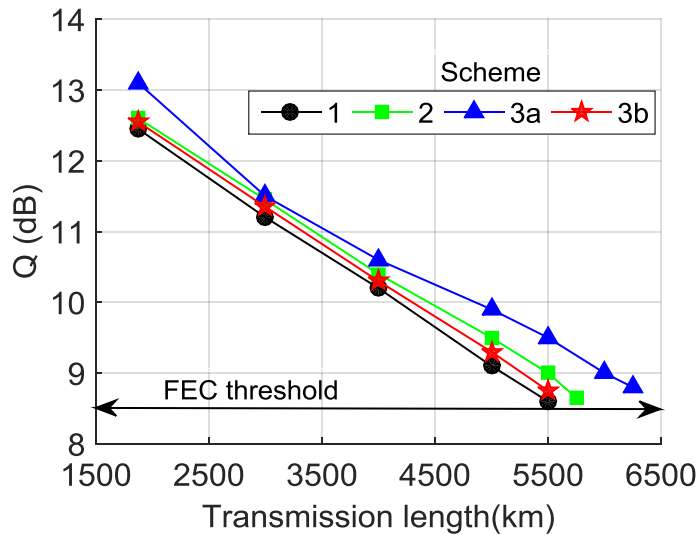
Figure 7. 27. Q factors vs. transmission distances at optimum launch power measured at 195.9THz (1530.33nm) for different pumping schemes

The Q factors versus transmission distances at corresponding optimum launch power for different pumping schemes is presented in Figure 7. 27. Scheme-3(a) showed a maximum Q factor of 13.1dB at optimum launch power and maximum transmission distance was achieved at 6150km with 738km reach extension than that of backward pumping (5412km). Scheme-2 also showed ~250km transmission reach enhancement compared with scheme-1 due to 0.2dB improved Q

factor, whereas scheme-3(b) achieved similar distance (5412km) like backward pumping only due to additional signal RIN penalty.
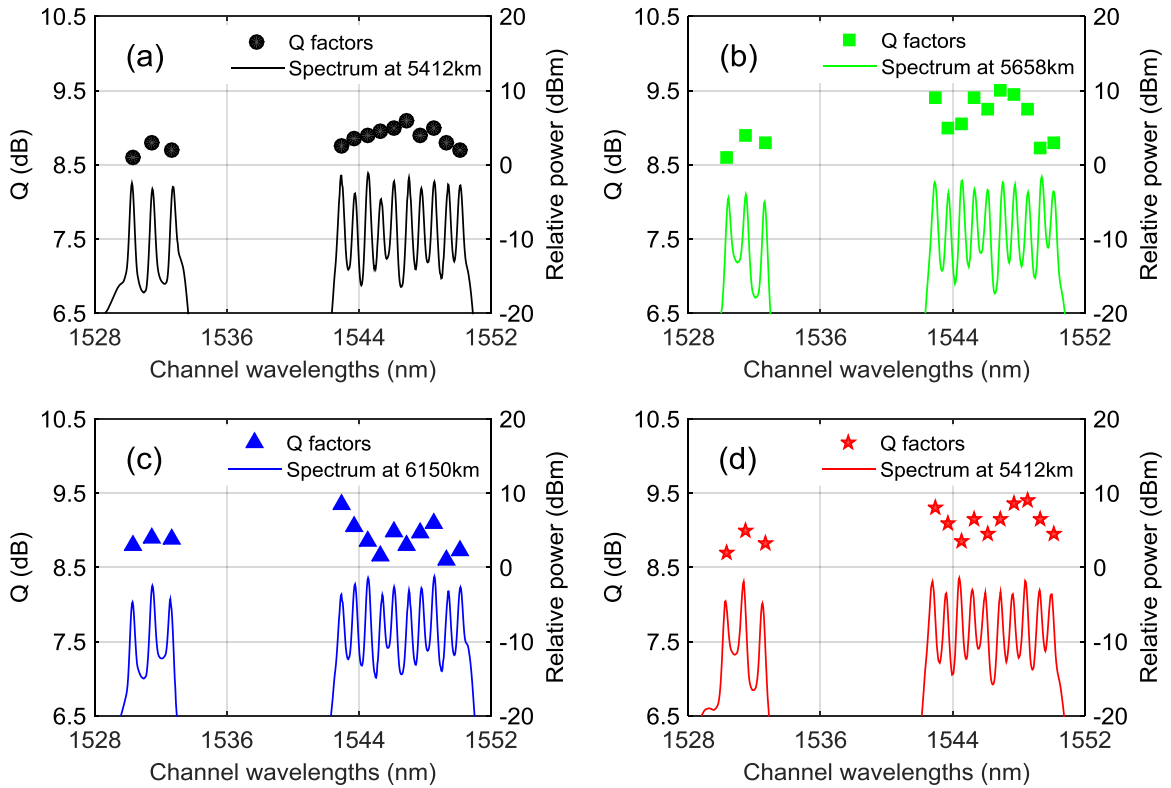
Figure 7. 28. Q factor of each signal channel and received spectra at respective maximum distance: (a) backward only pumping (scheme-1); (b) scheme-2; (c) scheme-3(a) and (d) scheme-3(b) considering hard decision - forward error correction (HD-FEC) threshold of Q = 8.5dB

The received spectrum and Q factor of each WDM signal at maximum reach were also measured and shown in Figure 7. 28, demonstrating Q factor above HD-FEC threshold of 8.5dB in each case. So, the benefit of improved noise performance with dual order forward pumping in broadband distributed Raman amplification resulted in extended transmission reach given that 1st order pump seed's power remains reasonably low (~ 21mW) and has very low pump RIN (~ -130dB/Hz) even with noisy 2nd order forward pump with RIN level about -120dB/Hz.

We also investigated the impact of different pump RIN of the 1st order seed on transmission performance. For this purpose we used the same semiconductor pump laser diode but drove it with low current which was enough to get 21mW output power. At low drive current, the pump RIN level was very high about ~ -120dB/Hz which subsequently transferred to signal and increased 1530.33nm signal RIN level up to ~4dB as shown in Figure 7. 29(a) and (b) respectively. The

additional signal RIN reduced the maximum Q factor (13.1dB) of scheme-3(a) to 12.7dB as shown in Figure 7. 29(c). In Figure 7. 29(d), due to the additional Q factor penalty the transmission reach was reduced down to maximum of 5658km which was still better than that of scheme-1 (5412km), mainly due to the proper choice of forward pump wavelengths and power which allows minimal RIN transfer to the signal.

So low power 1st order pump seed with low RIN (< -130dB/Hz) has to be used in the proposed dual order forward pumping scheme in order to get the best transmission performance. As a future work, we also suggest the use of a low RIN and broadband 1st order forward pump seed instead of the narrowband semiconductor laser diode for further OSNR improvement by allowing more gain from higher order forward pump without increasing the RIN transfer [159, 160].
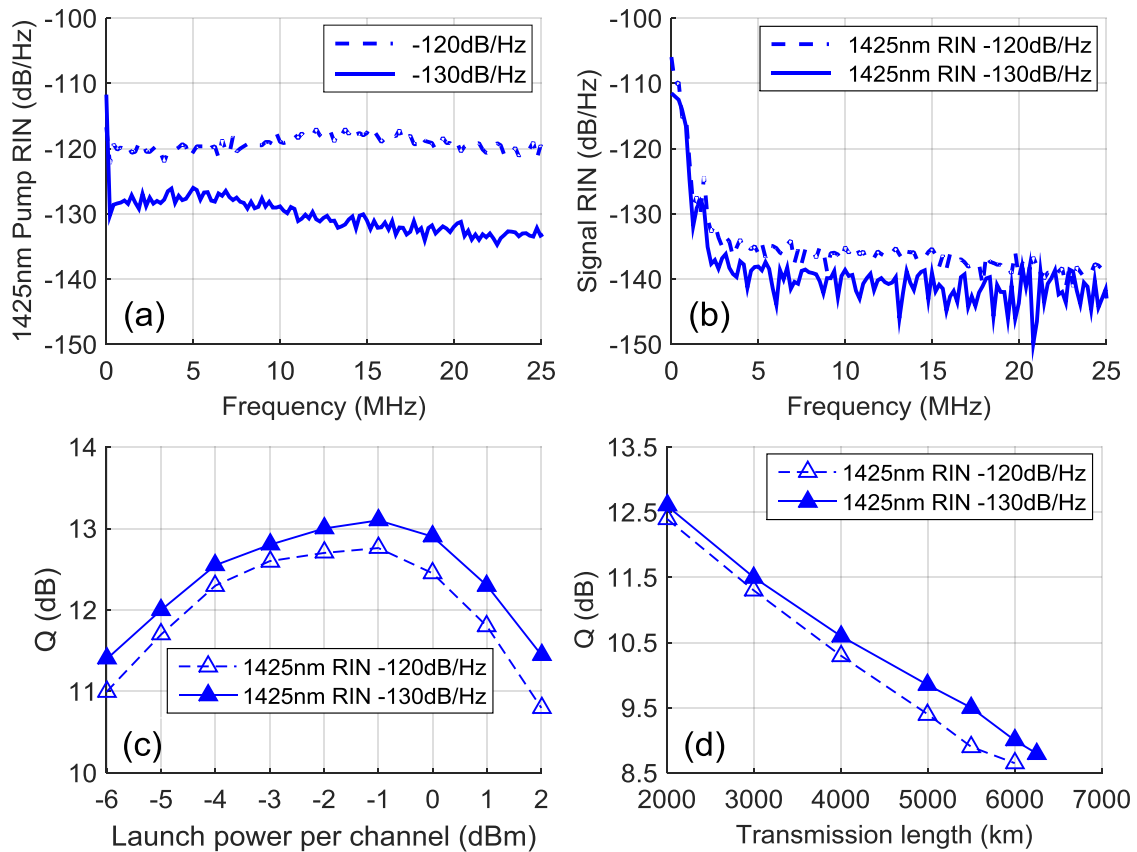
Figure 7. 29. Performance comparison of scheme-3(a): (a) using two RIN levels of the 1st order 1425nm forward pump by varying the drive currents and (b) signal RIN; (c) Q factors versus signal launch power per channel and (d) Q factors vs. transmission distance at optimum launch power measured at 1530.33nm signal

In conclusion, we have demonstrated the overall noise performance improvement and noise figure tilt reduction of a broadband distributed Raman amplifier using bidirectional amplification with

dual order forward pumping seeded by a first order pump without deteriorating the signal RIN performance. We have also investigated the impact of 1st order forward pump seed power and RIN level on the trade-off between noise figure improvement and net transmission performance. We have reported that despite the use of fibre laser with relatively high RIN level for second-order forward pumping, using ~21mW of 1st order forward pump seed with RIN level below -130dB/Hz shows no increase in signal RIN and improves transmission performance. Although the bi-directional pumping configuration requires additional pump lasers there is a significant advantage in transmission performance with the transmission reach of 13×120Gb/s DP-QPSK long haul transmission extended by a minimum of 14% up to 6150km compared with conventional backward only pumping.

7.3 Broadband Discrete Raman Amplification

Broadband discrete Raman amplification is another type of popular Raman amplification technique especially for metro or short haul transmission system. Majority of Raman amplified transmission systems use distributed amplification using the transmission fibre as the gain medium providing better OSNR and extended reach than conventional lumped amplifiers i.e. EDFA [195]. Discrete Raman amplifiers use a separate Raman gain fibre for amplification instead of using the transmission fibre as the gain medium as in distributed amplification, which may be advantageous for many operational reasons such as laser safety issues and so on.

7.3.1 Benefits and challenges

The well-known benefits of flexible gain bandwidth determined by Raman pump wavelengths and broadband operation by cascading suitably chosen multiple pumps are also present in discrete Raman amplifiers. Broadband operation mainly in C+L band can also be obtained by combining EDFAs operating at different bands but the technique leaves a small (~5nm) 'bandwidth gap' in the midst of C and L band requiring more passive components i.e. band couplers and splitters. Multi-pumped discrete Raman amplifier solves this problem and allows for all-Raman broadband and seamless, long haul transmission systems [17].

One of the main challenges in discrete Raman amplifier design is choosing the right fibre. Usually Raman gain fibres with smaller effective core area are chosen for discrete application for their higher Raman gain efficiency property, however the benefits may be outperformed by the additional nonlinear penalties limiting the transmission reach much lower than that of distributed amplification.

Gain fibres with higher Raman gain coefficient and small core diameter are mainly chosen for discrete Raman amplification. Most reported discrete Raman amplified systems used dispersion compensating fibre (DCF) as gain fibre which has two folds benefits: providing amplification and in-line dispersion compensation [114-116]. Broadband discrete Raman amplifiers are also very attractive in all-Raman amplified transmission systems providing seamless gain bandwidth for amplification unlike EDFAs and cost-effective solution with reduced numbers of required passive components.

There are some additional challenges in case of using different gain fibres in discrete Raman amplifiers. For example DCF will have additional dispersion in the system which will have pronounce effect in selecting proper transmission span lengths in case of dispersion compensated systems. Present transmission systems use coherent technology where dispersion effects are managed in receiver by DSP. So total dispersion map has to be remodeled in the DSP for additional dispersion by using DCF as gain medium.

Apart from choosing the right span length and dispersion map management in the DSP, signal nonlinear penalties and double Rayleigh scattering (DRS) induced multi-path interference (MPI) also deteriorates the system performances. Gain fibres with high nonlinear index will give rise to four wave mixing (FWM) products in WDM signal band which degrades the system performance. So improved nonlinearity compensation techniques has to be considered with high nonlinear fibre based discrete Raman amplifiers [196, 197]. Moreover, DRS significantly affects the OSNR performance and sets and upper limit on the maximum possible gain from the amplifier [195].

In this section, the design of broadband discrete Raman amplifiers for improved noise and nonlinear performances are discussed both numerically and experimentally. The design of multi-stage discrete Raman amplifiers for high output power, high gain and low noise figure performances are also investigated.

7.3.2 Design of advanced broadband discrete Raman amplifiers

In discrete Raman amplifier, gain fibres with high Raman gain co-efficient and small core area are usually preferred in order to improve the pump conversion efficiency. Highly nonlinear fibre (HNLF), dispersion shifted fibre (DSF) and DCF have already been used due to their high Raman gain properties [113, 198, 199]. Inverse dispersion fibre (IDF) has recently been proven as an alternative of DCF for in-line dispersion and nonlinearity management [200, 201].

The challenges of using these gain fibres are DRS induced MPI and nonlinear impairments due to high nonlinear index of fibre. DRS significantly deteriorates the OSNR performance and limits maximum gain of the amplifier. Separating the gain fibre lengths into two stages through an isolator [202], or amplifying in dual stage configurations with the same set of pump wavelengths have already been presented [203]. The main drawbacks of those configurations were poor pump conversion efficiency, as very high pump powers were needed to amplify both stages by reusing residual pumps, and large gain variations due to less flexibility of gain spectrum control at each stage. Moreover, nonlinear penalty, which could be detrimental due to the use of significantly longer lengths of the same gain fibre with very high nonlinearity in both stages, has not been analysed. Nonlinear penalty also increases with the length and the nonlinear refractive index parameter of the gain fibre, so proper choice of gain fibre length and nonlinear efficiency are required to optimize DRS and nonlinear penalty in designing discrete Raman amplifiers with high gain, low noise and nonlinear penalty.

In this section, we numerically demonstrate a design of broadband discrete Raman amplifiers in dual stage cascaded configuration pumping with only four backward 1st order pumps [204]. We report 19dB average net gain over 70nm bandwidth, over 20dBm output power, ~6dB noise figure and low nonlinear penalty. We investigate the performances of three different, commonly used Raman gain fibres: DCF, HNLF and IDF, in different combinations and determine the combination of gain fibres used in two stages for the best noise and nonlinear performance. We calculated the nonlinear impairment by determining the self-phase modulation (SPM) induced nonlinear phase shift (NPS) [205]. Noise performance was characterized by NF and output OSNR considering combined ASE and DRS noise contribution.

7.3.2.1 *Proposed amplifier design and simulation setup*

The amplifier configuration is shown in Figure 7. 30. It comprises of two stages, in which different combinations of three different gain fibres DCF, HNLF and IDF were investigated in each stage. We considered 70nm amplification bandwidth from 1530 to 1600nm. Only four depolarised cascaded 1st order Raman pumps: 1427nm, 1445nm, 1462nm and 1490nm were considered in backward pumping configuration at each stage to achieve total gain ripple ~1.6dB. Two separate stages were combined using a mid-stage isolator to restrict the evolution of DRS. Equal signal power per channel of -10dBm was considered at the input of the amplifier and mid-stage insertion loss from WDM coupler and isolator of 1dB was considered for signals.
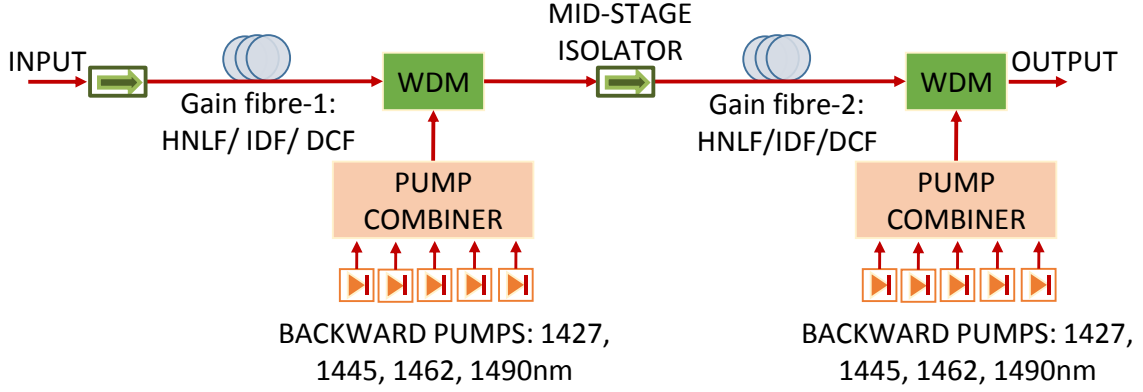
Figure 7. 30. Schematic diagram of a cascaded dual stage discrete broadband Raman amplifier

The complete numerical model for the evolution of signals, pumps and noise is based on standard average power model as mentioned in Eq. (7.1). Pump depletion, ASE noise, DRS, energy transfer due to interactions between pump-pump, pump-signal and signal-signal from either direction have been included in the model. Three different gain fibres: HNLF, IDF and DCF at different lengths were considered in the numerical simulation for performance characterisation of different features i.e. ASE and DRS noise, overall noise figure and NPS. To separately monitor the impact of different noise terms in discrete Raman amplifiers, forward and backward propagating ASE and DRS noises are defined separately in Eqs. (7.6) - (7.9).

$$\frac{dN_{ASE}^{+}}{dz} = -\alpha_v N_{ASE}^{+} + N_{ASE}^{+} \sum_{\mu>v} \frac{g_{\mu v}}{A_\mu} \left(P_\mu^{+} + P_\mu^{-} \right) + 2hv\Delta v \sum_{\mu>v} \frac{g_{\mu v}}{A_\mu} \left(P_\mu^{+} + P_\mu^{-} \right) \left(1 + \frac{1}{e^{\frac{h(\mu-v)}{kT}} - 1} \right) \quad (7.6)$$

$$\frac{dN_{ASE}^{-}}{dz} = \alpha_v N_{ASE}^{-} - N_{ASE}^{-} \sum_{\mu>v} \frac{g_{\mu v}}{A_\mu} \left(P_\mu^{+} + P_\mu^{-} \right) - 2hv\Delta v \sum_{\mu>v} \frac{g_{\mu v}}{A_\mu} \left(P_\mu^{+} + P_\mu^{-} \right) \left(1 + \frac{1}{e^{\frac{h(\mu-v)}{kT}} - 1} \right) \quad (7.7)$$

$$\frac{dN_{DRS}^{+}}{dz} = -\alpha_v N_{DRS}^{+} + N_{DRS}^{+} \sum_{\mu>v} \frac{g_{\mu v}}{A_\mu} \left(P_\mu^{+} + P_\mu^{-} \right) + \varepsilon_v N_{DRS}^{-} \quad (7.8)$$

$$\frac{dN_{DRS}^{-}}{dz} = \alpha_v N_{DRS}^{-} - N_{DRS}^{-} \sum_{\mu>v} \frac{g_{\mu v}}{A_\mu} \left(P_\mu^{+} + P_\mu^{-} \right) - \varepsilon_v \left(N_{DRS}^{+} + P_v^{+} \right) \quad (7.9)$$

Where, $N_{ASE}^{\pm}$ and $N_{DRS}^{\pm}$ represent the forward and backward propagating ASE and DRS noise power respectively at frequency v within a frequency interval Δv. The other parameters remain the same as described in Eqs. (7.1) - (7.3). The fibre parameters are given in Table 7. 6.

Table 7. 6. Summary of Raman gain fibre parameters [110, 111, 201, 204]

Parameters	HNLF	IDF	DCF
Pump attenuation, α_{1455} (dB/km)	0.75	0.3	0.8
Signal attenuation, α_{1550} (dB/km)	0.6	0.23	0.67
Effective area of fibre, A_{eff} (μm^2)	10.2	31	19
Raman gain co-efficient, g_R/A_{eff} ($W^{-1}km^{-1}$)	6.3	1.3	2.5
Rayleigh backscattering co-efficient, ε_{1550} (10^{-4} km^{-1})	9.2	1.2	7.1
Nonlinear refractive index, n_2 (10^{-20} m^2/W)	4.49	2.7	3.95
Nonlinear co-efficient, γ_{1550} ($W^{-1}km^{-1}$)	17.84	3.53	8.43
n_2/A_{eff} (10^{-8} W^{-1})	0.44	0.09	0.21
Dispersion (ps/nm/km) at 1550nm	-20.7	-44	-100

7.3.2.2 *Performance characterisation of single stage discrete Raman amplifiers*

Through numerical simulation considering the amplifier configuration described in Figure 7. 30, the performance of discrete Raman amplifier was investigated in single stage configuration by varying the lengths of different gain fibres in order to compare their noise and nonlinear performances. The target average net gain was fixed at ~10.8dB in each case with < 1.5dB gain ripple. Maximum pump power per wavelength was limited to 300mW. It was found that, NF values were degraded as the length of gain fibre were increased in single stage configuration, due to increasing DRS induced MPI noise. On the other hand, required total pump powers were reduced with increasing amplifier length until attenuation loss became dominant over Raman gain efficiency.

First of all we have numerically characterize the NF, NPS and output OSNR performances of IDF fibre at different lengths. We considered 5nm spaced WDM signals from 1530 to 1600nm over 70nm amplification bandwidth. Both ASE and DRS contributions were taken into consideration in wavelength dependent NF and OSNR calculation. NF values were calculated following the Eqs. (7.4) - (7.5). Output OSNRs were calculated as the following Eq. (7.8), considering the noise contributions both from ASE and DRS.

$$OSNR(dB) = 10\log 10(\frac{P_{out}}{P_{ASE} + P_{DRS}}) + 10\log 10(\frac{B_m}{B_o}) \tag{7.8}$$

Where, P_{out}, P_{ASE} and P_{DRS} are the signal power, ASE noise power and DRS noise power at the end of the amplifier. B_m and B_o represent the noise equivalent bandwidth and reference optical bandwidth respectively and both of those were considered as 125GHz. The NPS was calculated using the following Eqs. (7.9) - (7.10).

189

$$NPS = \gamma \int_0^L P_S(z)dz \tag{7.9}$$

$$\gamma = \frac{2\pi n_2}{\lambda_S A_{eff}} \tag{7.10}$$

Where, γ and P_S represents the nonlinear coefficient and signal power along the span length (L). In Eq. (7.10), nonlinear coefficient at specific signal wavelength (λ_S) was calculated from the ratio between nonlinear refractive index (n_2) and effective area (A_{eff}) of the gain fibre.
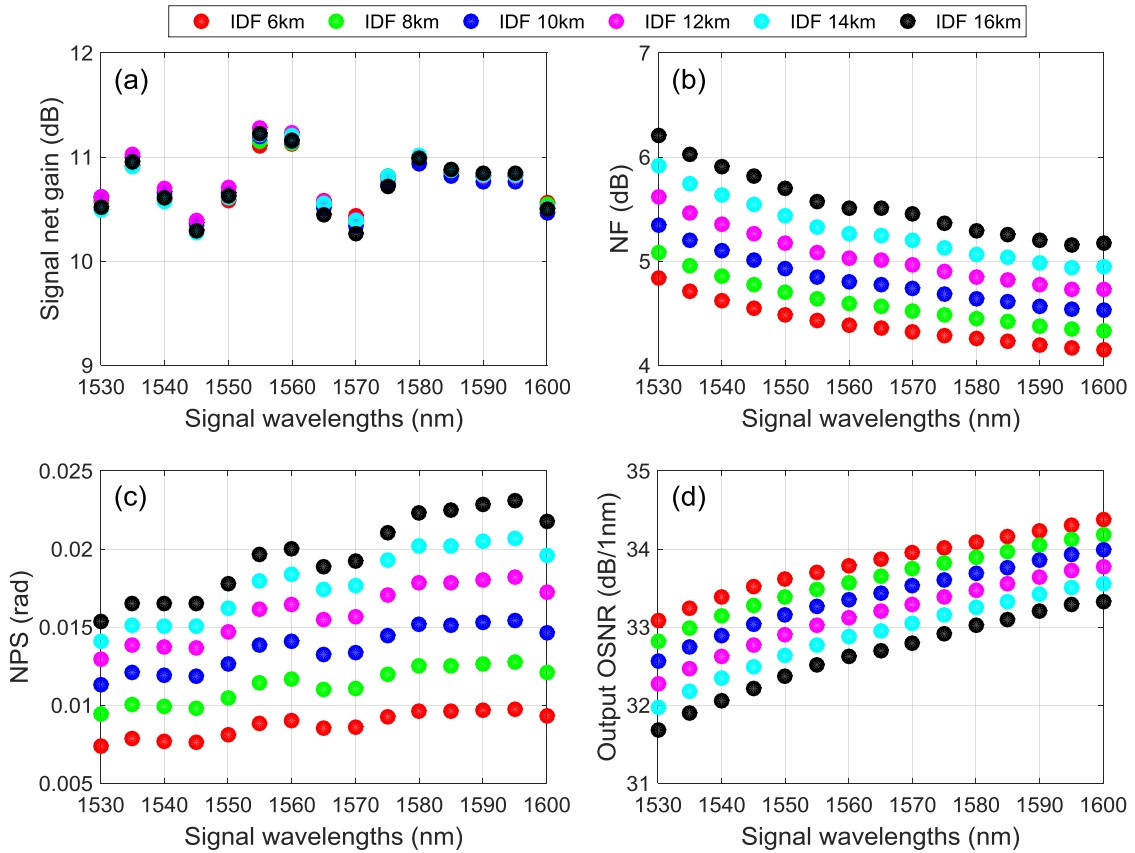
Figure 7. 31. Characterisations of IDF based single stage discrete Raman amplifier with varying lengths: (a) signal net gain (b) noise figure (c) nonlinear phase shift and (d) output OSNR

Figure 7. 31 shows the characterisation results with IDF fibre. The length of IDF is varied from 6km to 16km, 6km being the lowest possible length within the maximum 300mW pump power restriction. In order to maintain a fair comparison, we maintained the overall average net gain at 10.8~11dB for all the fibre lengths as shown in Figure 7. 31(a). As expected, low wavelength signals have higher NF due to being close to the longer wavelength pumps and thus have more

thermally generated noise (Figure 7. 31(b)). The tilt in noise figure could be minimised by forward pumping with shorter wavelength pumps in a bidirectional pumping configuration as described in case of broadband distributed Raman amplification in previous section [206]. In Figure 7. 31(b) and (c), both NF and NPS increased with increasing lengths of IDF, thanks to the impact of DRS and total average power along the span respectively. Output OSNR followed the opposite trend of NF as shown in Figure 7. 31(d). So, discrete Raman amplifier with shorter gain fibre length is the best in terms of noise and nonlinear performance but at the expense of pump power efficiency. Similar characterisations were carried out for DCF and HNLF with the same target net gain, gain ripple and pump power constraints.
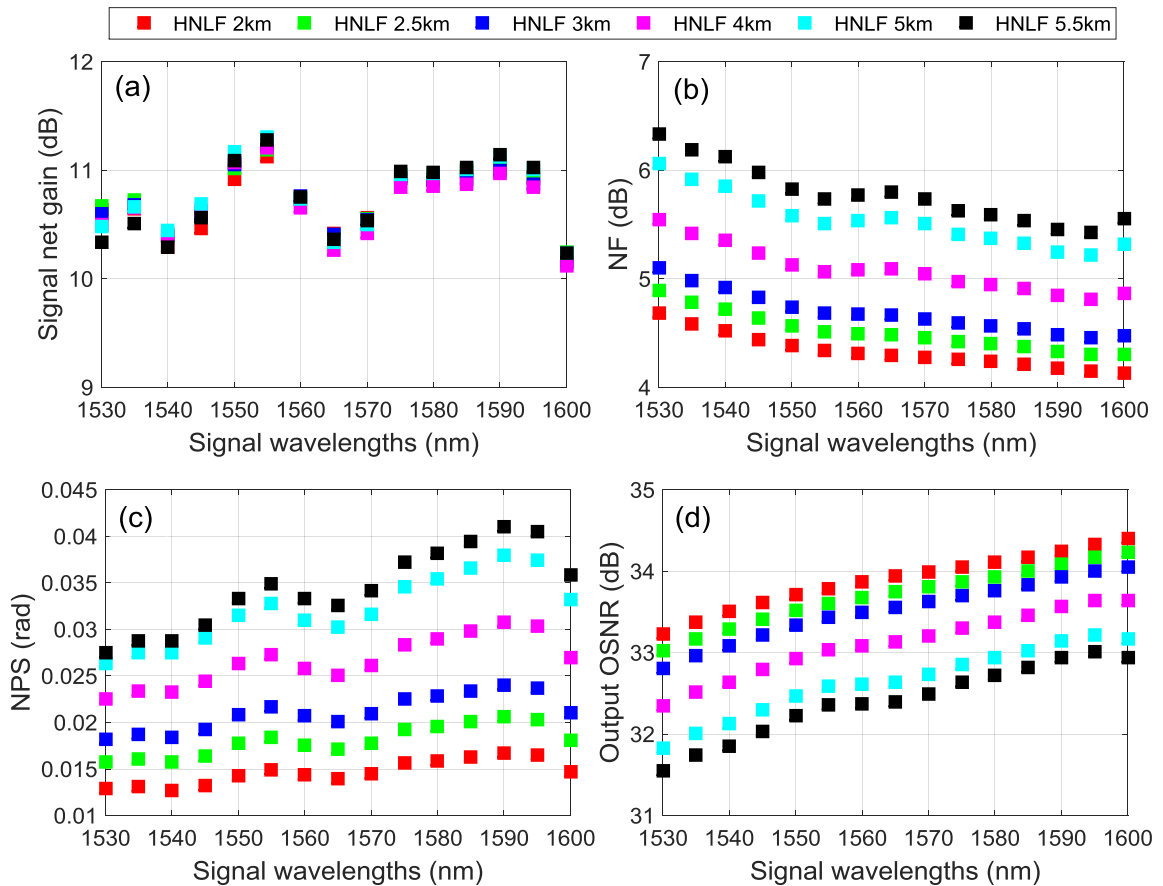
Figure 7. 32. Characterisations of HNLF based single stage discrete Raman amplifier with varying lengths: (a) signal net gain (b) noise figure (c) nonlinear phase shift and (d) output OSNR

The lengths of HNLF were varied from 2-5.5km keeping fixed average net gain 10.8-11dB. Similar performance trends were observed as IDF, showing shorter lengths of HNLF provided better NF, output OSNR and NPS performances. In Figure 7. 32(c), a sharp increase in NPS values

were obtained beyond HNLF length of 3km due to the accumulation of self-phase modulation (SPM) induced penalty in sufficiently long length of fibre with very high nonlinear co-efficient (Table 7. 6). Although the Rayleigh backscattering coefficient of HNLF was seven times higher than that of IDF, however it required shorter lengths of fibre to have similar net gain for having high Raman gain efficiency and that reduced the generation of more DRS noise. The overall NF of the amplifier performed similar to IDF based discrete amplifier up to 4km, giving NF < 6dB as shown in Figure 7. 32(b). In Figure 7. 32(d), degradation of output OSNR values were also observed with increasing HNLF lengths due to the increased noise contribution both from ASE and DRS.
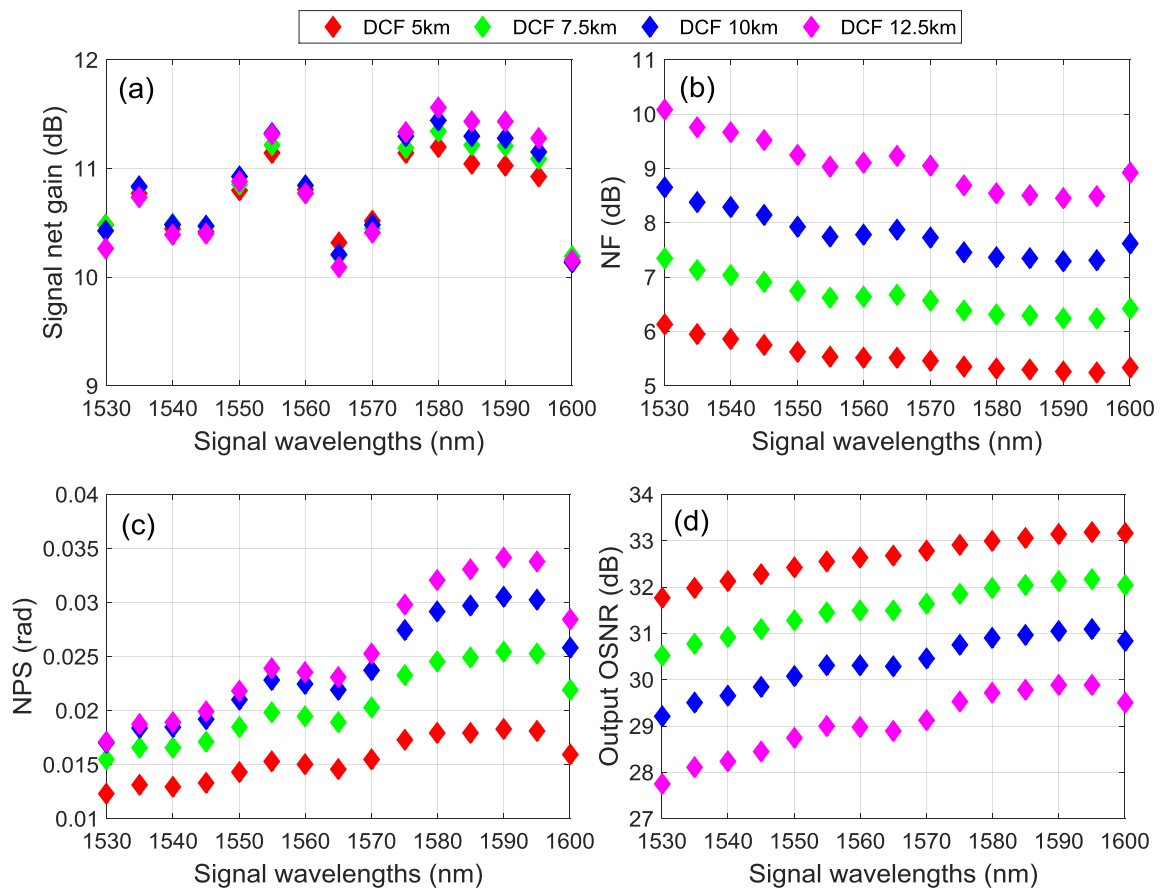
Figure 7. 33. Characterisations of DCF based single stage discrete Raman amplifier with varying lengths: (a) signal net gain (b) noise figure (c) nonlinear phase shift and (d) output OSNR

Figure 7. 33 shows the characterisation of DCF at different lengths varied from 5-12.5km within the pump power limit of 300mW per pump wavelength. The backward pump powers were optimized in order to get average net gain between 10.8~11dB with gain ripple below 1.5dB. DCF

also has very high Rayleigh backscattering coefficient than that of IDF and the overall average NFs were increased sharply with increasing fibre lengths due to the rapid growth of DRS induced noise over longer lengths. In Figure 7. 33(c), the longer signal wavelengths suffered from more SPM induced nonlinear phase shift because of higher path average power due to smaller attenuation in longer signal band. Finally similar trends in NF, NPS and output OSNR have also been observed, as shorter lengths being the best choice for low noise and NPS induced penalty. Pump powers used in the best possible lengths of each gain fibre are given in Table 7. 7.

Table 7. 7. Pump powers used in single stage of different gain fibres with the shortest characterized lengths

Pump (nm)	Pump power (mW)		
	HNLF 2km	IDF 6km	DCF 5km
1427	205	300	290
1445	95	185	180
1462	90	100	110
1490	113	200	165
Total	503	785	745

In the numerical simulation, frequency dependent Raman gain coefficients and fibre attenuation coefficients were considered for all the three gain fibre considered here as shown in Figure 7. 34(a) and (b) respectively. The Raman gain coefficients shown in Figure 7. 34(a) are given for a reference pump wavelength of 1455nm. IDF has the smallest attenuation coefficients in both pump and signal bands. The fibre attenuation coefficients of DCF shows similar values as HNLF in the 14xx band but increase sharply beyond conventional C band.
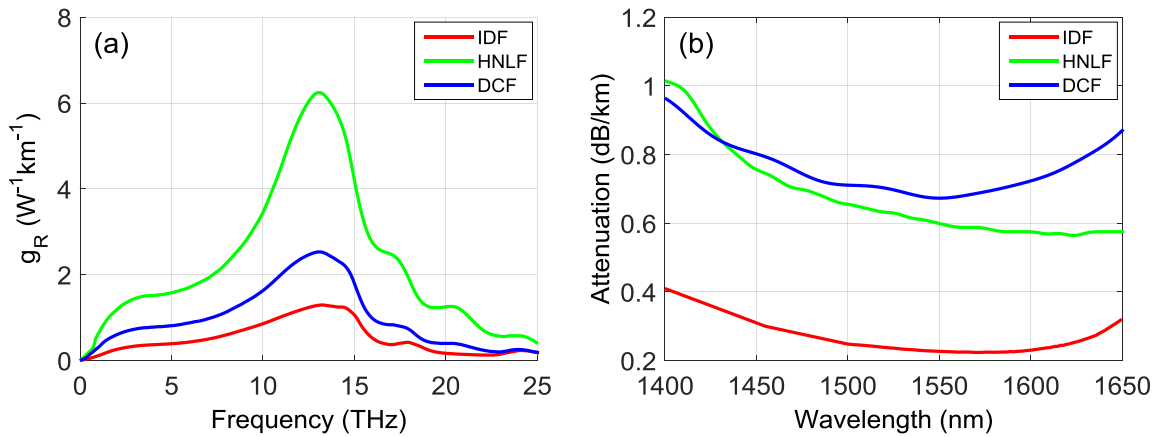
Figure 7. 34. Comparison of (a) Raman gain coefficients and (b) fibre attenuation coefficients among three different Raman gain fibres: IDF, HNLF and DCF [110, 111, 201]
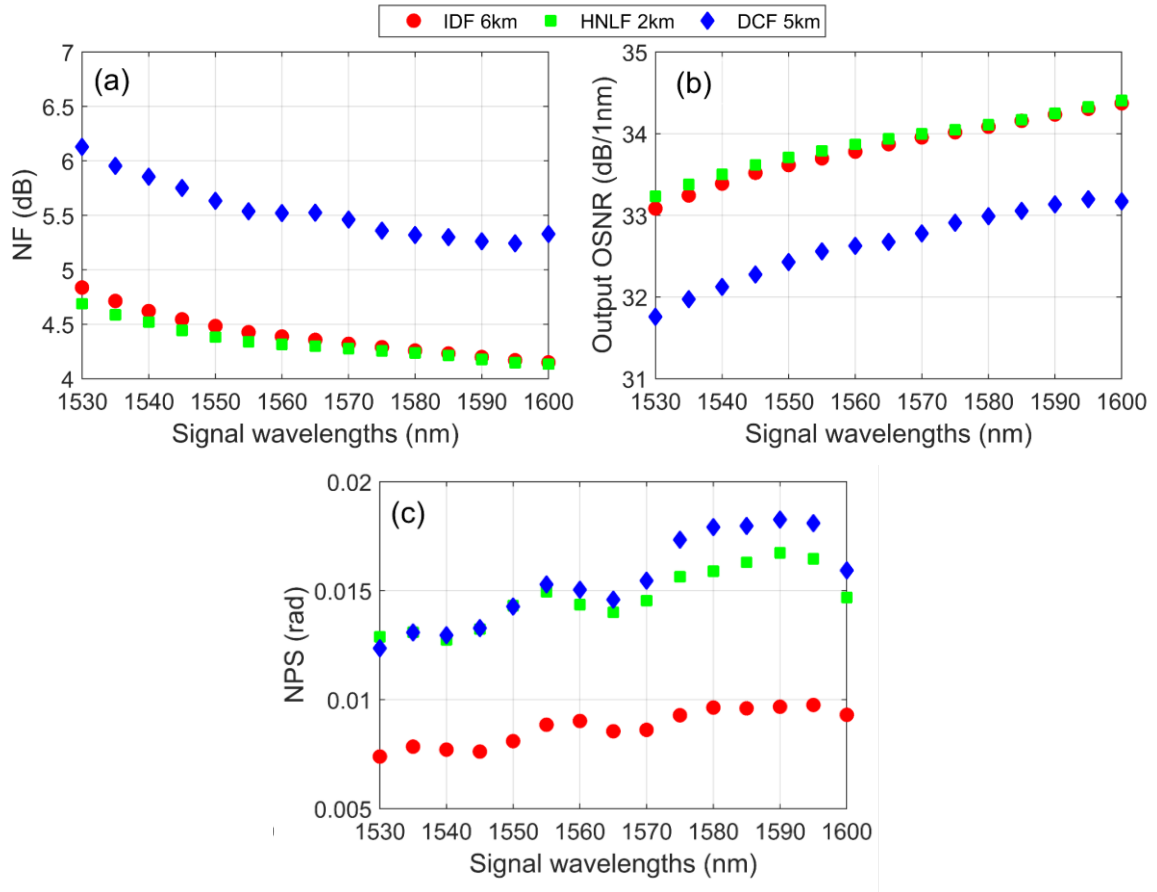
Figure 7. 35. Performance comparison of different single stage discrete Raman amplifiers with average target net gain of 10.8dB and at optimum length considered (a) noise figure (b) output OSNR and (c) nonlinear phase shift

Performance comparison of three different gain fibres in single stage configuration with the best performing shortest lengths is shown in Figure 7. 35. In Figure 7. 35(a) and (b), NF and output OSNR over 70nm bandwidth are almost similar for 6km IDF and 2km HNLF whereas 5km DCF shows more than 1dB penalty. Although HNLF shows similar noise performance as IDF but has worse nonlinear penalty that is similar to DCF as depicted in Figure 7. 35(c). Although DCF has lower nonlinear refractive index than HNLF as mentioned in Table 7. 7, however due to higher average power over longer length makes the nonlinear penalty as much as HNLF with half of the length. On the other hand, IDF has the lowest nonlinear penalty due to its larger effective area and lower nonlinear co-efficient than DCF and HNLF.

194
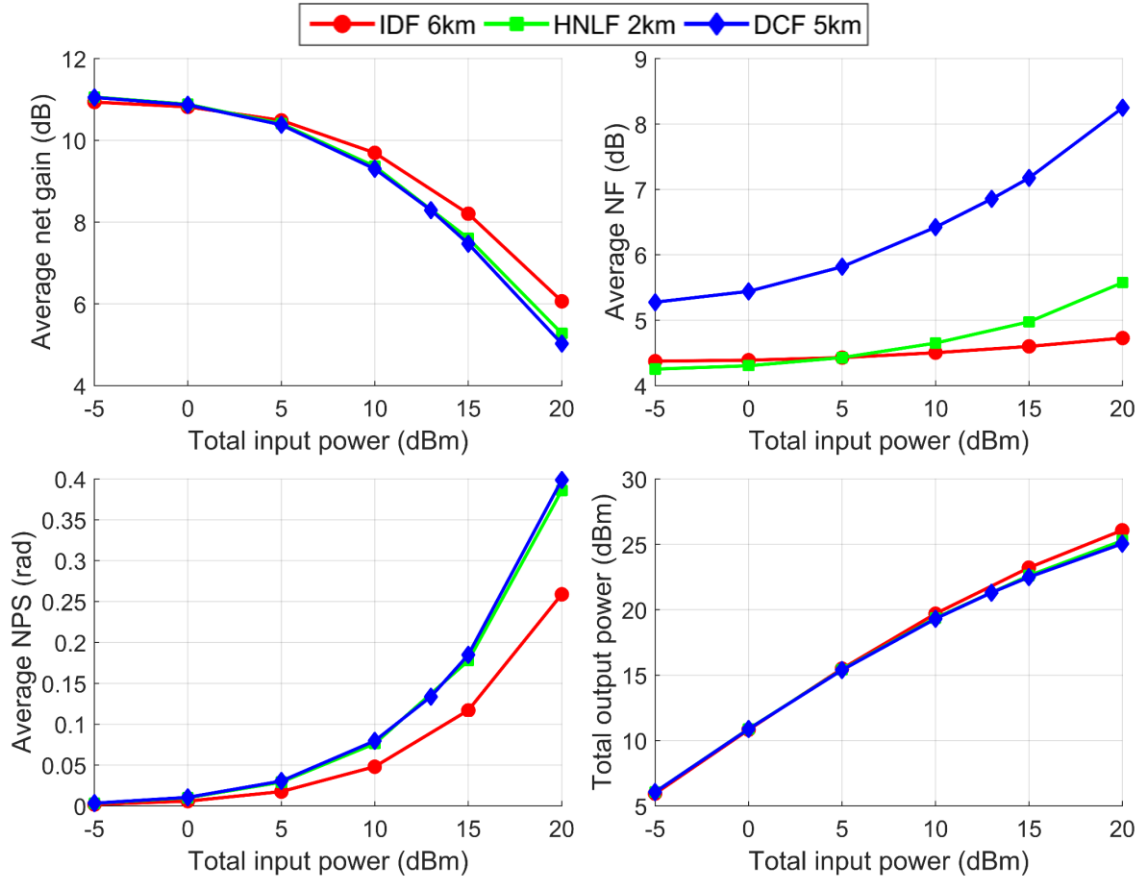
Figure 7. 36. Performance characterisation of single stage discrete Raman amplifiers with different gain fibres with increasing total signal power

We also investigated the performances with increasing total signal power for different gain fibres as shown in Figure 7. 36. The total signal power was distributed over 5nm spaced WDM signals in 70nm bandwidth. The gain ripple at each signal power was also limited to 2dB. The overall average net gain was reduced sharply due to more pump depletion beyond total signal launch power of 5dBm as shown in Figure 7. 36(a). In Figure 7. 36(b), DCF 5km shows the worst NF which increases sharply with increasing signal power, whereas HNLF 2km and IDF 6km shows similar noise performance and average NF does not increase rapidly as DCF 5km. As expected, increasing the signal power also increased the SPM induced NPS in all the fibre types as depicted in Figure 7. 36(c). HNLF and DCF gave almost similar NPS performances, with IDF being the lowest. Figure 7. 36(d) shows the total output power at the end of the amplifier, which also increases with increasing signal power up to 20dBm. The overall average net gain is reduced down to ~5dB at 20dBm total signal power due to the strong pump depletion, and at this small gain level output signal power is increased up to ~25dBm (Figure 7. 36(d)).

7.3.2.3 Performance characterisation of dual stage discrete Raman amplifiers

Total noise performance in a cascaded amplifier chain mainly depends on the noise contribution from the 1st stage amplifier. Usually higher net gain and lower noise figure are considered in the 1st stage to get better overall performance. Here, only IDF 6km and HNLF 2km have been used as the 1st stage which allowed us to investigate six different possible combinations of dual stage discrete Raman amplifier. Similar to the single stage, fifteen WDM signals with 5nm spacing over 70nm and -10dBm/channel were considered for the dual stage amplifier characterisation. The target average net gain from the combined dual stages was set to 19dB with a maximum ripple of 1.6dB.
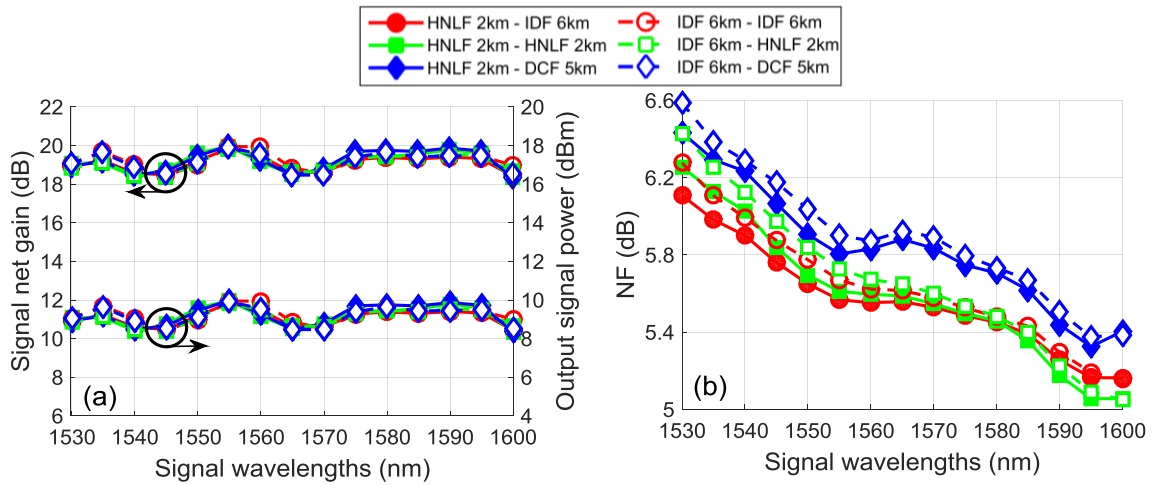
Figure 7. 37. Performance characterisations of dual stage discrete Raman amplifier (a) signal net gain and output power (b) noise figure

Figure 7. 37(a) shows the signal net gain and output power of signals in all the dual stage configurations considered here. It can be seen that, average total net gain is almost the same (~19dB) and average total output signal power is > 20dBm (~9dBm/channel) for all the schemes. Figure 7. 37(b) shows that all dual stage configurations with HNLF 2km based 1st stage (HNLF 2km - IDF 6km, HNLF 2km - HNLF 2km and HNLF 2km - DCF 5km) have better noise figure than its counterpart IDF 6km 1st stage based configurations because of having slightly better noise performance in the 1st stage as shown in Figure 7. 35(a) and (b). As expected dual stage amplifiers with DCF 5km in 2nd stage shows the worst noise performance regardless of their 1st stage configuration. HNLF 2km - IDF 6km shows the minimum noise figure (~6dB) with less than 1dB tilt across the 70nm bandwidth.
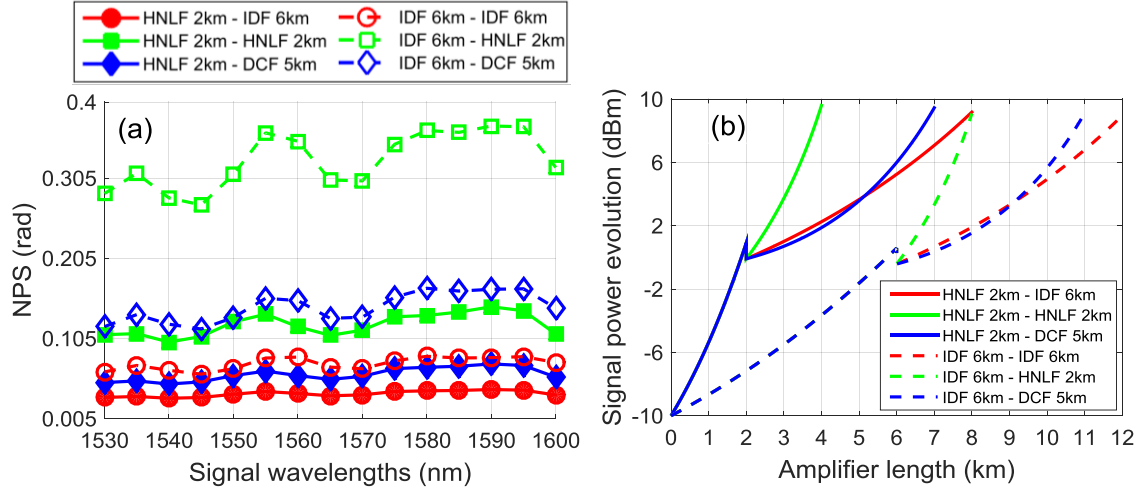
Figure 7. 38. Performance characterisation of dual stage discrete Raman amplifier at different gain fibre combinations: (a) NPS and (b) numerically simulated signal power evolution along the amplifier span

Total nonlinear phase shift for all signal wavelengths have also been calculated as shown in Figure 7. 38(a). NPS depends both on the nonlinear co-efficient of gain fibre and average signal power along the length of amplifier. Although IDF 6km shows better nonlinear performance than HNLF 2km in single stage characterisation (Figure 7. 35(c)) but in all dual stage combinations (IDF 6km – IDF 6km, IDF 6km – HNLF 2km and IDF 6km – DCF 5km), it shows worse performance than HNLF 2km 1st stage based counterpart. IDF 6km – HNLF 2km dual stage configuration has the highest nonlinear penalty, because HNLF has a nonlinear co-efficient ~5 times higher than IDF and average signal power is significantly higher in the 2nd stage. Nonlinear penalty is the lowest with HNLF 2km – IDF 6km configuration because IDF has the lowest nonlinear co-efficient and the best single stage NPS performance than both DCF and HNLF. Figure 7. 38(b) shows the signal power evolution of all dual stage amplifier configurations.

In summary, we have characterized the gain, noise and nonlinear performance of dual stage discrete Raman amplifiers with different combinations of three types of gain fibres: IDF, HNLF and DCF at optimum lengths. It is found that a dual stage discrete Raman amplifier design with >20dBm output power and ~6dB noise figure is possible with 2km HNLF and 6km IDF as 1st and 2nd stage combination respectively, showing the lowest NPS penalty of all the possible gain fibre combinations under study.

Although HNLF 2km - IDF 6km is the best solution in terms of noise and nonlinearity according to our design of a 19dB net gain, 20dBm output power discrete Raman amplifier, the availability of HNLF with zero dispersion wavelength < 1400nm would be the biggest challenge. IDF 6km – IDF

197

6km has the similar noise figure as with HNLF 2km 1st stage based configuration, but limited in terms of nonlinear penalty.

7.3.3 Experimental results

In this section, we demonstrate transmission performances of single stage and dual stage discrete Raman amplifiers with 10km IDF and 10km IDF-4km DCF respectively. Only IDF-DCF combination was chosen, as other gain fibre i.e. HNLF was not available for experimental characterisation. We were also limited by the available lengths of different Raman gain fibres to show experimental verification of the proposed dual stage discrete Raman amplifier design in the previous section. However the basic properties of dual stage discrete Raman amplifiers are presented here with available gain fibre lengths.
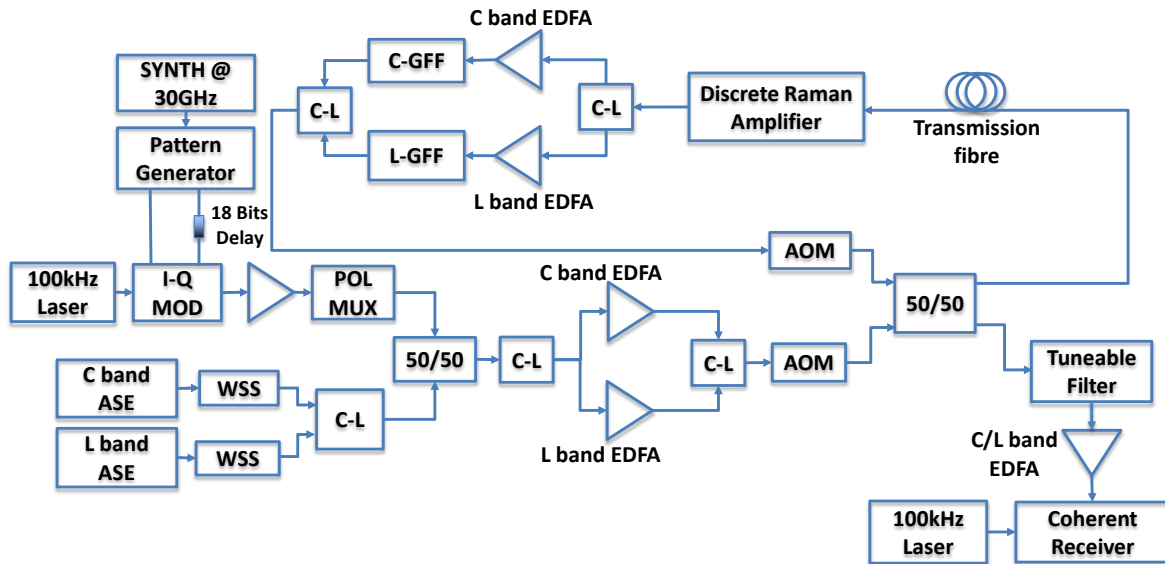
Figure 7. 39. Broadband transmission experiment setup in a recirculating loop with broadband discrete Raman amplifier in a single or dual stage configuration. Abbreviations: SYNTH = synthesizer, WSS = wavelength selective switch, AOM = acousto- optic modulator, GFF = gain flattening filter, POLMUX = polarisation multiplexer, MOD = modulator.

In Figure 7. 39, a broadband transmission experiment setup in a recirculating loop with discrete Raman amplifier in single or dual stage configuration is shown. In the transmitter, a narrowband (~100kHz linewidth) tuneable CW laser was modulated using IQ modulator to generate 120Gb/s DP-QPSK signal. The tuneable CW laser was used as the CUT. The 120Gb/s DP-QPSK modulated signal was then combined with spectrally shaped flat ASE noise generated from separate C and L band EDFAs. Two WSSs were used to generate 24 channels (12 channels per band) with 300GHz spacing over 70nm bandwidth from 1530nm to 1600nm. The broadband WDM input signal

198

consisting of 24 channels including a DP-QPSK modulated and 23 spectrally shaped channels were then applied into the loop through an AOM to synchronously control the loop switching along with another AOM in the loop as described in chapter 2. The input and output WDM signal after 20 recirculation in dual stage amplification scheme are shown in Figure 7. 40(a) and (b) respectively.
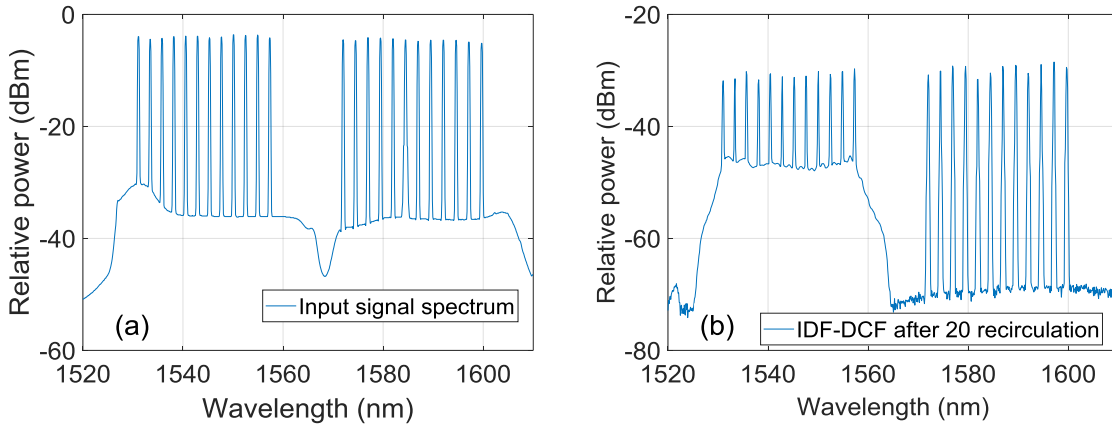
Figure 7. 40. (a) Input WDM signal into the loop and (b) output received spectrum after 20 recirculation in IDF 10km-DCF 4km dual stage discrete Raman amplifier configuration

The recirculating loop consisted of a transmission fibre based on SSMF followed by a single or dual stage discrete Raman amplifier. The single stage configuration included a 10km IDF fibre which was backward pumped by five 1st order pumps (1425, 1444nm, 1462, 1476, 1491nm) to obtain 14.5dB net gain to compensate the fibre loss of a 59km SSMF and passive component loss from input isolator and WDM. The dual stage discrete Raman amplifier consisted of a similar 1st stage preamplifier with 10km IDF, backward pumped by five 1st order pumps followed by a 2nd stage booster amplifier with low gain including a 4km DCF, also backward pumped by six 1st order pumps (1425, 1431, 1444nm, 1462, 1476, 1491nm). The dual stage design gave ~19.5dB average net gain and compensated for an 80km SSMF transmission span and passive component losses. The experimental setup of the dual stage discrete Raman amplifier is shown in Figure 7. 41.
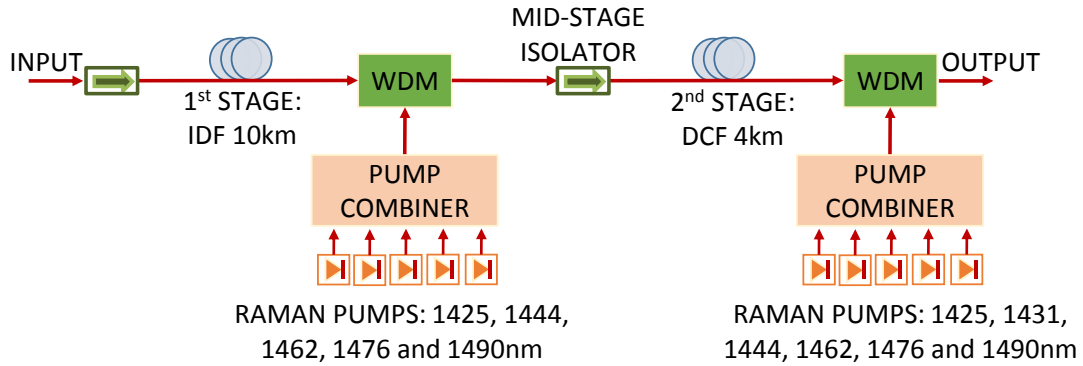
Figure 7. 41. Experimental design of a dual stage discrete Raman amplifier with IDF 10km and DCF 4km

At the receiver the signal is first filtered out using a narrowband tuneable band pass filter and then amplified before passing it to an optical front-end consisting of a polarisation diverse coherent receiver with 80GSa/s, 36GHz bandwidth oscilloscope. Transmission performance was characterized in terms of signal quality (Q factor) applying offline DSP.
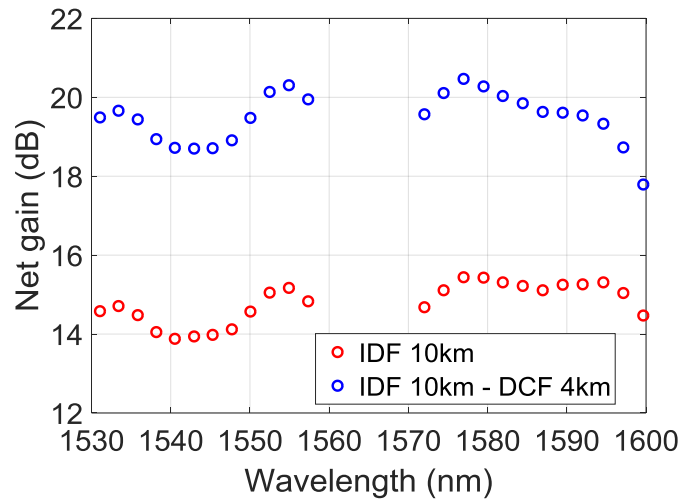
Figure 7. 42. Net gain comparison between single stage and dual stage discrete Raman amplifiers

The net gain performances of single and dual stage discrete Raman amplifiers are shown in Figure 7. 42. The average net gain of single and dual stage configuration were 14.5dB and 19.5 dB respectively with maximum 2dB gain variation across 70nm bandwidth. The 8~10nm gap between 1560 and 1570nm was due to the discontinuous bandwidth spectrum of C and L band EDFAs.
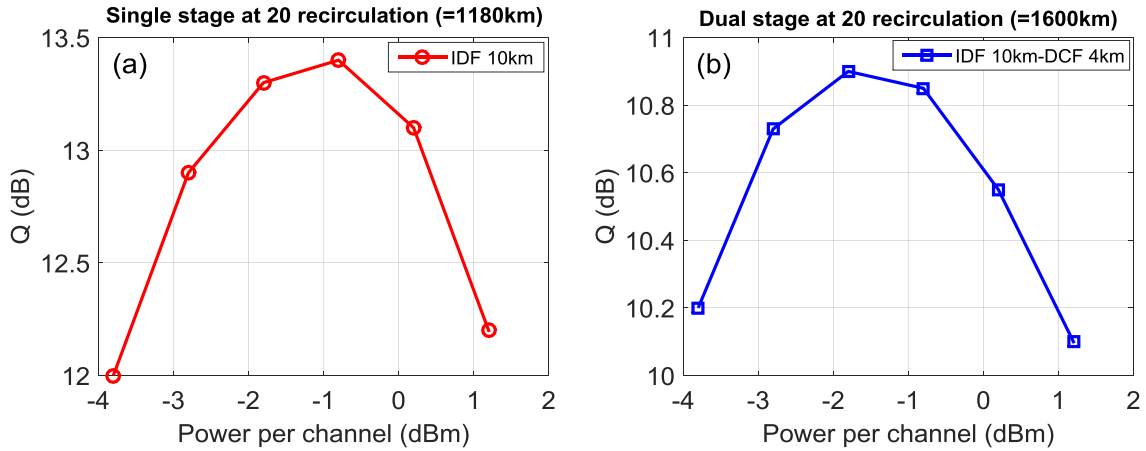
Figure 7. 43. Q factors vs. launch power per channel measured at 194THz signal in (a) single stage and (b) dual stage discrete Raman amplifier.

The Q factors vs. launch signal power per channel in single stage at 1180km and dual stage discrete Raman amplifier at 1600km are shown in Figure 7. 43(a) and Figure 7. 43(b) respectively. Although the Q factors were obtained after 20 recirculation, however total transmission distances were different due to different transmission span length of 59km and 80km for single and dual stage discrete Raman amplifier configuration respectively. In single stage configuration, the maximum Q factor at 1180km was measured as 13.4dB at optimum launch power per channel of -0.8dBm, whereas the optimum launch power obtained in case of dual stage configuration was 1dB lower at -1.8dBm because of additional nonlinear penalty from DCF 2nd stage. The maximum Q factor at optimum launch power was 10.9dB at 1600km in dual stage discrete Raman amplifier.
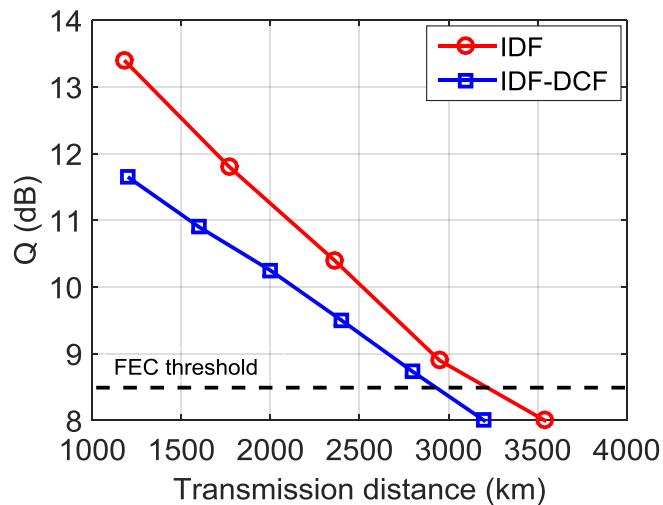
Figure 7. 44. Transmission reach comparison between single and dual stage discrete Raman amplifiers

The transmission reach comparison at corresponding optimum launch power between the IDF 10km based single stage and IDF 10km – DCF 4km based dual stage discrete Raman amplifiers is shown in Figure 7. 44. Single and dual stage discrete Raman amplifier compensate for 59km and 80km transmission span respectively. The Q performance degrades quite sharply with increasing number of recirculation. The dual stage discrete Raman amplifier shows lower Q values than that of single stage because of increased nonlinear penalty and noise figure as discussed in the simulation results of last section. At about 1200km transmission reach, dual stage configuration shows ~1.8dB Q factor penalty than that of single stage IDF based scheme. The slope of Q factor vs. transmission distances line for single stage configuration is much steeper than that of dual stage because it goes through more number of recirculation to obtain similar transmission distance as dual stage discrete Raman amplifier, which led to more accumulated amplifier noise, nonlinear penalties and also recirculating loop induced degradations. At the HD-FEC threshold of Q=8.5dB, the single stage discrete Raman amplifier shows only 250~300km additional transmission reach than dual stage scheme.

In the experimental characterisation, we were limited by different lengths of IDF and DCF. So it was not possible to try different lengths and Raman gain fibres to validate different amplifier configurations as shown through numerical simulation in the last section. In numerical simulation, we have shown that DCF 2nd stage based configuration performs worse than IDF or HNLF 2nd stage based configuration with equal 2nd stage gain contribution as shown in Figure 7. 37 and Figure 7. 38. So the performance of IDF 10km – DCF 4km based dual stage discrete Raman amplifier presented experimentally in this section can be further improved by using shorter length of IDF in the first stage and by replacing DCF with IDF or other Raman gain fibre with larger effective area and lower nonlinear coefficient.

7.4   Conclusions

In this chapter, we have shown the design of broadband distributed and discrete Raman amplifiers both numerically and experimentally. We propose an advanced design of broadband bidirectional distributed Raman amplification scheme in order to improve the noise figure tilt problem in conventional backward only pumping scheme without any additional signal RIN penalty from forward pumps. The benefits of the proposed bidirectional pumping scheme with proper choice of forward pump wavelengths have also been demonstrated through long-haul coherent WDM transmission experiment in a recirculating loop setup compared with other pumping schemes. A summary of transmission results are given below in Table 7. 8:

Table 7. 8. Summary of transmission results of broadband distributed Raman amplifiers

Pumping scheme	Scheme no.	Q factor @ 1845km (dB)	Maximum distance (km)
Backward only	1	12.4	5412
Forward pumping with only 2nd order pump	2	12.6	5658
Forward pumping with both 2nd order and 1st order (21mW) pumps (**proposed scheme**)	**3(a)**	**13.1**	**6150**
Forward pumping with both 2nd order and 1st order (49mW) pumps	3(b)	12.5	5412

Our proposed scheme-3(a) uses bidirectional pumping includes forward pumping with both 1365nm and 1425nm pumps at 216mW and 21mW powers respectively. It demonstrates a Q factor improvement of 0.7dB compared with conventional backward only scheme-1 enabling transmission reach enhancement of ~740km.

We have also shown design of high power, high gain dual stage discrete broadband Raman amplifier with improved noise and nonlinear performances by properly choosing the best combination of gain fibers (IDF, HNLF and DCF) in each stages. Through numerical characterisation of gain, noise and nonlinear performances, we have shown that a 70nm, dual stage discrete Raman amplifier with ~20dB net gain, >20dBm output power, ~6dB noise figure and lower nonlinear penalty can be designed by choosing HNLF 2km and IDF 6km as 1st and 2nd stage respectively within 300mW power per pump wavelength.

CHAPTER 8

CONCLUSIONS AND FUTURE WORKS

This thesis has investigated several aspects of the advanced design of Raman amplifiers including both distributed and discrete Raman amplifiers for high capacity and broadband long-haul transmission systems. Firstly, details on the numerical modelling of Raman amplifiers are presented with different amplifier characteristics such as: signal/noise power distribution, optical signal to noise ratio (OSNR), pump power requirement and so on. The performances of higher order pumped bidirectional distributed Raman amplifiers (DRAs) including ultra-long Raman fibre laser (URFL) based amplification techniques are also presented. Then improved designs of different bidirectional Raman fibre laser (RFL) based distributed Raman amplifiers (DRAs) have been explored experimentally for simultaneous reduction of amplifier spontaneous emission (ASE) noise and relative intensity noise (RIN) transfer from pump to signal. The RFL based DRAs presented here are consisted of 1365nm 2nd order pump(s) and 1st order pump(s) at 1455nm which has been created using the Rayleigh scattering in the fibre and feedback from FBGs placed at either end of the span. Experimental characterisation of signal or noise power distribution along the amplifier span, signal RIN and intra-cavity lasing mode structures are presented here for different span lengths in different lasing regimes: random distributed feedback (rDFB) laser, semi-rDFB type or weak Fabry-Perot lasing and Fabry-Perot based distributed cavity at different input reflection levels.

From the characterisation results, it has been reported that rDFB based DRA with backward pumping only configuration provides the highest signal power variation (SPV) giving worst ASE noise performance, however the signal RIN is minimum due to the absence of forward pump(s) propagating in the same direction of the signal. Inclusion of forward 1365nm pump improves the signal power distribution by increasing the forward gain contribution without increasing the signal RIN, however shows very poor pump conversion efficiency due to the lack of 1st order (1455nm) forward pump component at the absence of input FBG reflection. Pump power efficiency has been improved by including a very low input reflections from a weak input FBG or low Fresnel reflections (~3.4%) from a flat-cleaved FC-PC connector. However increase in the signal RIN level with the onset of weak Fabry-Perot lasing cavity along the amplifier span has been observed for

high forward pump power levels. Finally coherent transmission with DP-QPSK modulation formats has been carried out in a recirculating loop setup at different input reflection levels with increasing forward pump powers and it has been reported that in an 83km RFL based DRA, input reflection can be increased up to 10% and forward pump ratio of 21% can be used without any significant Q factor penalty.

We also experimentally demonstrated a novel signal RIN mitigation technique in bidirectional DRAs using a low RIN, broadband (~18nm) incoherent 1st order pump. In dual order forward pumped bidirectional DRA, the RIN from high power and noisy 2nd order pump (i.e. 1365nm) is distributed over the wide bandwidth of the broadband 1st order forward 1455nm pump which acts a seed with very low pump power (~20mW). The evolution of RIN is averaged out over the large bandwidth of this broadband source due to the non-degenerate four wave mixing process and subsequently transfer to the signal is also mitigated. The forward 1365nm pump power is also optimized for an 83km span DRA through long-haul coherent WDM transmission experiments in a recirculating loop setup. At optimum forward 1365nm pump power, a significant signal RIN reduction of more than 10dB is obtained compared with conventional low RIN and narrowband 1st order Raman pumps i.e. low RIN semiconductor pump. With improved OSNR and signal RIN performance, proposed dual order bidirectional pumped DRA can extend the reach of 10×120Gb/s DP-QPSK transmission system up to 7915km with 0.7dB Q factor improvement and 1250km transmission reach enhancement compared with low RIN, narrowband 1st order semiconductor pump.

Then a bidirectional DRA scheme using only the proposed broadband 1st order incoherent pump is also reported and the RIN and transmission performances are compared with other conventional narrowband 1st order sources. The maximum transmission reach up to 8332km is also reported using only 50mW of optimized 1st order broadband source as forward pump. The improved RIN performances allows transmission reach extensions of 1667km and 1250km compared with 1st order semiconductor forward pumped bidirectional DRA and backward only pumping respectively.

As any backward pumped distributed Raman amplification scheme is still the popular choice in terms of cost and energy efficiency in long-haul transmission system, we also report significant transmission performance improvement with the proposed broadband 1st order pump in backward dual order pumping configuration. Similar transmission reach (7915km) of dual order bidirectional pumped DRA including broadband 1st order pump has been achieved even with the proposed dual order backward pumped configuration without requiring additional forward pump sources.

Additional transmission reach of ~830km has been obtained compared with conventional backward pumping schemes with narrowband sources.

In this thesis, we have demonstrated how to design distributed Raman amplifiers with better SNR performance and minimum signal RIN penalty. We have shown an efficient design of broadband first order pump in order to be used in improved design of different higher order pumping configurations including RIN mitigated bidirectional pumping and simple backward only pumping. Now the only question can be, are these advanced DRA scheme going to be implemented in the next generation long-haul WDM coherent transmission systems? Due to the fact that, the generation of broadband 1st order pump requires an additional 2nd order 1365nm pump with high pump power (3~4W), which increases the cost and complexity of system design, our proposed DRA schemes may not be a preferred choice for service providers in next few years. However as modern high capacity transmission systems are going towards higher order modulation formats which require high SNR, our proposed bidirectional DRA schemes would definitely be one of the better solutions.

Then, a detail numerical and experimental design of broadband distributed and discrete Raman amplifiers combining multiple first order pumps is also reported in this thesis. In multi-pump broadband Raman amplifier there is a fundamental problem of high noise figure tilt due to high noise figure of low wavelength signals due to being close to the longer wavelength pumps. In order to reduce the noise figure tilt, we propose a novel dual order forward pumping scheme with a proper choice of forward pump wavelengths. In a 70nm wide (1530-1600nm) bidirectional DRA with 61.5km standard single mode fibre (SSMF) and four first order backward pumps, our proposed forward pumping with 1365nm and 1425nm 2nd and 1st order pump respectively improves the noise figure of the lowest signal wavelength by 1.2dB without any signal RIN penalty. The resultant improvement of noise performance shows better transmission performance of a 13×120Gb/s DP-QPSK system with 738km extended reach and 0.7dB improved Q factor compared with conventional backward only pumping.

Finally we also propose a dual-stage design of broadband discrete Raman amplifier with high gain (~19dB), high output power (~20dBm), low noise and low nonlinearity penalties. We numerically compare the performances (net gain, noise figure, nonlinear phase shift) of three different types of commonly used Raman gain fibres: highly nonlinear fibre (HNLF), dispersion compensating fibre (DCF) and inverse dispersion fibre (IDF) with varying lengths in different single and dual stage combinations. We demonstrate an optimum combination of HNLF 2km and IDF 6km in 1st stage

and 2nd stage respectively of a dual stage discrete Raman amplifier, which gives ~6dB noise figure, lowest possible nonlinear phase shift with respect to other gain fibre combinations.

Although the broadband amplifier design has been restricted in this thesis mainly in C and L band, however in principle Raman gain bandwidth can be achieved in any wavelength band provided that appropriate pumps are available with low enough fibre attenuation coefficients in that specific band. Proper Raman gain fibre with zero dispersion wavelength being outside of pump and signal band is required in order to avoid additional nonlinear penalties. Additional band splitting and combining are also required when amplification bandwidth extends beyond one Stokes shift (~13THz) to separate pump and signals remaining in the same wavelength band. So sub-band discrete Raman amplifiers can be designed in different spectral bands and combined using band combiners to get wideband gain bandwidth (i.e. 300nm) at the cost of lossy passive components.

8.1   Future Works

Distributed Raman amplification is the potential choice of future amplification technique in long-haul repeatered transmission systems due to the benefits of superior noise performance and wideband application in the low loss window of the transmission fibre. In Raman fibre laser based amplification, the amplification bandwidth can be increased up to 65~70nm covering C+L band by using multiple FBGs at 14xx wavelengths or by adding two extra 1st order seeds one in low wavelength (~1425nm) and other in higher wavelength (~1480nm). But the real problem of using multiple passive FBGs is the requirement of very high 2nd order 1365nm pump power due to the gain competition among the 14xx 1st order pumps. So better design is required to extend the bandwidth of higher order distributed Raman amplifiers. So far the design of RFL based DRA schemes have been limited to conventional C band application. With proper development of Raman pump lasers and efficient FBGs at specific wavelengths, RFL based DRA can also be designed at other wavelength bands.

Our proposed broadband (> 10nm, centred at 1450nm) and low RIN first order seed can replace multiple first order seeds and has the capability of extending the amplification bandwidth with proper design. One of the main issues of designing broadband incoherent first order pump is the requirement of high power 2nd order pump and a separate fibre section. In future, the design of broadband and incoherent semiconductor pump with reasonable high output power may improve the cost and power efficiency and increase the possibility in real system implementation.

Further optimization of amplifier span length in RFL based DRA is required for perfectly symmetric and quasi-lossless power profiles to be applied in mid-link optical phase conjugation (OPC) and Raman amplified nonlinear Fourier transform (NFT) based transmission system design respectively. While many techniques have been presented for the OPC applications, however more works needs to be done for wideband OPC and the Raman amplified NFT based systems. Improved design on the symmetry of signal power profiles over wide bandwidth is essential for broadband OPC system. Our novel design of broadband, low RIN 1st order pump can be used in bidirectional pumping configuration to obtain quasi-lossless signal transmission required for NFT based system.

Our proposed bidirectional broadband DRA scheme with improved noise figure performance can also be used for unrepeatered transmission systems. Further improved design can also be focused on broadband transmission with or without inline remotely pumped optical amplifier (ROPA) for the design of high-capacity unrepeatered transmission system with extended reach.

Finally, we have proposed high gain and high output power, low noise and low nonlinearity dual stage discrete Raman amplifier including highly nonlinear fibre (HNLF) and inverse dispersion fibre (IDF). However proper choice of HNLF with zero dispersion wavelength far away from the signal and pump bands is required to avoid increased four wave mixing induced nonlinearities. Further design improvement can be done for even high output power discrete Raman amplifier by adding more stages, however the nonlinear performance has to be optimized by choosing right fibre types. These improved broadband discrete amplifiers will be used in high capacity metro DWDM transmission systems.

Ultra-wideband Raman amplifiers covering the low loss window of silica fibre (1300~1650nm) can be designed combing sub-band amplifiers or by using pump and signal in different guard bands. The challenges include designing proper filtering methods between the sub-bands and also tackling the Raman power transfer from lower wavelength to higher wavelength effects in the later guard band approach. Moreover, the Raman gain tilt associated with Raman power transfer introduces additional nonlinear crosstalk which limits the transmission performance. So additional care has to be given in wideband amplifier design. All the above discussed scopes need proper research methodologies and efforts which are out of the scope of this thesis.

REFERENCES

[1]   F. Kapron, D. Keck, and R. Maurer, "Radiation losses in glass optical waveguides," *Applied Physics Letters,* vol. 17, pp. 423-425, 1970.

[2]   I. Hayashi, M. Panish, P. Foy, and S. Sumski, "Junction lasers which operate continuously at room temperature," *Applied Physics Letters,* vol. 17, pp. 109-111, 1970.

[3]   G. P. Agrawal, *Fiber-optic communication systems* vol. 222: John Wiley & Sons, 2012.

[4]   A. D. Ellis, N. M. Suibhne, D. Saad, and D. N. Payne, "Communication networks beyond the capacity crunch," *Philosophical Transactions. Series A, Mathematical, Physical, and Engineering Sciences,* vol. 374, p. 20150191, 2016.

[5]   R.-J. Essiambre, G. Kramer, P. J. Winzer, G. J. Foschini, and B. Goebel, "Capacity limits of optical fiber networks," *Journal of Lightwave Technology,* vol. 28, pp. 662-701, 2010.

[6]   P. Bayvel, R. Maher, T. Xu, G. Liga, N. A. Shevchenko, D. Lavery*, et al.*, "Maximizing the optical network capacity," *Philosophical Transactions of the Royal Society A: Mathematical, Physical and Engineering Sciences,* vol. 374, 2016.

[7]   R.-J. Essiambre and R. W. Tkach, "Capacity trends and limits of optical communication networks," *Proceedings of the IEEE,* vol. 100, pp. 1035-1055, 2012.

[8]   S. Kumar, *Impact of nonlinearities on fiber optic communications* vol. 7: Springer Science & Business Media, 2011.

[9]   S. Beppu, K. Kasai, M. Yoshida, and M. Nakazawa, "2048 QAM (66 Gbit/s) single-carrier coherent optical transmission over 150 km with a potential SE of 15.3 bit/s/Hz," *Optics Express,* vol. 23, pp. 4960-4969, 2015.

[10]   R. W. Tkach, "Scaling optical communications for the next decade and beyond," *Bell Labs Technical Journal,* vol. 14, pp. 3-9, 2010.

[11]   J. D. Downie, "High-capacity long-haul transmission using ultra-low loss optical fiber," in *17th Opto-Electronics and Communications Conference (OECC)* 2012, pp. 172-173.

[12]   D.-i. Chang, B. Clesca, S. Makovejs, and I. Davis, "Ultra-low loss fiber and advanced Raman amplification deliver record unrepeatered 100G transmission " presented at the SubOptic 2016, Dubai, UAE, 2016.

[13]   Y. Hadjar, N. Traynor, and S. Gray, "Noise figure tilt reduction in ultrawide-band WDM through second-order Raman amplification," *IEEE Photonics Technology Letters,* vol. 16, pp. 1200-1202, 2004.

[14]   M. Tan, P. Rosa, S. T. Le, I. D. Phillips, and P. Harper, "Evaluation of 100G DP-QPSK long-haul transmission performance using second order co-pumped Raman laser based amplification," *Optics Express,* vol. 23, pp. 22181-22189, 2015.

[15]   J. D. Ania-Castañón, "Quasi-lossless transmission using second-order Raman amplification and fibre Bragg gratings," *Optics Express,* vol. 12, pp. 4372-4377, 2004.

[16]   J.-X. Cai, H. G. Batshon, M. Mazurczyk, O. V. Sinkin, D. Wang, M. Paskov*, et al.*, "70.4 Tb/s capacity over 7,600 km in C+ L band using coded modulation with hybrid constellation shaping and nonlinearity compensation," in *Optical Fiber Communication Conference*, 2017, p. Th5B. 2.

[17]   L. E. Nelson, X. Zhou, B. Zhu, M. F. Yan, P. W. Wisk, and P. D. Magill, "All-Raman-amplified, 73 nm seamless band transmission of 9 Tb/s over 6000 km of fiber," *IEEE Photonics Technology Letters,* vol. 26, pp. 242-245, 2014.

[18]   A. Ghazisaeidi, "Coherent WDM Systems Using in-Line Semiconductor Optical Amplifiers," *arXiv preprint arXiv:1711.06108,* 2017.

[19]   D. Soma, Y. Wakayama, S. Beppu, S. Sumita, T. Tsuritani, T. Hayashi*, et al.*, "10.16 Peta-bit/s Dense SDM/WDM transmission over Low-DMD 6-Mode 19-Core Fibre across C+L

Band," in *43rd European Conference on Optical Communication*, Gothenburg, Sweden, 2017, p. Th.PDP.A.1.

[20] M. Tan, "Raman fibre laser based amplification in coherent transmission systems," Doctor of Philosophy, Aston University, Birmingham, UK, 2016.

[21] M. Tan, P. Rosa, S. T. Le, M. A. Iqbal, I. D. Phillips, and P. Harper, "Transmission performance improvement using random DFB laser based Raman amplification and bidirectional second-order pumping," *Optics Express,* vol. 24, pp. 2215-2221, 2016.

[22] C. R. S. Fludger, V. Handerek, and R. J. Mears, "Pump to signal RIN transfer in Raman fiber amplifiers," *Journal of Lightwave Technology,* vol. 19, pp. 1140-1148, Aug 2001.

[23] J. Ma, C. Jiang, and J. Wu, "Optimal design of ultrabroadband tellurite fiber Raman amplifier for wavelength-division multiplexing transmission systems," *Optical Engineering,* vol. 47, pp. 045007-0450075, 2008.

[24] H. J. Thiele, J. Bromage, and L. Nelson, "Impact of discrete Raman amplifier architecture on nonlinear impairments," in *28th European Conference on Optical Communication*, 2002, pp. 1-2.

[25] R.-J. Essiambre, P. Winzer, J. Bromage, and C. H. Kim, "Design of bidirectionally pumped fiber amplifiers generating double Rayleigh backscattering," *IEEE Photonics Technology Letters,* vol. 14, pp. 914-916, 2002.

[26] M. Seimetz, *High-order modulation for optical fiber transmission* vol. 143: Springer, 2009.

[27] S. Shimotsu, S. Oikawa, T. Saitou, N. Mitsugi, K. Kubodera, T. Kawanishi, *et al.*, "Single side-band modulation performance of a LiNbO 3 integrated modulator consisting of four-phase modulator waveguides," *IEEE Photonics Technology Letters,* vol. 13, pp. 364-366, 2001.

[28] Coherent WDM Technologies [Online]. Available: https://www.infinera.com/wp-content/uploads/2015/07/Infinera_Coherent_Tech.pdf

[29] K. Kikuchi, "Fundamentals of coherent optical fiber communications," *Journal of Lightwave Technology,* vol. 34, pp. 157-179, 2016.

[30] M. S. Faruk and S. J. Savory, "Digital Signal Processing for Coherent Transceivers Employing Multilevel Formats," *Journal of Lightwave Technology,* vol. 35, pp. 1125-1141, 2017.

[31] R.-M. Mu, V. Grigoryan, C. R. Menyuk, G. Carter, and J. Jacob, "Comparison of theory and experiment for dispersion-managed solitons in a recirculating fiber loop," *IEEE Journal of Selected Topics in Quantum Electronics,* vol. 6, pp. 248-257, 2000.

[32] P. Harper, "Long distance disperison managed soliton transmission experiments," Doctor of Philosophy, Aston University, Birmingham, UK, 1997.

[33] N. S. Bergano and C. R. Davidson, "Circulating loop transmission experiments for the study of long-haul transmission systems using erbium-doped fiber amplifiers," *Journal of Lightwave Technology,* vol. 13, pp. 879-888, 1995.

[34] G. Saavedra, M. Tan, D. J. Elson, L. Galdino, D. Semrau, M. A. Iqbal, *et al.*, "Experimental Analysis of Nonlinear Impairments in Fibre Optic Transmission Systems up to 7.3 THz," *Journal of Lightwave Technology,* vol. 35, pp. 4809-4816, 2017.

[35] R. Hui and M. O'Sullivan, *Fiber optic measurement techniques*: Academic Press, 2009.

[36] M. Taylor, "Observation of new polarisation dependence effect in long haul optically amplified system," *IEEE PhotonicsTechnology Letters,* vol. 5, pp. 1244-1246, 1993.

[37] Q. Yu, L. S. Yan, S. Lee, Y. Xie, and A. E. Willner, "Loop-synchronous polarisation scrambling technique for simulating polarisation effects using recirculating fiber loops," *Journal of Lightwave Technology,* vol. 21, pp. 1593-1600, 2003.

[38] S. Jansen, D. Van Den Borne, P. Krummrich, S. Spalter, G.-D. Khoe, and H. De Waardt, "Long-haul DWDM transmission systems employing optical phase conjugation," *IEEE Journal of Selected Topics in Quantum Electronics,* vol. 12, pp. 505-520, 2006.

[39] G. P. Agrawal, *Nonlinear fiber optics*: Academic Press, 2007.

[40] P. Rosa, "Quasi-lossless data transmission with ultra-long Raman fibre laser based amplification," Doctor of Philosophy, Aston University, 2014.

[41] G. P. Agrawal, *Lightwave technology: telecommunication systems*: John Wiley & Sons, 2005.

[42] S. J. Savory, "Digital filters for coherent optical receivers," *Optics Express,* vol. 16, pp. 804-817, 2008.

[43] J. Mårtensson, A. Berntson, M. Westlund, A. Danielsson, P. Johannisson, D. Anderson*, et al.*, "Timing jitter owing to intrachannel pulse interactions in dispersion-managed transmission systems," *Optics Letters,* vol. 26, pp. 55-57, 2001.

[44] M. Eiselt, M. Shtaif, and L. D. Garrett, "Contribution of timing jitter and amplitude distortion to XPM system penalty in WDM systems," *IEEE Photonics Technology Letters,* vol. 11, pp. 748-750, 1999.

[45] D. S. Millar, S. Makovejs, C. Behrens, S. Hellerbrand, R. I. Killey, P. Bayvel*, et al.*, "Mitigation of fiber nonlinearity using a digital coherent receiver," *IEEE Journal of Selected Topics in Quantum Electronics,* vol. 16, pp. 1217-1226, 2010.

[46] L. B. Du and A. J. Lowery, "Improved single channel backpropagation for intra-channel fiber nonlinearity compensation in long-haul optical communication systems," *Optics Express,* vol. 18, pp. 17075-17088, 2010.

[47] A. Ellis, M. McCarthy, M. Al-Khateeb, and S. Sygletos, "Capacity limits of systems employing multiple optical phase conjugators," *Optics Express,* vol. 23, pp. 20381-20393, 2015.

[48] A. D. Ellis, M. E. McCarthy, M. A. Z. Al Khateeb, M. Sorokina, and N. J. Doran, "Performance limits in optical communications due to fiber nonlinearity," *Advances in Optics and Photonics,* vol. 9, pp. 429-503, 2017.

[49] S. Makovejs, "High-speed optical fibre transmission using advanced modulation formats," Doctor of Philosophy, UCL (University College London), 2011.

[50] R. A. Shafik, M. S. Rahman, and A. R. Islam, "On the Extended Relationships Among EVM, BER and SNR as Performance Metrics," in *International Conference on Electrical and Computer Engineering*, 2006, pp. 408-411.

[51] B. Nebendahl, R. Schmogrow, T. Dennis, A. Josten, D. Hillerkuss, S. Koenig*, et al.*, "Quality metrics in optical modulation analysis: EVM and its relation to Q-factor, OSNR, and BER," in *Communications and Photonics Conference (ACP), 2012 Asia*, 2012, pp. 1-3.

[52] A. Bjarklev, *Optical Fiber Amplifiers: Design and System Applications*: Artech House, 1993.

[53] J.-M. Delavaux and J. Nagel, "Multi-stage erbium-doped fiber amplifier designs," *Journal of Lightwave Technology,* vol. 13, pp. 703-720, 1995.

[54] P. F. Wysocki, J. B. Judkins, R. P. Espindola, M. Andrejco, and A. M. Vengsarkar, "Broad-band erbium-doped fiber amplifier flattened beyond 40 nm using long-period grating filter," *IEEE Photonics Technology Letters,* vol. 9, pp. 1343-1345, 1997.

[55] P. F. Wysocki, N. Park, and D. DiGiovanni, "Dual-stage erbium-doped, erbium/ytterbium-codoped fiber amplifier with up to +26-dBm output power and a 17-nm flat spectrum," *Optics Letters,* vol. 21, pp. 1744-1746, 1996.

[56] B. T. Teipen and M. H. Eiselt, "107Gb/s DPSK-3ASK optical transmission over SSMF," in *Conference on Optical Fiber Communication (OFC), Collocated National Fiber Optic Engineers Conference (OFC/NFOEC)*, 2010, pp. 1-3.

[57] H. Chung, M. Lee, D. Lee, N. Park, and D. DiGiovanni, "Low noise, high efficiency L-band EDFA with 980 nm pumping," *Electronics Letters,* vol. 35, pp. 1099-1100, 1999.

[58] Y. Sun, J. W. Sulhoff, A. K. Srivastava, J. L. Zyskind, C. Wolf, T. Strasser*, et al.*, "An 80 nm ultra wide band EDFA with low noise figure and high output power," in *Integrated Optics and Optical Fibre Communications, 11th International Conference on, and 23rd European Conference on Optical Communications (Conf. Publ. No.: 448)*, 1997, pp. 69-72.

[59]   R. Olshansky, "Noise figure for erbium-doped optical fibre amplifiers," *Electronics Letters,* vol. 24, pp. 1363-1365, 1988.

[60]   Y. Miyajima, T. Komukai, T. Sugawa, and T. Yamamoto, "Rare earth-doped fluoride fiber amplifiers and fiber lasers," *Optical Fiber Technology,* vol. 1, pp. 35-47, 1994.

[61]   P. Morkel and R. I. Laming, "Theoretical modeling of erbium-doped fiber amplifiers with excited-state absorption," *Optics Letters,* vol. 14, pp. 1062-1064, 1989.

[62]   C. R. Giles and E. Desurvire, "Modeling erbium-doped fiber amplifiers," *Journal of Lightwave Technology,* vol. 9, pp. 271-283, 1991.

[63]   P. M. Becker, A. A. Olsson, and J. R. Simpson, *Erbium-doped fiber amplifiers: fundamentals and technology*: Academic Press, 1999.

[64]   I. A. Bufetov, M. A. Melkumov, S. V. Firstov, K. E. Riumkin, A. V. Shubin, V. F. Khopin*, et al.*, "Bi-doped optical fibers and fiber lasers," *IEEE Journal of Selected Topics in Quantum Electronics,* vol. 20, pp. 111-125, 2014.

[65]   S. Firstov, S. Alyshev, M. Melkumov, K. Riumkin, A. Shubin, and E. Dianov, "Bismuth-doped optical fibers and fiber lasers for a spectral region of 1600–1800 nm," *Optics Letters,* vol. 39, pp. 6927-6930, 2014.

[66]   N. Thipparapu, A. Umnikov, P. Barua, and J. Sahu, "Bi-doped fiber amplifier with a flat gain of 25 dB operating in the wavelength band 1320–1360 nm," *Optics Letters,* vol. 41, pp. 1518-1521, 2016.

[67]   J. K. Sahu, N. Thipparapu, A. Umnikov, P. Barua, and M. N. Velazquez, "Amplifier and laser demonstrations in Bi-doped silica optical fibers," in *International Conference on Fibre Optics and Photonics*, 2016, p. Tu2A. 2.

[68]   Z. Li, Y.-m. Jung, J. M. O. daniel, N. Simakov, P. C. Shardlow, A. M. Heidt*, et al.*, "Extreme Short Wavelength Operation (1.65 - 1.7 µm) of Silica-Based Thulium-Doped Fiber Amplifier," in *Optical Fiber Communication Conference*, Los Angeles, California, 2015, p. Tu2C.1.

[69]   Z. Li, S. U. Alam, J. M. O. Daniel, P. C. Shardlow, D. Jain, N. Simakov*, et al.*, "90 nm gain extension towards 1.7 µm for diode-pumped silica-based thulium-doped fiber amplifiers," in *The European Conference on Optical Communication (ECOC)*, 2014, pp. 1-3.

[70]   Z. Li, A. M. Heidt, N. Simakov, Y. Jung, J. M. O. Daniel, S. U. Alam*, et al.*, "Diode-pumped wideband thulium-doped fiber amplifiers for optical communications in the 1800 – 2050 nm window," *Optics Express,* vol. 21, pp. 26450-26455, 2013.

[71]   S. D. Agger and J. H. Povlsen, "Emission and absorption cross section of thulium doped silica fibers," *Optics Express,* vol. 14, pp. 50-57, 2006.

[72]   N. Simakov, Z. Li, S.-U. Alam, P. C. Shardlow, J. M. O. daniel, D. Jain*, et al.*, "Holmium Doped Fiber Amplifier for Optical Communications at 2.05 - 2.13 µm," in *Optical Fiber Communication Conference*, Los Angeles, California, 2015, p. Tu2C.6.

[73]   N. Simakov, Z. Li, Y. Jung, J. M. Daniel, P. Barua, P. C. Shardlow*, et al.*, "High gain holmium-doped fibre amplifiers," *Optics Express,* vol. 24, pp. 13946-13956, 2016.

[74]   T. Ivaniga and P. Ivaniga, "Comparison of the Optical Amplifiers EDFA and SOA Based on the BER and-Factor in C-Band," *Advances in Optical Technologies,* vol. 2017, 2017.

[75]   M. J. Connelly, "Wideband semiconductor optical amplifier steady-state numerical model," *IEEE Journal of Quantum Electronics,* vol. 37, pp. 439-447, 2001.

[76]   M. G. Oberg and N. A. Olsson, "Crosstalk between intensity-modulated wavelength-division multiplexed signals in a semiconductor laser amplifier," *IEEE Journal of Quantum Electronics,* vol. 24, pp. 52-59, 1988.

[77]   A. Elrefaie and C. Lin, "Performance degradations of multigigabit-per-second NRZ/RZ lightwave systems due to gain saturation in traveling-wave semiconductor optical amplifiers," *IEEE Photonics Technology Letters,* vol. 1, pp. 300-303, 1989.

[78]   P. Doussiere, F. Pommereau, J. Y. Emery, R. Ngo, J. L. Lafragette, P. Aubert, *et al.*, "1550 nm polarisation independent DBR gain clamped SOA with high dynamic input power range," in *Proceedings of European Conference on Optical Communication*, 1996, pp. 169-172 vol.3.

[79]   J. Sun, G. Morthier, and R. Baets, "Numerical and theoretical study of the crosstalk in gain clamped semiconductor optical amplifiers," *IEEE Journal of Selected Topics in Quantum Electronics,* vol. 3, pp. 1162-1167, 1997.

[80]   D. Schaafsma and E. Bradley, "Cross-gain modulation and frequency conversion crosstalk effects in 1550-nm gain-clamped semiconductor optical amplifiers," *IEEE Photonics Technology Letters,* vol. 11, pp. 727-729, 1999.

[81]   E. Tangdiongga, J. Crijns, L. Spiekman, G. Van den Hoven, and H. De Waardt, "Performance analysis of linear optical amplifiers in dynamic WDM systems," *IEEE Photonics Technology Letters,* vol. 14, pp. 1196-1198, 2002.

[82]   M. Itoh, Y. Shibata, T. Kakitsuka, Y. Kadota, and Y. Tohmori, "Polarisation-insensitive SOA with a strained bulk active layer for network device application," *IEEE Photonics Technology Letters,* vol. 14, pp. 765-767, 2002.

[83]   K. Morito, M. Ekawa, T. Watanabe, and Y. Kotaki, "High-output-power polarisation-insensitive semiconductor optical amplifier," *Journal of Lightwave Technology,* vol. 21, pp. 176-181, 2003.

[84]   K. Stubkjær, B. Mikkelsen, T. Djurhuus, N. Storkfelt, C. Jørgensen, K. S. Jepsen, *et al.*, "Recent advances in semiconductor optical amplifiers and their applications," in *Fourth International Conference on Indium Phosphide and Related Materials*, 1992, pp. 242-245.

[85]   P. A. Andrekson, P. Petropoulos, S. Radic, C. Peucheret, and M. Jazayerifar, "Fiber optical parametric amplifiers in optical communication systems," *Laser & Photonics Reviews,* vol. 9, pp. 50-74, 2015.

[86]   M. E. Marhic, N. Kagi, T. K. Chiang, and L. G. Kazovsky, "Broadband fiber optical parametric amplifiers," *Optics Letters,* vol. 21, pp. 573-575, 1996.

[87]   J. Hansryd, P. A. Andrekson, M. Westlund, J. Li, and P.-O. Hedekvist, "Fiber-based optical parametric amplifiers and their applications," *IEEE Journal of Selected Topics in Quantum Electronics,* vol. 8, pp. 506-520, 2002.

[88]   C. M. Caves, "Quantum limits on noise in linear amplifiers," *Physical Review D,* vol. 26, p. 1817, 1982.

[89]   P. A. Andrekson, C. Lundström, and Z. Tong, "Phase-sensitive fiber-optic parametric amplifiers and their applications," in *36th European Conference and Exhibition on Optical Communication*, 2010, pp. 1-6.

[90]   J. A. Levenson, I. Abram, T. Rivera, and P. Grangier, "Reduction of quantum noise in optical parametric amplification," *JOSA B,* vol. 10, pp. 2233-2238, 1993.

[91]   M.-C. Ho, K. Uesaka, M. Marhic, Y. Akasaka, and L. G. Kazovsky, "200-nm-bandwidth fiber optical amplifier combining parametric and Raman gain," *Journal of Lightwave Technology,* vol. 19, p. 977, 2001.

[92]   B. P. P. Kuo, J. M. Fini, L. Grüner-Nielsen, and S. Radic, "Dispersion-stabilized highly-nonlinear fiber for wideband parametric mixer synthesis," *Optics Express,* vol. 20, pp. 18611-18619, 2012.

[93]   I. Sackey, M. Jazayerifar, R. Elschner, T. Richter, C. Meuer, K. Petermann, *et al.*, "Non-reciprocal gain due to counter-propagating pumps in a polarisation-independent FOPA with diversity loop," in *European Conference on Optical Communication (ECOC)*, 2015, pp. 1-3.

[94]   F. Yaman, Q. Lin, and G. P. Agrawal, "A Novel Design for Polarisation-Independent Single-Pump Fiber-Optic Parametric Amplifiers," *IEEE Photonics Technology Letters,* vol. 18, pp. 2335-2337, 2006.

[95]   S. Takasaka and R. Sugizaki, "Polarisation Insensitive Fiber Optical Parametric Amplifier Using a SBS Suppressed Diversity Loop," in *Optical Fiber Communication Conference*, Anaheim, California, 2016, p. M3D.4.

[96]   V. Gordienko, M. F. C. Stephens, A. E. El-Taher, and N. J. Doran, "Ultra-flat wideband single-pump Raman-enhanced parametric amplification," *Optics Express,* vol. 25, pp. 4810-4818, 2017.

[97]   V. Gordienko, M. Stephens, and N. Doran, "Towards wide-bandwidth ultra-flat FOPAs," in *19th International Conference on Transparent Optical Networks (ICTON)*, 2017, pp. 1-4.

[98]   C. Headley and G. P. Agrawal, "Chapter 1 - Introduction," in *Raman Amplification in Fiber Optical Communication Systems*, ed Burlington: Academic Press, 2005, pp. 1-31.

[99]   Y. Emori, S. Kado, and S. Namiki, "Broadband flat-gain and low-noise Raman amplifiers pumped by wavelength-multiplexed high-power laser diodes," *Optical Fiber Technology,* vol. 8, pp. 107-122, 2002.

[100]   R. Stolen, "Fundamentals of Raman amplification in fibers," in *Raman Amplifiers for Telecommunications 1*, ed: Springer, 2004, pp. 35-59.

[101]   G. P. Agrawal, "Chapter 2 - Theory of Raman Amplifiers," in *Raman Amplification in Fiber Optical Communication Systems*, ed Burlington: Academic Press, 2005, pp. 33-102.

[102]   L. F. Mollenauer, M. Islam, and R. Stolen, "Experimental demonstration of soliton propagation in long fibers: loss compensated by Raman gain," *Optics Letters,* vol. 10, pp. 229-231, 1985.

[103]   P. Hansen, L. Eskildsen, S. Grubb, A. Vengsarkar, S. Korotky, T. Strasser, *et al.*, "442 km repeaterless transmission in a 10 Gbit/s system experiment," *Electronics Letters,* vol. 32, pp. 1018-1019, 1996.

[104]   T. Nielsen, A. Stentz, K. Rottwitt, D. Vengsarkar, Z. Chen, P. Hansen, *et al.*, "3.28-Tb/s transmission over 3 x 100 km of nonzero-dispersion fiber using dual C-and L-band distributed Raman amplification," *IEEE Photonics Technology Letters,* vol. 12, pp. 1079-1081, 2000.

[105]   K. Rottwitt and H. D. Kidorf, "A 92 nm bandwidth Raman amplifier," in *Optical Fiber Communication Conference*, 1998, p. PD6.

[106]   Y. Emori and S. Namiki, "100nm bandwidth flat gain Raman amplifiers pumped and gain-equalized by 12-wavelength-channel WDM high power laser diodes," in *Wavelength Division Multiplexing Components*, 1999, p. 177.

[107]   H. Bissessur, "State of the art in non repeated optical transmission," in *37th European Conference and Exhibition on Optical Communication*, 2011, pp. 1-3.

[108]   H. Bissessur, P. Bousselet, D. Mongardien, and I. Brylski, "Ultra-long 10 Gb/s Unrepeatered WDM Transmission up to 601 km," in *Optical Fiber Communication Conference*, 2010, p. OTuD6.

[109]   S. K. Turitsyn, J. D. Ania-Castañón, S. Babin, V. Karalekas, P. Harper, D. Churkin, *et al.*, "270-km ultralong Raman fiber laser," *Physical Review Letters,* vol. 103, p. 133901, 2009.

[110]   M. Takahashi, R. Sugizaki, J. Hiroishi, M. Tadakuma, Y. Taniguchi, and T. Yagi, "Low-loss and low-dispersion-slope highly nonlinear fibers," *Journal of Lightwave Technology,* vol. 23, pp. 3615-3624, 2005.

[111]   L. Grüner-Nielsen and Y. Qian, "Dispersion-compensating fibers for Raman applications," in *Raman Amplifiers for Telecommunications 1*, ed: Springer, 2004, pp. 161-189.

[112]   P. B. Hansen, G. Jacobovitz-Veselka, L. Gruner-Nielsen, and A. Stentz, "Loss compensation in dispersion compensation fiber modules by Raman amplification," in *Optical Fiber Communication Conference and Exhibit, 1998. OFC'98., Technical Digest*, 1998, pp. 20-21.

[113] T. Miyamoto, M. Tanaka, J. Kobayashi, T. Tsuzaki, M. Hirano, T. Okuno, *et al.*, "Highly nonlinear fiber-based lumped fiber Raman amplifier for CWDM transmission systems," *Journal of Lightwave Technology,* vol. 23, p. 3475, 2005.

[114] Y. Emori, Y. Akasaka, and S. Namiki, "Broadband lossless DCF using Raman amplification pumped by multichannel WDM laser diodes," *Electronics Letters,* vol. 34, pp. 2145-2146, 1998.

[115] A. Gnauck, G. Raybon, S. Chandrasekhar, J. Leuthold, C. Doerr, L. Stulz, *et al.*, "2.5 Tb/s (64x42. 7 Gb/s) transmission over 40x100 km NZDSF using RZ-DPSK format and all-Raman-amplified spans," in *Optical Fiber Communication Conference*, 2002, p. FC2.

[116] B. Zhu, L. Leng, L. Nelson, L. Gruner-Nielsen, Y. Qian, J. Bromage, *et al.*, "3.2 Tb/s (80 x 42.7 Gb/s) transmission over 20 x 100km of non-zero dispersion fiber with simultaneous C+ L-band dispersion compensation," in *Optical Fiber Communication Conference*, 2002, p. FC8.

[117] K. Mochizuki, N. Edagawa, and Y. Iwamoto, "Amplified spontaneous Raman scattering in fiber Raman amplifiers," *Journal of Lightwave Technology,* vol. 4, pp. 1328-1333, 1986.

[118] N. Olsson and J. Hegarty, "Noise properties of a Raman amplifier," *Journal of Lightwave Technology,* vol. 4, pp. 396-399, 1986.

[119] E. Desurvire, *Erbium-doped fiber amplifiers: principles and applications*: Wiley-Interscience, 2002.

[120] J. Bromage, "Raman amplification for fiber communications systems," *Journal of Lightwave Technology,* vol. 22, pp. 79-93, 2004.

[121] J. M. Senior and M. Y. Jamro, *Optical fiber communications: principles and practice*: Pearson Education, 2009.

[122] C. Headley and G. Agrawal, *Raman amplification in fiber optical communication systems*: Academic Press, 2005.

[123] J. Ania-Castañón and S. Turitsyn, "Noise and gain optimisation in bi-directionally pumped dispersion compensating amplifier modules," *Optics Communications,* vol. 224, pp. 107-111, 2003.

[124] M. Mermelstein, K. Brar, and C. Headley, "RIN transfer measurement and modeling in dual-order Raman fiber amplifiers," *Journal of Lightwave Technology,* vol. 21, p. 1518, 2003.

[125] D. K. Boiyo, S. Kuja, D. Waswa, G. Amolo, R. Gamatham, E. R. Kipnoo, *et al.*, "Effects of polarisation mode dispersion (PMD) on Raman gain and PMD measurement using an optical fibre Raman amplifier," in *AFRICON, 2013*, 2013, pp. 1-5.

[126] R. Neuhauser, P. Krummrich, H. Bock, and C. Glingener, "Impact of nonlinear pump interactions on broadband distributed Raman amplification," in *Optical Fiber Communication Conference and Exhibit, 2001. OFC 2001*, 2001, pp. MA4-MA4.

[127] T.-T. Kung, C.-T. Chang, J.-C. Dung, and S. Chi, "Four-wave mixing between pump and signal in a distributed Raman amplifier," *Journal of Lightwave Technology,* vol. 21, p. 1164, 2003.

[128] R. H. Stolen, E. P. Ippen, and A. R. Tynes, "Raman Oscillation in Glass Optical Waveguide," *Applied Physics Letters,* vol. 20, pp. 62-64, 1972.

[129] P. Rosa, G. Rizzelli, M. Tan, P. Harper, and J. D. Ania-Castañòn, "Characterisation of random DFB Raman laser amplifier for WDM transmission," *Optics Express,* vol. 23, pp. 28634-28639, 2015.

[130] L. F. Shampine, J. Kierzenka, and M. W. Reichelt, "Solving boundary value problems for ordinary differential equations in MATLAB with bvp4c," *Tutorial Notes,* vol. 2000, pp. 1-27, 2000.

[131] M. Alcon-Camas, A. El-Taher, J. Ania-Castanon, and P. Harper, "Gain bandwidth optimisation and enhancement in ultra-long Raman fibre laser based amplifiers," in *36th European Conference and Exhibition on Optical Communication (ECOC)*, 2010, pp. 1-3.

[132]   V. Karalekas, J. D. Ania-Castañón, J. Pérez-González, X. Chen, L. Zhang, and P. Harper, "Performance optimization of ultra-long Raman laser cavities for quasi-lossless transmission links," *Optics Communications,* vol. 277, pp. 214-218, 2007.

[133]   M. Tan, P. Rosa, M. A. Iqbal, I. Phillips, J. Nuño, and J. D. Ania-Castanon, "Rin mitigation in second-order pumped Raman fibre laser based amplification," in *Asia Communications and Photonics Conference*, 2015, p. AM2E. 6.

[134]   F. Gallazzi, G. Rizzelli, M. A. Iqbal, M. Tan, P. Harper, and J. D. Ania-Castañón, "Performance optimization in ultra-long Raman laser amplified 10× 30 GBaud DP-QPSK transmission: balancing RIN and ASE noise," *Optics Express,* vol. 25, pp. 21454-21459, 2017.

[135]   S. K. Turitsyn, S. A. Babin, A. E. El-Taher, P. Harper, D. V. Churkin, S. I. Kablukov*, et al.*, "Random distributed feedback fibre laser," *Nature Photonics,* vol. 4, pp. 231-235, Apr 2010.

[136]   P. Rosa, J.-D. Ania-Castañón, and P. Harper, "Unrepeatered DPSK transmission over 360 km SMF-28 fibre using URFL based amplification," *Optics Express,* vol. 22, pp. 9687-9692, 2014.

[137]   M. Nissov and H. Kidorf, "Chapter 5 - System Impairments," in *Raman Amplification in Fiber Optical Communication Systems*, ed Burlington: Academic Press, 2005, pp. 215-266.

[138]   M. Alcón-Camas and J. D. Ania-Castañón, "RIN transfer in 2nd-order distributed amplification with ultralong fiber lasers," *Optics Express,* vol. 18, pp. 23569-23575, 2010.

[139]   B. Bristiel, S. Jiang, P. Gallion, and E. Pincemin, "New model of noise figure and RIN transfer in fiber Raman amplifiers," *IEEE Photonics Technology Letters,* vol. 18, pp. 980-982, 2006.

[140]   J. Nuno and J. D. Ania-Castanón, "RIN transfer in second-order amplification with centrally-pumped random distributed feedback fiber lasers," *International Journal of Modern Physics B,* vol. 28, p. 1442005, 2014.

[141]   J. D. Ania-Castanón, T. J. Ellingham, R. Ibbotson, X. Chen, L. Zhang, and S. K. Turitsyn, "Ultralong Raman fiber lasers as virtually lossless optical media," *Physical Review Letters,* vol. 96, p. 023902, 2006.

[142]   J. D. Ania-Castañón, "Design and simulation of ultralong Raman laser links for optical signal transmission," in *Photonics North 2009*, 2009, p. 73862J.

[143]   M. Tan, P. Rosa, I. Phillips, and P. Harper, "Extended reach of 116 Gb/s DP-QPSK transmission using random DFB fiber laser based Raman amplification and bidirectional second-order pumping," in *Optical Fiber Communications Conference and Exhibition (OFC), 2015*, 2015, pp. 1-3.

[144]   I. Phillips, M. Tan, M. Stephens, M. E. McCarthy, E. Giacoumidis, S. Sygletos*, et al.*, "Exceeding the nonlinear-Shannon limit using Raman laser based amplification and optical phase conjugation," in *Optical Fiber Communications Conference and Exhibition (OFC), 2014*, 2014, pp. 1-3.

[145]   D. V. Churkin, S. A. Babin, A. E. El-Taher, P. Harper, S. I. Kablukov, V. Karalekas*, et al.*, "Raman fiber lasers with a random distributed feedback based on Rayleigh scattering," *Physical Review A,* vol. 82, Sep 22 2010.

[146]   M. Tan, P. Rosa, M. A. Iqbal, L. Son Thai, I. D. Phillips, S. K. Turitsyn*, et al.*, "Raman fibre laser based amplification in long-haul/unrepeatered coherent transmission systems," in *2017 19th International Conference on Transparent Optical Networks (ICTON)*, 2017, pp. 1-4.

[147]   M. Tan, M. A. Iqbal, S. K. Turitsyn, and P. Harper, "Mitigating RIN-penalty to enhance the transmission performance in distributed Raman amplification system," in *2017 Opto-Electronics and Communications Conference (OECC) and Photonics Global Conference (PGC)*, 2017, pp. 1-3.

[148] K. Technologies. Digital Communication Analyzer (DCA), Measure Relative Intensity Noise (RIN) [Online]. Available: http://literature.cdn.keysight.com/litweb/pdf/5989-5959EN.pdf

[149] C. J. O'Brien, M. L. Majewski, and A. D. Rakic, "A critical comparison of high-speed VCSEL characterisation techniques," *Journal of Lightwave Technology,* vol. 25, pp. 597-605, 2007.

[150] G. Rizzelli, M. A. Iqbal, F. Gallazzi, P. Rosa, M. Tan, J. D. Ania-Castañón*, et al.*, "Impact of input FBG reflectivity and forward pump power on RIN transfer in ultralong Raman laser amplifiers," *Optics Express,* vol. 24, pp. 29170-29175, 2016.

[151] G. R. Martella, M. A. Iqbal, P. Rosa, M. Tan, L. Krzczanowicz, I. Phillips*, et al.*, "Impact of Front-FBG Reflectivity in Raman Fiber Laser Based Amplification," in *CLEO: Science and Innovations*, 2016, p. SF1F. 6.

[152] G. Rizzelli, M. A. Iqbal, F. Gallazzi, P. Rosa, M. Tan, P. Corredera*, et al.*, "FBG Reflectivity Impact on RIN in Ultralong Laser Amplifiers," in *ECOC 2016; 42nd European Conference on Optical Communication; Proceedings of*, 2016, pp. 1-3.

[153] J. D. Ania-Castanon, V. Karalekas, P. Harper, and S. K. Turitsyn, "Simultaneous spatial and spectral transparency in ultralong fiber lasers," *Physical Review Letters,* vol. 101, Sep 19 2008.

[154] M. Krause, S. Cierullies, H. Renner, and E. Brinkmeyer, "Pump-to-Stokes RIN transfer in Raman fiber lasers and its impact on the performance of co-pumped Raman amplifiers," *Optics Communications,* vol. 260, pp. 656-661, 2006.

[155] C. Martinelli, L. Lorcy, A. Durecu-Legrand, D. Mongardien, S. Borne, and D. Bayart, "RIN transfer in copumped Raman amplifiers using polarisation-combined diodes," *IEEE Photonics Technology Letters,* vol. 17, pp. 1836-1838, Sep 2005.

[156] K. Keita, P. Delaye, R. Frey, and G. Roosen, "Relative intensity noise transfer of large-bandwidth pump lasers in Raman fiber amplifiers," *Journal of the Optical Society of America. B, Optical Physics,* vol. 23, p. 3, 2006.

[157] M. A. Iqbal, M. Tan, and P. Harper, "On the Mitigation of RIN Transfer and Transmission Performance Improvement in Bidirectional Distributed Raman Amplifiers," *Journal of Lightwave Technology,* pp. 1-1, 2018.

[158] M. A. Iqbal, M. Tan, and P. Harper, "Enhanced Transmission Performance Using Backward-Propagated Broadband ASE Pump," *IEEE Photonics Technology Letters,* vol. 30, pp. 865-868, 2018.

[159] M. A. Iqbal, M. Tan, and P. Harper, "Evaluation of RIN mitigated dual order bidirectional distributed Raman amplification using a broadband first order forward pump," in *European Conference on Optical Communication (ECOC 2017)*, Gothenburg, 2017, p. P1.SC1.13.

[160] M. A. Iqbal, M. Tan, and P. Harper, "Enhanced long-haul transmission using forward propagated broadband first order Raman pump," in *European Conference on Optical Communication (ECOC 2017)*, Gothenburg, 2017, p. P2.SC6.25.

[161] M. T. M. A. Iqbal, and P. Harper, "Transmission performance improvement using broadband incoherent counter-pumped distributed Raman amplification," in *Optical Fiber Communication Conference*, 2018, p. Th1C.2.

[162] M. A. Iqbali, M. Tan, and P. Harper, "RIN reduction technique for dual order forward pumped distributed Raman amplification," in *2017 Conference on Lasers and Electro-Optics Europe & European Quantum Electronics Conference (CLEO/Europe-EQEC)*, 2017, pp. 1-1.

[163] M. A. Iqbal, M. Tan, A. El-Taher, and P. Harper, "RIN and transmission performance improvement using second order and broadband first order forward Raman pumping," in *2017 Opto-Electronics and Communications Conference (OECC) and Photonics Global Conference (PGC)*, 2017, pp. 1-4.

[164] M. Morimoto, H. Ogoshi, J. Yoshida, S. Takasaka, A. Sano, and Y. Miyamoto, "Co-Propagating Dual-Order Distributed Raman Amplifier Utilizing Incoherent Pumping," *IEEE Photonics Technology Letters,* vol. 29, pp. 567-570, Apr 1 2017.

[165] D. Vakhshoori, M. Azimi, P. Chen, B. Han, M. Jiang, K. J. Knopp*, et al.*, "Raman amplification using high-power incoherent semiconductor pump sources," in *Optical Fiber Communication Conference*, 2003, p. PD47.

[166] G. Sun, Z. Cai, and C. Ye, "Dual-order Raman fiber laser with suppressed low-frequency pump-to-stokes RIN transfer," *Optics Communications,* p. 645, 2006.

[167] M. Schneiders, S. Vorbeck, R. Leppla, E. Lach, M. Schmidt, S. B. Papernyi*, et al.*, "Field transmission of 8 x 170 Gb/s over high-loss SSMF link using third-order distributed Raman amplification," *Journal of Lightwave Technology,* vol. 24, pp. 175-182, Jan 2006.

[168] S. Papernyi, V. Karpov, and W. Clements, "Third-order cascaded Raman amplification," in *Optical Fiber Communication Conference and Exhibit (OFC 2002)*, 2002, pp. FB4-FB4.

[169] V. Karalekas, J. D. Ania-Castanon, P. Harper, S. A. Babin, E. V. Podivilov, and S. K. Turitsyn, "Impact of nonlinear spectral broadening in ultra-long Raman fibre lasers," *Optics Express,* vol. 15, pp. 16690-16695, 2007.

[170] A. R. Sarmani, M. H. Abu Bakar, A. A. A. Bakar, F. R. M. Adikan, and M. A. Mahdi, "Spectral variations of the output spectrum in a random distributed feedback Raman fiber laser," *Optics Express,* vol. 19, pp. 14152-14159, 2011.

[171] S. Burtsev, H. de Pedro, C. Do-il, W. Pelouch, H. Fevrier, S. Ten*, et al.*, "150 × 120 Gb/s transmission over 3,780 km of G.652 fiber using all-distributed Raman amplification," presented at the Optical Fiber Communications Conference & Exhibition (OFC), 2015.

[172] M. Alcón-Camas and J. D. Ania-Castañón, "Relative intensity noise transfer in higher-order distributed amplification through ultra-long fiber cavities," in *Photonics North 2010*, Niagara Falls, Canada, 2010.

[173] J. C. Cheng, M. Tang, A. P. T. Lau, C. Lu, L. Wang, Z. H. Dong*, et al.*, "Pump RIN-induced impairments in unrepeatered transmission systems using distributed Raman amplifier," *Optics Express,* vol. 23, pp. 11838-11854, 2015.

[174] H. Kidorf, K. Rottwitt, M. Nissov, M. Ma, and E. Rabarijaona, "Pump interactions in a 100-nm bandwidth Raman amplifier," *IEEE Photonics Technology Letters,* vol. 11, pp. 530-532, 1999.

[175] V. E. Perlin and H. G. Winful, "Ultra-broadband Raman amplification with spatially diverse pumps," in *Lasers and Electro-Optics, 2002. CLEO '02. Technical Digest. Summaries of Papers Presented at the*, 2002, pp. 432-433 vol.1.

[176] X. Zhou and M. Birk, "100 nm broadband Raman amplification in NZ-DSF fiber with zero-dispersion wavelength around 1500 nm," in *Optical Amplifiers and Their Applications/Integrated Photonics Research*, San Francisco, California, 2004, p. JWB1.

[177] S. Namiki and Y. Emori, "Ultrabroad-band Raman amplifiers pumped and gain-equalized by wavelength-division-multiplexed high-power laser diodes," *IEEE Journal of Selected Topics in Quantum Electronics,* vol. 7, pp. 3-16, 2001.

[178] J. Ania-Castañón, A. Pustovskikh, S. Kobtsev, and S. Turitsyn, "Simple design method for gain-flattened three-pump Raman amplifiers," *Optical and Quantum Electronics,* vol. 39, pp. 213-220, 2007.

[179] M. A. Iqbal, G. R. Martella, F. Gallazzi, M. Tan, P. Harper, and J. D. Ania-Castañón, "Performance improvement of broadband distributed Raman amplifier using bidirectional pumping with first and dual order forward pumps," in *18th International Conference on Transparent Optical Networks (ICTON)* 2016, pp. 1-4.

[180] B. Min, W. J. Lee, and N. Park, "Efficient formulation of Raman amplifier propagation equations with average power analysis," *IEEE Photonics Technology Letters,* vol. 12, pp. 1486-1488, 2000.

[181] W. Zhang, J. Peng, X. Liu, and C. Fan, "An analytical expression of equivalent noise figure for distributed fiber Raman amplifiers with Rayleigh scattering," *Optics Communications,* vol. 199, pp. 231-236, 2001.

[182] P. Xiao, Q. Zeng, J. Huang, and J. Liu, "A new optimal algorithm for multipump sources of distributed fiber Raman amplifier," *IEEE Photonics Technology Letters,* vol. 15, pp. 206-208, 2003.

[183] A. Mowla and N. Granpayeh, "Design of a flat-gain multipumped distributed fiber Raman amplifier by particle swarm optimization," *Journal of the Optical Society of America A,* vol. 25, pp. 3059-3066, 2008.

[184] X. Liu and B. Lee, "Optimal design of fiber Raman amplifier based on hybrid genetic algorithm," *IEEE Photonics Technology Letters,* vol. 16, pp. 428-430, 2004.

[185] X. Liu and B. Lee, "Optimal design for ultra-broad-band amplifier," *Journal of Lightwave Technology,* vol. 21, pp. 3446-3455, 2003.

[186] H.-m. Jiang, K. Xie, and Y.-f. Wang, "Pump scheme for gain-flattened Raman fiber amplifiers using improved particle swarm optimization and modified shooting algorithm," *Optics Express,* vol. 18, pp. 11033-11045, 2010.

[187] H. M. Jiang, K. Xie, and Y. F. Wang, "Novel design of flat gain spectrum Raman fiber amplifiers based on ant colony optimization," *IEEE Photonics Technology Letters,* vol. 23, pp. 1823-1825, 2011.

[188] Z. Tong, H. Wei, and S. Jian, "An efficient method to optimize gain spectra of fiber Raman amplifiers pumped by multiple laser diodes," *Microwave and Optical Technology Letters,* vol. 35, pp. 381-383, 2002.

[189] K. Deb, *Multi-objective optimization using evolutionary algorithms* vol. 16: John Wiley & Sons, 2001.

[190] E. Zitzler, "Evolutionary algorithms for multiobjective optimization: Methods and applications," 1999.

[191] C. Fludger and K. J. Cordina, "Changes in Raman gain coefficient with pump wavelength in modern transmission fibres," in *Optical Amplifiers and Their Applications*, 2002, p. OMC3.

[192] S. Kado, Y. Emori, S. Namiki, N. Tsukiji, J. Yoshida, and T. Kimura, "Broadband flat-noise Raman amplifier using low-noise bidirectionally pumping sources," in *27th European Conference on Optical Communication*, 2001, pp. 38-39.

[193] M. A. Iqbal, M. Tan, L. Krzczanowicz, G. Rizzelli, F. Gallazzi, A. E. El-Taher*, et al.*, "Noise Performance Improvement of Broadband Distributed Raman Amplifier Using Dual Order Bidirectional Pumping," in *Asia Communications and Photonics Conference 2016*, Wuhan, 2016, p. AF4G.2.

[194] A. E. El-Taher, J. D. Ania-Castañón, V. Karalekas, and P. Harper, "High efficiency supercontinuum generation using ultra-long Raman fiber cavities," *Optics Express,* vol. 17, pp. 17909-17915, 2009.

[195] M. N. Islam, "Raman amplifiers for telecommunications," *IEEE Journal of Selected Topics in Quantum Electronics,* vol. 8, pp. 548-559, 2002.

[196] L. Krzczanowicz, M. A. Iqbal, I. Phillips, M. Tan, P. Skvortcov, P. Harper*, et al.*, "Low transmission penalty dual-stage broadband discrete Raman amplifier," *Optics Express,* vol. 26, pp. 7091-7097, 2018.

[197] M. A. I. L. Krzczanowicz, I. Phillips, M. Tan, P. Skvortcov, P. Harper, and W. Forysiak, "Low penalty, dual stage, broadband discrete Raman amplifier for high capacity WDM/metro networks," in *Optical Fiber Communication Conference*, San Diego, USA, 2018, p. W3D.3.

[198] T. Miyamoto, T. Tsuzaki, T. Okuno, M. Kakui, M. Hirano, M. Onishi*, et al.*, "Raman amplification over 100 nm-bandwidth with dispersion and dispersion slope compensation

for conventional single mode fiber," in *Optical Fiber Communication Conference and Exhibit (OFC 2002)*, 2002, pp. 66-68.

[199] J. Bromage, H. Thiele, and L. Nelson, "Raman amplification in the S-band," in *Optical Fiber Communication Conference and Exhibit (OFC 2002)*, 2002, pp. 383-385.

[200] I. Nasieva, J. Ania-Castanon, and S. Turitsyn, "Nonlinearity management in fibre links with distributed amplification," *Electronics Letters,* vol. 39, pp. 856-857, 2003.

[201] K. Mukasa, K. Imamura, I. Shimotakahara, T. Yagi, and K. Kokura, "Dispersion compensating fiber used as a transmission fiber: inverse/reverse dispersion fiber," *Journal of Optical and Fiber Communications Reports,* vol. 3, p. 292, 2006.

[202] D. Hamoir, J. Y. Boniort, L. Gasca, and D. Bayart, "Optimized, two-stage architecture for Raman amplifiers," *Optical Amplifiers and Their Applications, Proceedings,* vol. 44, pp. 96-98, 2001.

[203] S. A. E. Lewis, S. V. Chernikov, and J. R. Taylor, "Characterisation of double Rayleigh scatter noise in Raman amplifiers," *IEEE Photonics Technology Letters,* vol. 12, pp. 528-530, May 2000.

[204] M. A. Iqbal, M. Tan, L. Krzczanowicz, P. Skvortcov, A. El-Taher, I. D. Philips*, et al.*, "Performance characterisation of high gain, high output power and low noise cascaded broadband discrete Raman amplifiers," in *19th International Conference on Transparent Optical Networks (ICTON)*, 2017, pp. 1-4.

[205] T. Miyamoto, M. Tanaka, J. Kobayashi, T. Tsuzaki, M. Hirano, T. Okuno*, et al.*, "Highly nonlinear fiber-based lumped fiber Raman amplifier for CWDM transmission systems," *Journal of Lightwave Technology,* vol. 23, pp. 3475-3483, Nov 2005.

[206] M. A. Iqbal, M. Tan, L. Krzczanowicz, A. E. El-Taher, W. Forysiak, J. D. Ania-Castañón*, et al.*, "Noise and transmission performance improvement of broadband distributed Raman amplifier using bidirectional Raman pumping with dual order co-pumps," *Optics Express,* vol. 25, pp. 27533-27542, 2017.